EME 2016

August 20-21

17th International EME Conference

Venice – Italy

Organized by

"Laguna Veneta Contest Team – IQ3LX"

www.iq3lx.it

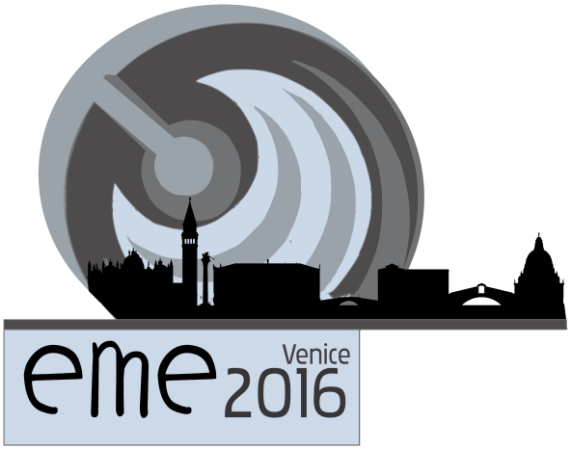

Conference Proceedings

ISBN: 979-12-200-1222-5

Published in 2016 by "Laguna Veneta Contest Team – IQ3LX"

With the patronage of A.R.I.

Editors: Giulio Pico IW3HVB, Corrado Feltrin IK3YBX

Printed in Italy by AREAGRAPHICA

Organizing Committee:

Giulio Pico IW3HVB

CEO @EME2016

Licensed on 1998, Industrial Engineer ,15 years of experience as Transmission Network Designer on microwave links, Active VHF EME operator and DXpeditioner since 2010.

Corrado Feltrin IK3YBX

SUPERVISOR @ EME2016

Corrado Feltrin – Supervisor IK3YBX since 1994. Specialist and Software Developer for TIM.

Roberta Foffano

LOGISTICS AND COLLATERAL PROGRAM @ EME2016

Roberta Foffano – Conference Logistics Coordinator Twenty five years of Experience in Conference Organization.

Aldo Pico IK3COJ

TECHNICAL COORDINATOR @ EME2016

Aldo Pico – Technical Area Coordinator IK3COJ since 1983, Thirty years of experience in radio engineering, one of the pioneers of microwave EME in Italy.

Fabio Cazzin IW3FVZ

WEBMASTER @ EME2016

Fabio Cazzin – Vice President, WebMaster IW3FVZ since 1988, System Integrator and Internet Service Provider, CEO of NS3. President of the A.R.I. Section in Mestre.

Sandro Segreto IZ3ZMF

PROVISIONS @ EME2016

Sandro Segreto – Provisions Coordinator IZ3ZMF since 2013, A young force, dedicated to the Ham proselytism between Boy Scouts, Radiocommunication area. Sales Manager.

IK3GHY

SUPERVISOR@EME2016

Giorgio Murador - Supervisor IK3GHY since 1986, Another Italian pioneer in microwave EME.

Summary

The digital version of the proceedings book, along with other documents, media, and software, are available for download at www.eme2016.org

Welcome to the 17th edition of the International EME Conference

We are very glad to be hosts for this edition of the International EME Conference.

It has been a demanding task, but a rewarding one for sure.

130 participants from 20 countries covering 5 continents are big numbers, and we have to thank you before anyone else for your presence.

The contents of the conference papers are top notch, with topics spacing from Dish Contruction to the latest results in digital techniques, so a well deserved Thank you! We address to the lecturers.

We thank all the volunteers from A.R.I. Local Chapters of Mestre and Treviso for their collaboration and support. Thanks to A.R.I. national and regional managements for their enthusiastic contribution.

We can't forget to thank all of our commercial sponsors who strongly believed in this project, for their technical and financial help.

A very special thank you goes also to the collateral program staff!

We hope for you all to enjoy your stay here in Venice, and we look forward to the next one!

73. The EME 2016 Organizing Committee.

Sponsors List:

IK1UVL & IK3XTV - Signal polarity in V/UHF bands Chapter 2

Giorgio Marchi & Flavio Egano (email: ik3xtv@gmail.com ; marchi.uwl@gmail.com)

EME 2014 – Parc du Radome, Pleumeur Bodou France
Chapter I: Ionospheric interactions with EME signals

Synopsis:

Cap. I – 2014

Ionosphere's meteorology: QSB in 2 m.

Building an Excel sheet for 2 m Faraday calculations.

Panoramic of polarity on moon passes

Cap. II - 2016

Spatial offset as function of distance and direction.

Extension of Excel sheet to other V/UHF bands

Analysis of polarity for each band.

Numbers and orders of magnitude of qualitatively known characteristics.

EME 2016 – Chapter II . Signal Polarity in V/UHF bands

Hello, nice to meet you again. Why Chapter II?

Background, Chapter I

We both operate on the 2 m band, and had decided to investigate Faraday and QSB effects, so common on this band.

In the 2014 France meeting, we showed you our studies on what happens in the ionosphere to a 2 m signal.

Specifically: the type of QSB one can expect, and the polarity of the returning wave over a full moon pass.

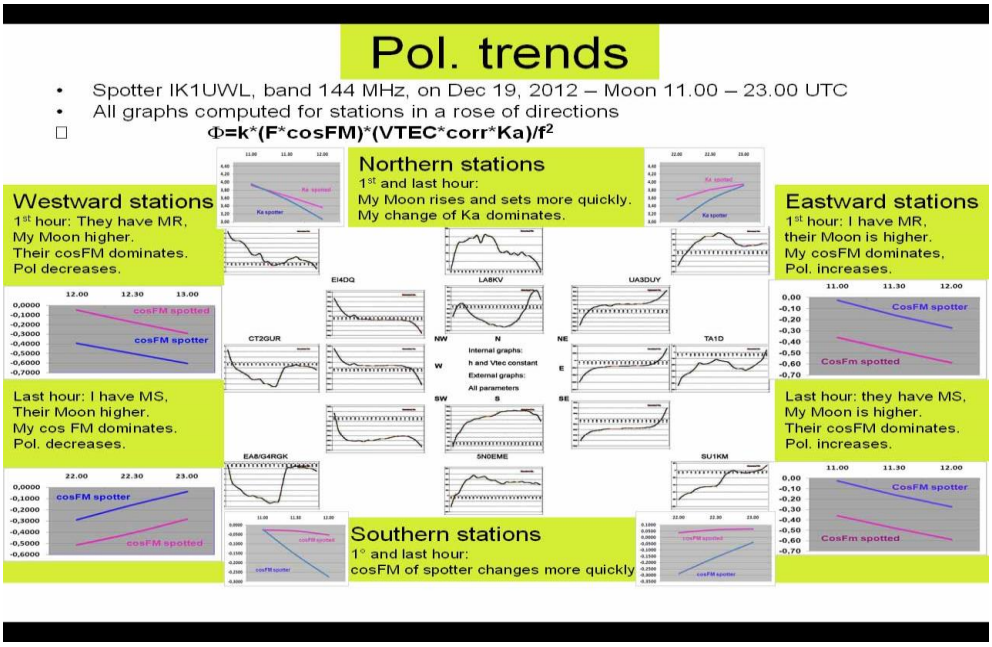

All the polarity calculations were made with an Excel sheet we built.

	Date	Call	Loc.	Lat.	Long.	Lat. mag.	Corr. Day	Corr.night	F	Incl.	Decl.	Loc conv.	Conv. Lat.	Calc. F	Dourbes
2	16/12/2012	SP4MPB	KO03HT	53,81	20,63	50,65	0,93	0,20	0,44958	68,77	4,54				
3															
4	UTC	localtime(ref.DRB)	Az (°)	El (°)	h (km)	Ka	VTEC Drbs	Corr.	¥TEC loc.	STEC	cosFM	Rot.(°)	Rot.(rad)	Offset P1	P1(0,180)
5	10.00	11.04	129	8,3	187	3,64	15,52	0,45	14,24	51,84	-0,3367	-512,6	-8,95	61,6	61,6
6	10.30	11.34	135	11,6	185	3,27	15,00	0,45	13,72	44,79	-0,4171	-548,7	-9,58	64,5	64,5
7	11.00	12.04	142	14,5	182	2,95	14,08	0,45	12,80	37,78	-0,4912	-545,0	-9,51	68,0	68,0
8	11.30	12.34	149	17,0	182	2,70	13,82	0,45	12,54	33,90	-0,5543	-551,9	-9,63	71,7	71,7
9	12.00	13.04	156	19,0	182	2,53	13,68	0,45	12,40	31,36	-0,6042	-556,5	-9,71	75,6	75,6
10	12.30	13.34	163	20,6	185	2,40	13,68	0,45	12,40	29,74	-0,6435	-562,1	-9,81	79,7	79,7
11	13.00	14.04	171	21,7	187	2,32	14,10	0,45	12,82	29,73	-0,6716	-586,4	-10,23	84,5	84,5
12	13.30	14.34	178	22,2	197	2,28	12,11	0,45	10,83	24,66	-0,7093	-512,9	-8,95	88,8	88,8
13	14.00	15.04	186	22,1	201	2,28	10,53	0,45	9,25	21,07	-0,6866	-424,9	-7,42	86,4	93,6
14	14.30	15.34	193	21,5	221	2,31	10,55	0,45	9,27	21,40	-0,6751	-424,2	-7,40	82,2	97,8
15	15.00	16.04	201	20,3	259	2,36	10,00	0,45	8,72	20,60	-0,6495	-393,0	-6,86	77,4	102,6
16	15.30	16.34	208	18,7	307	2,45	7,89	0,45	6,61	16,17	-0,6129	-291,0	-5,08	73,4	106,6
17	16.00	17.04	215	16,5	326	2,59	6,32	0,33	5,38	13,95	-0,5641	-231,1	-4,03	69,6	110,4
18	16.30	17.34	222	14,0	369	2,75	5,26	0,20	4,69	12,89	-0,5045	-191,0	-3,33	66,1	113,9
19	17.00	18.04	229	11,0	406	2,95	4,47	0,20	3,90	11,51	-0,4317	-145,9	-2,55	62,8	117,2
20	17.30	18.34	235	7,7	417	3,20	4,63	0,20	4,06	12,99	-0,3538	-135,0	-2,36	60,2	119,8
21	18.00	19.04	241	4,2	432	3,41	4,34	0,20	3,77	12,84	-0,2686	-101,3	-1,77	58,0	122,0
22	18.30	19.34	247	0,8	451	3,48	3,95	0,20	3,38	11,77	-0,1804	-62,4	-1,09	56,1	123,9
...															
36	Date	Nomin	Loc.	Lat.	Long.	Lat. mag.	Corr. Day	Corr.night	F	Incl.	Decl.	Loc conv.	Conv. Lat.	Calc. F	Dourbes
37	16/12/2012	PA3FPQ	JO22XE	52,19	5,96	50,61	0,93	0,20	-0,43860	66,93	0,23				
38															
39	UTC	localtime(ref.DRB)	Az (°)	El (°)	h (km)	Ka	VTEC Drbs	Corr.	¥TEC loc.	STEC	cosFM	Rot.(°)	Rot.(rad)	Offset P2	P2(0,180)
40	10.00	10.05	116	2,0	192	4,21	14,74	0,45	13,48	56,76	-0,2023	329,0	5,74	55,4	55,4
41	10.30	10.35	122	5,8	187	3,93	16,05	0,45	14,79	58,16	-0,2974	495,6	8,65	57,6	57,6
42	11.00	11.05	128	9,4	187	3,52	15,52	0,45	14,26	50,13	-0,3869	555,6	9,70	60,1	60,1
43	11.30	11.35	135	12,8	185	3,13	15,00	0,45	13,74	42,98	-0,4725	581,9	10,16	63,4	63,4
44	12.00	12.05	141	15,8	182	2,82	14,08	0,45	12,82	36,10	-0,5427	561,3	9,80	66,6	66,6
45	12.30	12.35	148	18,4	182	2,58	13,82	0,45	12,56	32,35	-0,6055	561,2	9,79	70,4	70,4
46	13.00	13.05	155	20,6	182	2,40	13,68	0,45	12,42	29,82	-0,6558	560,2	9,78	74,5	74,5
47	13.30	13.35	163	22,3	185	2,28	13,68	0,45	12,42	28,27	-0,6956	563,4	9,83	79,4	79,4
48	14.00	14.05	170	23,5	187	2,20	14,10	0,45	12,84	28,25	-0,7199	582,6	10,17	83,7	83,7
49	14.30	14.35	178	24,0	187	2,17	12,11	0,45	10,85	23,49	-0,7319	492,6	8,60	88,7	88,7
50	15.00	15.05	186	24,0	201	2,16	10,53	0,45	9,27	19,99	-0,7304	418,4	7,30	86,2	93,8
51	15.30	15.35	193	23,3	221	2,19	10,53	0,45	9,27	20,29	-0,7151	415,6	7,25	81,9	98,1
52	16.00	16.05	201	22,0	259	2,25	10,00	0,45	8,74	19,66	-0,6844	385,4	6,73	76,9	103,1
53	16.30	16.35	208	20,3	307	2,33	7,89	0,45	6,63	15,44	-0,6444	285,2	4,98	72,8	107,2
54	17.00	17.05	215	18,0	326	2,48	6,32	0,33	5,39	13,37	-0,5905	226,2	3,95	68,8	111,2
55	17.30	17.35	222	15,4	369	2,64	5,26	0,20	4,70	12,40	-0,5258	186,8	3,26	65,1	114,9
56	18.00	18.05	229	12,3	406	2,85	4,47	0,20	3,91	11,12	-0,4483	142,8	2,49	61,7	118,3
57	18.30	18.35	235	8,9	417	3,11	4,63	0,20	4,07	12,64	-0,3655	132,4	2,31	59,0	121,0

Results were checked by comparison with real decodes of the same stations lasting at least one hour. For our research, we built a big library of station pairs.

Our Excel sheet

Building the sheet for each pair of stations is a lot of work, due to the amount of data necessary. These are: Moon position during the pass, ionospheric density and thickness for that date, the geomagnetic field above that locator.

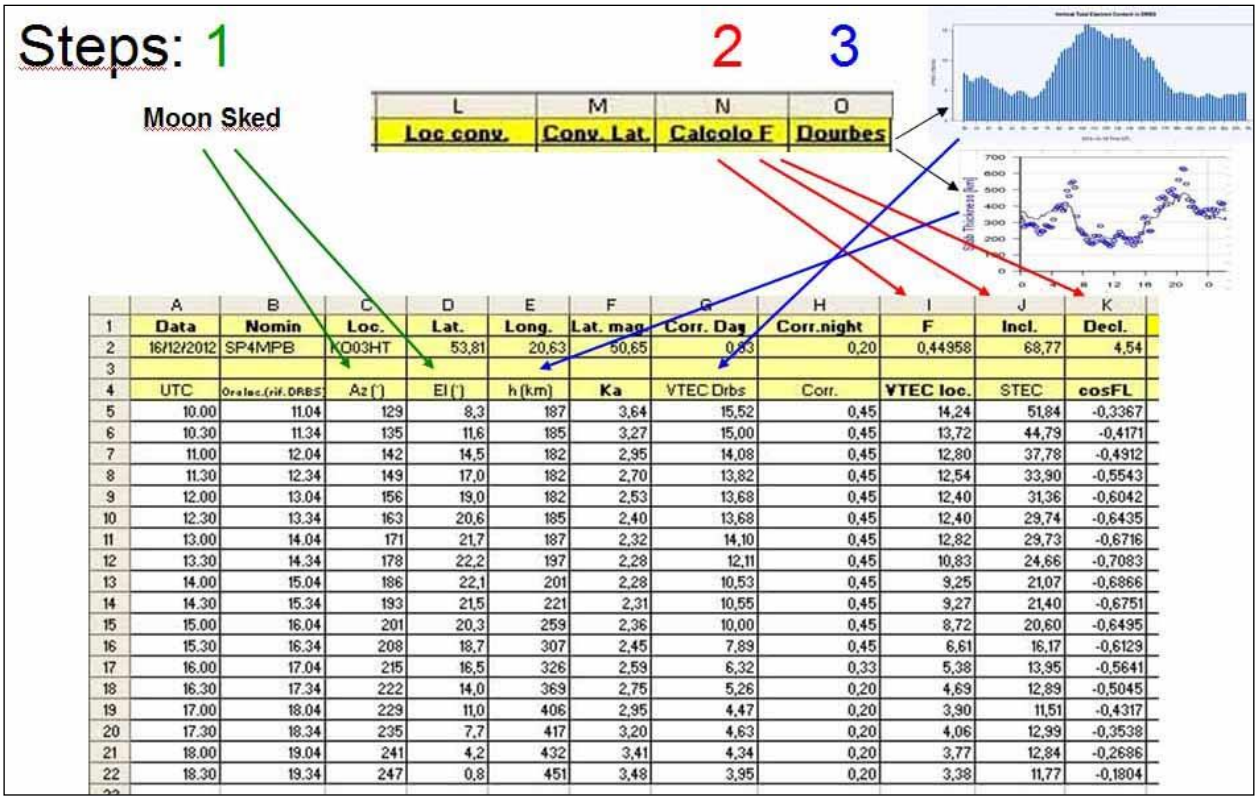

	A	B	C	D	E	F	G	H	I	J	K
1	Data	Nomin	Loc.	Lat.	Long.	Lat. mag.	Corr. Day	Corr.night	F	Incl.	Decl.
2	16/12/2012	SP4MPB	JO03HT	53,81	20,63	50,65	0,83	0,20	0,44958	68,77	4,54
3											
4	UTC	Oraloc.(rif.DRBS)	Az (°)	El (°)	h (km)	Ka	VTEC Drbs	Corr.	VTEC loc.	STEC	cosFL
5	10.00	11.04	129	8,3	187	3,64	15,52	0,45	14,24	51,84	-0,3367
6	10.30	11.34	135	11,6	185	3,27	15,00	0,45	13,72	44,79	-0,4171
7	11.00	12.04	142	14,5	182	2,95	14,08	0,45	12,80	37,78	-0,4912
8	11.30	12.34	149	17,0	182	2,70	13,82	0,45	12,54	33,90	-0,5543
9	12.00	13.04	156	19,0	182	2,53	13,68	0,45	12,40	31,36	-0,6042
10	12.30	13.34	163	20,6	185	2,40	13,68	0,45	12,40	29,74	-0,6435
11	13.00	14.04	171	21,7	187	2,32	14,10	0,45	12,82	29,73	-0,6716
12	13.30	14.34	178	22,2	197	2,28	12,11	0,45	10,83	24,66	-0,7083
13	14.00	15.04	186	22,1	201	2,28	10,53	0,45	9,25	21,07	-0,6866
14	14.30	15.34	193	21,5	221	2,31	10,55	0,45	9,27	21,40	-0,6751
15	15.00	16.04	201	20,3	259	2,36	10,00	0,45	8,72	20,60	-0,6495
16	15.30	16.34	208	18,7	307	2,45	7,89	0,45	6,61	16,17	-0,6129
17	16.00	17.04	215	16,5	326	2,59	6,32	0,33	5,38	13,95	-0,5641
18	16.30	17.34	222	14,0	369	2,75	5,26	0,20	4,69	12,89	-0,5045
19	17.00	18.04	229	11,0	406	2,95	4,47	0,20	3,90	11,51	-0,4317
20	17.30	18.34	235	7,7	417	3,20	4,63	0,20	4,06	12,99	-0,3538
21	18.00	19.04	241	4,2	432	3,41	4,34	0,20	3,77	12,84	-0,2686
22	18.30	19.34	247	0,8	451	3,48	3,95	0,20	3,38	11,77	-0,1804

The sheet converts the ionospheric data for the station's location, calculates the increase of ion density due to oblique passage (Ka), and finds the magnetic field component in the wave's direction (cosFM).

Results for each station

Putting these data in Faraday's rotation formula and adding the polar offset gives us a table of the rotations of the up going and down going waves.

SP4MPB (tx)

Rotaz. (°)	Rotaz.(rad)	Offset P1
-512,6	-8,95	61,6
-548,7	-9,58	64,5
-545,0	-9,51	68,0
-551,9	-9,63	71,7
-556,5	-9,71	75,6
-562,1	-9,81	79,7
-586,4	-10,23	84,5
-512,9	-8,95	88,8
-424,9	-7,42	-86,4
-424,2	-7,40	-82,2
-393,0	-6,86	-77,4
-291,0	-5,08	-73,4
-231,1	-4,03	-69,6
-191,0	-3,33	-66,1
-145,9	-2,55	-62,8
-135,0	-2,36	-60,2
-101,3	-1,77	-58,0
-62,4	-1,09	-56,1

Wave going up

PA3FPQ (rx)

Rotaz. (°)	Rotaz.(rad)	Offset P2
329,0	5,74	55,4
495,6	8,65	57,6
555,6	9,70	60,1
581,9	10,16	63,4
561,3	9,80	66,6
561,2	9,79	70,4
560,2	9,78	74,5
563,4	9,83	79,4
582,6	10,17	83,7
492,6	8,60	88,7
418,4	7,30	-86,2
415,6	7,25	-81,9
385,4	6,73	-76,9
285,2	4,98	-72,8
226,2	3,95	-68,8
186,8	3,26	-65,1
142,8	2,49	-61,7
132,4	2,31	-59,0

Wave coming back

Final results in 2m

Notwithstanding the choice of two relatively near stations (1000 km), so that the ionospheric density is similar, we see that the two factors, Ka and cosFM, have an important influence in causing different rotations.

So, on 2 meters, the rotation varies appreciably, going up and down during the Moon pass.

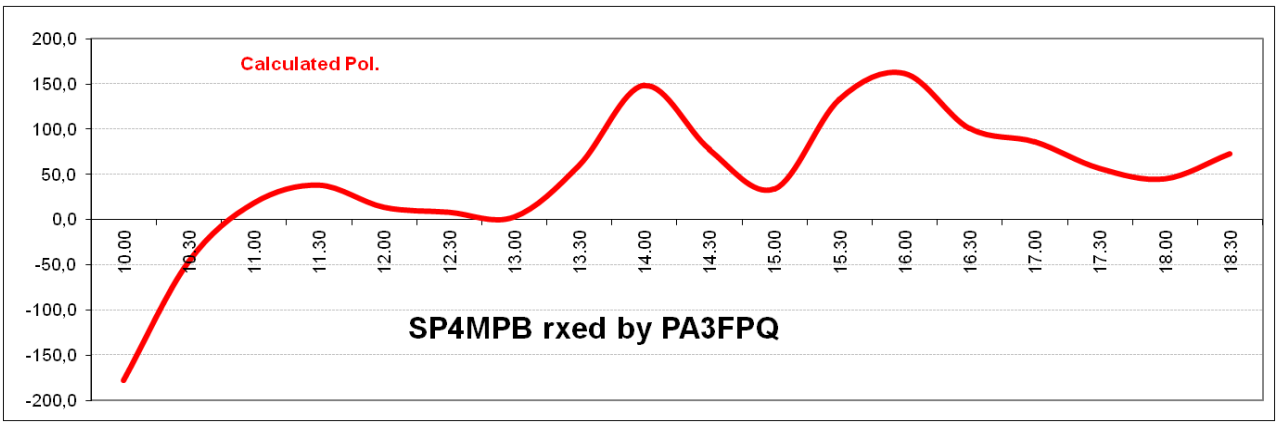

Chapter II

Using this library, we intend to show and expand the polarity issue for the V/UHF bands.

Polarity is the sum of Spatial Offset and Faraday rotation.

Spatial Offset is dependent only on the relative location of the stations..

Faraday is dependent on frequency, ionosphere's density, and on Moon's position

From our library: Spatial Offsets

With a simple shift of the field chosen for the polarity graph, we easily obtain from each Excel sheet in our library the graph of Polar Offset.

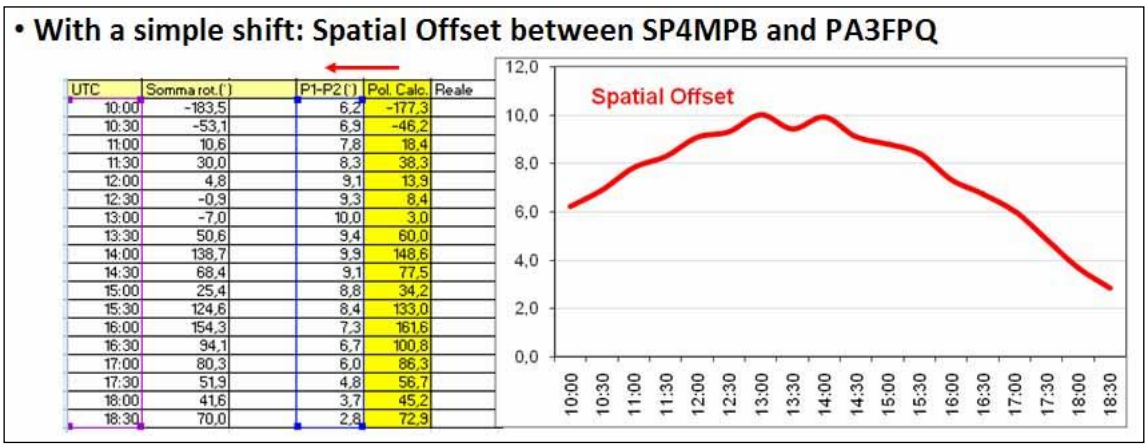

UTC	Somma rot.(°)	P1-P2(°)	Pol. Calc.	Reale
10:00	-183,5	6,2	-177,3	
10:30	-53,1	6,9	-46,2	
11:00	10,6	7,8	18,4	
11:30	30,0	8,3	38,3	
12:00	4,8	9,1	13,9	
12:30	-0,9	9,3	8,4	
13:00	-7,0	10,0	3,0	
13:30	50,6	9,4	60,0	
14:00	138,7	9,9	148,6	
14:30	68,4	9,1	77,5	
15:00	25,4	8,8	34,2	
15:30	124,6	8,4	133,0	
16:00	154,3	7,3	161,6	
16:30	94,1	6,7	100,8	
17:00	80,3	6,0	86,3	
17:30	51,9	4,8	56,7	
18:00	41,6	3,7	45,2	
18:30	70,0	2,8	72,9	

Since it is independent from frequency, our library data are valid for all bands.

Spatial Offset

An easy way to calculate the angle between the planes of two antennas in different places of the world is to calculate for each the angle respect earth's polar axis, then make the difference between them.

P=arctg((sin**Lat***cos**El**-cos**Lat***cos**Az***sin**El**)/cos**Lat***sin**Az**)

Spatial Offset = P1 – P2

These angles depend on the latitude, and on Moon's direction.

Latitude is a constant; Moon's direction varies during the pass.

The differences between polar offsets increase with station distance so spatial offset can become an important factor of polarity.

For example TI2SW 9000 km west of IK1UWL

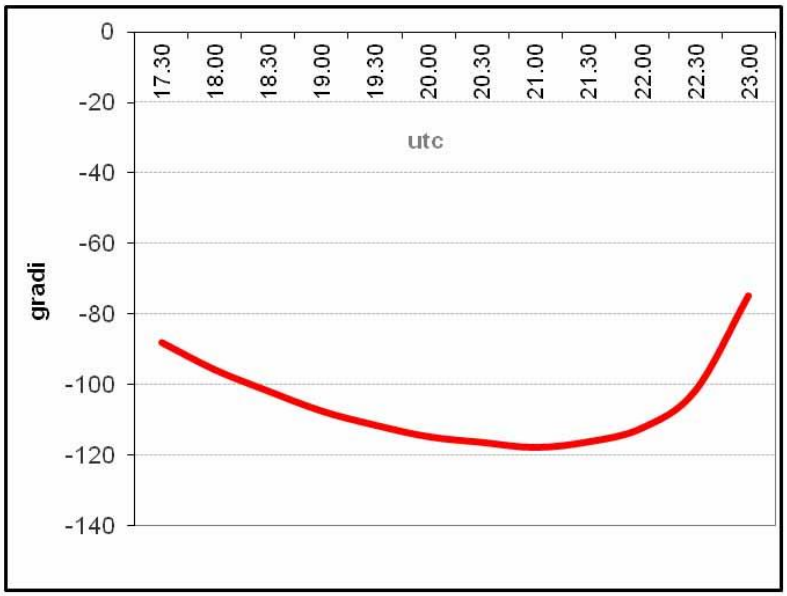

Offset, change with distance and direction

From our big library, we have extrapolated graphs for many stations placed in different directions and at different distances.

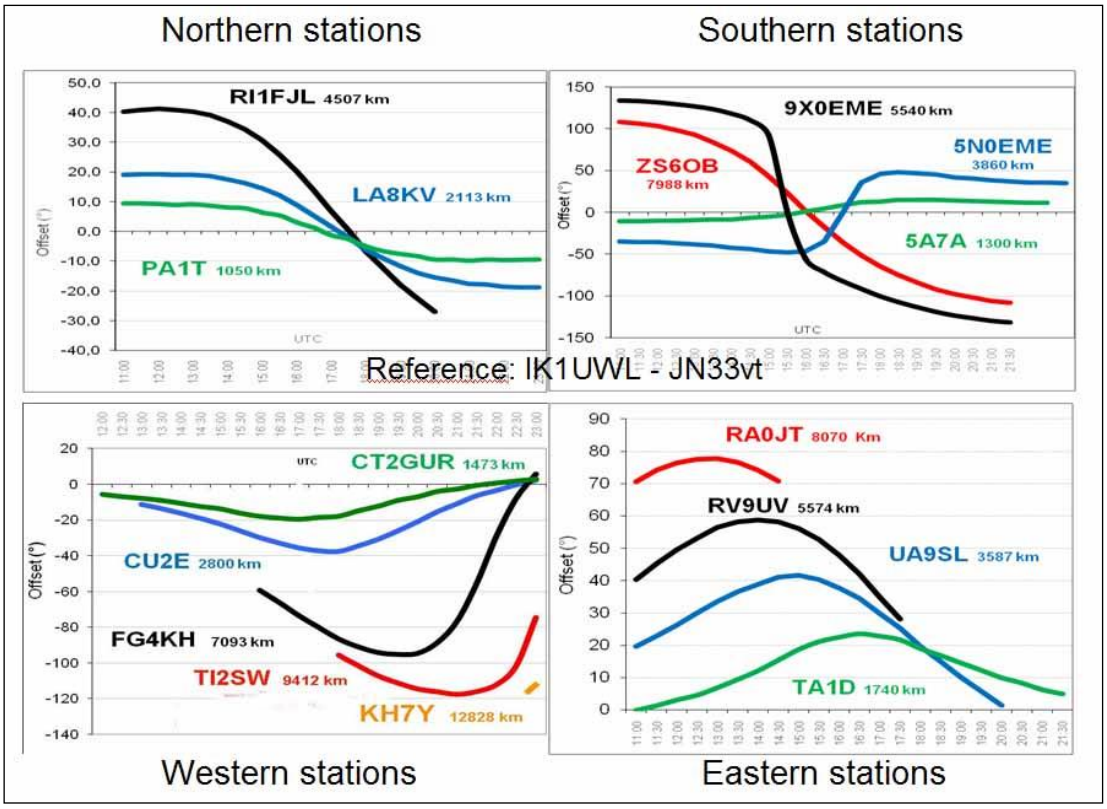

When the main difference is only in latitude, the graphs have an S shape, and offset tends to zero with Moon in the middle of the pass.

When the difference is mainly longitude, the offset is maximum with Moon in the middle of the pass, and does not change sign.

Offsets can reach and pass 90°. If greater, since the phase is not important, the effective offset is the supplement of the calculated value (but the full value must be used for polarity calculation).

Conversion to other bands

In our sheets we did put in the coefficient k/f^2 which has a value for 2 m of 1,14.

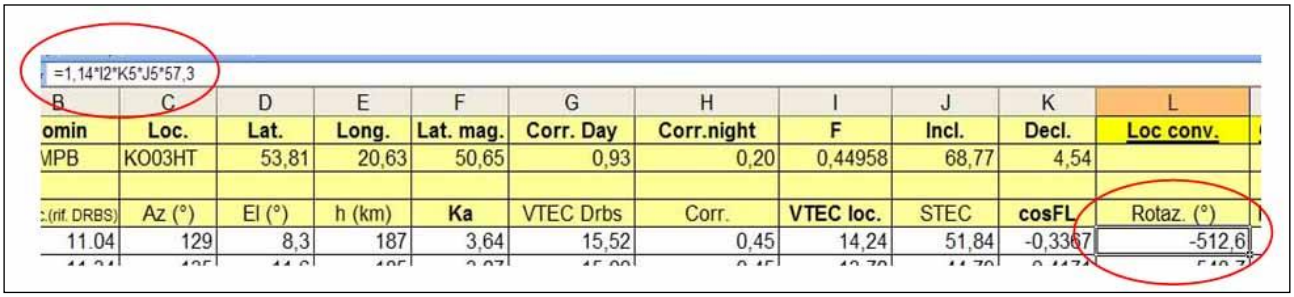

B	C	D	E	F	G	H	I	J	K	L
omin	Loc.	Lat.	Long.	Lat. mag.	Corr. Day	Corr.night	F	Incl.	Decl.	Loc conv.
MPB	KO03HT	53,81	20,63	50,65	0,93	0,20	0,44958	68,77	4,54	
(rif. DRBS)	Az (°)	El (°)	h (km)	Ka	VTEC Drbs	Corr.	VTEC loc.	STEC	cosFL	Rotaz. (°)
11.04	129	8,3	187	3,64	15,52	0,45	14,24	51,84	-0,3367	-512,6

These are the different values for the other VHF and UHF bands:

6m – 9,46; 70cm – 0,127; 23cm – 0,0123

Changing the coefficient in the formula transforms the sheet to what would happen if the two stations were operating on this different band. Our library can be easily transformed to show what would happen on different bands for the same pair and in the same conditions.

4 bands (6m, 2m, 70 cm, 23 cm)

Using the same pair, SP4MPB by PA3FPQ, we show you the superimposed graphs of polarity rotation when operating on these four bands.

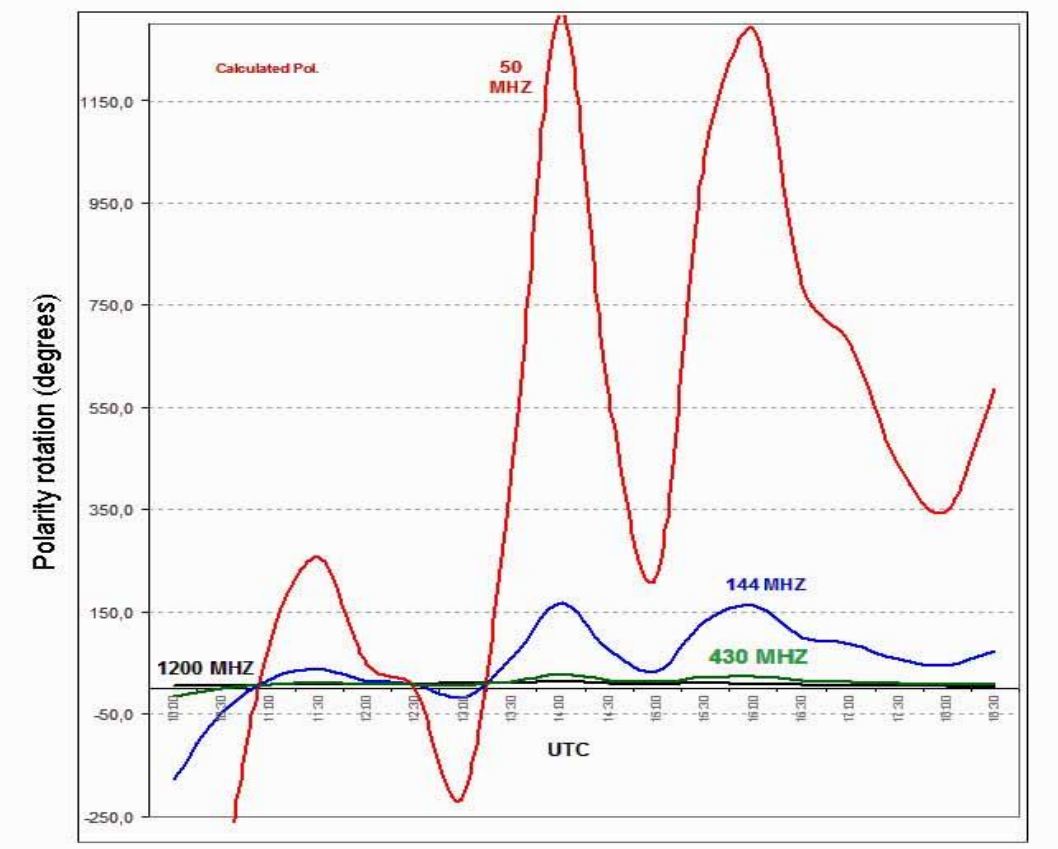

Rotation due to Faraday is enormous on the lower band, and gradually becomes smaller with decreasing frequency. There is a factor 9 for each jump.

These graphs use Faraday calculated for an unperturbed ionosphere.

Let's see in more detail what happens on each band.

VHF bands, unperturbed ionosphere

In VHF, polarity is determined mainly by Faraday rotation, which is much bigger than spatial offset.

Faraday rotation is obtained multiplying a frequency dependent coefficient, the geomagnetic field component in the wave's direction, and the ionosphere's electron content encountered. In order of importance, parameters influencing Faraday, for an unperturbed ionosphere, are:

-- the angle between the Geomagnetic field and Moon's direction which can vary from very small values to almost 90°

-- the obliquity coefficient which measures the increase of length of the passage through the ionosphere, function of moon's elevation

-- the electron density of the ionosphere

VHF bands, turbulent ionosphere

Superimposed on the average evolution of Faraday rotation during a Moon pass, there can be a more quick fluctuation due to the effect of ionospheric winds.

Winds cause undulations and waves (TIDs), so free electron density varies in space and time, causing rotation fluctuations.

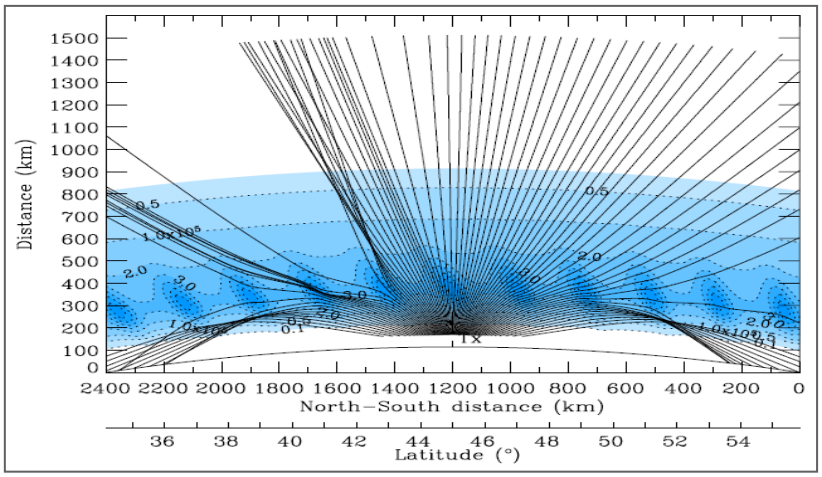

Australian scientist of the University of Sydney, Cleo Loi, has made the very interesting discovery of plasma tubes in Earth's magnetosphere. These structures are important because they cause signal distortions that could affect trans-ionospheric communication.

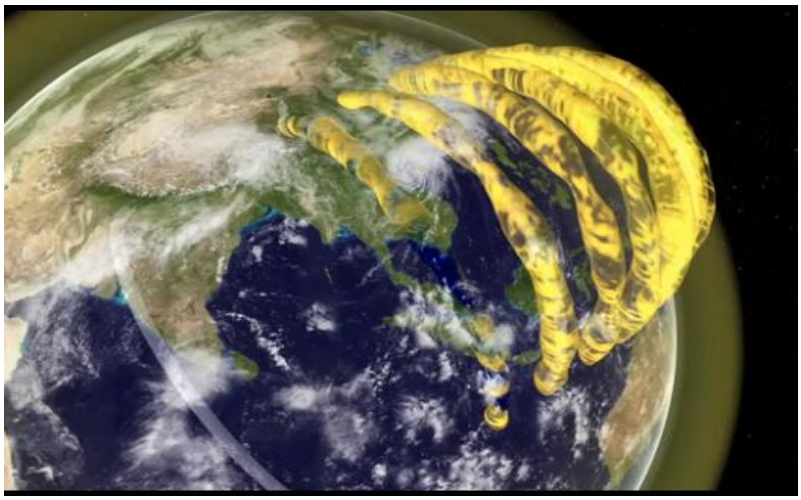

The complex plasma ducts are created in the atmosphere when this is ionized by sunlight. The plasma interacts with the earth's magnetic field, creating field-aligned ducts of plasma. These structures of plasma are at about 600 km above the Earth's surface, in the upper ionosphere.

50 MHz band

Typical sky noise temperature is 3600 °K (very high).

On this band Faraday rotates with high speed many thousands of degrees over a Moon pass. So there is a quick shift between horizontal and vertical polarization.

Spatial offset is absolutely irrelevant.

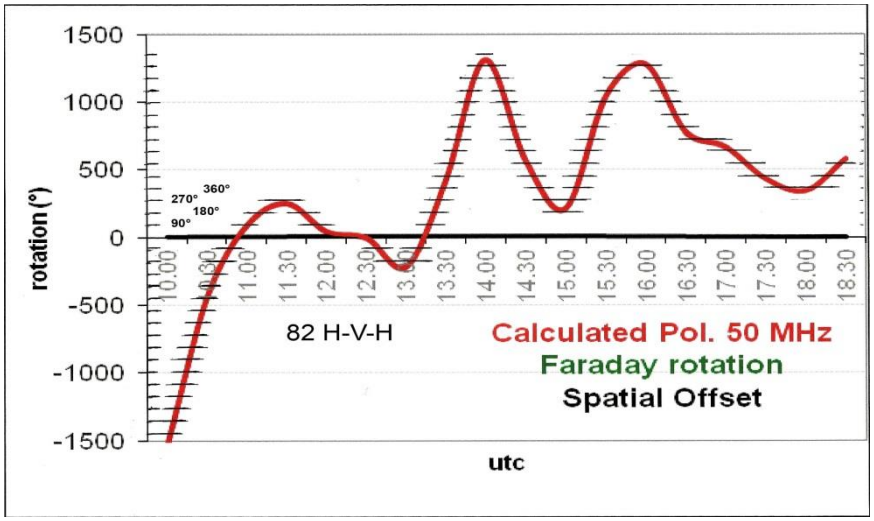

In this case, in the first 90 minutes rotation is 1800°, so the speed is 20°/1'.

This is just typical; we have found many cases with even higher rotation speeds.

Let's consider what this entails.

Effect of rotation speed on a JT65 qso

JT65 alternates 1' periods of transmission and reception.

We are considering a case in which the received signal, when polarity is optimum, is 3 dB above the minimum decoding limit.

3 dB is the attenuation when the polarity is +-60°.

So, during the time that polarity is between 60° and -60°, decodes are possible.

Beyond -60° through 90° until the successive 60°, there are no decodes.

Part of the favourable period is occupied by transmission, so the number of consecutive periods favourable for decodes decreases to half.

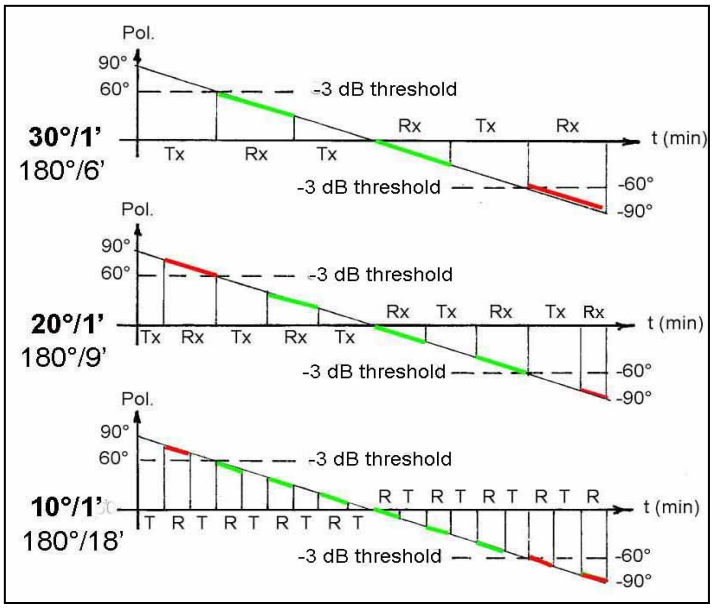

In this graph, we show the effect of rotation speed for three typical cases.

A JT65 qso takes 5-6 minutes overall if decodes happen consecutively, rare case.

On this band, this condition is very rare, so a qso can take a much longer time.

144 MHz band

Typical sky noise temperature is 300 °K (moderate).

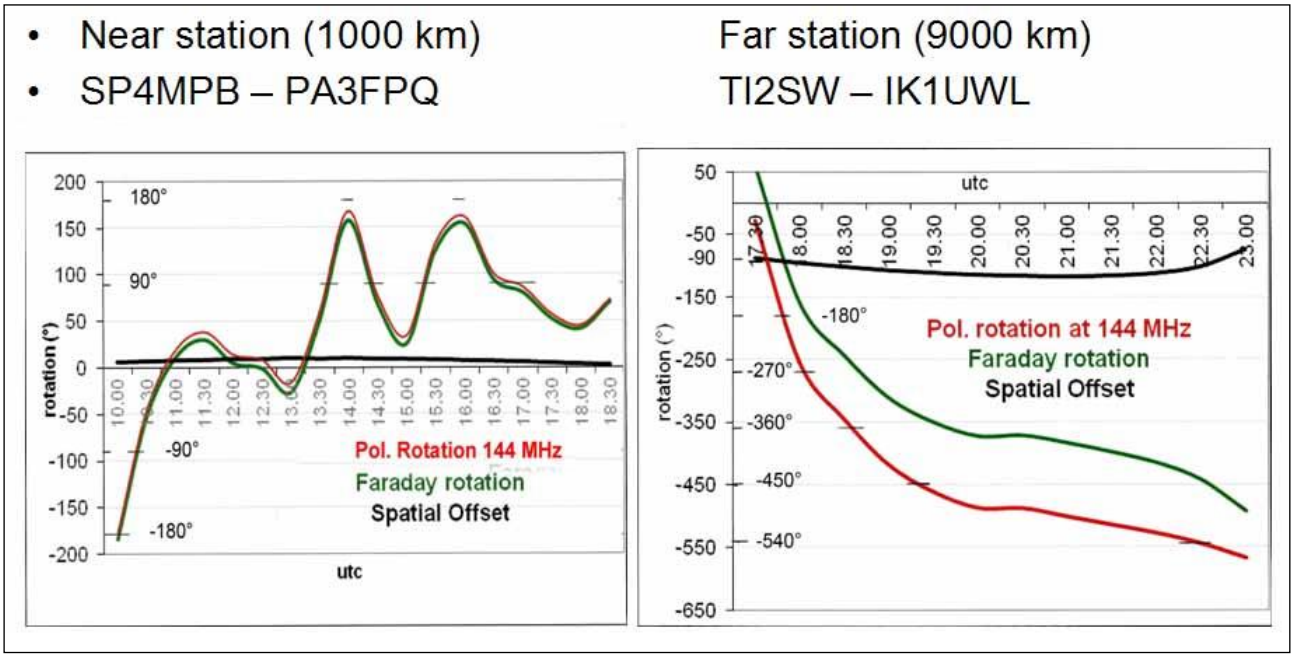

On this band there are typically <u>overall rotations of hundreds of degrees</u>, so spatial offset can influence the time when polarity is favourable, but is overridden by Faraday, both for near and for distant stations.

Speed of rotation change is much lower, of the order of 90°/30', so during a Moon pass, there are tens of favourable periods followed by tens of unfavourable periods.

On this band cross yagis are usable, and this is a coomon trend to overcome Faraday.

UHF bands

In the UHF bands the dominant factor becomes spatial offset, which can reach and pass half turn, in which case the supplement counts since phase does not count.

Therefore, distance between stations has the biggest influence.

432 MHz band

Typical sky noise temperature is 85 °K (low).

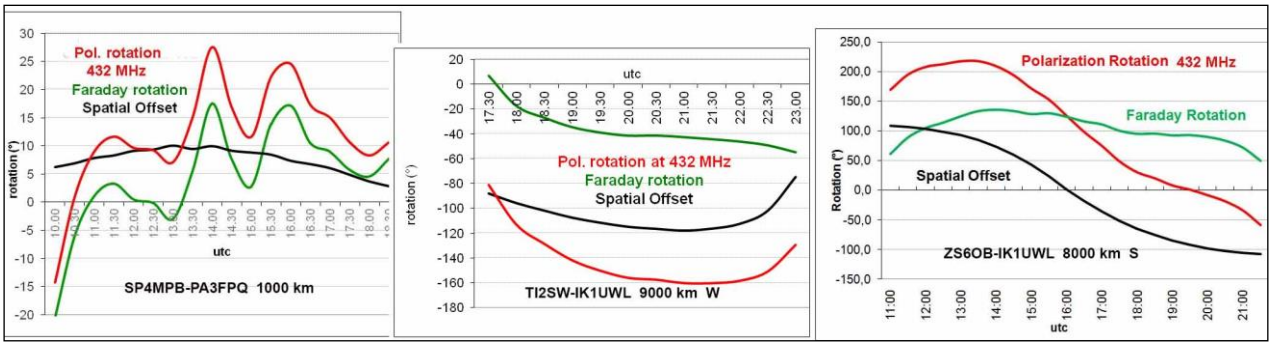

Here <u>Faraday rotation is of the order of tens of degrees</u>, often smaller than spatial offset.

For distant stations, the length of unfavourable periods is big, so it would be very useful having some way to control rx polarization, such as crossed yagis (not easy to build).

V-H-V transitions are few and far apart..

Cross pol. or circular pol. Is possible when moving to parabolic dishes. This is the obvious trend on this band, when sizable dishes are possible.

1296 MHz band

Typical sky noise temperature is 68 °K (very low).

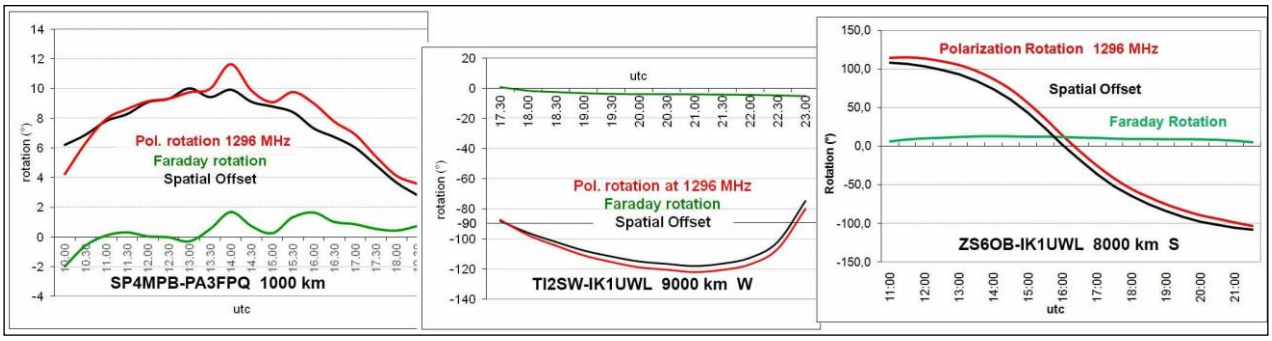

On this band Faraday is practically non existent, so spatial offset becomes the dominant factor.

Fortunately, on this band dishes predominate on yagis, and so circular pol., which is the best solution for these problems, is achievable.

VHF/UHF bands overview

VHF bands are dominated by Faraday, UHF bands are dominated by Spatial Offset

Going from 6 m to 23 cm, polarity changes with decreasing speed.

From peaks of the order of 1200°/h on 6m (because of Faraday), we tend towards 10°-20°/h on 23 cm (due to Spatial Offset).

So when single polarity of the receiving antenna is in use, favorable and unfavorable periods increase in length and decrease in number.

Our Excel sheet has allowed us to get some numbers and orders of magnitude of characteristics, known in practice, of these bands.

References

- Aspects of Weather and Space Weather in the Earth's Upper Atmosphere: The Role of Internal Atmospheric Waves by Michael C. Kelly.

- INGV istituto nazionale di Geofisica e Vulcanologia.

-Total Electron Content Studies of the Ionosphere John A. Klobuchar, Air Force Cambridge Research - Laboratories L. G. Hanscom Field, Massachusetts.

- The Potential of Broadband L-Band SAR Systems for Small Scale Ionospheric TEC Mapping (Remote Sensing Technology Institute, German Aerospace Center (DLR) Oberpfaffenhofen, D – 82234 Wessling, Germany)

- Institute of Communication and Navigation, German Aerospace Center

- Geomagnetism Tutorial Whitham D. Reeve Reeve Observatory Anchorage, Alaska USA

- Frederick University, 7 Y. Frederickou St., Palouriotisa, Nicosia 1036, Cyprus

- Electron density measurements of the plasmasphere – experimental observations and modelling studies

- Cooperative Research Centre for Satellite Systems Department of Physics, La Trobe University Bundoora, Australia

- Propagation Factors in Space Communications (NATO)

- Seasonal variations of storm-time TEC at European middle latitudes Royal Meteorological Institute (RMI), Belgium

- Radio Wave Propagation by Lucien Boithias, published by North Oxford Academic

- Cleo Loi, Australian astrophysicist graduate at the University Of Sydney School Of Physics.

- CAASTRO , ARC Centre of Excellence for All-sky Astrophysics- Australia

-Science Foundation for Physics - The University of Sydney

-The Murchinson widefield Array

-Density duct formation in the wake of a travelling ionospheric disturbance: Murchison Widefield Array observations (Journal of Geophysical Research)

G4DDK - An investigation into EME LNA safe operating levels

Sam Jewell (e-mail: jewell@btinternet.com)

A great deal has been written about the possible safe maximum input operating levels for very low noise preamplifiers. Some informed people have recommended that power should be left on the preamp during transmit, whilst others believe this may be a problem due to overdrive and turn the supply power off during transmit. Exactly how much signal input can be sustained without damage doesn't seem to have been extensively investigated, possibly due to the expense of testing many active devices to their inevitable destruction.

There is also a grey area where preamplifiers may still continue to operate, but with degraded performance. It has been widely reported that some preamplifiers have exhibited degraded noise figure whilst continuing to have normal gain.

In this paper I explore failure levels in the popular VLNA23 EME preamplifier and try to reproduce the degraded noise figure phenomenon. The results are likely to be applicable to other preamplifiers using similar active devices in the front end.

The very low noise amplifier (VLNA) for 23cm was introduced during the Weinheim VHF meeting in 2006. It is based on a modified design format by Tommy Henderson, WA5AGO (with his permission). It features self supporting input matching components in order to minimise losses in the high electron mobility transistor (HEMT) input. Any losses in the matching circuit add directly to the device's inherent noise figure, increasing it by as much as several tenths of a dB, depending on the quality of the components used (Q and Equivalent Series Resistance or ESR). The arrangement and 'value' of the components used in the VLNA23 preamp for 23cm allows typically 0.25dB noise figure (17k) to be readily achieved. See fig for the simplified matching circuit.

Further work on the VLNA by RW3BP identified the Mitsubishi MGF4919 as a suitable device to improve the noise figure below that possible with the NEC NE32584 used the first version of the VLNA. Further, the use of extended source leads, in the form of wire loops, allowed the input match (return loss) to be increased from typically 3dB to better than 10dB and depending on adjustment etc, to better than 14dB. It should be stressed that the shape and steepness of the sides of the return loss response characteristic means that the value changes rapidly with adjustment and a good quality network analyser is required to achieve the best matching results. In a low noise preamplifier the match does NOT affect noise performance, but if a filter is placed ahead of the preamp a poor return loss can have drastic effects on filter passband frequency response. Measurement of noise figure is less uncertain with good preamplifier input match.

The resulting preamplifier, incorporating many of RW3BP's improvements, has been designated the VLNA23. Variants for 70, 13 and 9cm have also been developed. Only the VLNA23 has been used in the investigations cited in this paper. To date almost 2000 VLNAs have been produced. Approximately 80% of these have been VLNA23 kits and built modules, the rest being mainly for 70cm and 13cm with a few for 9cm.

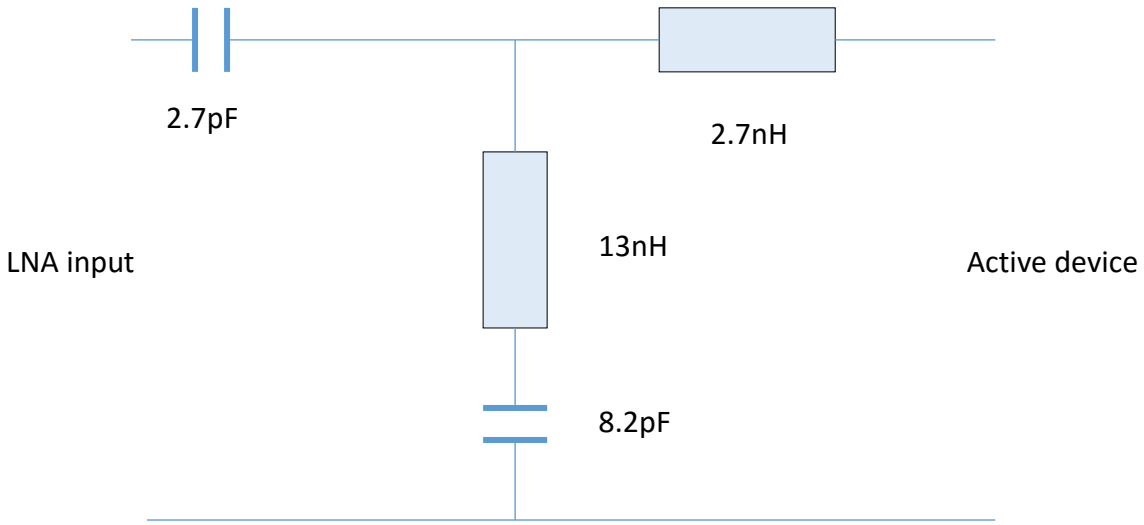

Fig 1 Input noise matching circuit for the VLNA23

Reported faults with the VLNA

Apart from the obvious failures due to RF overload (where the operator accidentally transmits directly into the preamplifier from either the RF input or the RF output) there have been several instances where the noise figure of the preamplifier has been seen to increase but the gain has remained normal. Note that I have deliberately said preamplifier and not VLNA as this failure has also been reported by a number of operators, and observed by myself, in at least two popular 144MHz P-HEMT equipped preamplifiers. Typically, the noise figure increases by up to a dB or so whilst the gain remains as originally measured. Some operators may be unaware of the existence of this problem at first as the system noise appears normal, but signal reports and sun noise measurements seem to indicate otherwise. Indeed there have been numerous requests on the various moon reflectors as to whether this condition is even possible, since it is so unusual. Yes it is!

LNA devices

In recent years there has been a revolution in the availability of low cost, very low noise, devices. This has been driven by the need to reduce satellite TV LNB noise figures (noise temperatures) to allow the use of small dish receive systems [a pity really as bigger TVRO dishes are great for EME]. In parallel with the need for lower noise figures there has been an increasing demand for high dynamic range devices for use in mobile radio systems such as GSM and UMTS.

Most early LNAs used bipolar transistors. These have been largely superseded by what we commonly call GaAs FETS or metal–semiconductor field-effect transistor (MESFET), such as the popular Mitsubishi MGF1302. More recently High electron mobility transistors (HEMT), also known as heterostructure FET (HFET) or modulation-doped FET (MODFET) have become the device technology of choice.

HEMTS are field-effect transistors incorporating a junction between two materials with different band gaps or heterojunction as the channel rather than a doped region.

HEMTs are now gradually giving way to an improved HEMT known as a Pseudo Morphic HEMT (P-HEMT) device and both of these device types are used in the VLNA and in the front end of

numerous other low noise preamplifiers. In the VLNA a HEMT is used in the first stage and a P-HEMT in the large signal second stage.

HEMT and P-HEMT reliability

Researching the reliability of these devices in learned research papers I found that little has been written on the noise figure degradation effect and almost all the research seems to have been focused on gain and power output (P1dB) degradation under various conditions of temperature and input level excesses. There is certainly room for a student to study this effect in more detail as a degree thesis.

I was left with the option of doing my own testing to try to reproduce the noise figure increase effect and if successful to find what was the cause. Going beyond noise figure degradation, the VLNA inevitably fails. At what level does this happen? I am neither a device physicist nor an academic so my testing here details my results but does not identify the cause of the actual phenomenon. In the conclusions, relying on a reliable source, I do speculate on the likely cause, however.

Test method

In order to ascertain what level of input signal can safely be applied to the VLNA it is not sufficient to test just a single example as this might give misleading results. A better method is to test a large number of VLNAs and record the levels at which complete failure occurs. If degradation of the noise figure, with normal gain, is observed this is noted. The results of the testing should ideally be consistent, but inevitably some spread in results will be seen. Of course testing to destruction is both wasteful and expensive, but there is no other convenient way to do the tests.

In these tests the same VLNA23 was used (Nr 1328) and after each test the input and second stage devices were changed to eliminate anomalies due to cumulative effects.

As there is some disagreement in the community as to whether preamplifiers are more robust powered up whilst transmitting, or should be powered down, both conditions were tested.

Since the failure mechanism is possibly related to thermal effects due to RF, the tests were conducted at 3 minute and then 1 hour intervals at each power level in the test.

Many tests were run and as some of these could last as much as eight hours, the whole testing session was run over a period of several weeks. A great deal of test data was generated. Only a few representative results tables are included in the paper. The tests are ongoing and it is expected that some further results will be presented at the Conference.

A Marconi Instruments 2024 signal generator was used as the test signal source. This was used with an MCL ZHL series broadband amplifier to generate sufficient signal to drive the amplifier under test. A 10dB attenuator was used between the generator and the ZHL amplifier. The output of the VLNA under test was connected to either an HP8592L spectrum analyser to measure level or HP8970A noise figure meter when testing for noise figure, with an HP346A (5dB ENR) noise head then substituted at the VLNA input.

The reason for using the amplifier was to generate sufficient signal power to ensure that the amplifier was driven into an area of operation where the effect should be observed - and beyond. A very short lead was used to connect the broadband amplifier to the preamplifier under test to ensure minimal mismatch loss on the connecting lead as the preamplifier input

match, although good, is far from a perfect resistive 50R. On 'reflection' an isolator should have been better at the preamplifier input.

Fig 2 shows the test set up. After each test and device replacement the preamplifier was re-aligned for noise figure, gain and input match. Although there was some small variation in the actual measured noise figure, gain and input match each time, best effort was made to make these as similar as possible. Changes of less that 0.05dB in NF and changes of more than approximately1dB in gain were ignored. Input return loss was adjusted to better than 10dB in each case.

The test signal at 1296MHz was gradually increased in small power increments, starting from the widely accepted 'safe level' of 0dBm. This signal was injected into the VLNA23 input and the output terminated in a good quality 50R SMA termination. The VLNA23 was either powered up or left unpowered, depending on the test in progress.

After leaving the preamp to 'soak' at each power level for a set time, the noise figure and gain (not match) were re-measured. If there was no noticeable change in performance the test was repeated at the next higher power level. This continued until either the 'wanted' increase in noise figure was observed or the preamplifier showed complete failure.

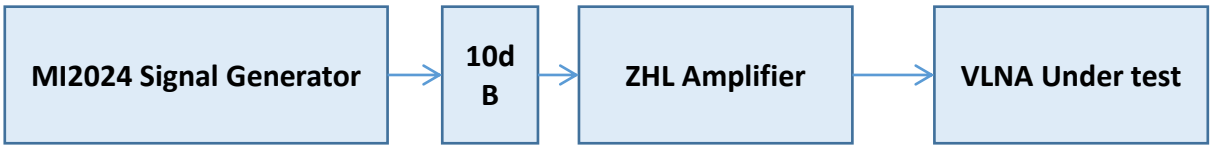

Figure 2. Test Setup

Results

The following shows the initial VLNA23 test measurements before the series of tests were begun.

VLNA23 Nr 1328

Initial measurements:

Noise figure measured at 0.25dB, gain 37.5dB, Input return loss 10dB

Drain voltage Tr1 =1.15V, Tr2 =2.93V

The first series of tests involved increasing the power input by a small amount with VLNA23 power on, soak at that level for 3 minutes, then remeasure, and note noise figure and gain. The noise figure and gain numbers are those measured after the soak period at the power level in the top row of the table.

Input level (dBm)	+4	+10	+13	+14	+15	+16	+17	+18	+19	+20	+21	+22	+23	+24
Noise figure (dBm)	0.27	0.28	0.31	0.32	0.33	0.33	0.33	0.32	0.33	0.38	0.39	0.38	0.41	Failed
Gain (dB)	38.3	38.4	38.6	38.6	38.6	38.6	38.6	38.6	38.2	38.5	38.5	38.4	38.5	

Table 1. Power on and input level gradually increase. Soak for 3 minutes at each power level.

Input level (dBm)	0	+7	+10	+13	+15	+17	+20
Noise figure (dB)	0.28	0.28	0.28	0.28	0.29	0.58	Failed
Gain (dB)	38.0	38.1	38.2	38.2	38.1	38.0	

Table 2. Power on and input increased in slightly larger increments. Soak for 3 minutes. Note the noise figure degradation at the +17dBm measurement level.

Input level (dBm)	0	+5	+10	+17	+20
Noise Figure (dB)	0.27	0.26	0.27	0.68	Failed
Gain (dB)	37.9	37.5	37.8	37.5	

Table 3 Power on and again a noise figure degradation was seen. Soaked for 3 minutes at each power level.

To investigate if the length of time of abusive power affected the results another series of tests, still with power on, was conducted with a soak time of 1 hour at each level.

Input level (dBm)	0	+6	+10	+13	+15	+17	+20
Noise figure (dB)	0.31	0.31	0.32	0.32	No measurement	0.32	Failed
Gain (dBm)	37.6	37.6	37.5	37.4		37.4	

Table 4. Power on. Soak for 1 hour each level

The test was then repeated with power off.

Input level (dBm)	0	+10	+13	+15	+17	+20	+21
Noise figure (dB)	0.31	0.32	0.30	0.32	0.34	0.4	Failed
Gain (dBm)	38.4	38.6	38.2	38.0	37.8	37.8	

Table 5. Power off but soaked for 1 hour at each level.
Only a small degradation seen at +20dBm before complete failure at +21dBm input.

Input level (dBm)	0	+6	+10	+13	+15	+17	+20
Noise figure (dB)	0.31	0.32	0.32	0.32	no results	0.54	Failed
Gain (dBm)	37.6	37.6	37.4	37.4		37.4	

Table 6. Power on and soaked for one hour at each level.
Noise figure degradation is again seen at the +17dBm input level.

The table below shows another test with power off and soaked for 1 hour. This time there was no apparent degradation before complete failure at +19dBm input level

Input level (dBm)	0	+7	+10	+13	+15	+17	+19
Noise figure (dB)	0.28	0.28	0.28	0.28	0.30	0.28	Failed
Gain (dBm)	38.4	38.4	38.4	38.4	38.3	38.25	

Table 7. Power off. Soaked for one hour at each level.

Conclusions

The results show some quite large anomalies due probably to the measurements having been taken over a period of some weeks. However they do show that the degraded noise figure effect is seen in a reasonable proportion of the tests and occurs between about +15 and +20dBm input level. Beyond +20dBm the preamp tends to fail completely. The period of the test, up to 1 hour, makes little if any difference to the results. This seems to point to both degradation and failure happening quite quickly when the preamp is abused by too much RF input and is consistent with relay contact effects.

There are a number of key conclusions:

Complete failure of the input stage was most common. Degradation in noise figure was less common. The four examples included in the above tables were the only ones seen in around 20 tests (~20%)

The VLNA23 is able to sustain a much higher input level, without damage, than expected. A level up to +15dBm was repeatedly obtained without apparent damage for soak durations of up to 1 hour both for power on and power off.

The MGF4919 generally didn't fail completely until the input level exceeded+20dBm, power on or off. No failures of the second stage (ATF54143) were experienced.

4. Although not part of these tests, the same degradation effect has been noted in several ATF53189 equipped preamplifiers. The ATF53189 is an Avago E-pHEMT device, so the effect doe not seem to be limited to conventional HEMT technology.

Recommendations

Although the VLNA23 is clearly able to stand more power input, without damage, than is usually accepted it is still a good idea to limit maximum input to 0dBm to give a good margin of protection.

Sequencer delay should be at least 100ms to allow relay contact bounce to cease. Older relays may require increased delay as the weakened contacts may bounce for longer.

Very high power systems might need two protection relays in tandem!

DJ5HG - On the Theoretical and Practical Limits of Digital QSOs

Klaus von der Heide, (email: Klaus@v-d-Hei.de)

Introduction

A usual digital communication system consists of hardware and software. In order to reach maximum sensitivity, every hardware component must be carefully tuned to optimal power or lowest noise. This paper deals with the part of the system which is implemented in software on the PC. The theoretical lower bound of digital information transfer is analysed under the special constraints of radio amateur QSOs.

Weak-signal communication systems usually are evaluated by the relation of the required energy per information bit Eb to the noise power per Hz bandwidth N0 = kBT with the Boltzmann-constant kB and the equivalent noise-temperature T. In a spaceprobe, the value Eb/N0 determines the number of information bits that can be communicated with a limited battery. In an optimized BPSK-sytem, Eb/N0 is the SNR at the input of the decoder. On the other hand, radio amateurs use the SNR at the audio output of an SSB-transceiver, i.e. in a bandwidth of 2500 Hz. Unfortunately, digital modes with different periods cannot be compared directly in this case. The transformation between both scales is easily performed by

SNR = Eb/N0 + 10*log10(number_infobits / period / bandwidth)

Eb/N0 = SNR − 10*log10(number_infobits / period / bandwidth)

For the threshold sensitivity SNR=−24 dB of JT65 in bandwidth 2500 Hz we get

Eb/N0 = −24 − 10*log10(72 / 47.8 / 2500) = +8.2 dB

C.E.Shannon found by mathematical treatment [1] that confident communication only is possible if

Eb/N0 > ln(2) or in dB: Eb/N0 > 10*log10(ln(2)) = −1.6 dB

Applied to the usual EME-case of transmission of about 70 bits within about 50 seconds we get the minimum possible SNR in bandwidth 2500 Hz (for communication at 100% correct decode):

SNR > −1.6 + 10*log10(70 / 50 / 2500) = −34.1 dB.

Therefore, at least theoretically, a gain of 10 dB over JT65 could be possible.

In 1959 Shannon refined the lower bound of communication as a function of the number k of information bits encoded as transmitted blocks, and of the code rate r which is the relation of the number of information bits k in a block and the number of resulting bits n of the transmitted block, and finally of the required block error rate PW [2]. This lower bound is called the sphere-packing lower bound.

Figure 1 shows the sphere-packing bound (for r = 0) over the number of information bits encoded in blocks, and the Eb/N0 at which interplanetary communication systems reach the low block error rate PW = 10-4 [3]. Figure 1a adds the sphere-packing bound for lower code rates, and the Plotkin-bound [4].

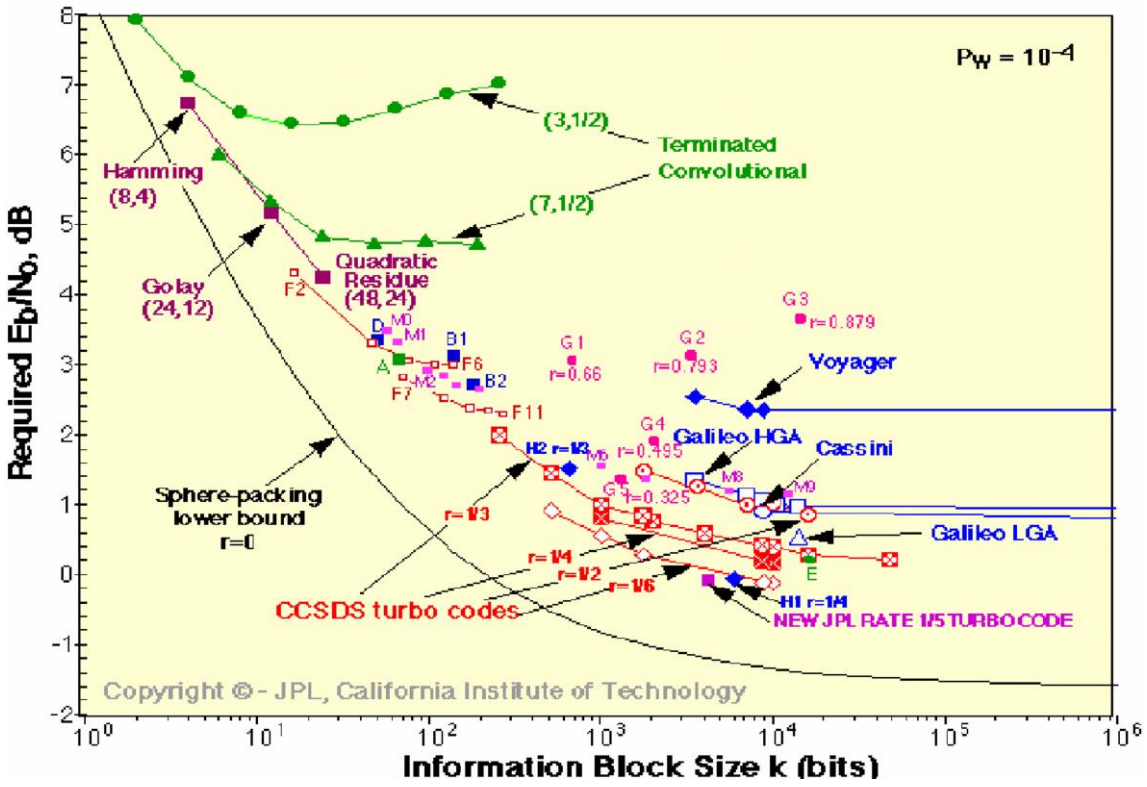

Figure 1. Evaluation of some codes and spacecrafts by the JPL for the block error rate PW=10-4 .

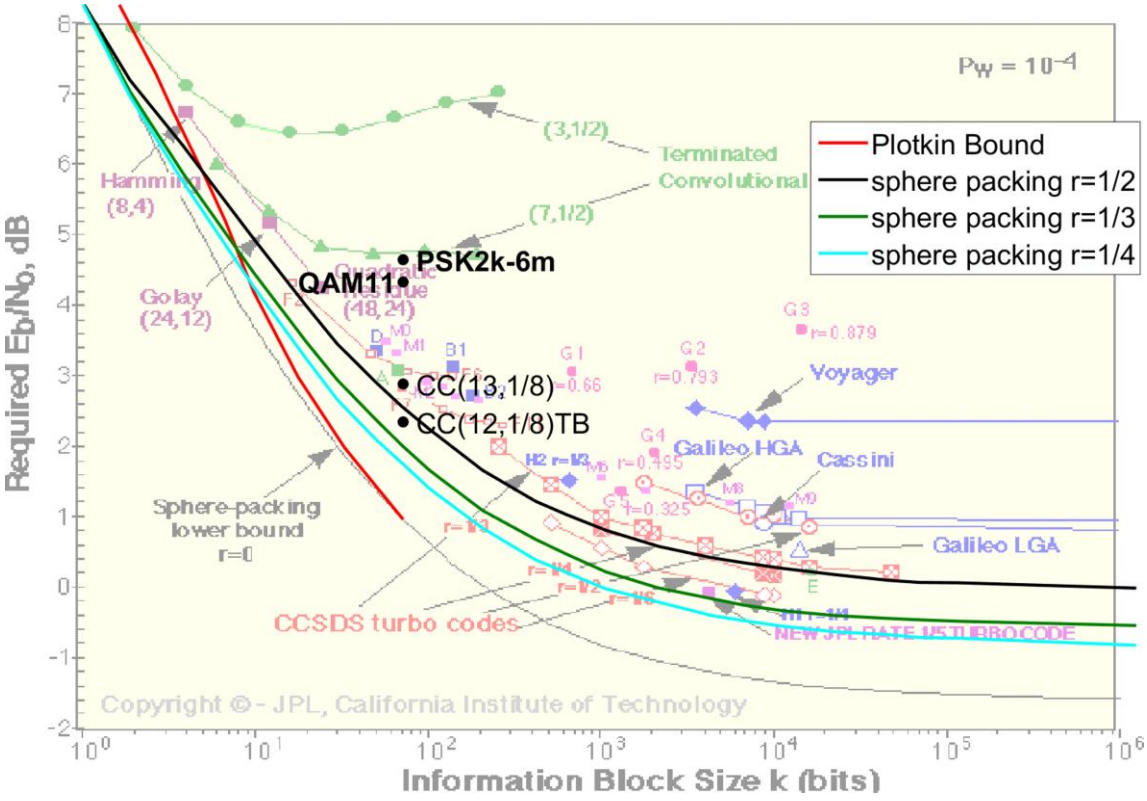

Figure 1a. This figure adds to Figure 1: the sphere-packing bound for r = 1/2, 1/3, and 1/4 [6], and the Plotkin bound (for any r). There is obviously some distance between the interplanetary communication and the sphere-packing bound for r = 0, but they nearly reach the limits set by the lower code rates. Also added are two codes found by the author and used in PSK2k and in the experimental mode QAM11. The required Eb/N0 of the modes PSK2k and QAM11 are considerably worse compared the the codes. This is caused by the necessary synchronization and phase-recovery (see Chapter 4 of this paper).

In contrast to commercial and scientific communication, we are interested to transmit small blocks of about k=60 bits of information, and we are happy if the rate of successful decodes is just PW=50%. So the question is: Where are our weak-signal systems in a diagram for PW=0.5? This is shown in Figure 2. The modes used by radio amateurs obviously are more or less far away from the theoretical limit. It is profitable to know the reasons, because the goal of a design of a weak-signal mode should be to approach the limit. We will now discuss the main three topics.

Codes for the Radio-Amateur Weak-Signal Modes

Figure 2 shows a gap in the required Eb/N0 of 6 dB between uncoded transmission and lower bound for optimally encoded transmission at the typical number k = 60 of information bits in a weak-signal QSO. A good code should approach the lower bound as near as possible, and decoding on a usual PC must be possible in about a second or less, but it's gain cannot be larger than 6 dB.

Convolutional Codes (CC) are a large class with selectable code rate r = 1/2, 1/3, ... , 1/16, and smaller. The distance between the lower bounds for codes with r = 1/2 and those with r = 0 is 1.6 dB at k = 60 . We therefore should choose a code with low rate (r = 1/8 ... 1/16).

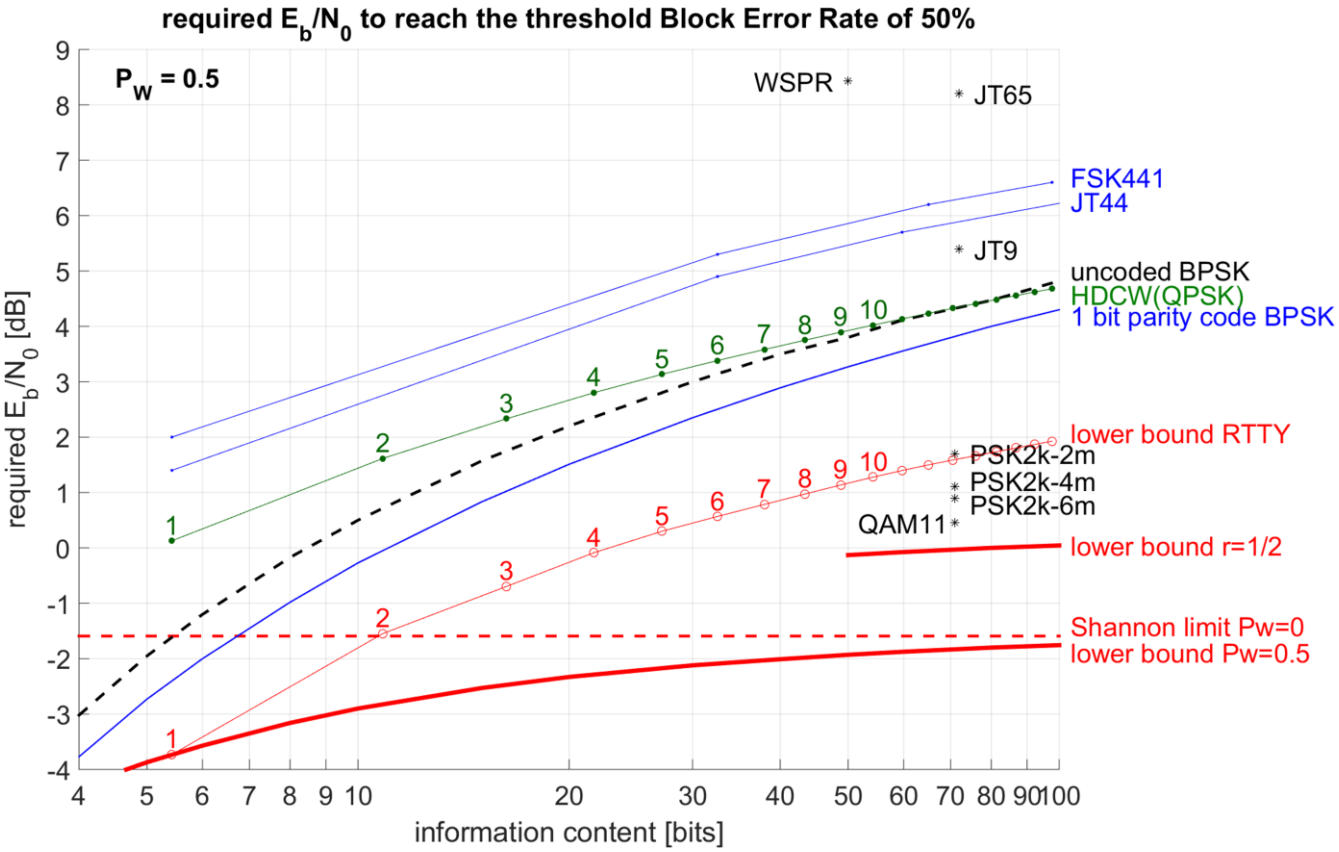

Figure 2. A diagram corresponding to Figure 1, but for PW = 0.5 looks quite different. The reason is that there is a considerable probability for receiving a correct block out of pure noise. Especially 1-bit-blocks are correct by 50% even if there is no signal. The horizontal scale of the diagram therefore is limited to the interesting region k = 4 ... 100. The green line named "lower bound RTTY" means an alphabet of 43 characters encoded by the optimal Hadamard43-code. JT44 and HDCW also belong to this class of character-oriented transmissions. The synchronization of single character-blocks causes a loss of about 3 dB (see Chapter 4).

A second parameter of convolutional codes is the so-called constraint length cl . Large constraint length makes the code better, but increasing cl by 1 nearly doubles the decoding time of the usual Viterbi-decoder. This limits cl to less than 16 or even lower. In addition, cl should not be larger than k/4. Otherwise the overhead of the long tail decreases the code performance.

A very effective method to increase the performance of convolutional codes is tail-biting. Given the constraint length cl (and r < 1/3), tailbiting makes the code much better if k is within the interval 4*cl ... 20*cl. Figures 3 and 4 show results of the author's simulations. The encoding of tail-ended and tail-biting convolutional codes is explained in the documentation of PSK2k [5]. The author decodes tail-biting blocks by applying the normal Viterbi-decoder to the concatenation of five times the received block enclosed by (1/r) * (cl – 1) zeros at the beginning and at the end. The result is an array of cl – 1 + 5*k bits. Bits cl+2*k ... cl+3*k–1 are taken as the k decoded information bits. This procedure surely could considerably be improved. The results presented here were obtained with this simple algorithm.

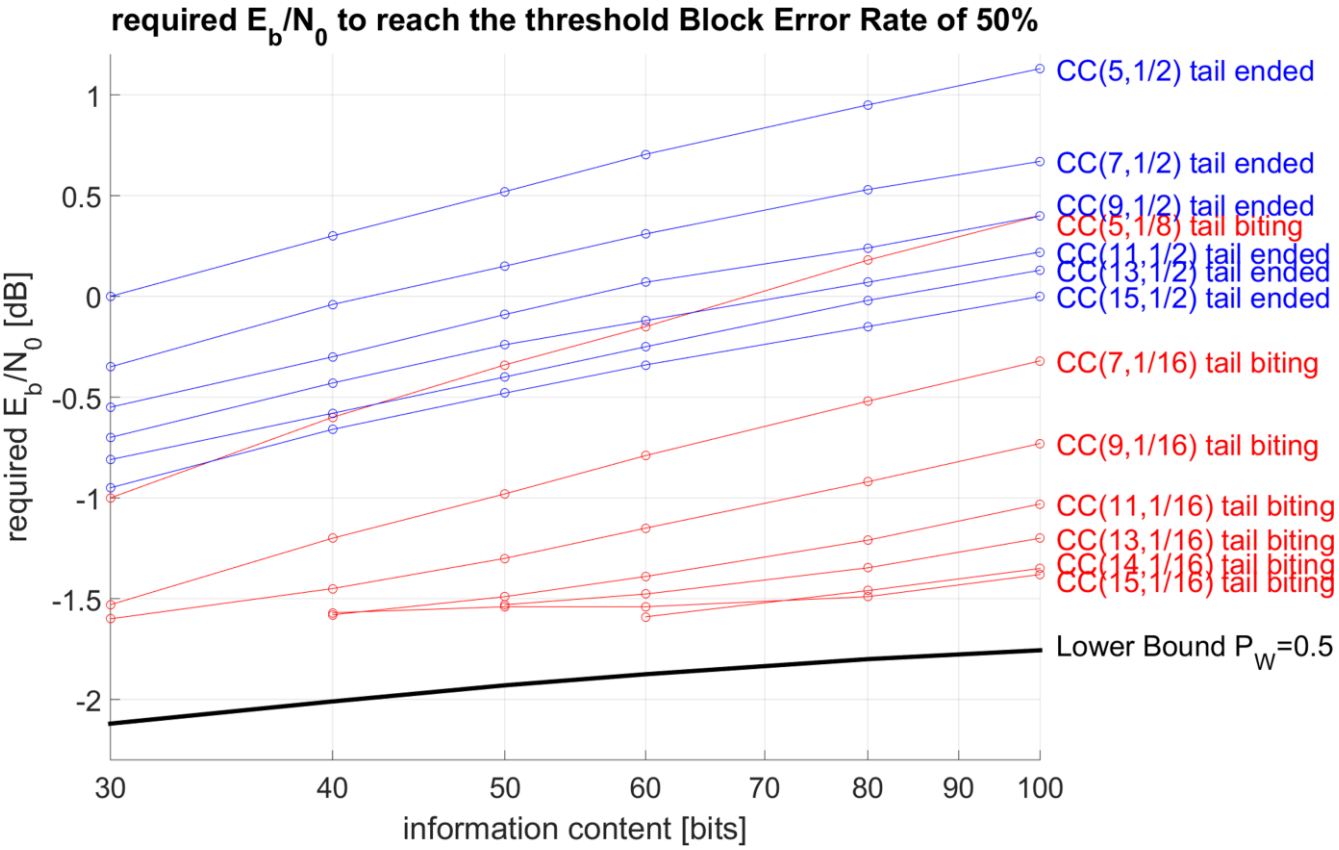

Figure 3. Required Eb/N0 to reach the threshold block error rate of 50% by selected convolutional codes. The codes are named by CC(cl, r). All codes are taken from the author's web page [7]. In the essential region of k = 60 ... 70, some codes approach the theoretical lower bound to less than 0.4 dB distance.

We can conclude from Figures 3 and 4 that the convolutional codes with r = 1/16 and cl = 12, 13, and 14 are very good codes for the case of weak-signal applications in amateur radio. If the application does not allow such low code rates we must accept a loss. In the case of PSK2k-2m, the SSB-bandwidth does not allow a Baud-rate larger than 2000. This limits the number of bits of the codeword which can be sent within a short meteorscatter ping to about 250 including all additional pilote bits sent for synchronization and phase recovery. Therefore, the code rate cannot be lower than r = 1/2. This causes a loss of 1.6 dB. The 4m- and 6m-modes use r = 1/4 and r = 1/8 with a much lower loss. 1/3 of the transmitted bits are pilote

bits. This overhead causes an additional loss of 10*log10(3/2) = 1.8 dB. The sensitivity of PSK2k-2m therefore should be

Eb/N0 of the CC(13,1/2) at k = 71 taken from Figure 3: −0.1 dB

loss by adding the pilote (1 pilote bit per 2 codeword bits): 1.8 dB

the sum is the theoretical Eb/N0 of PSK2k-2m: 1.7 dB

in scale with bandwidth 2500 Hz: SNR = 1.7 + 10*log10(71 / 0.129 / 2500) = −4.9 dB

This fits well to the experiments [8] with the existing PSK2k-receiver where −6 dB and −4 dB resulted in block error rates 90% and 0% resp. We can conclude this chapter 2 with the satisfactory message that there exist well usable codes for weak-signal applications which approach the theoretical lower bound better than 0.4 dB. The next chapter will show that this unfortunately only is true for PSK.

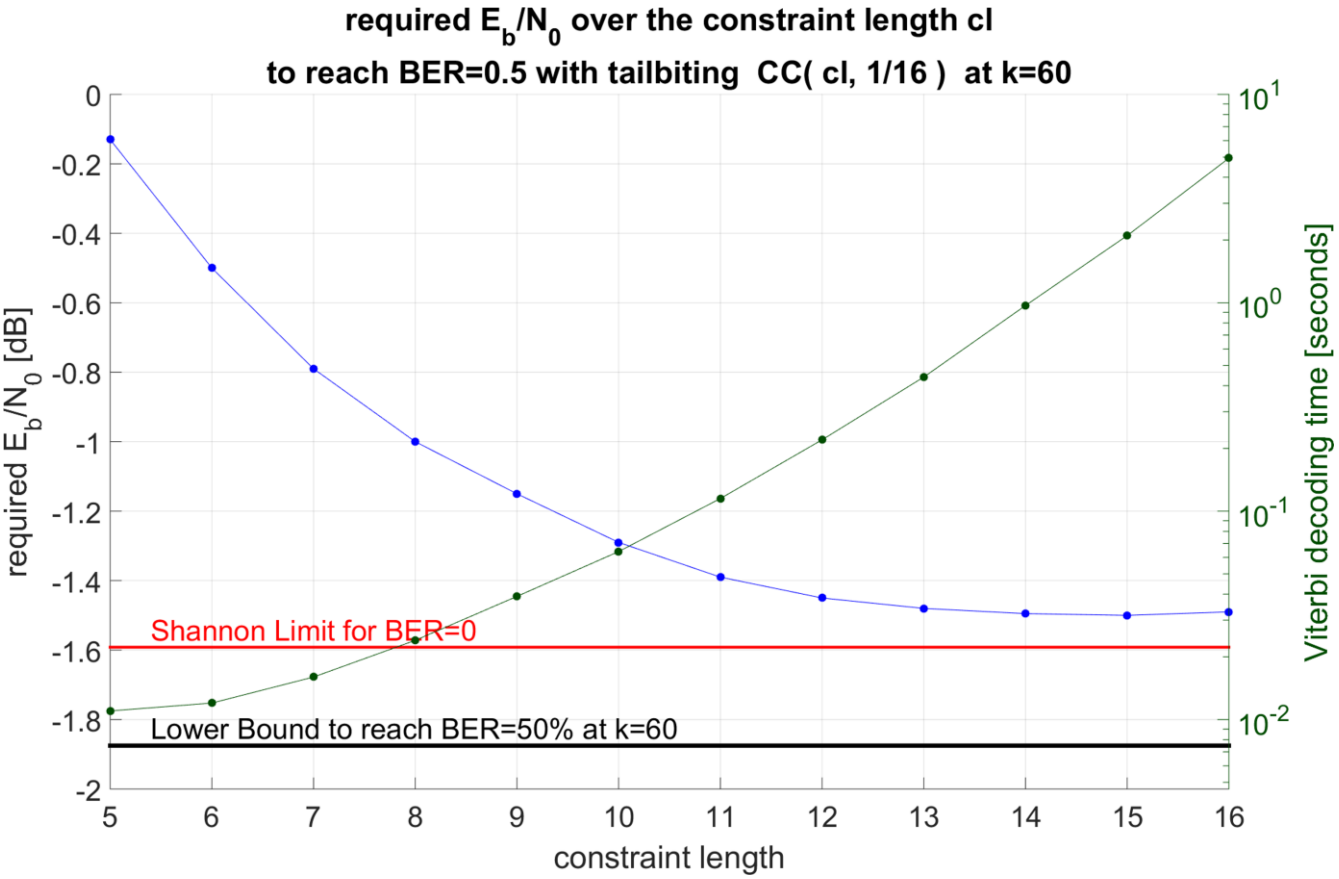

Figure 4. Required Eb/N0 to reach the threshold block error rate of 50% by convolutional codes with different constraint length cl and fixed r = 1/16 (blue line), and decoding time on a PC (green line). A useful code obviously is the tail-biting CC(13, 1/16).

Modulation and Demodulation

Figure 5 compares the bit error rates at very low signal levels for some modulation types. It is obvious that PSK is much better than all other types. The difference of the required Eb/N0 gets even larger with decreasing signal levels. At bit error rate 0.1, FSK and PSK differ by 6 dB (horizontal distance in Figure 5), at bit error rate 0.4, the difference already approaches 12 dB. Such large error rates (or corresponding small Eb/N0 values) are quite normal if low-rate codes are used. Let for example be r = 1/16, that means the number of transmitted bits is 16 times larger than the number k of information bits. If the codeword is received with Eb/N0 = −1.5 dB (the threshold sensitivity of CC(13,1/16)), then the energy per codeword bit is 12 dB less: −13.5 dB. We get the corresponding bit error rate of PSK from Figure 5. It is 0.38.

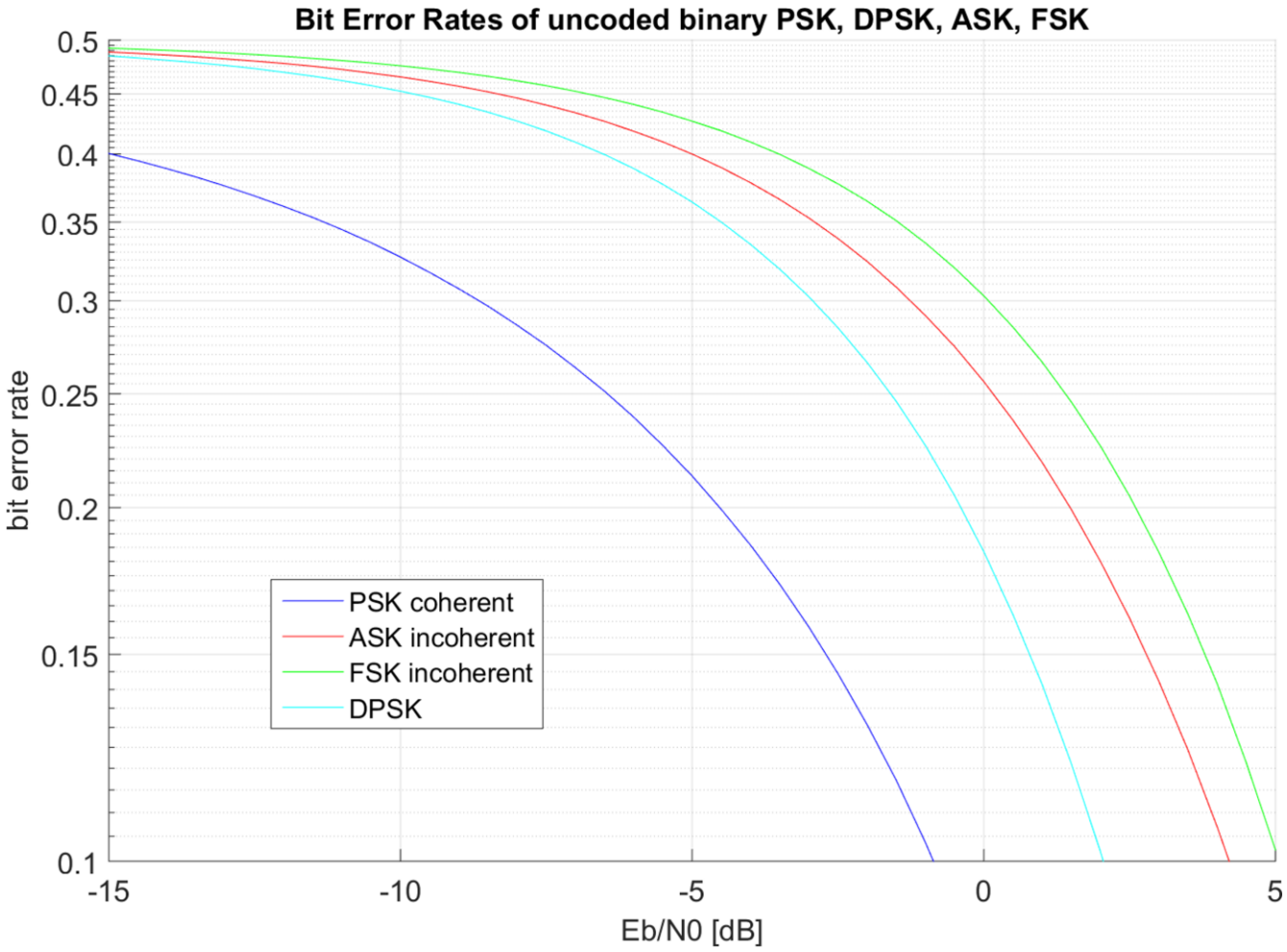

Figure 5. The bit error rates of modulation types differ very much at the same energy Eb/N0 in case of very low signal levels. The (horizontal) difference between PSK and FSK at the bit error rate 0.4 is nearly 12 dB, while it is 6 dB at the bit error rate 0.1.

The Eb/N0 to get the same bit error rate with FSK is 11 dB worse. I.e. if the same code is used combined with FSK instead of PSK, the transmitter must use more than 10 times the power needed by PSK. This shows that low-rate codes cannot be used conveniently with FSK.

A corresponding calculation with the higher-rate code CC(15,1/2) yields a difference of 6 dB between PSK and FSK. But if PSK with the low-rate code is compared to FSK with the high-rate code, then the difference is 8 dB.

ASK is about 1 dB more sensitive than FSK in the weak-signal area. It has the additional advantage of insensitivity to spreaded radio channels (FAI, aurora). On the other hand, there are the well known disadvantages of ASK, mainly the electromagnetic interference.

DPSK has nearly the same sensitivity as BPSK at large signal levels. It is even better than BPSK down to about Eb/N0 = 5 dB if phase recovery of BPSK has to be supported by an additional pilote.

m-FSK is a good choice for uncoded communication. Figure 6 shows the symbol error rates of m-FSK for different values of m. The error rates are considerably reduced for Eb/N0 > 2 dB at large m. But, following the argumentation of above, error correcting codes are nearly unusable.

An example for m-FSK is JT44. It uses a 43-FSK. A transmitted block consists of 22 symbols which are sent 3 times in sequence within 25 seconds. The 50% block error rate (all 22 symbols correct) is reached at the symbol error rate $1 - 0.5(1/22) = 0.031$. It follows from figure 6 that Eb/N0 = +3.3 dB yields this symbol error rate in a 43-FSK. The JT44-block contains 66 data symbols interleaved by 69 synchronization symbols.

The synchronization therefore causes a loss of 10*log10(135/66) = 3.1 dB. The transformation to SNR in 2500 Hz yields the 50%-threshold to get all 22 characters of the transmitted text fully correct:

SNR = 3.3 + 3.1 + 10*log10(22*log2(43) / 25 / 2500) = −20.8 dB

This theoretical lower bound fits well to the practical observation. It follows directly from Figure 2 that JT44 seems to be better than JT65. This is true only on non-fading channels, where JT44 needs only half the energy of JT65 to communicate an information bit. In contrast to PSK, coding cannot lead to considerable gain in sensitivity if FSK is used. But it does a good job in case of fading.

Our conclusion of this chapter is: BPSK is the only modulation for communication with very weak signals. In case of uncoded transmission, m-FSK may be a good alternative.

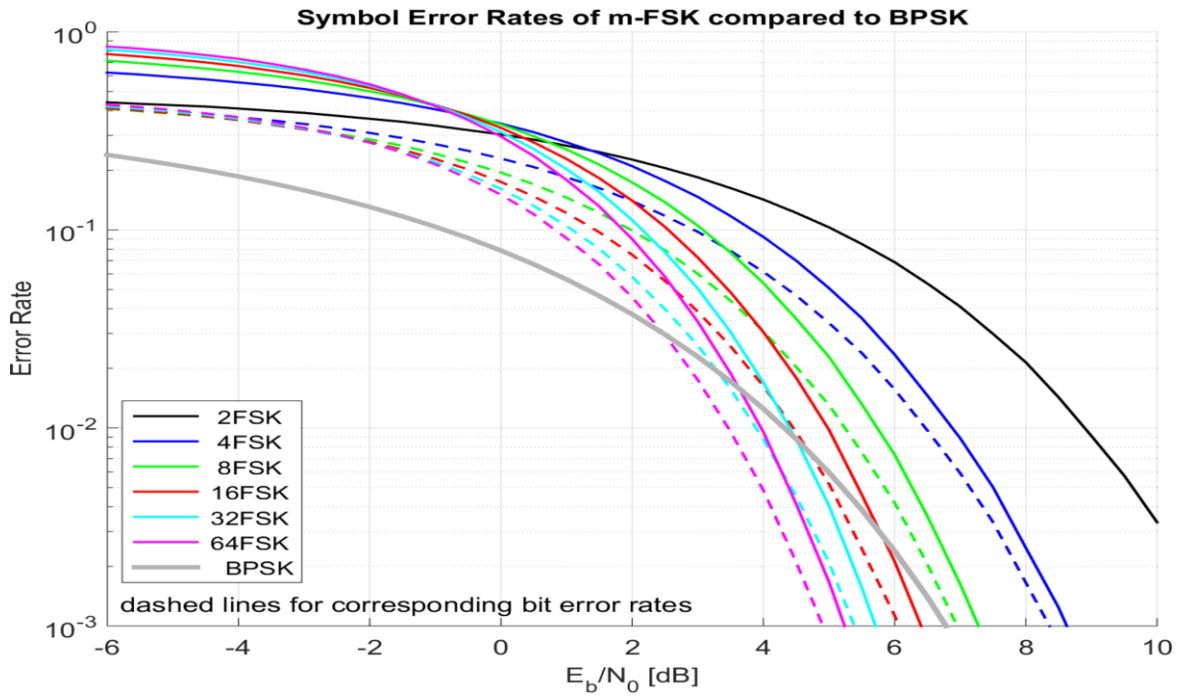

Figure 6. Symbol Error Rates of m-FSK and corresponding bit error rates (dashed lines)

Synchronization and Phase Recovery

If small blocks are used in a weak-signal communication, it is very difficult to find the block in time-domain and in frequency-domain. This problem is exhaustively discussed in [9], and the author made a contrution to it on the last EME-conference [10].

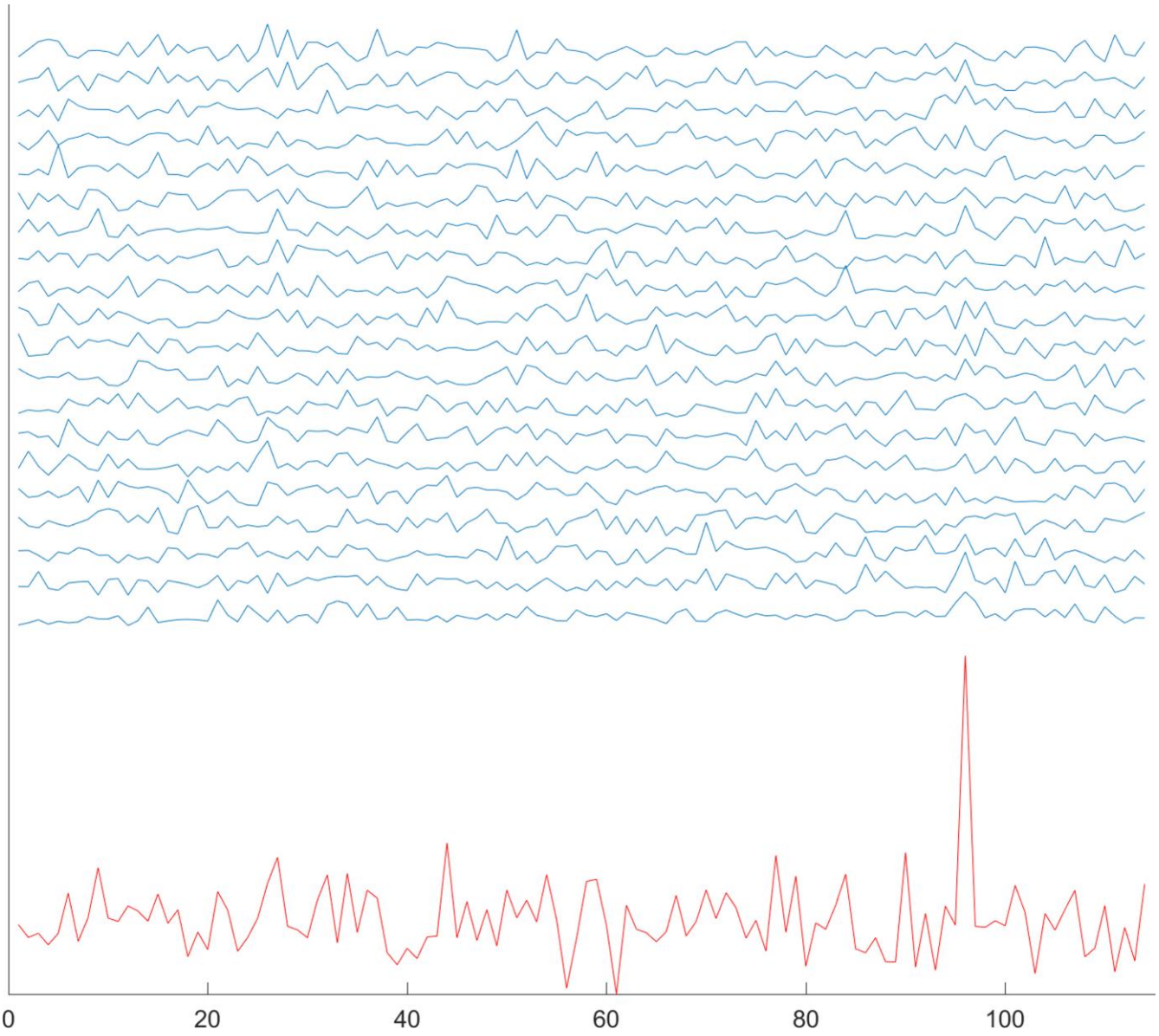

Figure 7. Example for the search of the pilote pattern of QAM11 (length 283 bits) at SNR = −29 dB and phase distortion of coherence length 5 s (corresponding to 28 bits). The pattern was divided into 20 overlapping segments of length 28. The complex input signal is filtered by all segments. The absolute-values of all 20 outputs are shown above. None of them has a significant indication of a hit, but the sum (the lower line) clearly has.

The search for a weak signal in frequency domain may be supported by a waterfall-diagram. But this does not work in case of PSK, and it fails completely for signals with SNR lower than about -28 dB in 2500 Hz bandwidth. Therefore the only solution is the exhaustive search on all parallel channels within a given bandwidth. The spacing of the channels is proportional to the Baud-rate. A high Baud-rate reduces the search in frequency domain. This fits well to the demand for low-rate codes. The search in time-domain can easily be realized by interleaving the data-bits with a fixed binary pattern of low autocorrelation. The author prefers Hadamard-codes. In order to profit from the sensitivity of coherent PSK, the pattern must be divided into

segments of length less than the coherence time. The correlation is performed with all segments and the results are absolutely added at correct delays. Figure 7 gives an example for the Hadamardcode of 283 bits and coherence length corresponding to 28 bits. The reverse pattern was divided into 20 overlapping segments of length 28 which where taken as the filter-coefficients of 20 filters. The figure shows the absolut-values of the individual filter outputs (already correctly shifted) and the sum of these outputs. The phases of the filteroutputs at the hit are good estimates of the carrierphase. A simple interpolation yields the development of the carrierphase over the whole length of the inputsignal. At this length of the pilote pattern, BPSK is 12 dB more sensitive than FSK, and the sensitivity even increases with longer patterns. The author uses this method of synchronization and phase-recovery in PSK2k with the interleaving sequence d1 p1 d2 d3 p2 d4 d5 p3 d6 d7 p4 d8 ... where di and pi denote data resp. pilote bits with index i.

The very simple experimental modes QAM11 and QAM66 use a tail-biting CC(12,1/8) to generate 568 data bits out of 71 information bits. The pilote also has 568 bits (see the appendix). But there is no interleaving of pilote and data. The data are modulated on the sinewave carrier (full amplitude), and the pilote bits are shifted by a halve bit and modulated on the cosinewave (halve amplitude). This Offset-QAM reduces the principal loss caused by sending the pilote to 10*log10 ((energy of data) / (energy of pilote and data)) = −1.0 dB.

The reduction of the power for the pilote leads to an increase of the rate of failure of the synchronization at very low signal levels. Nevertheless, this tradeoff between synchronization failure and decoding failure leads to a 50%-threshold-SNR of −32 dB in 2500 Hz bandwidth on the AWGN-channel (Eb/N0 = 0.46 dB). That is a gain of 8 dB compared to JT65. And it is about 2.5 dB above the corresponding sphere packing bound (see Figure 1a). If we subtract the known losses, 1 dB loss by the pilote transmission and 0.5 dB loss by the used code, the remaining distance from the theoretical lower bound only is 1 dB. It is caused by different reasons, synchronization failures for example.

On a fading channel, the phase must be recovered as a function of time over the whole receiving period. If the coherence time for example is 1 second then there are only 11 noisy pilote bits within this time segment to support the phase recovery. The recovered phase therefore may be very noisy which reduces the sensitivity considerably. Figure 8 shows the block error rates of QAM11 and QAM66 for different coherence times. The phase recovery for PSK or QAM generally fails if the coherence time is less than 1 / Baudrate.

FSK vs. PSK

As long as the phase recovery is successful, PSK and QAM are more sensitive than FSK. But if the phase distortion by the radio channel is too large, only FSK and ASK are usable. It is interesting to get a closer look to the transition region. Let the coherence time of phase distortion be 0.4 s. From Figure 8 we get a block error rate of 90% at -25 dB.

If the transmission period now is compressed to 1/6 (QAM66), and the power correspondingly increased by 7.8 dB, then QAM66 will run with a block error rate of only 6% at a 6 times larger bit rate, but with the same Eb/N0. The reason is the increase of sensitivity of PSK with lower (i.e. more stretched) phase distortion.

See Figure 8 for the dependency of sensitivity on the coherence time in case of QAM11/66.

Thus PSK sets a lower bound for the rate bits / (coherence time). In other words: if the coherence time is low, you have to use a high bitrate. To communicate the high bit rate on a weak radio channel you are forced to transmit with appropriate high power. The energy per bit remains the same as in Figure 1.

On the other hand, the transmitting power is limited for radio amateurs.

Therefore the demands for PSK cannot be satisfied in some cases. This especially concerns EME-contacts with strong libration fading on GHz-bands. If PSK does not work we must accept the general loss of other modulations plus the loss of coding gain which adds to at least 5 dB. This is not weak-signal communication, but bad-channel communication.

A further problem arises on channels with both, frequency-spreading and time-spreading. Time spreading leads to intersymbol interference (ISI), if the Baudrate is higher than 1 / (time spreading). PSK cannot be used on such over-spreaded channels. An example is aurora, but not EME.

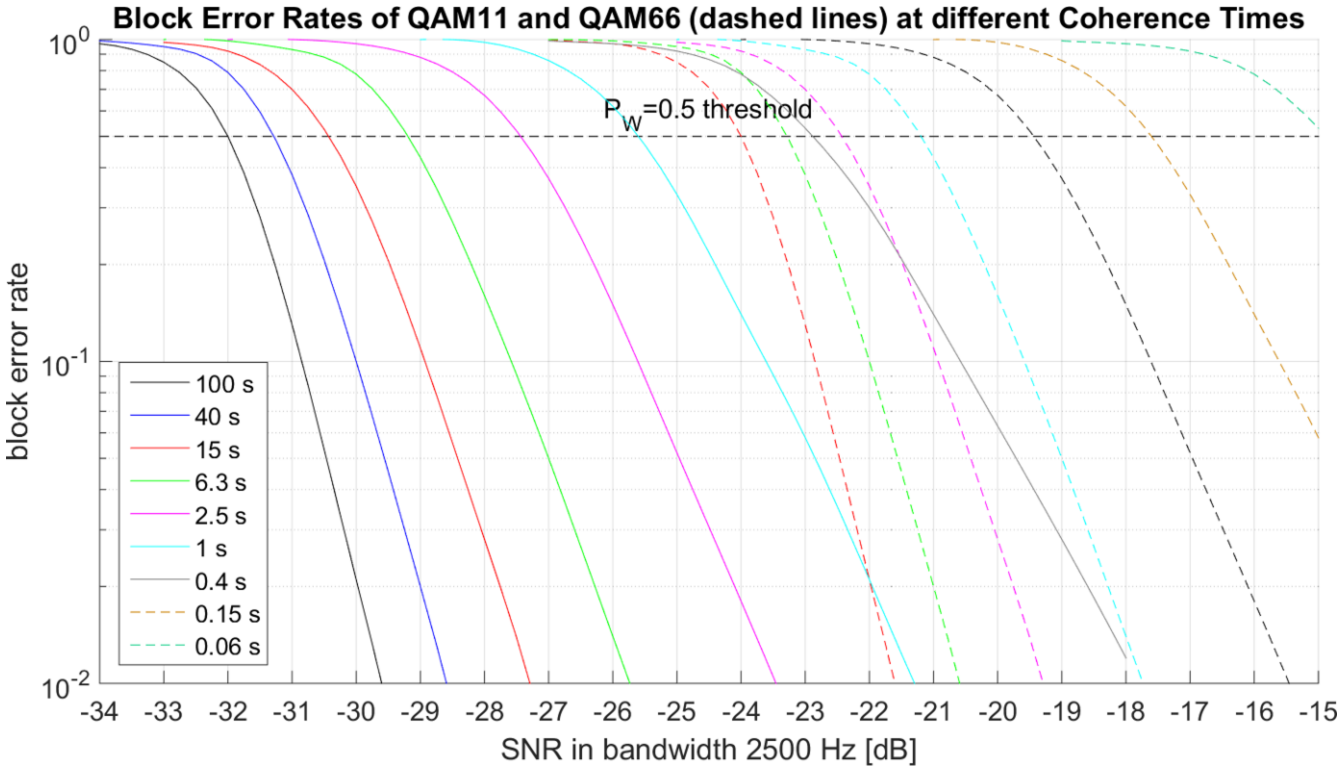

Figure 8. Block error rates of QAM11 and QAM66 for different coherence times.

References

[1] C.E. Shannon, A Mathematical Theory of Communication, The Bell System Technical Journal, Vol. 27, pp.379-423, 623-656, (1948)

[2] C.E. Shannon, Probability of Error for Optimal Codes in a Gaussian Channel, The Bell System Technical Journal, Vol. 38, pp. 611-656, (1959)

[3] original URL http://www331.jpl.nasa.gov/public/AllCodesVsSize.GIF

[4] M. Plotkin, Binary codes with specified minimum distance, IRE Transactions on Information Theory, 6:445-450, (1960)

[5] http://www.dj5hg.de/digitalmodes/psk2k_documentation.pdf (chapter 5)

[6] S. Dolinar, D. Divsalar, and F. Pollara, Code Performance as a Function of Block Size, TMO Progress Report 42-133, (1998)

[7] http://www.dj5hg.de/code/codes.html

[8] K. von der Heide, FSK441 vs. PSK2k by Simulation Experiments, DUBUS vol. 42/2, pp. 67-77, (2012)

[9] K. von der Heide, Modulation, Demodulation, and Block Localization for Digital Weak- Signal Modes, DUBUS vol.42/3, pp.63-75, (2013)

[10] K. von der Heide, A Coherent Digital Mode for EME, EME 2014 conference, pp. 129-134

Appendix: QAM11 (QAM66)

Source Code: 56 bits of information plus 15 check bits for final error detection (71 bits)

Channel Code: CC (12, 1/8) tail-biting and interleaved, results in 8*71 = 568 bits

Pilote Sequence: Hadamard-283 interleaved with the encoded receiver-address of 284 bits

Receiver Address: 54 address bits plus 17 check bits = 71 bits encoded with CC (12, 1/4) TB

Modulation: QAM, data on sine with amplitude 0.89, pilote on cosine with amplitude 0.45

Baud-rate: 8000 / 720 = 11.1111 (66.6666)

Total Bandwidth: 12 Hz (72 Hz)

Length of Transmission: 568.5 * 720 / 8000 = 51.165 s, period 60 s (8.5275 s no fixed period)

ZS6EME - Optimized EME reception with Linrad and WSJT under multi-polarization configuration

Alex Artieda (email: zs6eme@linkrf.ch)

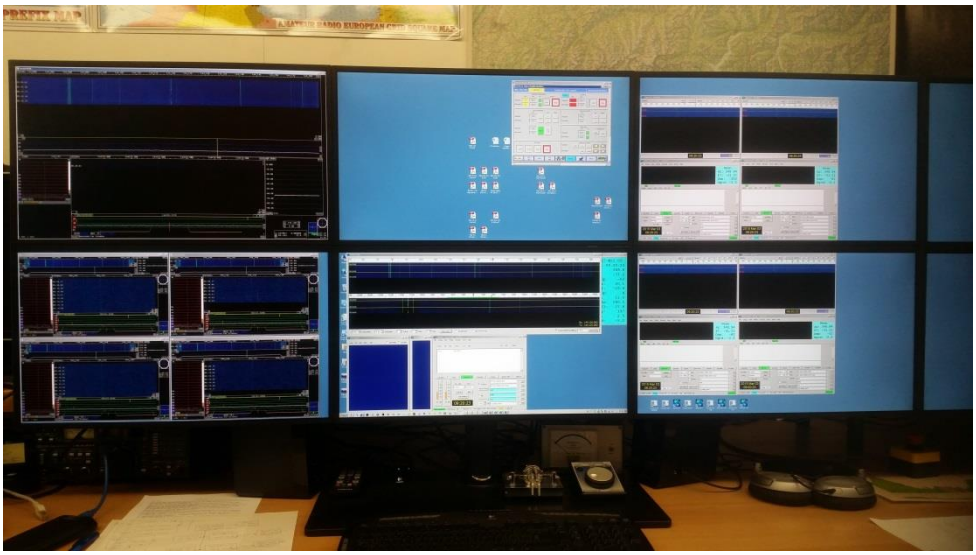

Fig1. HB9Q 144 Mhz Station with multipol. System

Introduction

EME operators are searching always the best RX performance in their systems. Since the advent of MAP65 many configurations was proposed to beat the infamous Faraday Rotation. My main contribution has been the design and production of more than 200 IQ + radios to exploit to the maximum the outstanding features on Linrad and MAP65, specially in 50, 144 and 432 MHz

This paper is not a trial of which software works better, it is simply a basis for setting up a multi polarization system that allows us to make appropriate comparisons and, maybe at the end, gain some extra performace.

However, a recurring comment within the EME community (most of the time not well documented) regarding the differences between MAP65 and WSJT has captured my attention in the last years and has motivated me to try to understand those differences in decoding (if exist) without marginalizing any specific software.

The system I propose is very similar to others but with some differences, is based on the "do" and "do nots" committed previously. The title of my presentation refers to WSJT; however a multi-polarization system based on Linrad is a powerful tool, not only for digital operators, has tremendous advantages for CW as we will see later

Because of erroneous observations (mainly a priori and without scientific basis) that WSJT decodes better than MAP65, this guide opens a door to a real analysis. A suitable SW and HW platform is needed (and properly configure) to make appropriate comparisons, simple observations are not enough. Then the data collected can be integrated, analyzed and conclusions can emerge, is a very long process, this is just the beginning.

Previous multi polarizations systems

Many systems were proposed in the last years but after a deep analysis I consider only two of them as serious systems.

The analog approach

Carsten DM1CG, use in DK0KK an "analog" approach to split the signal coming from the antennas in different phase angles.

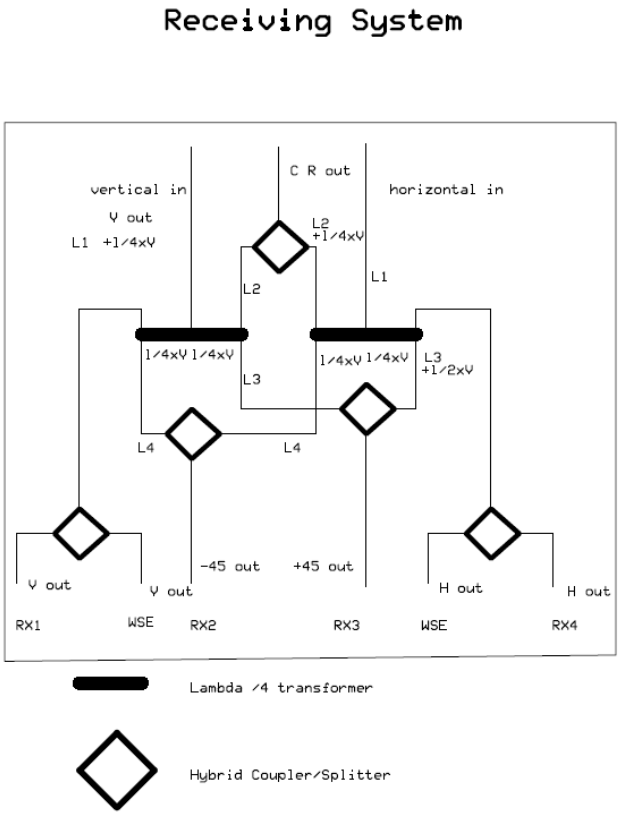

Fig2.DK0KK Analog phase splitter

This is a "state of the art" phase splitter/shifter based on passive analog parts like coax cables, splitters and hybrid couplers. That system demand a complex instrument (Vector Network Analyzer) to calibrate the phase shift on each port to reduce "at maximum" phase errors due improper implementation. This way to reach different phase on the signal works as great as the investment on dedication and precision during the setup but "add" the intrinsic problem than any analog part you add on the system has some tolerances (expressed in +/- decimal degrees) on the phase shift, same for the amplitude (in tenth of dB's). The sum of errors makes the system hard to be properly duplicated and calibrated but not impossible, never the less Carsten have the knowhow and the instruments and is well proved he did a good job.

The Digital approach

Roger W3SZ uses Linrad as an Input to digitize the analog baseband. The Linrad MASTER is in charge to open the audio A/D converter who is attached to a WSE 4ch receiver. Then he send the digital stream to 4 different Linrad SLAVES and MAP65, each slave receive the RAW data from the Linrad MASTER and later each Linrad SLAVE is set (just with the polarization control) to a different angle, H, V +45 and -45 (in practice you can open as much Linrad SLAVES you want and configure each to any desired angle with just one mouse click). Then the output of each Linrad SLAVE is send to a dedicate WSJT program, WSJT knows nothing about the polarization of the signal, is the Linrad SLAVE who will be fix at witch angle the operator wants

to receive, this make the digital approach very useful for CW operators because you can listen the audio on one single Linrad and rotate the polarization control with the mouse "on fly" until you have the strongest signal in your headset, no more complex mechanical systems to rotate antennas and feeds like in the past.

(About W3SZ setup: see http://www.nitehawk.com/w3sz/LinradMAP65.htm)

Linrad and WSJT under multi-polarization configuration

This is the system I propose based on the Digital approach of W3SZ:

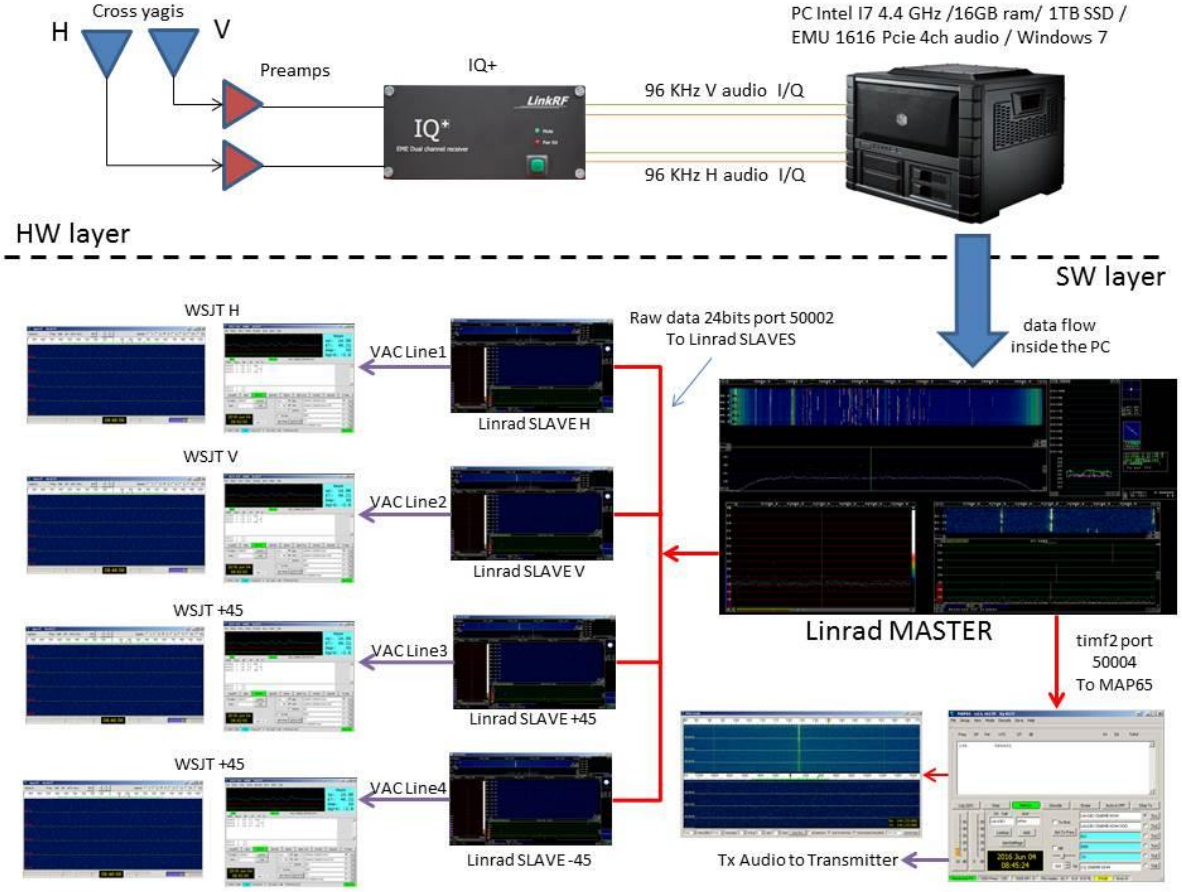

Fig3 Multi-polarization system with Linrad as a core

The multi-polarization system allows us to receive the same signal, coming from the same antenna during the same period of time and using the same analog Front-end hardware; that means the integrity of the data is guarantee and is presented at the same time, in the same way, to different software's. Many wrong configurations just tap the IF line and use two different receptors and/or computers with different A/D converters (audio cards), this could be ok when you compare radio HW but is not the properly way for compare two or more different software's in a fair way. I saw other wrong configurations were the signal after the preamps is just split with a simple BNC "T". We cannot trust in that configuration due the distortion on the phase integrity of the analog signal they introduce.

Special considerations

This is a complex system and not easy to implement and use. There are special conditions to be considered before embarking on the tedious but fruitful, adventure of set up similar system. It is not an impossible task but I will detail some points that should not be avoid/overlooked. Currently there are 4 similar systems installed in different parts of the world and its operators are more than satisfied with the results.

THE ANTENNA and FRONT-END

Is a must to have a dual polarization antenna, the configuration could be in "+" or "X", what is important is minimize the loss in the coax cables, use properly antenna combiners (same model and manufacture). The preamps need to have (if possible) the same gain and NF (matched pairs) and again same model and manufacture will help. Your radio need to be a "real" Dual channel radio for adaptive polarization, both receptors need to share the same local oscillator with a signal with the same phase and amplitude (this is a pre-condition for adaptive polarization). Today the IQ+ (with more than 200 units in service) is a good example, also the WSE converters and only few other digital SDR radios. The use of USB SDR dongles is not possible, at least on the way they are commercialized, if you are able to "lock" two SDR USB receptors with the same LO then you are in business, if not will not work.

THE COMPUTER

This is the core of your system, what I propose is use just on PC to run all programs at the same time. WSJT and MAP65 demanding huge amount of RAM and disk processing, same as Microprocessor capabilities. I test the system in different PC configurations and the minimum you must have is an I5 Intel processor with a clock speed of at least 3GHz, 8GB RAM and if possible a SSD disk instead of traditional mechanical disk. In that system all software runs together and you will not have overlap during decoding process (the las seconds of a RX period) with the upcoming TX period. Keep the old computers for internet browsing and emails. The top performance computer for this task is the similar we are using in HB9Q and in my QTH: I7 Intel processor 4Ghz clock, 16GB RAM and 4 Solid State Disk in RAID0 configuration. Regarding the disk: if your disk system is to slow the data processing will be delayed by the Disk controller and this will create a bottleneck increasing the demanding of the processor. I use RAID0 because this increase the read and write process in a dramatic way. When a mechanical normal disk have today a media of 150MB/s one single SSD will give you 500MB/s and 4 SSD in RAID0 give you up to 1,500MB/s, the escalation is not lineal BUT if you consider RAID0 disk configuration be aware if one disk fail you will loss the entire PC, a periodically backup with some software like Acronis is required to restore the PC in case of a disk failure, in a computer with that characteristics running 5 Linrad's, MAP65 and 4 WSJT plus browser and antenna controller will hit the processor no more than 60% for 2 or 3 seconds, the idle will be no more than 20%, enough performance.

MONITORS

Just one single monitor is not enough to run the system, a lot of information will be available on your screen and switching from one program to another in a single monitor is impossible. Today most of the PC's come with video cards capable to run 2 monitors simultaneously. Never the less after test the system in different location we found the absolute minimum numbers of displays in 2 (a little complicate), a minimum in 3, ideal is 4. HB9Q use 6 monitors per station, personal with 4 is enough. You will need a second graphic adapter, nothing fancy, just with multiport capability, ZS6JON is using a small USB video adapter (very cheap) with good results.

MORE THAN ONE PC

If you don't have an I5 or I7 computer with those characteristics you can off-load the work in two or 3 slow computers. Just consider the impact regarding space, duplicated mouse and keyboards, never the less will work. Linrad don't demand huge resources, you can keep Linrad MASTER and SLAVES in one PC and run MAP65 and WSJT in another one or even in two. Timing is very important; you must share the same internal network (preferred without network switches or hubs in between). A good NTP program to synchronize the clock is a must.

OPERATING SYSTEM

I test the configuration under Windows 7 / 8 / 10 but for sure you can run the system in a native Linux or OS, is just a matter of configuration, totally possible for sure.

CW ONLY OPERATORS

The system is much simple and will demand just one single PC with I3 processor or even less, if you are not interested in digital you don't need huge of PC power, just 1 Linrad properly configured and that's all, you will be able to beat the Faraday Rotation just with one click with your mouse but your Front-End must be based in dual polarization Antennas and receiver.

COMPILE YOUR OWN LINRAD

Linrad by default don't have implemented the option to follow the frequency selected in Linrad MASTER by the Linrad SLAVES, due the fact my system is very similar to Roger W3SZ he create a special files called ***extra_w3sz_hb9dri.c*** and ***users_w3sc_hb9dri.c ,***those files allow you to compile Linrad to allow all Linrad SLAVES are on the same frequency you select on Linrad MASTER and NOT in MAP65, later I will explain why.

LINRAD AND MAP65 CALIBRATION

Just installing the programs is not enough to reach top performance, you must do some calibration previous any collection of data and post analysis is done. The list is a must and cannot be avoided:

In Linrad MASTER calibrate IQ image rejection

In Linrad MASTER and SLAVES calibrate the Noise Blanker (Total amplitude and phase) with a pulse generator similar like Leif SM5BSZ propose in his page or like the SIGP-1 I design and produce in the past, (have a look in http://www.linkrf.ch/SIGen.html)

In MAP65 you don't need to calibrate Image rejection

In MAP65 don't use the Noise blanker, the Linrad NB is much better

In MAP65 calibrate the Dphi

PATIENCE, a lot of PATIENCE: The setup process is long and very complicate but when is done is done, never the less use the system demand some training, you will need to follow some concatenated process to start and stop the system, and errors in the start/stop will be translated not necessary in a non-working system but will produce completely wrong data, if this is combined with a poor PC performance the dissatisfaction is guaranteed.

HOW THE MULTI-POLARIZATION SYSTEM WORKS

Linrad MASTER is the core of your system, when you click in any frequency in Linrad MASTER and your Linrad's are compiled with the properly files the Linrad SLAVES will go, all together, to the same frequency, this allow your WSJT's are all in the same frequency. In Roger's W3SZ configuration the Linrad MASTER follow the frequency you select in MAP65, this is nice but has one problem, normally when you are in MAP65 during RX periods you can quickly click and select another adjacent frequency were you consider a potential signal is, you try manually several times forcing decodes and many times you will find decodes on the high resolution graph when the wide decoder don't decode, this automatically will change the Linrad SLAVES frequency destroying the RX period, that means in that implementation you cannot change with MAP65 the frequency during a RX period without destroying the RX period in WSJT because MAP65 will change Linrad MASTER and also the Linrad SLAVES, in that way on my system I can move freely in MAP65 without altering the RX period on WSJT, the disadvantage is I need to change manually the RX frequency in MAP65 and Linrad MASTER when I want MAP65 and WSJT decoding the same signal but I don't see a problem on that.

Linrad MASTER send, via the network, two kind of data in different ports: it sends ***raw data 24 bit format to port 50002*** (this is the input configuration port for Linrad SLAVES's) and ***timf2 blanker out to port 50004*** (this is the input configuration for MAP65).

The Frequency configuration is done creating a folder in your root named C:/Lin2ft and placing inside a file ***Radio0file,*** Linrad MASTER will write the frequency in that file and Linrad SLAVES will read the frequency also from that file, in that way Linrad MASTER and Linrad SLAVES are in frequency sync.

Having the Linrad Master and Linrad SLAVES on the same frequency Linrad MASTER will send, via the network, the same raw data to MAP65 and Linrad SLAVES, but only the data send to MAP65 will be the output of the Linrad NB, the data send to the Linrad SLAVES doesn't have the NB applied, for that reason you must calibrate the NB in Linrad SLAVES too. This allows us to switch on/off the NB in every particular angle and see if the NB have influence or not. MAP65 will start decoding immediately, now is the moment for the Linrad SLAVES to send the audio output to a specific polarization into WSJT.

To do that you must have Virtual Audio Cable installed and configure, you must have 4 Virtual Audio cables. Then you will configure the Linrad SLAVE H to output the audio to VAC1 (Virtual audio cable 1), Linrad SLAVE V to VAC2, Linrad SLAVE +45 to VAC3 and Linrad SLAVE -45 to VAC4.

Then, in each Linrad SLAVE you must configure the polarization selector to the respective polarization like that:

Linrad SLAVE H | Linrad SLAVE V | Linrad SLAVE +45 | Linrad SLAVE -45

Fig4. Linrad SLAVES polarization angle controls

Pay attention the polarization is selected in "FIXED" and not in Adaptive as it is by default.

Now just install WSJT in 4 different subfolders and rename the icons in your desktop to reflect each shortcut to their respective polarization angle pointing to the properly copy of WSJT. This is how it looks:

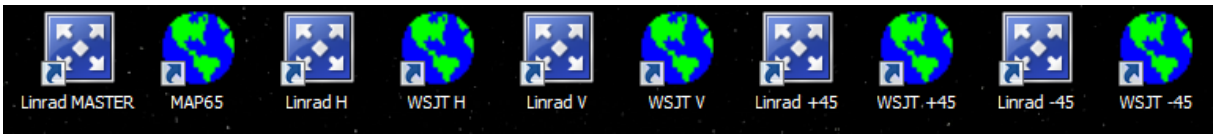

Fig5. Icons distribution in your desktop

The order (starting from the left) show the way you MUST start the programs and keep in mind than Linrad even if they start in SSB (pressing D) are not giving audio output into their respective VAC cables until you click random in any frequency, then you will have audio output. Same for the Linrad MASTER

Now you must configure the WSJT input in each copy to their respective VAC, keeping the output to the ***Microsoft Sound Mapper- Output***

Now just click in any frequency, in the waterfall of the Linrad MASTER and all Linrad SLAVES will follow the frequency but now you must configure the "cero beat" to have the signal on WSJT exact on the frequency you want. Linrad has not USB or LSB selector, works based on the BFO concept (Beat Frequency Oscillator) for that reason is a must to inject a stable signal in a well know frequency, let said 144.150 MHz, then move the BFO red vertical bars (exist 3 of them, use the upper red bar) until the 3 bars are aligned in the center, this correspond to "cero", look the next figures:

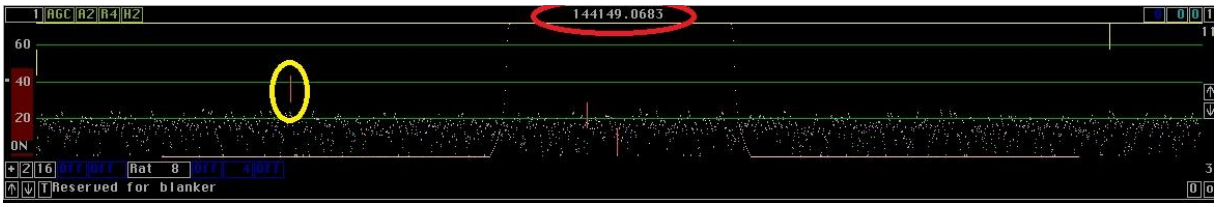

Fig6. BFO displaced to the left (yellow circle)

Fig6.shows how it looks after the installation, pay attention to the upper vertical red bar showed in a yellow circle, probably this upper red bar is on the right, doesn't matter, the frequency is selected in 144.150 MHz but because the BFO is displaced look the real frequency in the upper center flag with a red circle, it shows 144.149.0683, means you are not at cero, just move the red vertical bar until the 3 red vertical bars are aligned on the "cero", like in the next figure:

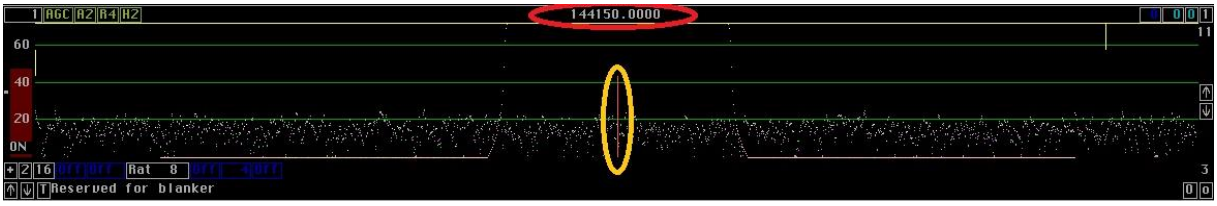

Fig7. BFO at "CERO", yellow circle, Frequency read 144.150 MHz (red circle)

Fig7. The BFO vertical bars are all aligned on the center, look the frequency in the red circle, reads 144.150 MHz, and now your Linrad MASTER is sending the audio in the real frequency you select with no Linrad BFO intervention.

The next step will be adjust the same BFO bars on each Linrad SLAVE until the carrier in 144.150 MHz match the CERO DF position on the WSJT waterfall. With that you complete the

frequency calibration and you are sure than any frequency you select on Linrad MASTER will fall in the center (DF=0) in each WSJT.

The output Filter in each Linrad SLAVE need to be open just enough to cover the bandwidth in WSJT, this is approx. 4 KHz, just using the yellow vertical lines just above the BFO to have just the amount you need. In my Linrad SLAVES this is how the BFO looks, displaced to the left until the 144.150 MHz carrier match the DF=0 :

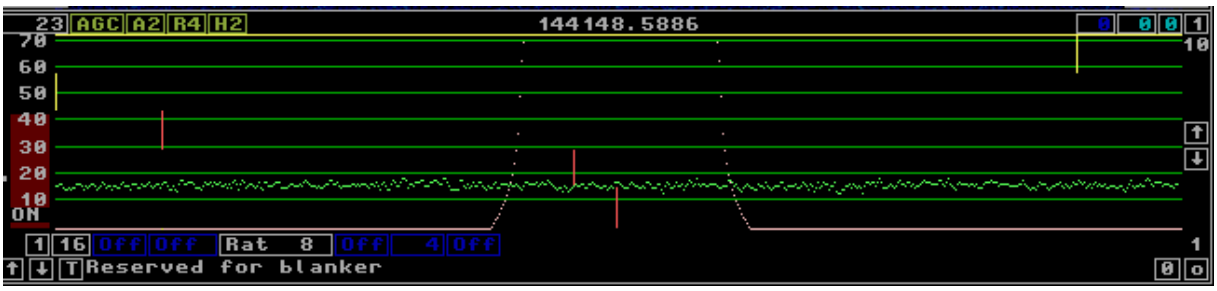

Fig8. Linrad SLAVES BFO position and filter size

Fig8.The BFO first vertical bar is displaced to the left, means I'm receiving in USB, a common error for those who fail in the setup is to having the first vertical bar displaced to the right, this will place the Linrad SLAVES in LSB mode and no decodes will happens, the yellow vertical lines correspond to the filter.

A REAL CASE IN ZSJON STATION

John ZSJON operate in 144 MHz with a modest Yagi array, his antennas are 4 times 9 elements in Horizontal and 4 times 6 elements in Vertical, a mismatched antenna system far away from the optimal for adaptive polarization. John will replace soon his antenna for 4 times 12 elements in vertical and horizontal.

In November 2015 John install an IQ+ radio together with MAP65, he was very happy to have 90KHz of bandwidth and multiple decodes with MAP65, never the less when DL1RPL move to Mayote (FH) and Reunion (FR) he had a lot of problems to work the DXpedition. He try two entire moon pass with no decodes looking for FH/DL1RPL, I visit him the 21 of November and we deploy the Multi polarization System, we didn't manage before because he has not enough Monitors on his PC, never the less with 3 monitors running I deploy the system just in 1 hour (fully configured and calibrated) and he was able to complete a QSO with solid decodes in one of the WSJT configure as multi-polarization program but no decodes or traces at all in MAP65, days later the 03.12.2015 he works FR/DL1RPL, in the same way was WSJT and not MAP65 who decodes. If John remains just on MAP65 he will never have the chance to sum two new DXCC. It was worth the new configuration? Ask John.

HB9Q, 4 YEARS OF EXPERIENCE

The System I propose here is in service in HB9Q for almost 3 years but HB9Q start to using previous Multi-polarization system with MAP65 and WSJT more than 4 years ago. We can full fill this presentation of examples but always will down as a simple anecdotal and a priori observations. Never the less if you ask Dan HB9CRQ (head of HB9Q) he does not conceive the idea of operating without the two programs in parallel. The system is in service in 144 and 432 MHz

IS WSJT BETTER THAN MAP65?

I don't' think so, what I believe is both programs behave (in terms of decodes) pretty much the same and if exist a difference is not more than1%. How both software can decode "the

same" when WSJT is looking just for 4KHz of bandwidth and MAP65 90 KHz.? I think exist a trade-off compromise about Wide-decoding, sensitivity and confidence to avoid false decodes.

Maybe is a matter of interpretation and your goals you establish about performance. What is clear is sometimes WSJT decodes when MAP65 doesn't but I see many times the inverse relation when MAP65 beat WSJT in very low SNR ratios, is very difficult (and non-professional) to just assume WSJT is better than MAP65.

I think, and this needs to be confirmed in the next years (when enough data is collected and analyzed properly with the correct Methodology and Metrology), in some specific cases WSJT, under Multi-polarization configuration, decodes when MAP65 not. These specific cases are statistically very small (less than 1% for SNR -27 to -30dB) but if those particular cases are in relation with a new DXCC or rare grid then the value to implement such a complex system is tremendous and correspond to each individual to evaluate and balance the cost/benefit of this system. Not because the differences are less than 1% we will neglect that differences exist, especially when pushing to the limits our software and Hardware could be translated in just 1 DXCC more in your list, is a matter of individual decision I guess.

THE FUTURE

Having the HW and software properly configure future comparison can be done away from anecdotal observations only if we collect enough amounts of data and process that data correctly; I grab on few TB of data recorded in HB9Q and hundreds of logs from WSJT and MAP65 but the individual effort to grab on the data is tremendous, first, I think, we need to standardize stations size and propagation conditions, delete the non-usable data, find errors, false decodes and duplicates etc. That scape from my scope of time and interest never the less even if the benefit seems to be very small now every fraction of dB really counts for me (I'm by my own, not any more using big antennas like in HB9Q) and if the Multi-polarization system allow me to gain that fractions of dB's in my SNR: Welcome!!

Note: This paper is a brief description of the Multi-polarization system, a step by step guide, easy to follow is not the idea, never the less If a good number of potential users are interested I can consider to write one and publish on my homepage.

73 de Alex, ZS6EME (HB9DRI)

Zs6eme (at) linkrf (dot) ch

K2UYH - Stress Offset Dish for 1296

Allen Katz (e-mail:alkatx@tcnj.edu)

Abstract

This paper reviews stress dishes and describes the construction of a stress offset dish for 1296 EME. Stress parabolic reflectors offer a lightweight, high-gain antenna ideally suited for EME on the lower microwave bands. They require minimum skill for construction and can produce gains in excess of 25 dB, depending on size and frequency. This type of antenna also can be easily and inexpensively constructed. Further, the offset design offers advantages for EME not only in gain for a given area, but also in mounting as it can be easily placed very close to the ground.

Introduction

This paper is an update of earlier papers on stress dish construction. The use of stress dishes for portable EME operation has been a long term interest to me. I produced the first stress dish while still in high school. Stress dishes can be produced in a form that is highly portable, making them ideal for temporary and dxpedition operation.

Fig. 1 - First stress dish (30') constructed by K2UYH in 1960.

Parabolic reflectors have been extensively used for EME. This popularity is due no-doubt to two outstanding features. First, the performance of a parabolic reflector is basically frequency independent. The reflector once constructed can be used on a variety of frequency bands depending on the feed antenna used. This feature is highly desirable as the antenna can be used on more than one band during portable operation. Secondly, if the reflector's surface tolerance is maintained, the antenna's gain efficiency is independent of size. This is not the case for array type antennas, where losses due to the phasing harness increase with array size.

On 1296, dishes have a major advantage over yagi antennas because circular polarization can be easily implemented. Almost all *regular* 23 cm EME stations are circularly polarized. The use of circular polarization provides an effective gain increase of 3 dB. Thus a reflector type antenna with a circular polarized feed can have half the *effective* area of a yagi and still have as much *effective* gain.

Dish antennas tend to be heavier and of greater size than yagis. Stress dish designs can at least partially solve the problem of weight. However, they tend to be more fragile and appropriate care must be taken. For very small dishes (< about 4' dia. on 23 cm), aperture blockage by the feed can be a concern. An offset dish eliminates the feed blockage problem, and generally provides higher gain efficiency than a conventional dish. Thus a circularly fed, offset stress dish would appear to be an ideal antenna for portable 1296 EME operation.

However, if you are flying, the length of the longest piece of your antenna can be an issue. The spokes (petals) of an offset dish are twice the length of a conventional dish of the same area. Consequently, a full dish can be packed in a container of half the length, and cause less attention at an airport. When I made my dxpedition trips, I decided to use a conventional stress dish.

More recently, I have revisited my old offset dish designs and concluded they can offer advantages over a conventional dish.

Fig. 2 - 7.5' offset dish with 1296 circular feed.

Dish Basics: The relationship between the diameter and depth of a parabolic reflector is given by the equation:

$$X^2 = 4fY \quad (1)$$

where X is radius of the reflector, Y is the depth, and f is the focal distance. The shape of the curve for example of a 7' diameter dish with a focal distance to diameter ratio (f/d) of 0.55 is shown in Figure 3. The deeper a dish, the shorter the focal distance and the wider the beam width of the optimum feed antenna.

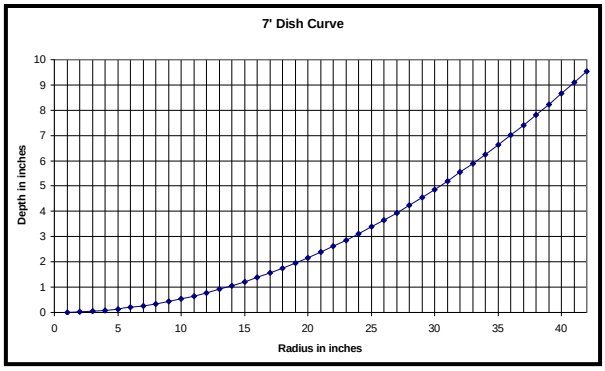

Fig. 3 – Curve of 7' dish with f/d = 0.55.

Offset Dishes:

Offset dishes are just a portion of a parabola of revolution (conventional parabolic dish). The antennas discussed in this paper use about a quarter of a conventional dish reflector. By using only part of a normal *full* dish for the reflector, the feed antenna can be moved away from the center of the reflector, where most of the RF energy is located. The feed can be located to one side of the reflector, where little or no RF energy is present – as shown in Figure 4a. The feed must still be located at the focal point of the parabolic curve. The feed must also have higher gain, since it should *ideally* only illuminate the reflector area. (As noted, the offset dish is only a *fraction* of the full dish. Hence the feed antenna must have higher gain to produce a smaller beam). This arrangement generally enables an offset dish to have a higher efficiency than a conventional dish – higher gain/area ratio. The table in Figure 4b shows the relationship between the f/d of a complete reflector, and the f/d for which the feed should be designed to properly illuminate an offset dish. As can be seen, a deeper dish should be used to keep the focal distance a reasonable length.

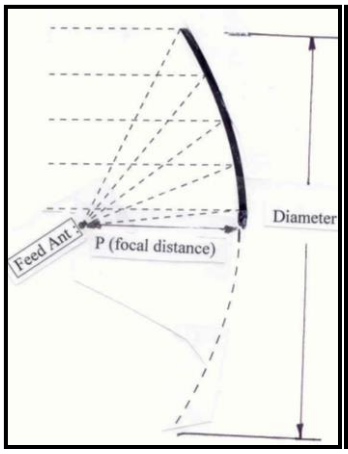

Surface f/d	Reflector f/d
0.90	0.46
0.85	0.44
0.80	0.43
0.75	0.41
0.70	0.40
0.60	0.36
0.55	0.34
0.50	0.32
0.45	0.30
0.40	0.28

Fig. 4 – a) The feed is located to one side of the reflector, b) Relationship between reflector f/d and equivalent f/d for feed.

The offset dish besides having greater efficiency than a convention dish has an added advantage for EME. It can be mounted very close to the ground and still fully track the Moon. Consequently, a relatively small mount can be used, and when not in use the dish laid on the ground.

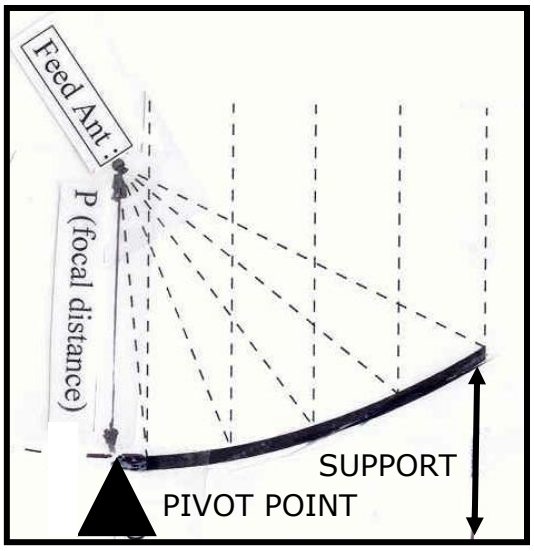

Fig. 5 - The offset dish can be laid on ground (pointing up) when not in use.

Stress Principle: When a beam (dish spoke) is loaded at its end, it deforms in an approximate parabolic curve. This principle from mechanics is the basis of the stress parabolic reflector. The heavy structure that supports the surface of most parabolic reflectors is replaced by a set of spokes, which are bent into an approximate parabolic shape with guy lines. The deflection of a typical spoke is illustrated in Figure 6.

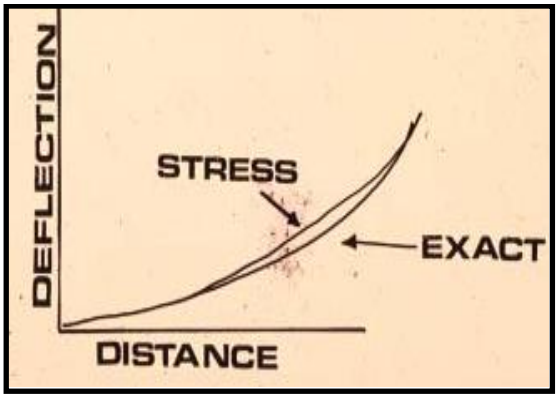

Fig. 6 - Deflection of typical reflector spoke.

Each spoke is basically a cantilever beam. The equations of bending predict a parabolic curve for small deflections. The amount of deflection for most parabolic reflectors is not *small*; neither is the loading perpendicular to the beam (adding the effects of column action to the total deformation). For these reasons, mathematical predictions of the exact curve are rather complex.

Data from numerous models and actual working reflectors reveal that the relative shape is insensitive to material and cross-sectional area. The greatest error occurs along the third quarter of the spoke's length and is always is in the direction of too great a deflection. The curve is also insensitive to the angle (α) the guy line makes with the reflector's normal. A slightly better curve is provided by larger angles. Shape is also related to the focal point to diameter ratio (f/d) and the diameter of the dish. Smaller f/d ratios yield greater bending and hence greater error. Likewise, as dish diameter is increased, the absolute error increases in proportion to size. Figure 7 shows experimentally determined root mean squared (RMS) error for 12' stress dish.

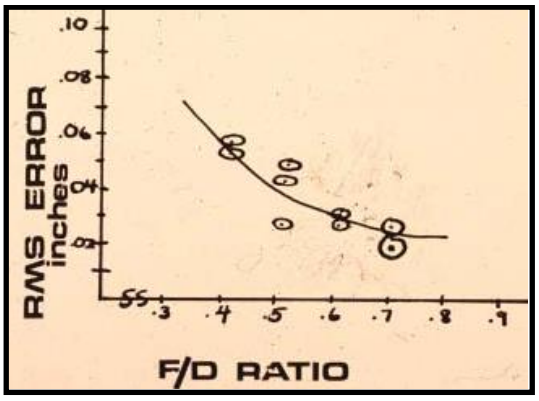

Fig. 7 - RMS error of a 12’ stress dish as a function of f/d ratio.

The maximum spoke error (for a length of 6’ and an f/d of 0.5) is about 0.5” and its approximate RMS error 0.4”. A dish constructed from such a spoke would have a loss in gain due to surface error respectively of less than 0.1 dB, 1 dB and 2.5 dB on the 70, 23 and 13 cm bands. This performance is obtained without any curve measurement; only the bending of the spoke to a depth corresponding to the desired f/d ratio. Figure 8 shows how RMS error varies with f/d and dish diameter.

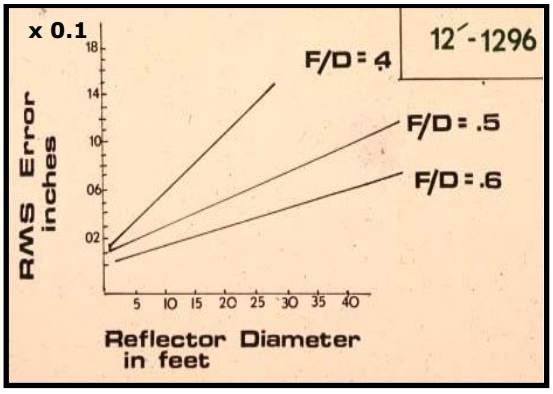

Fig. 8 - Effect of f/d ratio and dish diameter on surface accuracy.

Figure 9 shows the relationship between loss in gain in dB and RMS error in wavelengths.

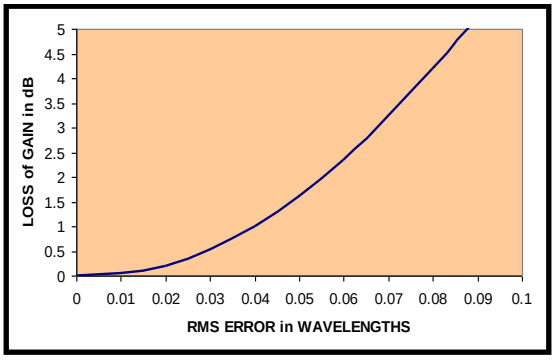

Fig. 9 - Gain loss due to RMS surface error.

In practice, a stress reflector's surface accuracy can be significantly improved by correcting the curve. Generally some form of correction is desirable for reflectors of greater than about 8' in diameter at 1296 and above. Surface error correction can be achieved by either pre-stressing the spokes beyond their *elastic limit* in a manner that corrects for the stress curve's error – this was the approach taken by K2RIW and N2UO for their stress dishes. Alternately back guying or the addition of a rigid circle at the point of maximum error (approximately ¾ the length of the spoke) can be used for correction. This was the method I used. Variations of these approaches have been used to extend the usable frequency range of stress dishes above 13 cm. On 432 MHz, stress dishes with diameters greater than 40' have been built with success. W5LUA used a 24' stress dish for years on 23 and 13 cm.

Fig. 10 - N2UO's 10' stress dish with 1296 feed.

Construction

To demonstrate the stress offset dish concept, a reflector with a radius of 7.5' was fabricated for use primarily on 1296. If the reflector was a full dish, it would correspond to a 15' dish. In the case of an offset dish, only about a quarter of a conventional dish's surface is used. This surface was produced from just five 7.5' lengths of ½" x ¾" wood molding stock – readily available at the local Home Depot. (Larger cross section spokes are suggested for a more permanent reflector). These *spokes* were attached to a hub made from a 1' radius wedge shaped (quarter of a circle) piece of ½" plywood with two bolts.

Fig. 11 - The *spokes* are attached to a plywood center hub with two bolts.

A 3’ overlap was used. It would have been preferable to make channels into which the wooden spokes could be inserted for attachment. (I used this method of attachment for a 70 cm 20’ portable stress dish that I produced more than 20 years ago). This arrangement is stronger and makes assembly and disassembly quicker – but with only five spokes, the added time was not considered insignificant.

To overcome the problem of the “longest piece” during transportation, the center hub of the reflector can be extended. The hub could have been increased in size to 2.5’. This change would have allowed the spokes to be reduced to a more convenient 5’ length.

A partial rim around the outside of the reflector was made with 3.5’ lengths of ½” x ½” wood modeling stock with two small (8-32) bolts as shown in Figure 6. The 3.5’ length was chosen to produce a reflector with an equivalent (full reflector) f/d ratio of about 0.3. This corresponds to a feed beamwidth of about 90°. (This beamwidth matches reasonably well a dual dipole feed). Using equation 1 shows the dish’s focal distance is about 4.5’.

Fig. 12 - An outside rim is formed from 3.5’ lengths of ½” x ½” modeling strips.

A 3.5’ length of 2” x 3” lumber was used for the main feed support.

Fig. 13 - The dish is attached to the feed support by a 2” x 2” block.

This piece was initially attached to the plywood center section using a small wood block as shown in the figure. However, it was found that additional support was needed, and right angle

steel brackets were later added to hold the feed in place. Nylon ropes were run from the feed support to eye bolts at the ends of each spoke. The length of these lines was adjusted so that the radius (X distance) of each spoke was 7.5'. The feed support was also used for attaching the dish to the mount.

Feed Antenna

Orthogonal dual dipoles with a quadrature hybrid to produced circular polarization were used as the feed antenna. Dual dipoles were chosen because of their relative small size. (A septum horn would be an excellent choice of feed for this reflector, but its size and weight could be a problem, when it is carried as luggage on an airliner). The feed was attached to about a 1' length of 1" x 1" lumber. This was attached to a second approximately 1.5' length of 1" x 1" stock using a single 3/8" bolt, which was in turn attached to the feed support by another single 3/8" bolt. Extra mounting holes were drill in the feed support to allow the position of the feed to be raised or lowered. This arrangement provided several degrees of freedom in adjusting the position of the feed for optimum performance. Feed mounting details are shown in Figure 14.

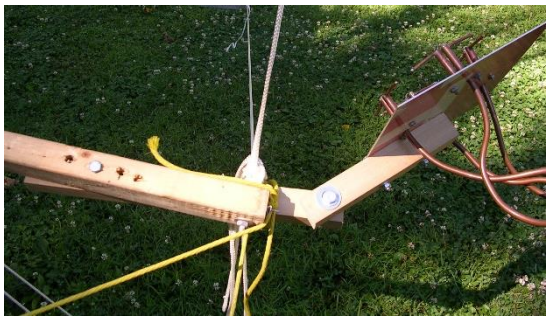

Fig. 14 - The feed is mounted using several supports to allow optimum positioning.

Covering:

The dish was covered with Aluminum screening. This material is available in the US in 3' width by 25' long rolls, which is sufficient to cover the dish, for relatively low cost. The screening was first rolled over the top of the stressed dish and cut to the required size. The remaining screening was flipped over to match the cut end with the shape of the dish, and rolled over the center portion of the dish. This process was repeated a third time for the bottom section – see Figure 15.

Fig. 15 - Aluminum screening is tied to the spokes using wire.

One of the extra corner pieces from the top was used to cover the small remaining area at the bottom (vertex) of the reflector. The screening is attached to the spokes using small gage (~ #24) wire. The wire is run through the mesh and around the spokes and then wrapped (tied) together. The process of attaching the mesh takes only a few minutes. The Aluminum mesh can be removed and rolled around the 4' 2" x 3" members for transport/shipping.

Testing

This offset dish for 1296 was originally constructed in a single weekend and tested for sun noise. The dish worked as planned and yielded > 8 dB of Sun noise. This was > 3 dB more than a 15' loop yagi that was used as a reference. It is presently disassembled and in storage for use in a future EME dxpedition.

Conclusion

The offset dish design shown in this paper illustrates a relatively inexpensive and simple way of producing antennas for 23 cm EME, and possibly 13 and even 9 cm EME. It is particularly useful for temporary and portable operation because it can be quickly assembled and taken apart. It also can be mounted very close to the ground and with a relatively simple mount. The 7.5' offset dish provides performance equivalent to about an 8' diameter circular dish, yet can be disassembled into a small lightweight package.

Acknowledgement

The author wishes to acknowledge the contributions to stress parabolic reflector design of K2RIW, W2IMU, VE7BBG, N2UO (ex-LU6DW) and many other amateurs.

References

1. J. Ruze, "Antenna Tolerance Theory – A Review," Proceedings of the IEEE, April, 1966.

2. A. Katz, "Simple Parabolic Anetenna Design," CQ, August, 1966.

3. R. Turrin, "A Parabolic Reflector Antenna for 1296 MHz," Technical Report No. 5, Crawford Hill VHF Club, Homdel, NJ, 1970.

4. J. Janky, R. Taggart, "Two Hundred Dollar Station Tunes in Satellites," Microwaves, August, 1970.

5. R. Turrin, "A Circular Polarized Feed Antenna for 1296 MHz," Technical Report No. 9, Crawford Hill VHF Club, Homdel, NJ, 1971.

6. R. Knadle, "A Twelve-Foot Stress Parabolic Dish," QST, August, 1972.

No. 9, Crawford Hill VHF Club, Homdel, NJ, 1971.

7. A. Katz, "20' Portable Stress Dish," 432 and Above EME Newsletter, Oct. 1980,

http://www.qsl.net/pa3csg/Boek/BoekH3/art3-8.htm

8. A. Katz, "Small Station EME on 70 and 23 cm Using JT44/65,"

http://www. nitehawk.com/rasmit/jt44_50.html..

9. P. Wade, "W1GHZ Online Microwave Antenna Handbook, Chapter 5,

http://www. w1ghz.cx/antbook/app-5a.pdf.

Appendix

CD/Mount Parts List

1 - Hub of 1’x1”x1” plywood with corners cutoff at 3.5” in and holes drilled as shown in Figure 4.

16 - 2”x0.5”x0.75” wood molding stock clamps with holes drilled 0.75” in from the ends.

8 - *Spokes* of 40.5”x0.5”x0.75” wood molding stock with holes drilled at 0.5” and 2” in from one end.

8 - *Rim segments* of 32.5”x0.5”x0.75” wood molding stock with holes drilled at 0.5” from both ends.

8 – Trapezoidal shaped pieces of aluminum screening cut as shown in Figure 5.

40 – ¼” bolts 2.5” long, nuts and washers.

8 – 10-32 eye bolts, nuts and washers.

8 – 10-32 bolts 1.5” long, nuts and washers.

2 – Aluminum poles 1.25” dia x ~ 3’.

1 – Aluminum pole 1.25” dia x ~ 1.5’.

5 – 1” pipe nipples.

2 - 1” pipe flanges for mounting on hub.

1 – I” pipe tee.

1 – 1” pipe elbow

3 – Hose clamps.

50’ – Nylon rope.

OK1DFC - Portable MW EME 9 – 6 – 3 cm

Zdenek Samek OK1DFC (email: ok1dfc@seznam.cz)

What we need?

- First accept that problem does not exist, just only challenge
- I will need something where to install antenna and move it in AZ and EL.
- Control antenna in real time
- Choice right antenna
- TRV with PLL LO and IF TRX with PLL LO
- SW and aceccories as GPS, SDR etc.

Make a QSO is just for fun after that.....

Azimuth and Elevation

- Stability
- Easy to build
- Construction simple as possible
- Zero back slash in AZ and EL

Mesh dish

3,2m is usable for 432, 1296, 2320 MHz for 3400 MHz is problem with surface accuracy and 1,8m solid dish is giving almost same result

Solid Dish

180cm dish for satellite reception
F/D 0,38
Very good usable for 9cm - 6cm and 3cm


Mechanical parts important for axe stability of dish


Test in 3cm band. Looking for
maximum of Sun noise


TRVs


3400 MHz
• 100W RF
• 0,7dB N/F DB6NT
• Septum feed OK1DFC and Chaparral ring

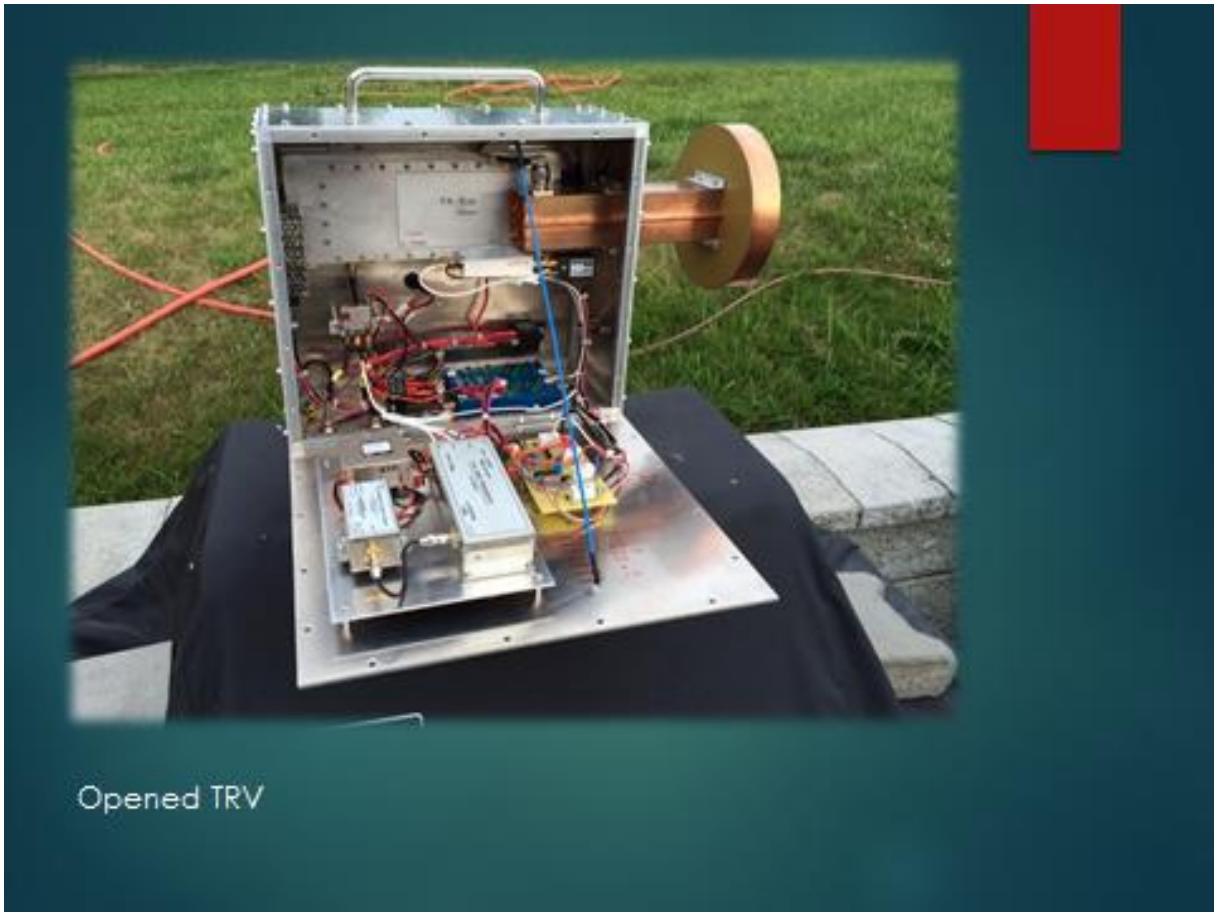

HB9Q EME 3400 MHz

PA3DZL EME 3400 MHz

OK1KIR RS 3400 MHz


5760 MHz
5760 MHz / 144 MHz
• 100W RF DB6NT
• 0,9dB N/F DB6NT
• Septum feed OK1DFC

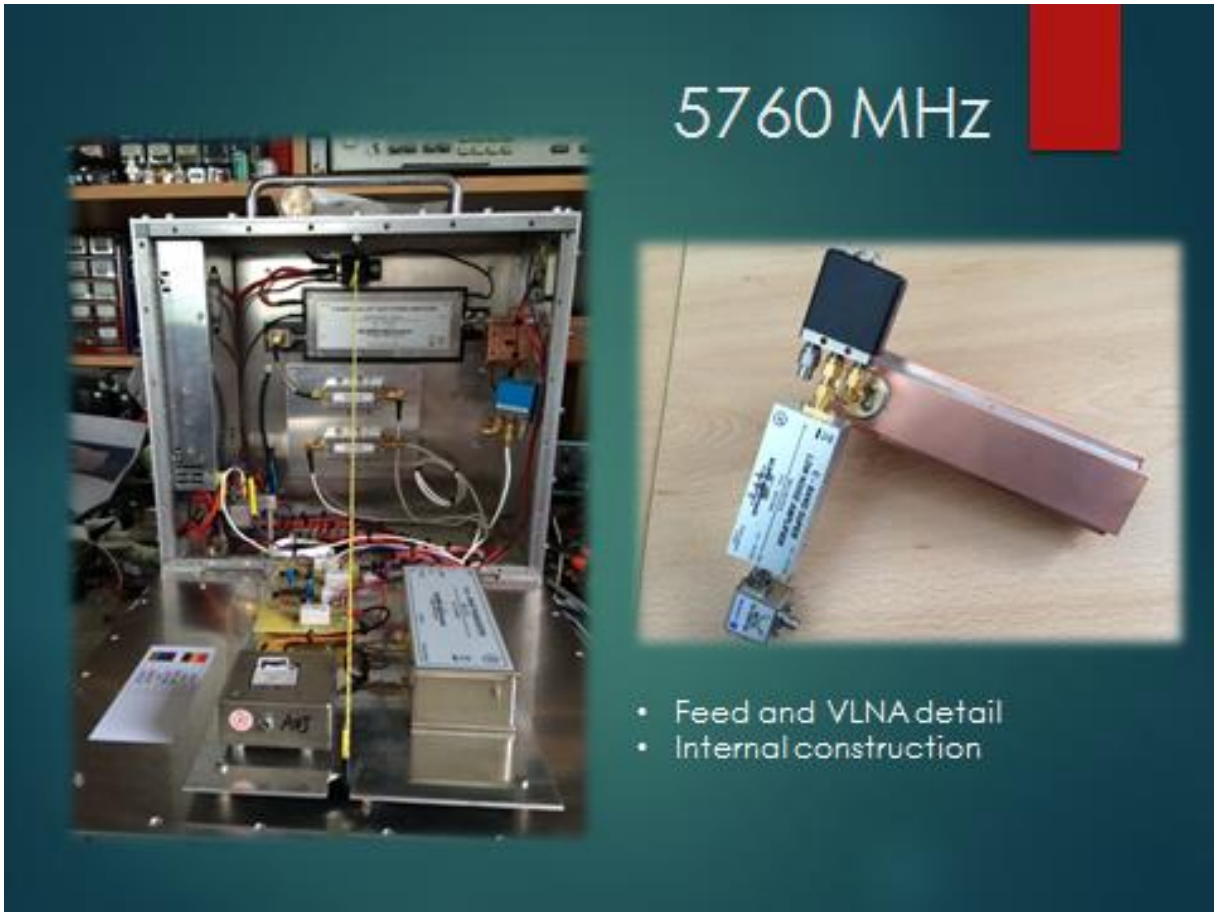
5760 MHz
• Feed and VLNA detail
• Internal construction

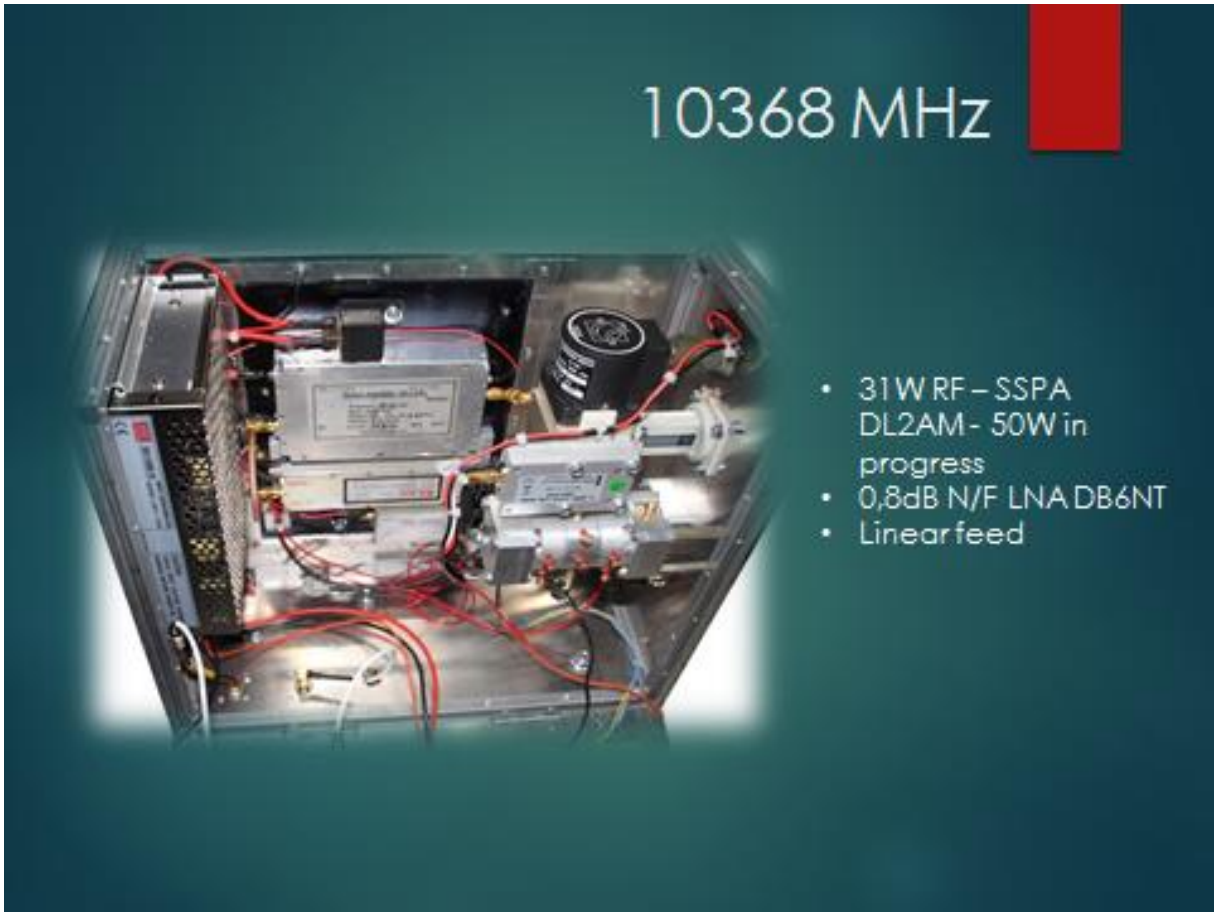
10368 MHz
• 31W RF – SSPA DL2AM - 50W in progress
• 0,8dB N/F LNA DB6NT
• Linear feed

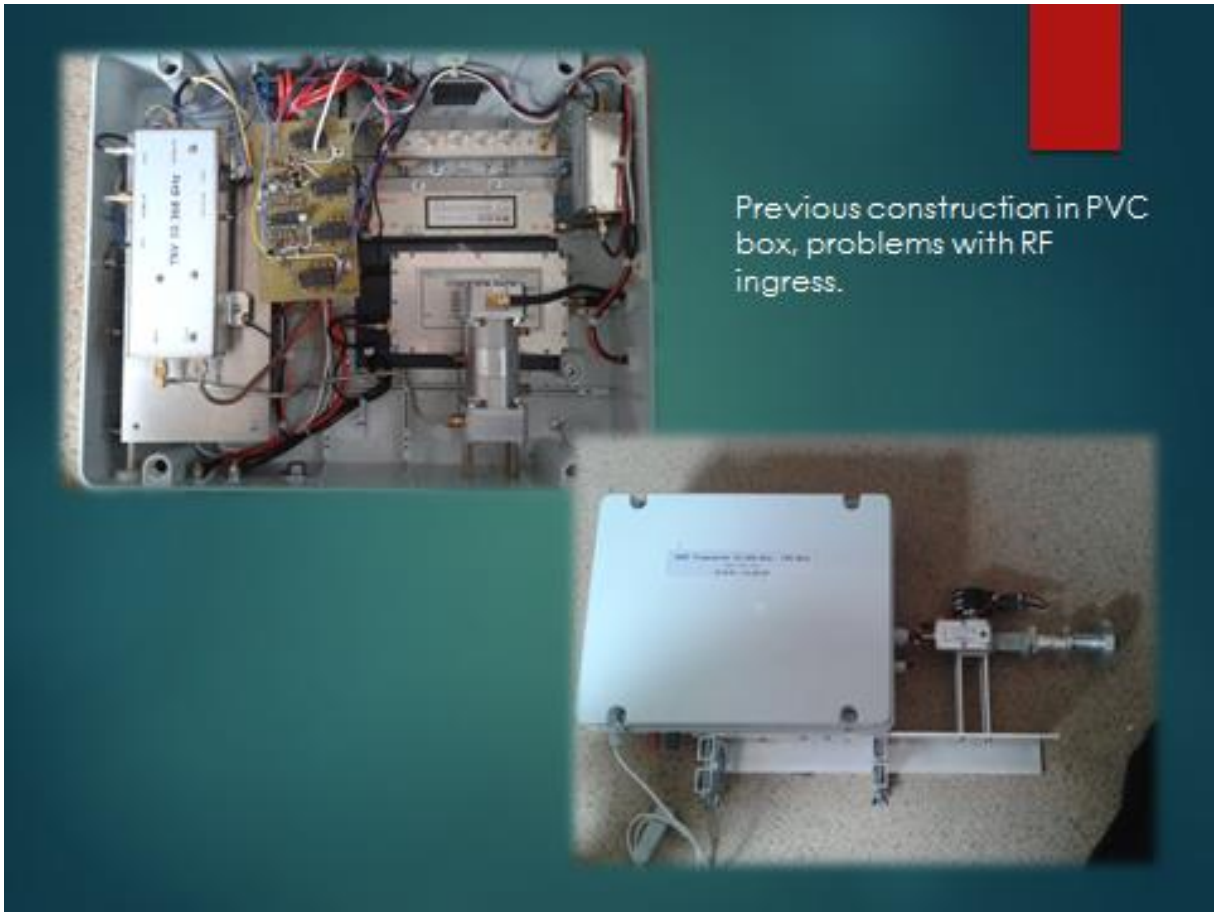
Previous construction in PVC box, problems with RF ingress.


New TRV in Alu box and RF detection

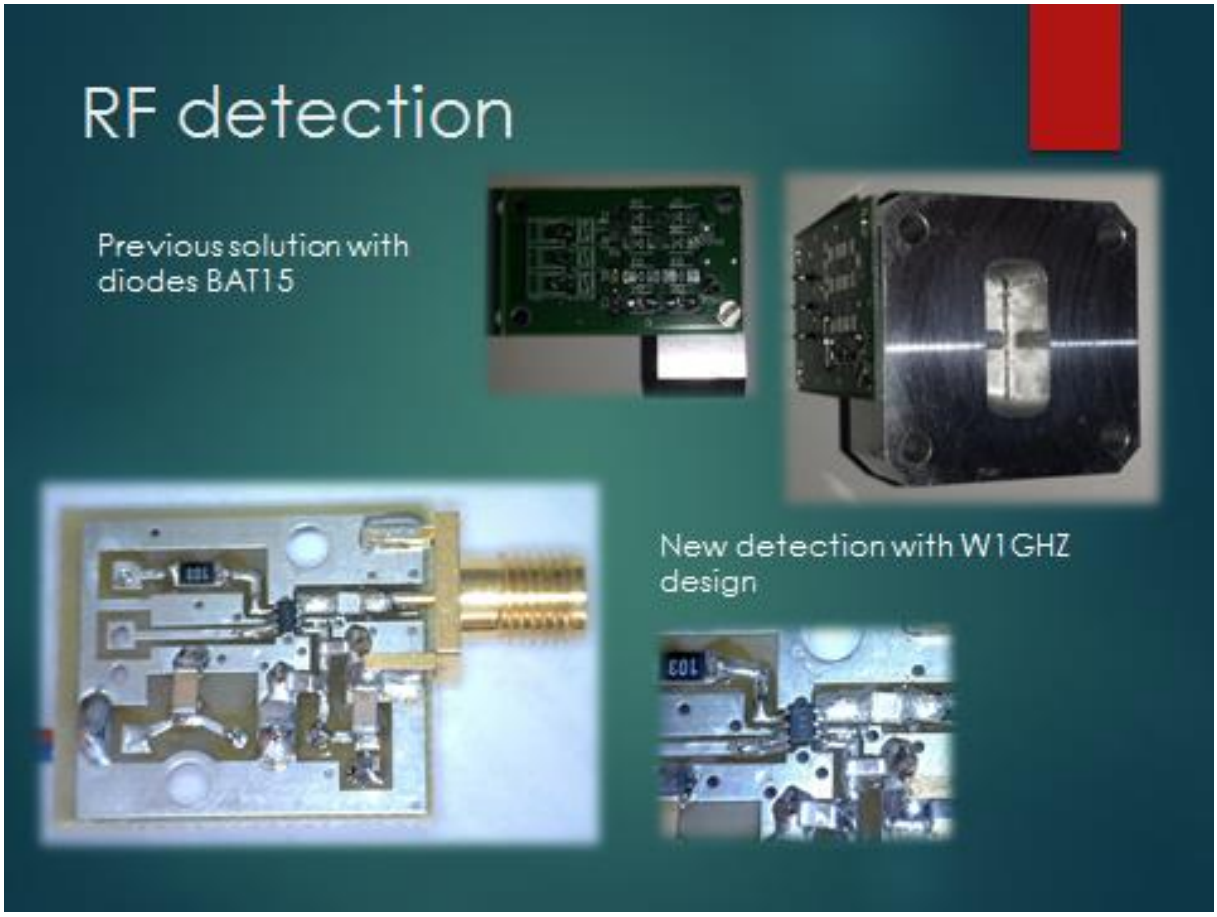
RF detection
Previous solution with diodes BAT15
New detection with W1GHZ design

RF detection LTC5508

TYPICAL APPLICATION

300MHz to 7GHz RF Power Detector

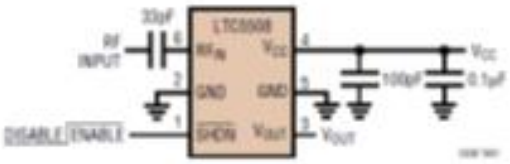

Output Voltage vs RF Input Power

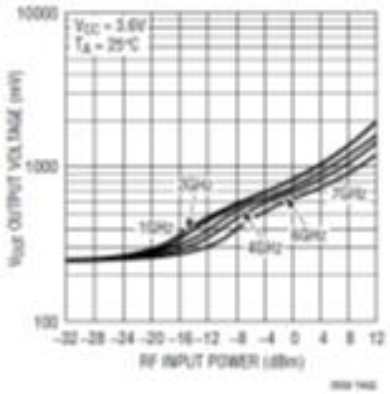

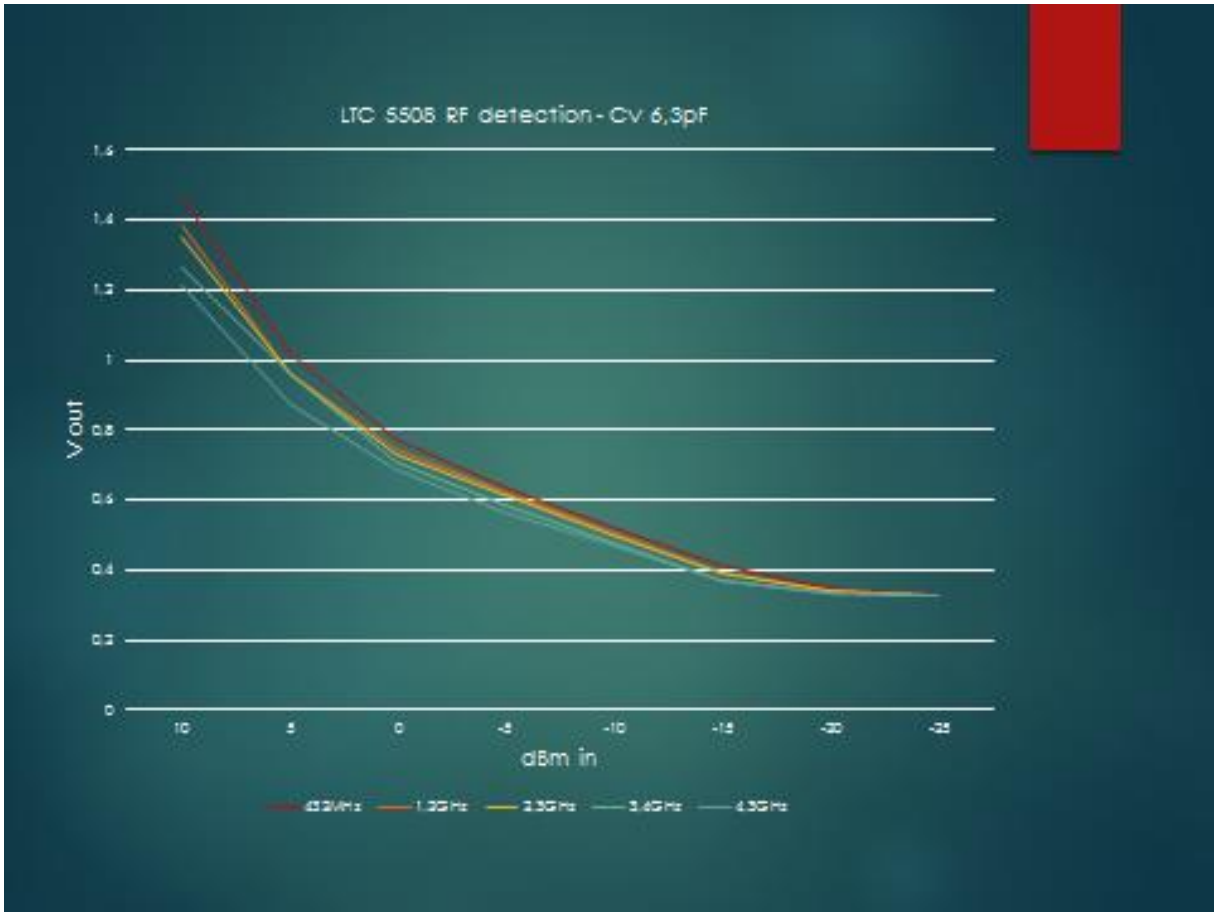

IC9100 and Sequencer

IF site

Previous - IC756 PROII - 28MHz

- Necessary to have other small 2m TRV
- Not so good SDR part

Now - IC9100 - 144 - 432 - 1296 MHz direct

- Internal TCXO 3ppm
- Possible to lock with 10 MHz GPS normal
- 20dB ATT because maximum RF power for accidently connected TRV with full RF is 1W

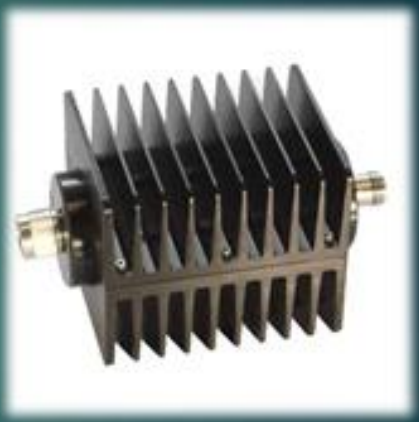

IC9100 a PLL LO GPS

Solution by David VK3HZ

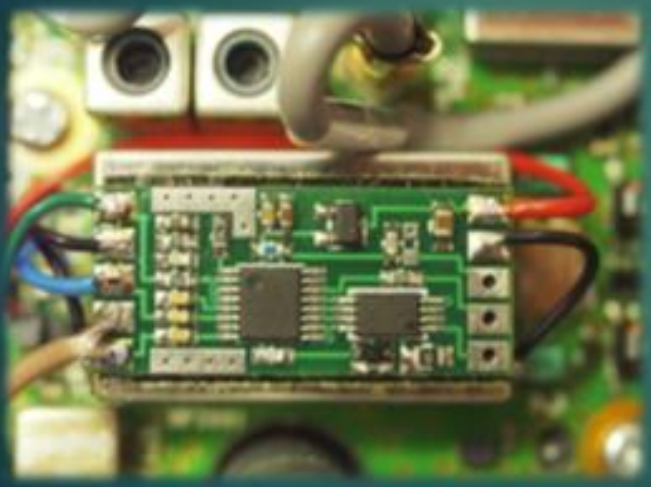

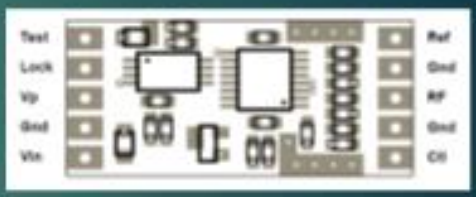

PLL GPS 10MHz

SW and accessories

- SDR – 14
- Signalhound
- PC – with good RAM
- GPS for PC clock control
- GPS – 10 MHz for PLL LOs
- JT SW – JT65C - JT4F 10 GHz etc.
- SDR HD
- MicroHam USB interface

SDR

Signalhound 10Hz-4,4GHz

Spectrum analyzer and tracking generator
- Possible to lock with GPS 10 MHz
- Tracking works also as a CW generator
- Possible to use as a SDR RX up to 9cm

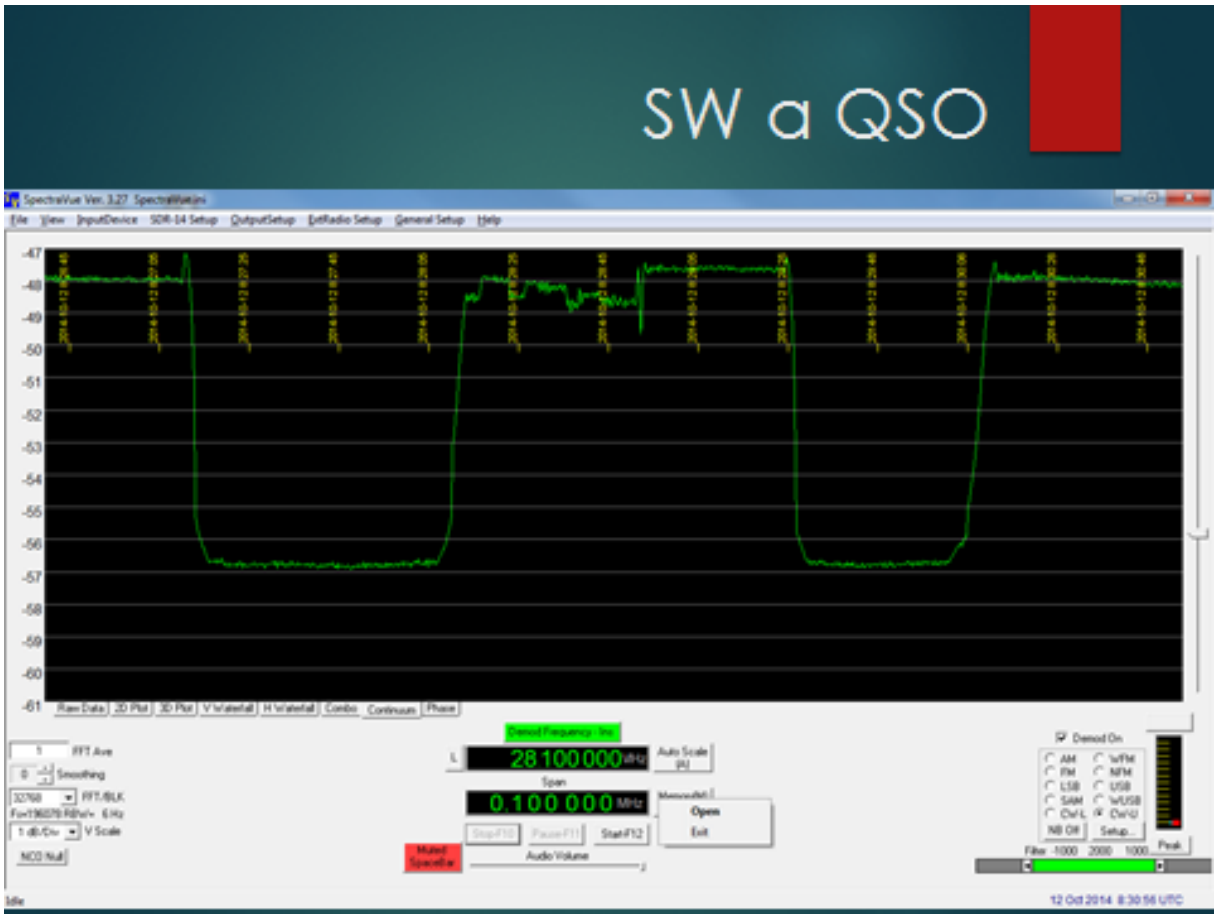
SW a QSO
28 100 000
0.100 000

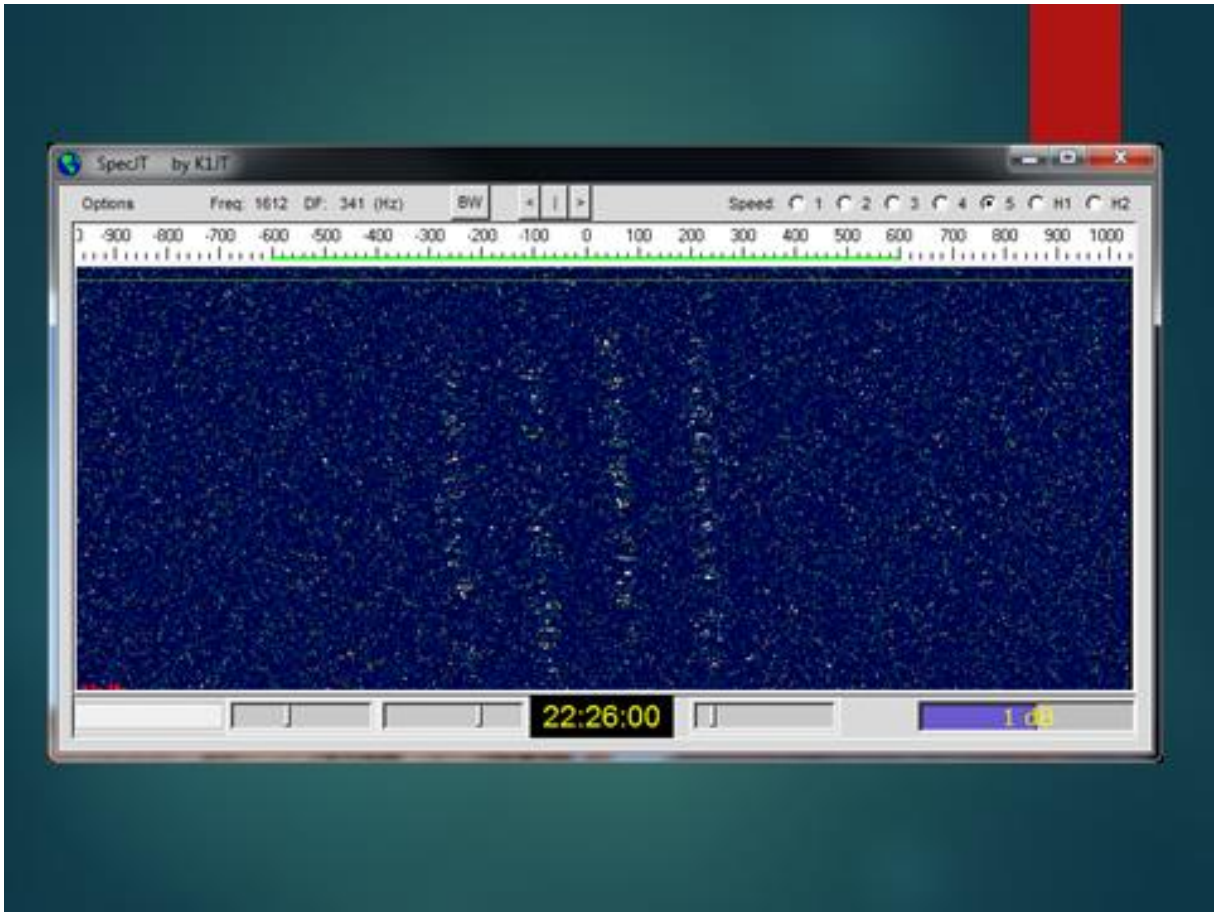
SpecJT by K1JT
Options
Freq: 1612 DF: 341 (Hz)
BW
Speed
22:26:00

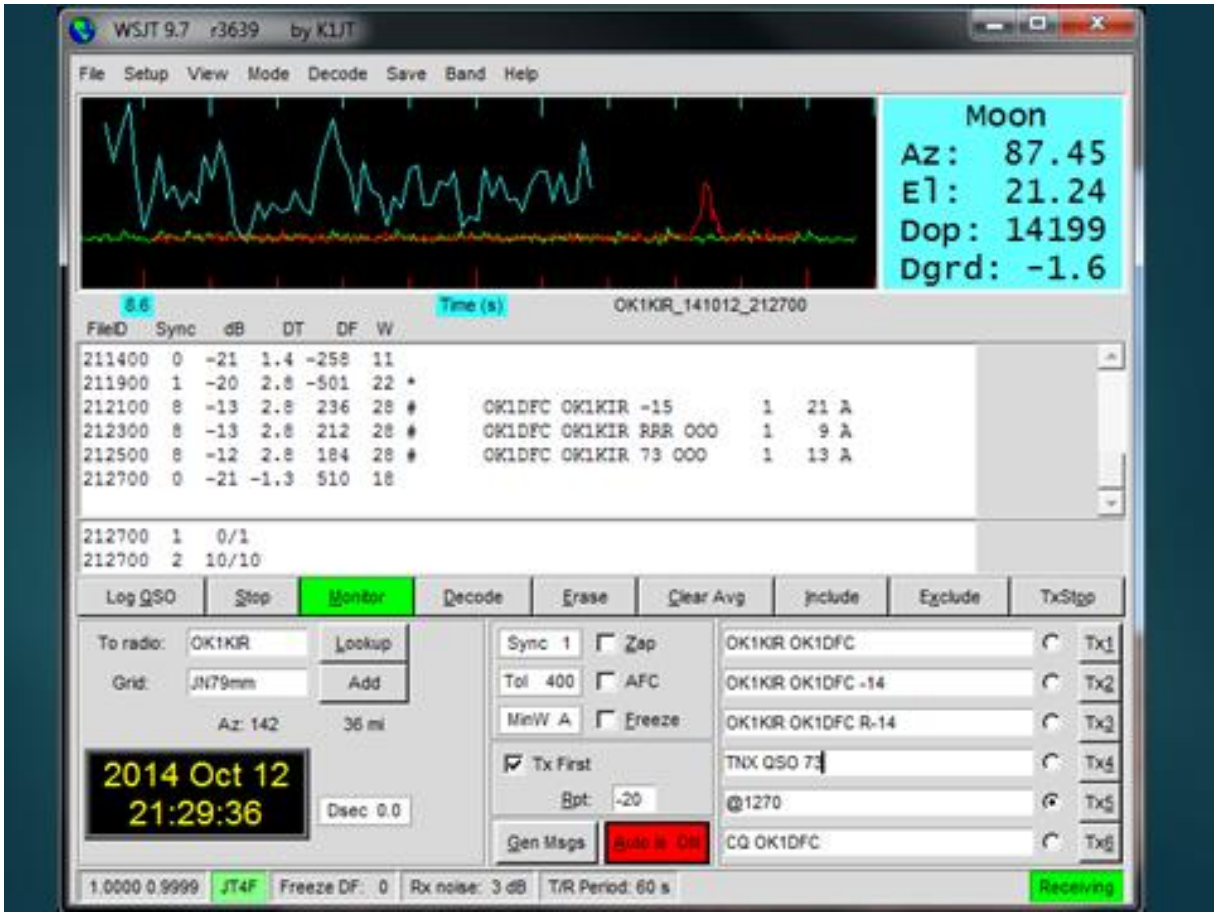
WSJT 9.7 r3639 by K1JT
File Setup View Mode Decode Save Band Help
Moon
Az: 87.45
El: 21.24
Dop: 14199
Dgrd: -1.6
OK1KIR_141012_212700
FileID Sync dB DT DF W
211400 0 -21 1.4 -258 11
211900 1 -20 2.8 -501 22 *
212100 8 -13 2.8 236 28 # OK1DFC OK1KIR -15 1 21 A
212300 8 -13 2.8 212 28 # OK1DFC OK1KIR RRR OOO 1 9 A
212500 8 -12 2.8 184 28 # OK1DFC OK1KIR 73 OOO 1 13 A
212700 0 -21 -1.3 510 18
212700 1 0/1
212700 2 10/10
Log QSO Stop Monitor Decode Erase Clear Avg Include Exclude TxStop
To radio: OK1KIR
Grid: JN79mm
Lookup
Add
Az: 142
36 mi
2014 Oct 12
21:29:36
Dsec 0.0
Sync 1
Zap
Tol 400
AFC
MinW A
Freeze
Tx First
Rpt: -20
Gen Msgs
OK1KIR OK1DFC
OK1KIR OK1DFC -14
OK1KIR OK1DFC R-14
TNX QSO 73
@1270
CQ OK1DFC
Tx1
Tx2
Tx3
Tx4
Tx5
Tx6
1.0000 0.9999 JT4F Freeze DF: 0 Rx noise: 3 dB T/R Period: 60 s
Receiving

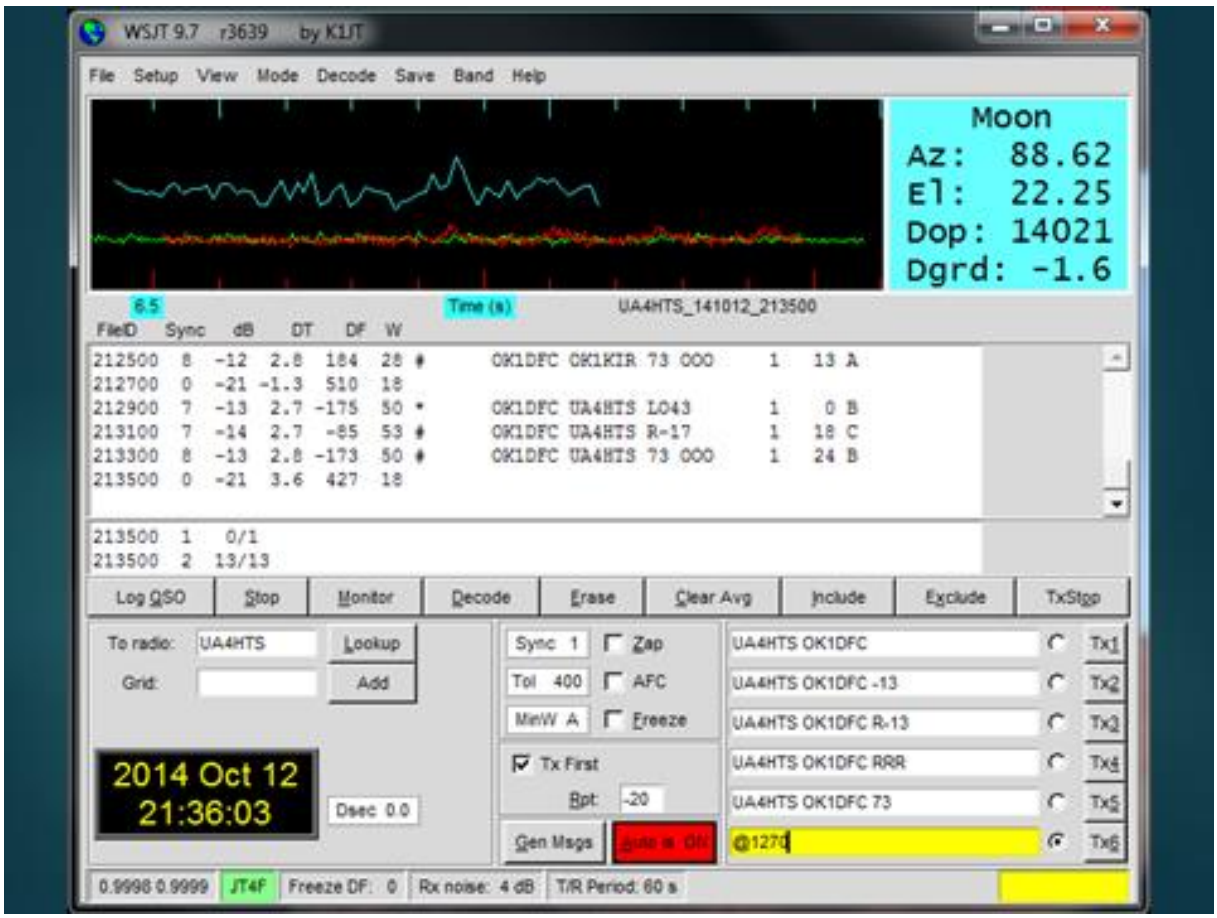
WSJT 9.7 r3639 by K1JT
File Setup View Mode Decode Save Band Help
Moon
Az: 88.62
El: 22.25
Dop: 14021
Dgrd: -1.6
UA4HTS_141012_213500
FileID Sync dB DT DF W
212500 8 -12 2.8 184 28 # OK1DFC OK1KIR 73 OOO 1 13 A
212700 0 -21 -1.3 510 18
212900 7 -13 2.7 -175 50 * OK1DFC UA4HTS LO43 1 0 B
213100 7 -14 2.7 -65 53 # OK1DFC UA4HTS R-17 1 18 C
213300 8 -13 2.8 -173 50 # OK1DFC UA4HTS 73 OOO 1 24 B
213500 0 -21 3.6 427 18
213500 1 0/1
213500 2 13/13
Log QSO Stop Monitor Decode Erase Clear Avg Include Exclude TxStop
To radio: UA4HTS
Grid:
Lookup
Add
2014 Oct 12
21:36:03
Dsec 0.0
Sync 1
Zap
Tol 400
AFC
MinW A
Freeze
Tx First
Rpt: -20
Gen Msgs
UA4HTS OK1DFC
UA4HTS OK1DFC -13
UA4HTS OK1DFC R-13
UA4HTS OK1DFC RRR
UA4HTS OK1DFC 73
@1270
Tx1
Tx2
Tx3
Tx4
Tx5
Tx6
0.9998 0.9999 JT4F Freeze DF: 0 Rx noise: 4 dB T/R Period: 60 s

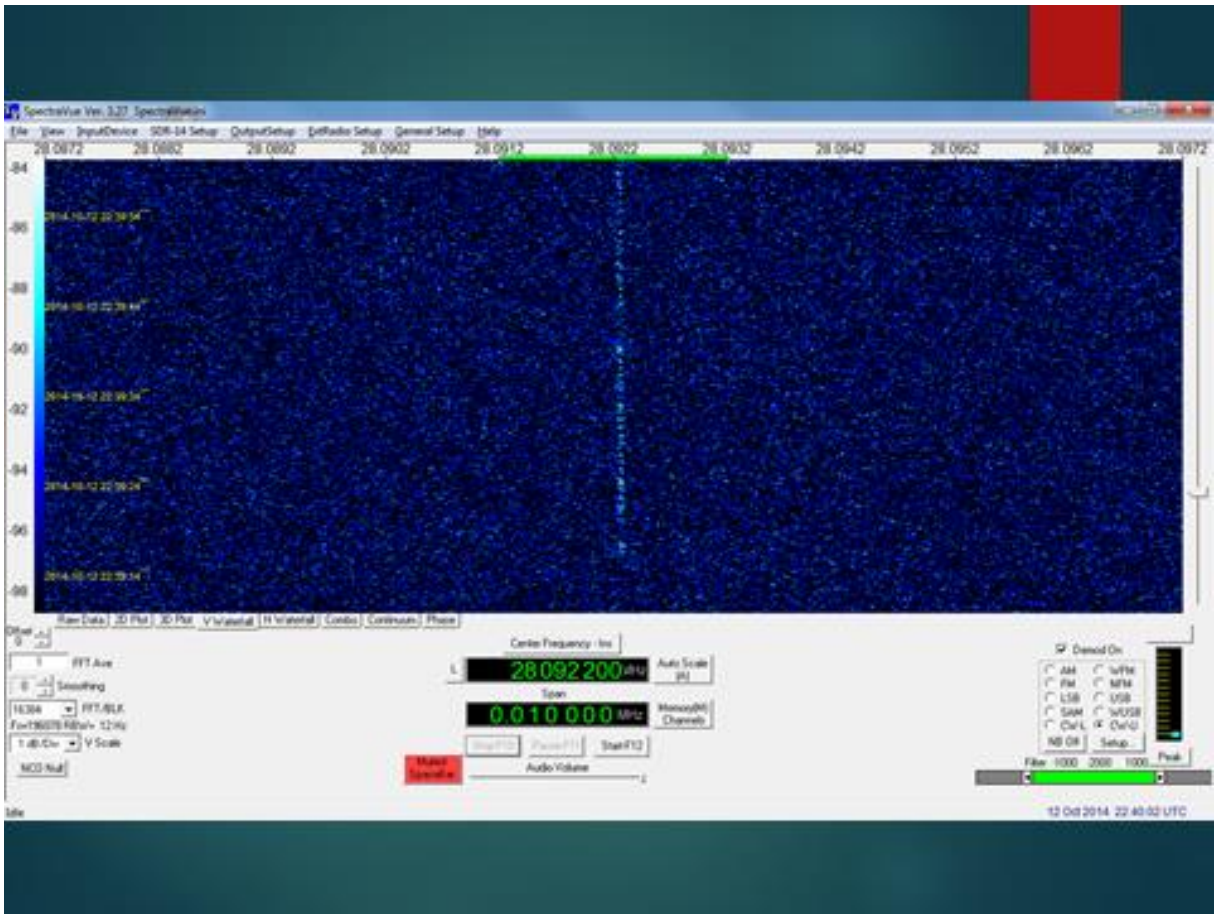

Thank you for your attention and see you via Moon

K1JT, High-Accuracy Prediction and Measurement of Lunar Echoes

Joe Taylor (email: joe@princeton.edu)

Introduction

For me, one of the fascinations of amateur Earth-Moon-Earth (EME) communication is the range of interesting physics that accompanies it. Motivated in part by a need to test a new software program called EMEcho, and also by a desire to see how well I could predict and measure the phenomena of Doppler shift, frequency spread, and polarization of EME signals using amateur equipment, I recently made an extensive series of lunar echo measurements at 144 and 432 MHz. This paper describes how the measurements were made and presents a selection of results.

Doppler shifts of EME signals are caused by continuous changes in the total line-of-sight distance between a transmitter, reflecting or scattering spots on the lunar surface, and a receiver. The relevant rates of change are usually dominated by Earth rotation, which at the equator amounts to about 460 m/s. As a consequence, two-way Doppler shifts can be as large as ±440 Hz at 144 MHz, ±4 kHz at 1296 MHz, and ±30 kHz at 10 GHz. Different reflection points on the lunar surface produce slightly different Doppler shifts, so the echo of a monochromatic signal is spread out over a small and predictable frequency range. The full range of spread can be as large as 4 Hz at 144 MHz and 300 Hz at 10 GHz. However, at VHF and UHF a majority of reflected power is returned from a region near the center of the lunar disk, so the observed half-power Doppler spread is always considerably less than the full limb-to-limb amount.

A smooth moon would produce a specular reflection that preserves linear polarization and reverses the sense of circular polarization. A rough moon (on the scale of one wavelength) would produce diffuse echoes and significant depolarization; cross-polarized return echoes might be just a few dB weaker than the dominant polarization. At VHF and UHF frequencies the circumstances are closer to the specular limit. Received echoes should be almost fully polarized, and with linear polarization they should have a polarization angle that depends on geographic locations of the transmitter and receiver and the amount of ionospheric Faraday rotation.

Together with our knowledge of solar-system dynamics, the relevant physics is such that EME Doppler shifts can be calculated with high accuracy (parts in 1010, or better) for any time and any terrestrial location. Maximum Doppler spread across the full lunar disk is also predictable. Faraday rotation depends on latitude, moon elevation, time of day, solar activity, and ionospheric "weather"; the resulting effects are generally not predictable in detail. For optimum efficiency, EME operators must know about and take account of this full range of phenomena, both predictable and otherwise.

1. Equipment Setup

I used single-station echo tests to measure Doppler shift, frequency spread, and polarization during the moon pass of January 2-3, 2015. My equipment was that of the 144 MHz EME station at K1JT and the 432 MHz station at W2PU, the Princeton University Amateur radio Club. The two stations are configured in a similar way. Both have four dual-polarization Yagis — 4×2Mxp28's at 144 MHz [1] and 4×15LFA-JT's at 432 MHz [2]. Both stations use a single low-loss feedline for transmitting and separate LNAs and receive feedlines for each polarization. The receivers use dual-channel down-converters to produce four baseband signals, I and Q (in-phase and quadrature) for each polarization. WSE converters by SM5BSZ [3] were used at 144 MHz, and the IQ+ receiver by HB9DRI [4] at 432 MHz. Four-channel sound cards (M-Audio Delta44) digitize the I/Q signals at 96000 samples per second, and in normal EME operation all further processing takes place in the computer programs Linrad [5] and MAP65 [6]. For this echo experiment my new program EMEcho was used in place of MAP65. Transmitter power was about 500 W at the antenna, at each station.

2. EMEcho Software

EMEcho is a new program designed to make reliable tests of lunar echoes from an amateur EME station. It goes beyond the Echo mode available in WSJT in two important ways. Doppler calculations are done with state-of-the-art accuracy, based on the Jet Propulsion Laboratory's DE405 planetary ephemeris [7]. In addition, EMEcho takes full advantage of a dual-polarization system by measuring the polarization as well as the frequency and strength of echo signals.

The basic echo-testing cycle is similar to that used in program WSJT. The cycle repeats every six seconds, starting at 0, 6, 12, … seconds of a UTC minute. A fixed-frequency tone is transmitted for 2.3 s, the echo is received and recorded about 2.5 s later, and the spectrum is computed, displayed, and (if desired) recorded in a disk file. In a dual-polarization MAP65-compatible system, spectra can be displayed for both the matched linear polarization and the orthogonal polarization.

3. Measurements

A six-second measurement cycle means that some 8400 2.3-second pulses were transmitted at each station over the full moon pass. A few of the return echoes were rejected for failing a simple interference test; the remainder were averaged in groups of 10 to produce about 800 sets of polarized spectra. Measurements are reported here for both 144 and 432 MHz. They include frequency profiles of the echoes with bin spacing 0.37 Hz, Doppler shifts accurate to around 0.1 Hz, and polarization angles accurate to a few degrees.

3.1 Doppler Shift and Doppler Spread

Figure 1 is a grayscale plot showing matched-polarization and cross-polarized echo strengths as a function of frequency and time. No ad hoc frequency adjustments have been made; the plotted "Frequency Offset" is that of the received spectrum relative to the predicted Doppler shift. The Doppler shift, in turn, is based on station location, UTC according to the internet-synchronized computer clock, and the JPL DE405 planetary ephemeris. The grayscale chosen for Figure 1 is logarithmic, so as to emphasize the weakest features.

Figure 1

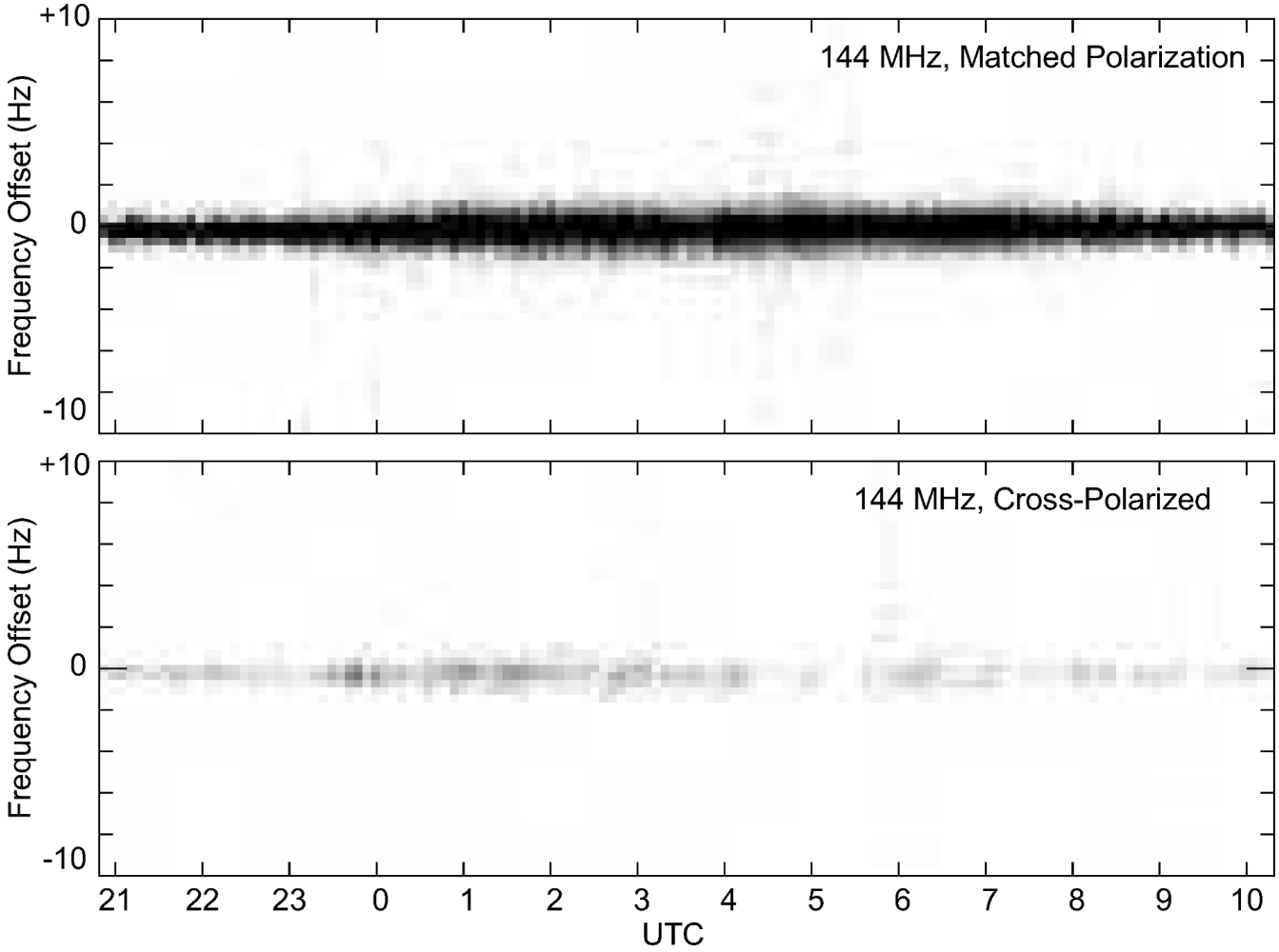

It's easy to see that the frequency width of return echoes is greater in the middle of the run than near either end. These differences are consistent with the predicted dependence of Doppler spread during the course of a moon pass. Further details of this effect can be seen in Figure 2, where spectra have been averaged over about an hour near the times of minimum and maximum libration rate. Dashed curves represent the echo profile around 2130 UTC, shortly after moonrise, while solid curves are the average spectral profile around 0330 UTC, near lunar culmination.

Figure 2

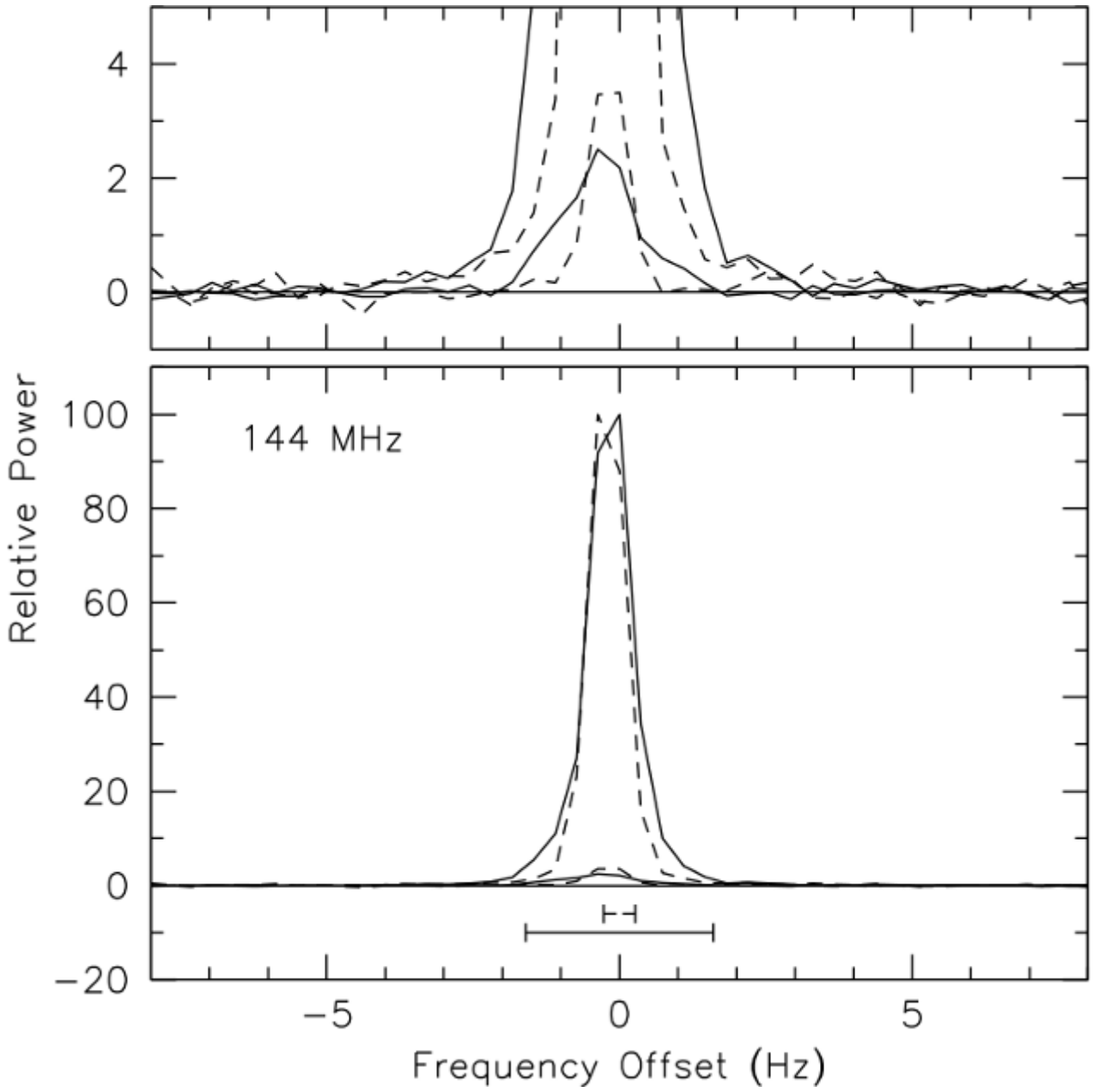

Figures 3 and 4 display the corresponding results obtained at 432 MHz. Again the measured frequency offsets are essentially zero (within the measurement uncertainties). Doppler spreads are rather more than 3 times larger than at 144 MHz, owing to the higher frequency and the somewhat larger size of the lunar reflecting region. Cross-polarized echo signals are essentially undetectable in the grayscale plot and only barely visible in the expanded view (upper panel) of Figure 4. It is interesting to see that at both frequencies the weak wings of the spectral profile extend out to the full calculated limb-to-limb Doppler spread — as they should, with adequate sensitivity. These effects have been noted before by EME operators: see, for example, references [8] and [9].

Figure 3

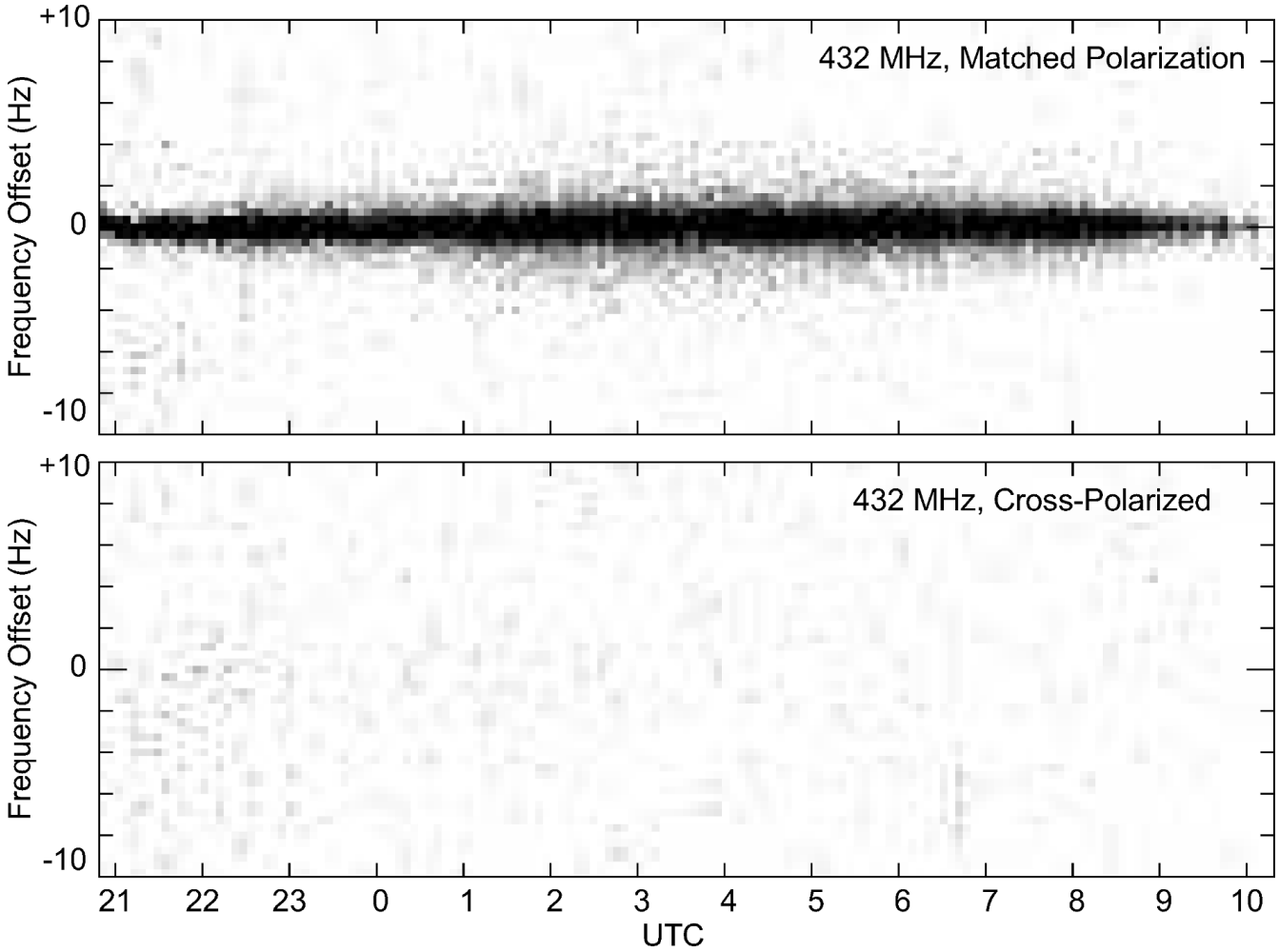
+10
0
-10
Frequency Offset (Hz)
432 MHz, Matched Polarization
+10
0
-10
Frequency Offset (Hz)
432 MHz, Cross-Polarized
21
22
23
0
1
2
3
4
5
6
7
8
9
10
UTC

Figure 4

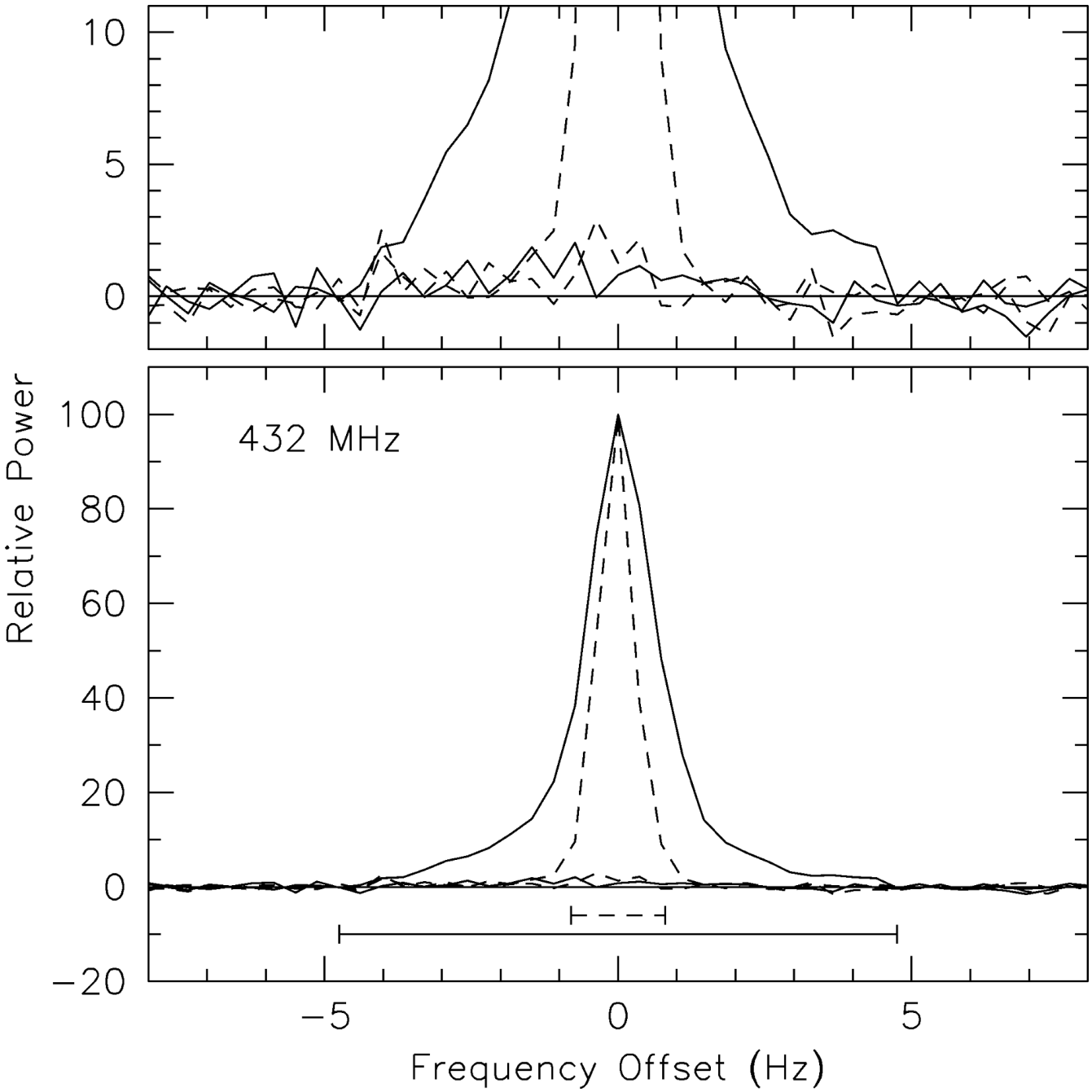

I consider the Doppler calculations used in this paper to be the best achievable with today's knowledge of solar system dynamics. The JPL DE405 ephemeris represents a numerically integrated model of the solar system based on several hundred years of astronomical observations, radar observations of planets out as far as Saturn, and tracking observations of many interplanetary spacecraft. Positions and velocities of the Earth and Moon (and many other solar system objects) are tabulated in a data file suitable for numerical interpolation. Doppler calculations in EMEcho include the following steps:

Convert geodetic coordinates of the antenna to geocentric coordinates, accounting for the Earth's oblateness.

Convert UTC to UT1 and to LAST (local apparent sidereal time). Note that UTC runs at an essentially constant rate defined by the average of many atomic clocks, plus occasional leap seconds. UT1 represents the actual measured rotation of the Earth. UTC and UT1 can differ by up to ± 0.9 s.

Compute 3-dimensional position and velocity of the antenna with respect to center of Earth.

Convert UTC to ET (Ephemeris Time), accounting for all leap seconds up to the present.

Interpolate the DE405 ephemeris to obtain the 3-dimensional position and velocity of center of moon relative to center of Earth.

Combine results of items 3 and 5 to get position and velocity of antenna with respect to moon.

Calculate Doppler shift from the line-of-sight component of velocity obtained in item 6.

Achieving the accuracies required to produce the results presented in Figures 1 through 4 requires knowledge of antenna coordinates to better than one km and clock accuracy better than one second. The transmitter frequency in the antenna's reference frame must also be specified accurately: for example, 144.118 MHz rather than 144 MHz. The Doppler calculations must avoid certain shortcuts and approximations that have typically been used in amateur EME-related software, including my own programs WSJT and MAP65.

Figure 5 illustrates some potential consequences of ignoring one or more of the warnings mentioned above. To produce this graph I used GPS-measured coordinates of the W2PU antenna and calculated Doppler shifts at a nominal frequency of 1.0000 GHz, at frequent intervals from moonrise to moon set on January 2-3, 2015, the date of my echo-test observations. The horizontal straight line at zero represents my supposed state-of-the-art calculation. The ten numbered curves show the differential effects of various changes, omissions, or assumptions in the Doppler calculation, as follows:

Antenna moved 1 km East.

Antenna moved 1 km North.

Antenna moved to 1 km higher elevation.

UTC clock error +1 s.

Frequency changed to 1.0001 GHz.

Time difference UT1-UTC ignored.

Nutations ignored.

Calculation of moon position based on a closed-form series expansion rather than interpolation of the DE405 ephemeris.

Doppler calculation made by program EME Planner, by VK3UM [10].

Doppler calculation made by program EME System, by F1EHN [11].

Figure 5

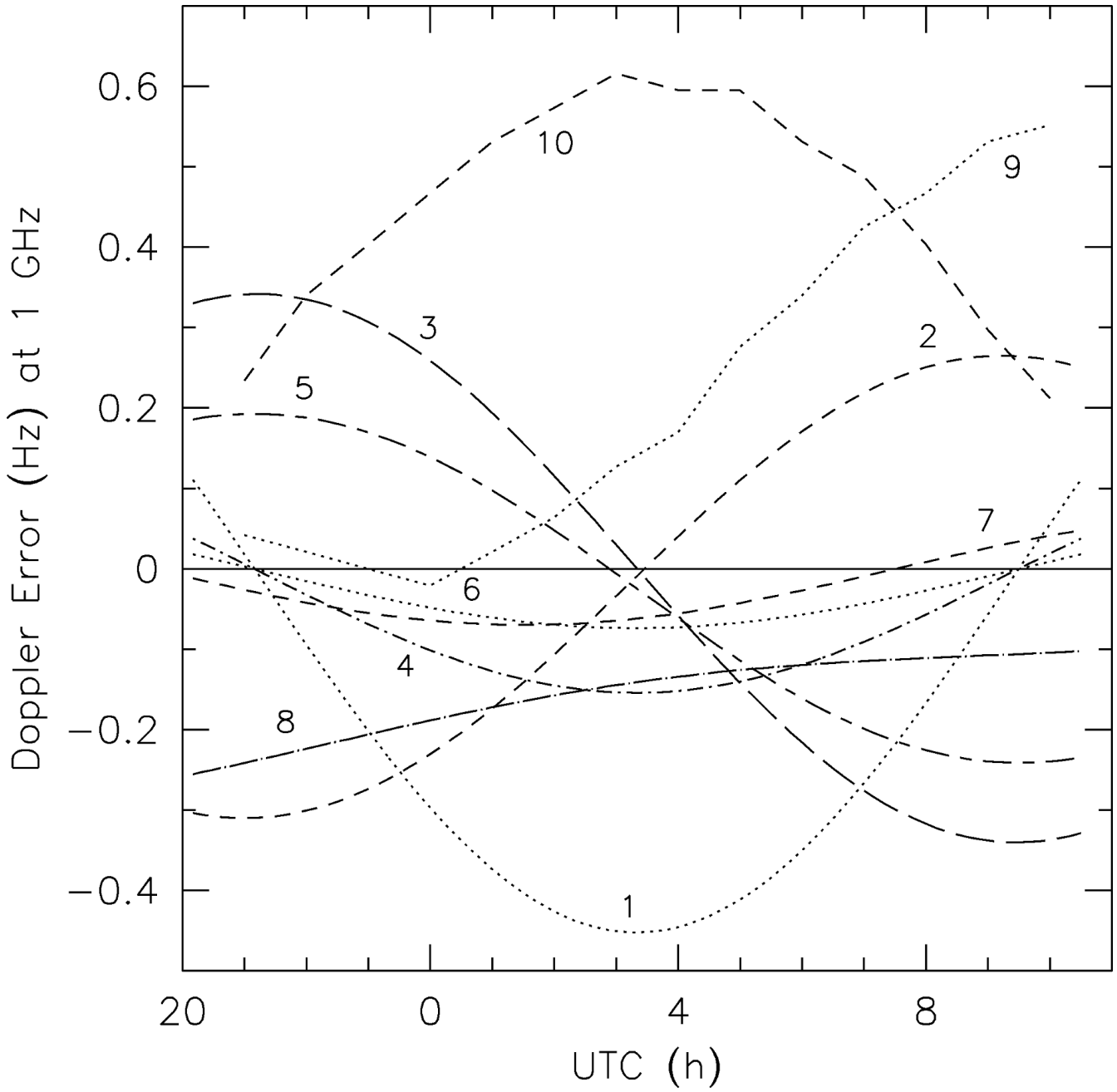

I call particular attention to several points relating to Figure 5. First, the Doppler calculations in EME Planner and EME System are very good — in this example, accuracies better than 1 Hz at 1 GHz, through a full moon pass. Note that in order to obtain this accuracy you must start with very accurate station coordinates: a six-digit Maidenhead locator is not good enough. Your computer clock must be synchronized to UTC and your software must be updated with the latest leap seconds. And you must use the actual transmitter frequency, not just the frequency of the band edge, for example. Careful use of EMEcho should give Doppler predictions even better than those of EME Planner and EME System, accurate to about 1 Hz at 10 GHz.

3.2 Polarization

In addition to Doppler shift and Doppler spread, my experiment yielded polarization measurements at both 144 and 432 MHz. The polarized spectra recorded on disk were averaged over five-minute intervals. The resulting polarization angles are plotted in Figure 6. A solid line connects sequential measurements at 144 MHz. As shown by the scale at left, these angles increased gradually from about 60 degrees to 200 degrees in the two hours around local sunset. The angles then decreased through some 1080 degrees — three full turns — over the next five hours. Subsequent angles decreased only slightly more from 0400 UTC (an hour before local midnight) until moon set, about two hours before sunrise.

Polarization angles measured at 432 MHz are plotted as filled triangles in Figure 6, using the scale at right. Note that the left and right scales are in the ratio of 9 to 1. The close tracking of the scaled results at the two frequencies is an excellent confirmation that Faraday rotation scales inversely as the square of frequency.

Figure 6

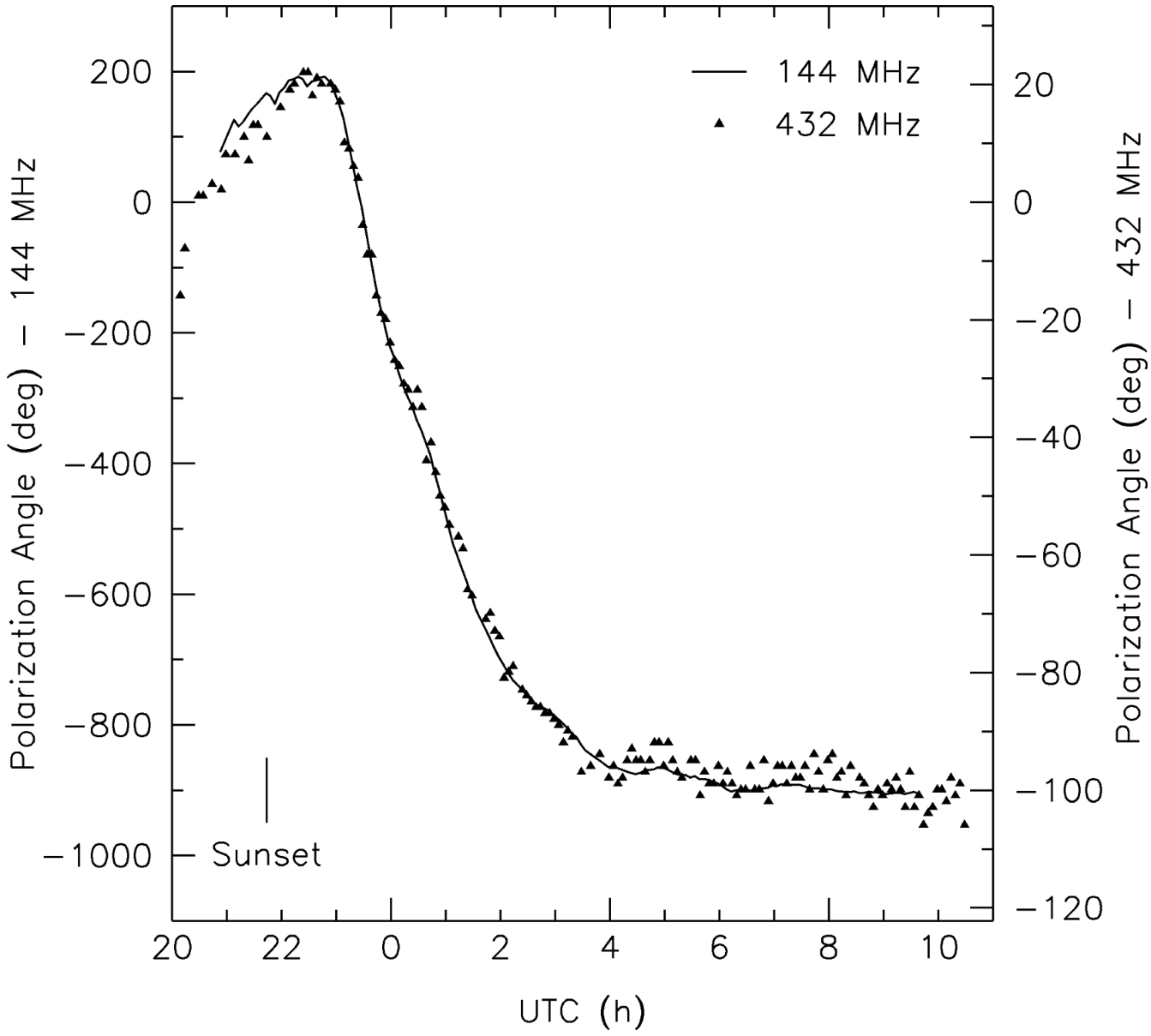

4 Conclusion

Program EMEcho requires a MAP65-compatible EME station and was written mainly for my personal use. However, all of its features except the dual-polarization capability have been incorporated into the WSJT-X, the latest program version in the WSJT project [12]. WSJT-X also offers a number of features such as automatic rig control and Doppler tracking, which make it especially attractive for amateur EME communication on any band.

References

[1] http://www.m2inc.com

[2] Joe Taylor, K1JT, and Justin Johnson, G0KSC. Dubus, 4/2014, p 53.

[3] http://www.sm5bsz.com/linuxdsp/optrx.htm

[4] http://www.linkrf.ch/

[5] http://www.sm5bsz.com/linuxdsp/linrad.htm

[6] http://physics.princeton.edu/pulsar/K1JT/map65.html

[7] ftp://ssd.jpl.nasa.gov/pub/eph/planets/fortran/userguide.txt

[8] http://www.sm5bsz.com/sm5frh/sm5frh.htm

[9] http://physics.princeton.edu/pulsar/K1JT/EME2010_K1JT.pdf

[10] http://www.vk3um.com/eme%20planner.html

[11] http://www.f1ehn.org/

[12] http://physics.princeton.edu/pulsar/K1JT/wsjtx.html

Figure Captions

Figure 1 — Measured echo power at 144 MHz as a function of frequency offset and time. Upper: linear polarization angle matched to that of the echo. Lower: orthogonal linear polarization.

Figure 2 — Frequency structure of echoes at 144 MHz near meridian transit (solid line) and near 2130 UTC, a time of minimum libration rate (dashed line). The upper panel uses an expanded vertical scale to show the weakest spectral features. Horizontal bars in the lower panel indicate the full range of predicted Doppler spread. The pair of curves with intensity a few percent of maximum show the measured cross-polarized power, which in this case may be mostly a result of minor alignment imperfections in the K1JT antenna. Horizontal bars in the lower panel indicate the full limb-to-limb ranges of predicted Doppler spread.

Figure 3 — Measured echo power at 432 MHz as a function of frequency offset and time. Upper: linear polarization angle matched to that of the echo signal. Lower: the orthogonal linear polarization.

Figure 4 — Frequency structure of echoes at 432 MHz near meridian transit (solid line) and near 2130 UTC, a time of minimum libration rate (dashed line). The upper panel uses an expanded vertical scale to show the weakest features. Horizontal bars in the lower panel indicate the full limb-to-limb ranges of predicted Doppler spread.

Figure 5 — Examples of contributions that might affect the accuracy of computed Doppler shifts.

Figure 6 — Measured polarization angles at 144 MHz (left scale) and 432 MHz (right scale).

F2CT - REF-DUBUS CONTEST 2015 MAY 16-17

Guy Gervais (email: f2ct@wanadoo.fr)

Abstract

In may 2014 , first tests on 10GHz EME were made with Cassegrain 13m PB8 dish with a non optimized linear feed . During 2014 REF-Dubus EME some qsos via the Moon were achieved but the echoes level was around 6dB/noise . After some investigations we found that the feedhorn was not optimized and note at the focal point.

So we decide to design a new feed with the help from Jean Pierre Blot , antennas engineer , OM6AA Rata and Bert PE1RKI.

The new simulations and design draft from Jean-Pierre Blot were sent to Bert PE1RKI and to Rata OM6AA

10GHz Septum feed 10GHz Simulation

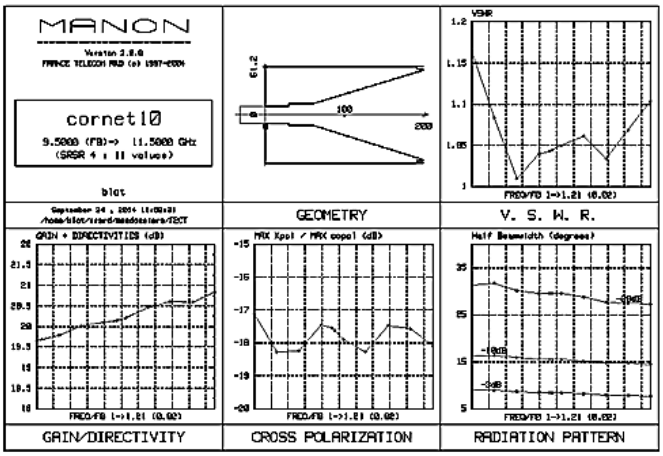

sub-réflecteur position

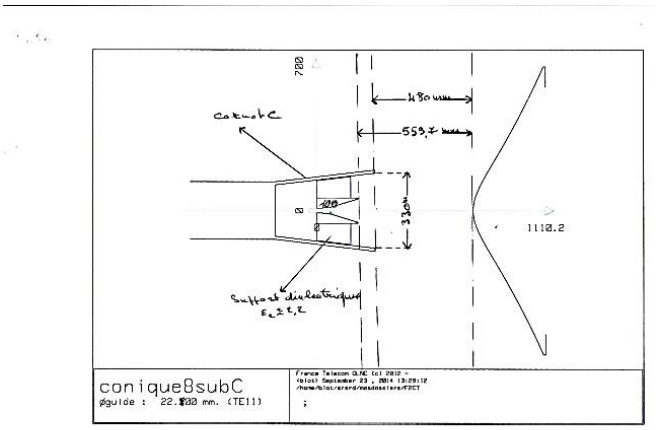

RL @ 10,4 GHz : 34,5dB

10 GHz setup :

Isolation RHCP/LHCP : 28dB

10GHz septum feed inside C band feed:

- *Receiving:*
- 10,6 GHz LNA with 0,6 dB NF and 26 dB gain on RHCP (Right Hand Circular Polarization)
- 10,450/10,368GHz switchable converter for JAs
- *Transmitting*:
- 50 W SSPA on LHCP (Left Hand Circular Polarization)
- Home-brew transverter 432MHz/10GHz

The Shack :

PB8 with 10GHz set up

Results:

Sun noise test on Friday May 15th at 15h15 utc : 24,7dB (SF 129)

Saturday May 16th 05h00 utc:

- Moon noise : 5,5 dB 1kHz BW
- Echoes : 23,5dB / 1kHz BW
- TM8PB send first CQ on CW sur 10368,088MHz ;
- We stopped at 0930 utc and came back at 1300 utc till 1500 utc after a big failure on the AZ tracking system (PB8 aperture : +/- 0,137° @ 3dB)

Sunday May 17th 05h45 utc:

- JA window : JA4BLC : JA6CZD ; JA1WQF ;
- Unfortunately we miss VK3NX
- We stopped between 10h30 and 13h00 utc and put down the feed and setup at 1600 utc just before the rain and wind !

- 41 stations identified:
- 34 Stations heard/worked in CW :
- Germany : DF1OI ; DL7YC ; DL0EF ;
- England: G4NNS
- Canada : VE4MA ; VE6TA ;
- Denmark : OZ1LPR ;OZ1FF ;
- Spain: EA3HMJ (JT)
- Estonia : ES5PC
- US : K2UYH ; WA3LBI ; WA6PY
- France: F1PYR ; F6KEH ;
- Holland : PA0BAT ; PA3DZL ; PA7JB ;
- Italy : IZ2DJP ; IW2FZR ;
- Japan : JA1WQF ; JA4BLC ; JA6CZD ;
- Luxembourg : LX1DB
- Norway : OH2AXH ; OH2DG ;
- Romania : YO2BCT ; YO3DDZ ;
- Russia : UA3PTW ; UA4HTS ;
- Poland: SP6JLW
- Sweden : SM6CKU ;
- Switzerland : HB9SV ; HB9BHU ;
- Czech Rep : OK1CA ; OK1KIR ; OK2AQ ;

Stations worked in SSB :

- DL0EF ; F1PYR ; LX1DB ; OZ1LPR ;

Louder stations : DL0EF ; OH2AXH ; SP6JLW ; OZ1LPR ; DL7YC ; LX1DB ; OK1CA ; OK1KIR;PA0BAT; UA4HTS;

Projects:

We plan to test soon PB8 on 24GHz but we must still work on the automatic tracking system because we need an accuracy better tha 0,05°.

On June 13/14 TM8PB team will participate at the 5,7 GHz Dubus contest.

Many thanks to all ORPB society members for their oustanding help

- Lucien Macé F3ME : PB8 tracking system and PB8 assembly
- André Gilloire : PB8 assembly
- Sylvain Meyer F6DBI : PB8 assembly
- Jean-Pierre Blot : 10GHz feedhorn design
- Olivier Boeffard : tracking system

2015-05-29 Guy F2CT

TM8PB op

F2CT - Activity week-end 2015 october 24-25

Guy Gervais (email: f2ct@wanadoo.fr)

Abstract

In may 2015, new tests on 10GHz EME were made with Cassegrain 13m PB8 dish with an optimized septum feed. More than 25 qsos were made in CW and SSB with only some watts at feed due to high losses in the coaxial RX/TX links.

So we decide to design a 24GHz feed with the help from Jean Pierre Blot, antennas engineer.

The new simulations and design draft from Jean-Pierre Blot:

24 GHz feed Simulation

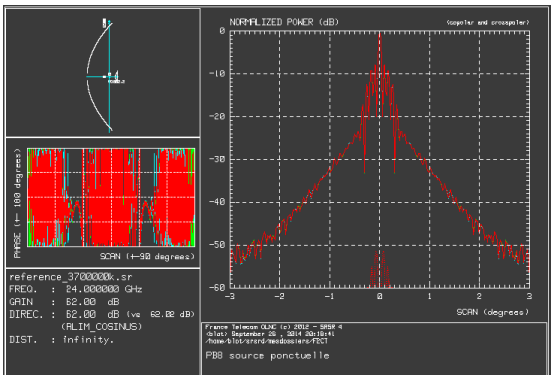

sub-réflecteur position

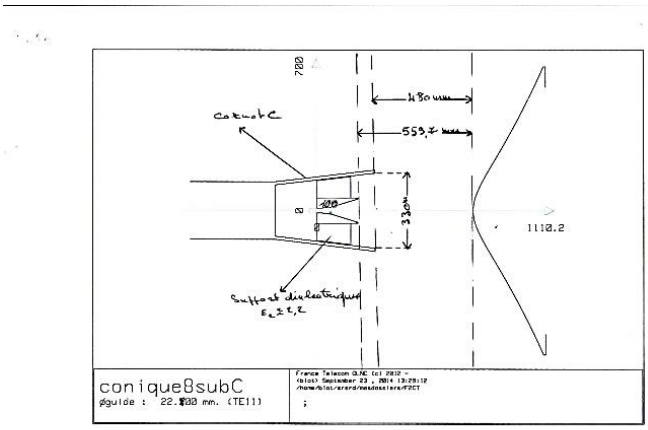

feed assembly

- RL @ 24048 GHz: - 30dB

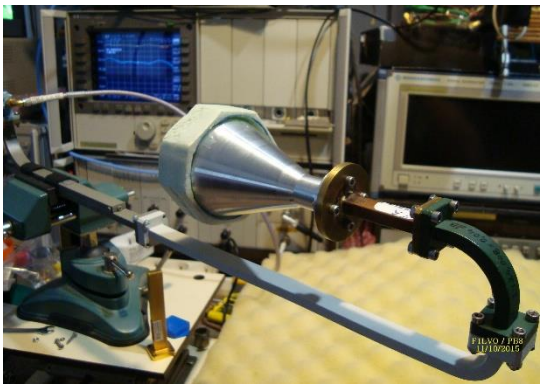

24 GHz setup :

- receiving:
- DB6NT LNA 1,5 dB NF
- Homebrew converter 432/24048 MHz

- Transmitting:
- 12 W SSPA
- Homebrew transverter 432MHz/24 GHz

The Shack :

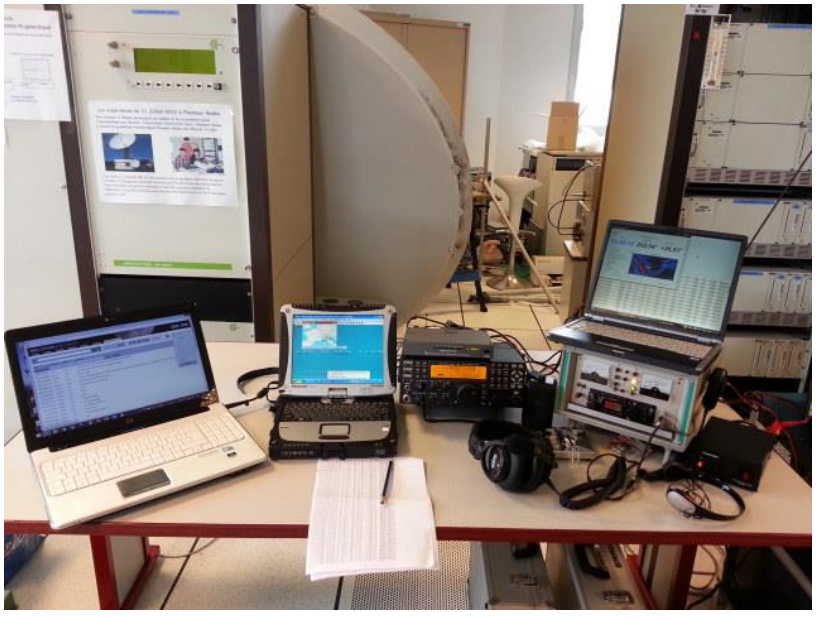

K3 + 432/28MHz tvt + Doppler shift compensation

PB8 with 24 GHz set up

Results :

- Sun noise test on saturday october 24 th at 1400 utc : 17,7dB (SF 106.3)

Saturday october 24: 17h30 utc:

- Moon noise: 2,8 dB / 1kHz BW
- Echoes: 6,5dB / 1kHz BW

Sunday October 25 th 1830 utc:

- Australia: VK3NX; VK7MO (JT)
- Germany: DL7YC only RX
- England: G3WDG; G4NNS
- Denmark: OZ1FF (JT)
- Spain: EA3HMJ (JT)
- US: W5LUA
- France: F1PYR; F2CT
- Netherland: PA0BAT
- Japan: JA1WQF; JA4BLC; JA6CZD
- Luxembourg: LX1DB
- Sweden: SM7FWZ only RX
- Czech Rep: OK1CA; OK1KIR

Stations worked in SSB:

- LX1DB; 55/53;

Stations worked in CW:

- LX1DB; OK1CA; OK1KIR; JA4BLC; PA0BAT

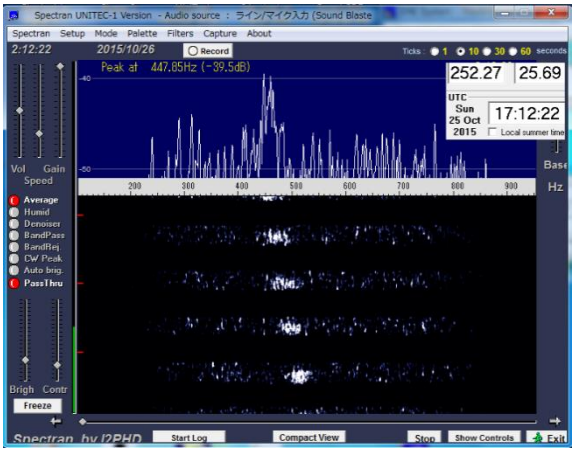

JA4BLC echoes

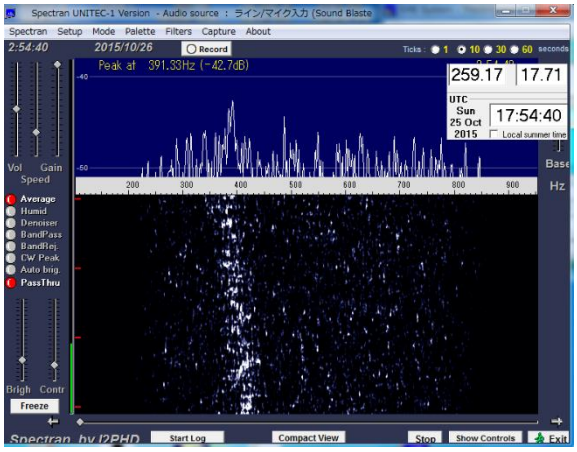

F2CT at JA4BLC

Stations heard in CW and JT: G3WDG; OZ1FF; F1PYR;

On Monday morning, we put down the 24GHz feed system and found two failures:

- Feed horn was at 4 lambdas from the phase center
- a ground solder on the TX semi rigid coax was broken ; power at the feed was only 2,48W !!!

Projects :

We plan to make a new 24GHz optimized feed and to put the 45W TWT just near the feed.

Now the position accuracy on the new automatic tracking system accuracy is better than 0,05°.

On 24GHz, PB8 aperture is 0,067°.

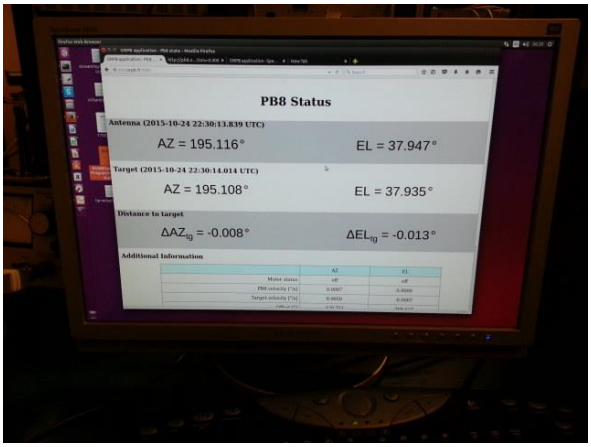

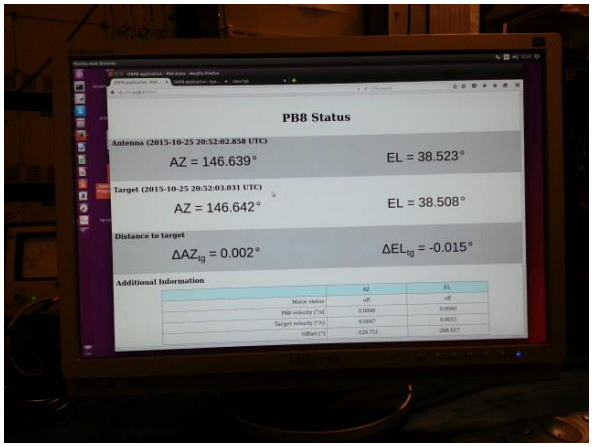

On the upper line the Moon target; on the lower the real position of PB8; the error is between 0,008 and 0,015 ° !

ORPB society received his new call sign F4KJM that will be used during 2016 EME events.

The 6cm EME beacon will be soon on 5760,188 MHz with 20W at feed.

Call sign will be F4KJM/B;

F4KJM will participate into the next Dubus and Arrl microwave contests

Many thanks to all ORPB society members for their oustanding help

- Lucien Macé F3ME : PB8 tracking system design and PB8 assembly
- André Gilloire : PB8 assembly
- Sylvain Meyer F6DBI : PB8 assembly
- Jean-Pierre Blot : 24 GHz feedhorn design
- Olivier Boeffard : tracking system design

2015-11-10 Guy F2CT

TM8PB/F4KJM op

Patronages for the EME2016 Conference:

Associazione Radioamatori Italiani

National Management Committee

Veneto Regional Committee

Mestre Local Chapter

Treviso Local Chapter

Laguna Veneta Contest Team

Amsat Italia

DUBUS

Collegio dei Periti Industriali e dei Periti Industriali Laureati di Venezia

G3WDG - Experiences with Circular Polarisation on 10GHz

Charlie Suckling (e-mail: charlie@sucklingfamily.free-online.co.uk)

Introduction

Newcomers to 10GHz EME often ask whether they should use linear polarisation (LP) or circular polarization (CP). While CP has been adopted as the "standard" for a number of years, many stations are still using linear. CP requires more investment in both the time and effort required to build a feed, or the higher cost of buying one ready-made. For smaller stations, who might want to try out their tropo systems on EME, the attraction of using LP is clear. My expectations of CP, based on experience on the lower microwave bands, and some publications (Ref 1), was that it would have identical performance to LP in terms of signal to noise ratio on the EME path, be 3dB down with stations using LP, and might offer some advantage in having narrower spectral width.

The objective of this work was to explore experimentally what CP has to offer, apart from the clear advantage of being immune from spatial offset losses which can be encountered when linear polarization is used.

Building and testing a feedhorn

I do not have access to machine tools, so I investigated a number of designs with respect to construction difficulty (and of course performance related to antenna efficiency and G/T). The designs that seemed most suitable were the 0.692 and 0.760 wl "Kumar" types of SM6FHZ (Ref 2), which use readily available tubing sizes, so that use of a lathe would not be required. SM6FHZ noted that the 0.760 wl feed might be more forgiving of constructional tolerances, but as it had lower predicted efficiency with my 0.3 f/D 3m dish, both versions were built for later comparison. These feeds are also very compact and lightweight. To date, only the 0.692 wl feed has tried and as it had excellent performance, on-air tests of the 0.760 wl version have not yet been performed.

The first problem to be overcome was how to mark out the location of the septum, and also the positions of the feed probes, with sufficient accuracy. The second problem was to be able to fabricate the septum itself with high dimensional accuracy, and lastly to find ways of soldering it all together. Photographs of some key stages in the construction are shown in Fig 1, including method of cutting the pipe, marking out the position of saw cuts for the septum, the use of photo etching to define the dimensions of the septum, employing solder paste to ensure good quality soldering, and SM6PGP's method of locating the choke in the correct position (Ref 3). Further details are given in Ref 4.

The return loss and isolation of the feed were measured, both with the horn radiating into free space, and with a metal plate held firmly over the mouth of the feed. The latter measurement showed little change in the return loss and the isolation dropped to a few tenths of a dB, indicating that the resistive loss was low and the axial ratio must be good. With a poor axial ratio, the reflection from the shorting plate would have caused as a significant change in return loss and a higher isolation figure.

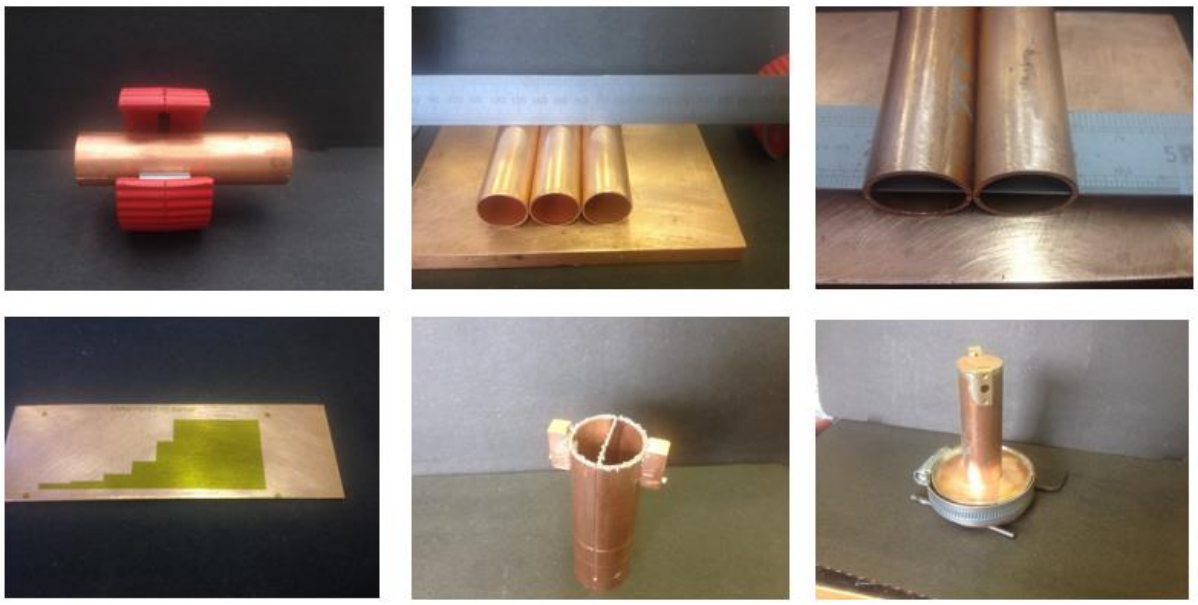

Fig 1 Some key stages in the construction of the feedhorn

Attempts were made to measure the axial ratio of the feed, by rotating a waveguide to coax transition connected to the transmission detector on the scalar analyser, but this was difficult to do accurately owing to stray reflections. The results looked promising however, and were confirmed by an EME test with OK1KIR, who have the ability to rotate their LP feed to defined angles. The results of this test are shown in Fig 2.

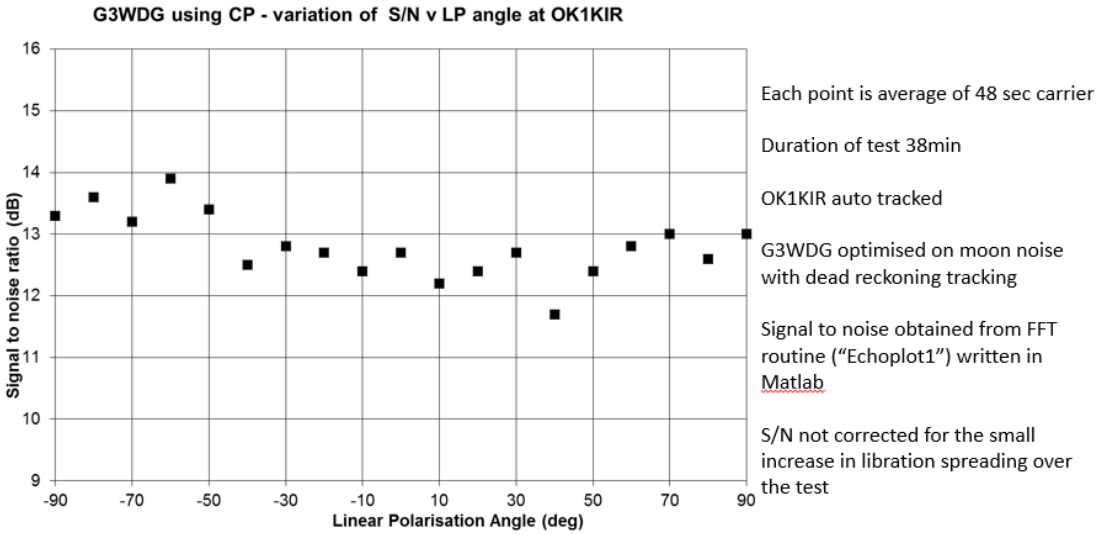

Fig 2 Signal to noise ratio of G3WDG's CP signal at OK1KIR as a function of LP angle

Development of software to measure S/N ratio of EME signals

While it may have been possible to adapt existing software to analyse the S/N of EME signals, I decided to write some custom software to perform the measurements I was interested in. Two Matlab programs were written, 'Echo" to obtain repeated echoes automatically similar to WSJT-X's Echo mode, and a modified version ('Echoplot') to analyse single tone recordings of other stations. The 'Echo' program generates a 1000Hz tone for 3s, records and saves the first 2.5 sec of the echo as a wave file, performs a FFT of the 2.5s echo, displays a linear power

graph of the echo and saves this as an image file. In addition, the FFTs of each individual echo are added together, displayed with a dB scale, and saved after each echo as an image file.

Signal to noise ratio is then obtained by averaging the noise level of the added echoes either side of the 1000Hz echo tone, sufficiently far away from the spreading of the signal, and subtracting the average of the two from the peak signal as shown in Fig 3, and finally correcting for (S+N)/N to S/N. Doppler correction used OK2AQ's Matlab Dopp software (Ref 5) controlling a 58MHz DDS in the 28/144MHz transverter.

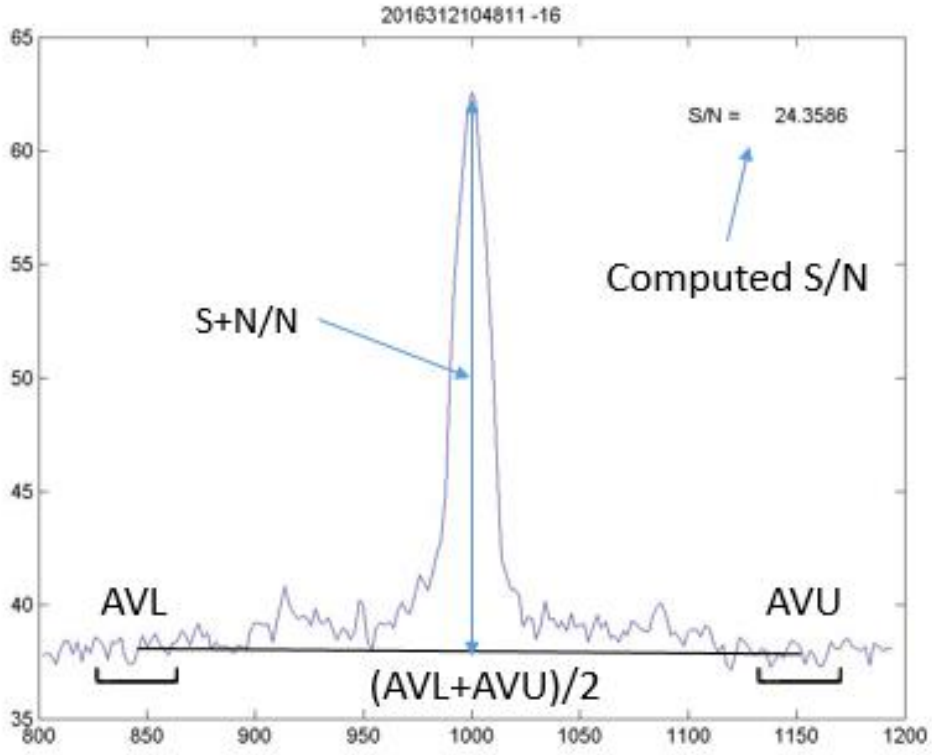

Fig 3 Obtaining the S/N ratio of an echo

The reason for adding echoes before obtaining the S/N is that as the echoes are added the variation in the noise level is reduced allowing a more accurate value to be obtained, as shown in Fig 4.

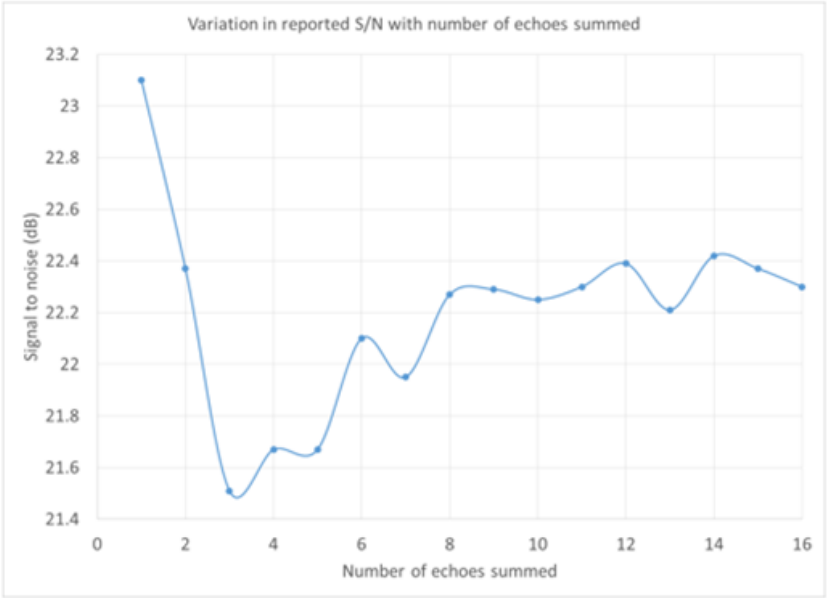

Fig 4 Reduction in S/N error by using multiple echoes

The relative accuracy of the Echo program in determining S/N was checked by performing a series of echo tests at different TX power levels, from 100W down to 0.5W. The following results were obtained:

Power	actual dB difference	measured S/N difference
100W	0	0
50W	-3.0	-2.8
2W	-17.0	-16.7
0.5W	-23.0	-22.3

Checking sense of CP: RHCP or LHCP?

Following on from the tests with OK1KIR to check axial ratio, the next set of tests were done to verify that I had identified the feed's TX and RX ports correctly. To achieve this, I reconfigured my feed so that preamp could be switched between the TX and RX ports of the feed remotely. The loss to the TX port was about 0.5dB higher than to the RX port, reducing system sensitivity by about 1dB according to EMECalc with moon noise included.

The first tests CP to CP tests were with HB9Q, and showed a stronger signal using my TX port compared to the RX port, which was unexpected! WSJT-X waterfall plots of HB9Q's signal are shown in Fig 5.

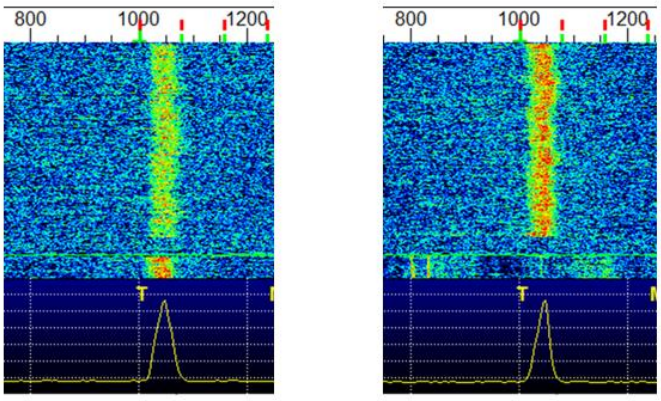

Fig 5 HB9Q's CP signal received at G3WDG using RX and TX ports

Analysis of the recordings using Echoplot showed the difference in S/N between the TX and RX ports to be 6.4dB, allowing for the extra loss in the path from the preamp to the TX port. I was surprised to see such a small difference between RHCP and LHCP. Experience with cross-polarised LP signals on 10GHz was more in the region of 10-11dB difference in levels.

A second CP-CP test was done shortly after, with LX1DB. This time the signal was stronger on my RX port, and Echoplot measured the difference in levels (Cross Polar Discrimination or XPD) as 8.0dB, as shown in Fig 6. Later visual checks at HB9Q showed that their feed's TX/RX ports had been reversed.

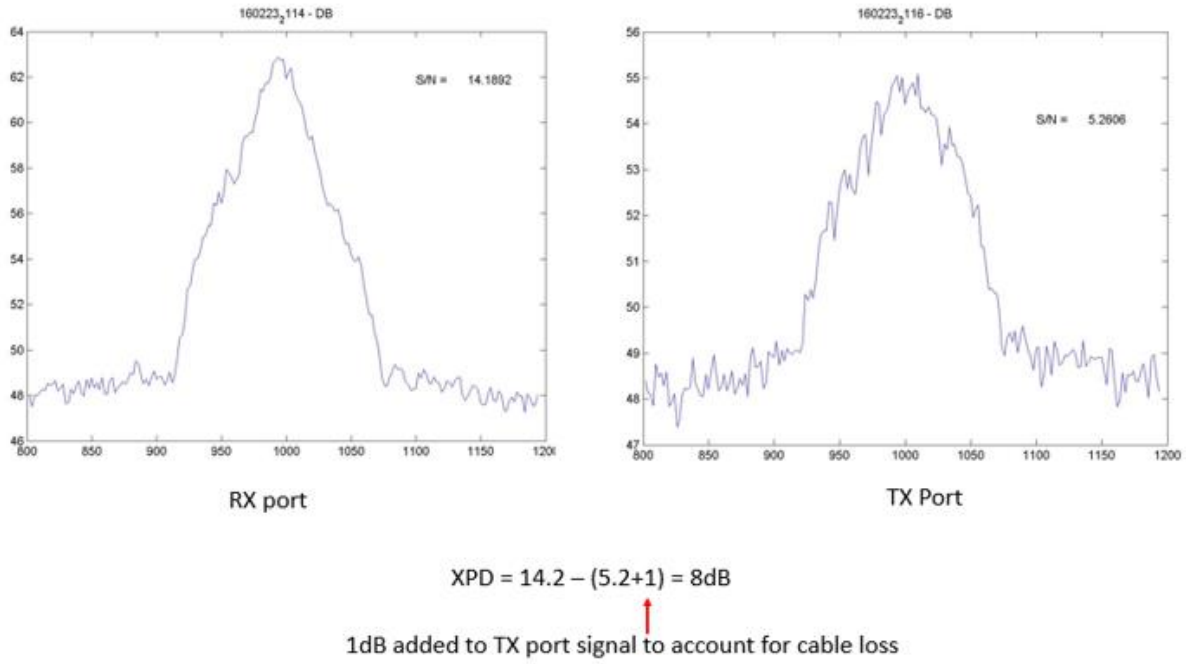

Fig 6 CP signal from LX1DB received on RX and TX ports of G3WDG's CP feed

After these tests I checked again how to identify the TX and RX ports of a septum feed, and found a clear definition in SM6FHZ's paper, reproduced in Fig 7.

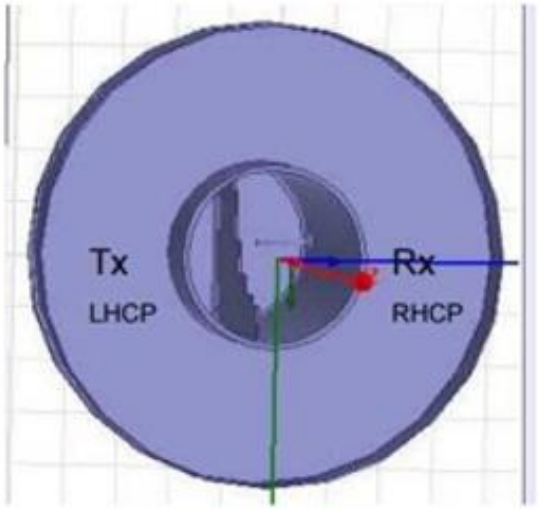

Fig 7 Identification of TX and RX ports on a septum feed

Looking into the mouth of the horn, with the thinnest segment of the septum at the bottom, the RX port is on the right and the TX port on the left. The TX port actually generates LHCP, but this is reversed by reflection from the dish to produce the standard RHCP. It does not matter whether the launches are probe or waveguide, it is whether they are to the left or right of the septum that defines the sense of CP.

Echo tests to compare CP to CP and LP to LP

In order to see whether CP to CP and LP to LP produce comparable levels of EME signals, a series of own echo tests were done over a number of days around the March 2016 perigee. On each day, one feed was installed and a series of tests made in sequence, while the signal width reduced towards the minimum for that day. At the time of minimum signal width, the feeds were swapped quickly and tests resumed. In this way, data could be taken at the same values of signal width to enable fair comparisons to be made, as the S/N was found to vary with signal width. On the next day, the sequence of feeds used was reversed. The LP feed used was identical in dimensions to the CP feed, except that it was fed from the rear by a tapered waveguide. In this way it was hoped that the radiation patterns of the LP and CP feeds would be the same. Receive sensitivity on CP was 0.4dB worse than LP (feed to preamp SMA-WG transition), while TX loss on LP was 0.7dB higher (extra SMA interconnect cable).

The moon elevation was always between 15-35 degrees. In past tests, echo signal levels, and moon/sun noise, have been reasonably constant over this range. Output power at the feed was 80W for all tests.

As noted above, it was found that the measured S/N was strongly dependent on the width of the signal. This can be seen in Fig 8, where the results of a number of tests on different days are shown. It can also be seen that the signal levels for the CP echoes were lower than for the LP echoes. Taking the average over a set of 8 tests, the CP echoes measured 1.3dB lower than for LP. Taking into account the differences in loss on transmit and receive, from a system performance point of view the CP echoes should have been 0.3dB stronger, making the actual CP echoes some 1.6dB down.

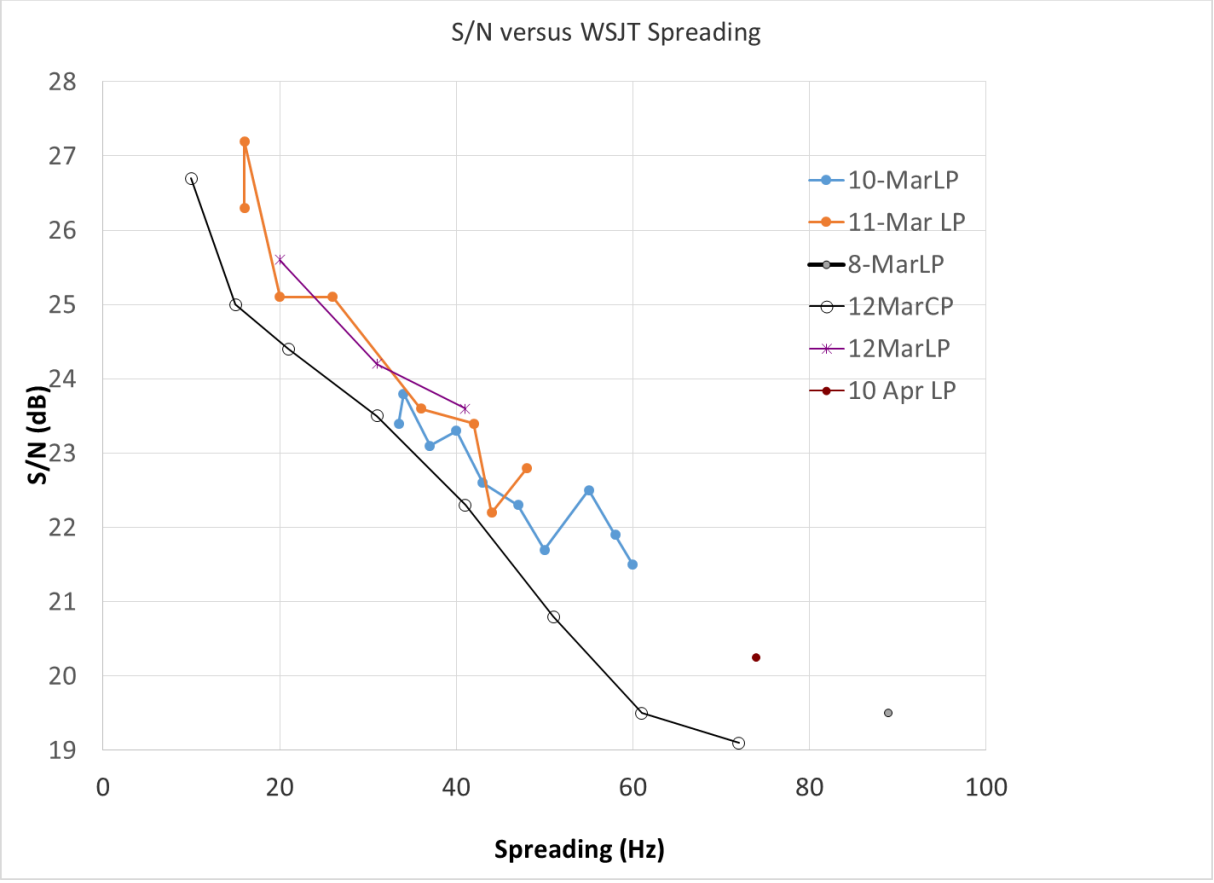

Fig 8 Variation of signal strength versus signal spreading (WSJT-X predicted 'Width')

Comparison of Echo shapes

Prior to the use of the Echo software, attempts were made to use some error-corrected WSJT-X 'fast' modes, which had message lengths shorter than 2.5s, to compare decoding success with LP and CP. The theory was, that narrower signals would produce more decodes under conditions where the signal spreading was equal to or larger than the tone spacing. Echoes were obtained with a number of JT9 'fast' modes, and JTMSK, and no significant differences could be seen between LP and CP. In fact with modes requiring high signal coherence, such as JTMSK, LP seemed slightly superior (probably owing to the higher S/N, discovered later).

Following this, it was noticed when using Echo, every return looked different. In a set of 16 echoes for example, some were very narrow, while others were wider. Examples of LP and CP individual echoes, all obtained with a spreading of 41Hz, are shown in Figs 9. For the same spreading, Fig 10 shows the accumulated plot of 16 echoes, on a log scale. From these tests, no significant difference in signal width were observed. Archives of these files can be made available on request.

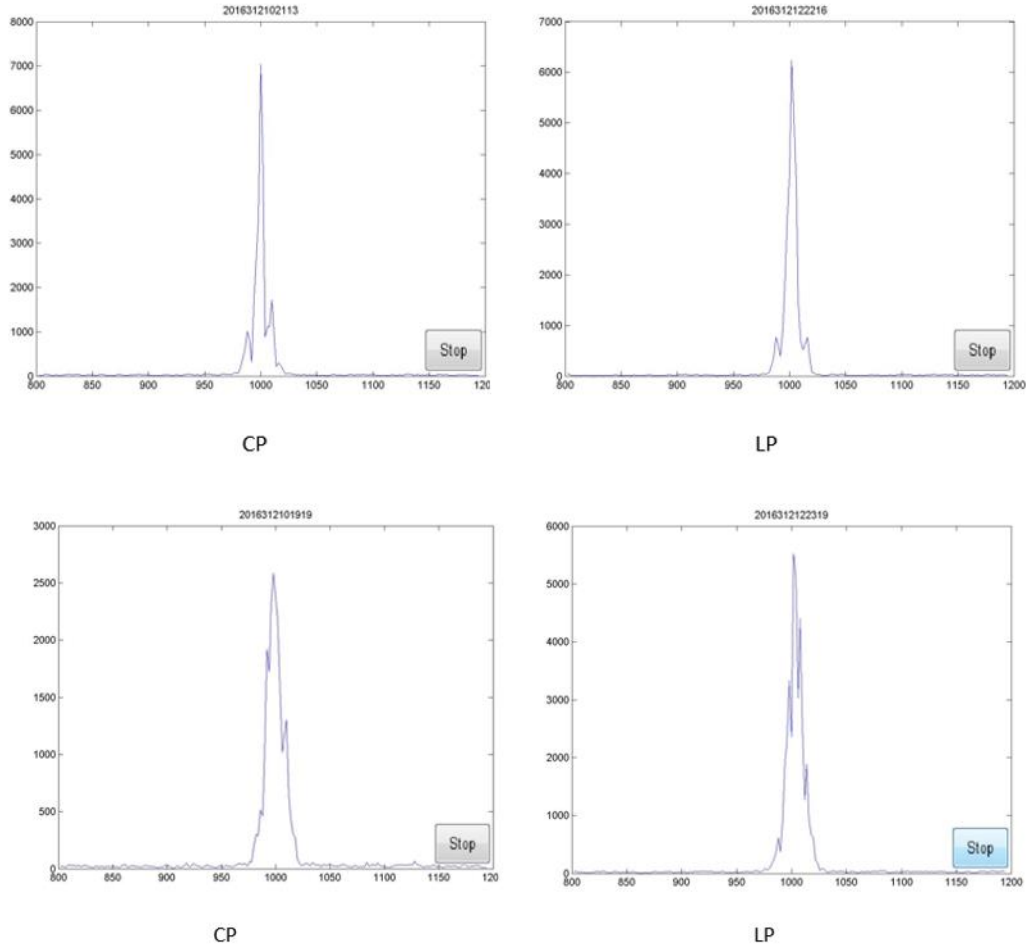

Fig 9 Linear power plots of individual echoes, with predicted signal width of 41Hz

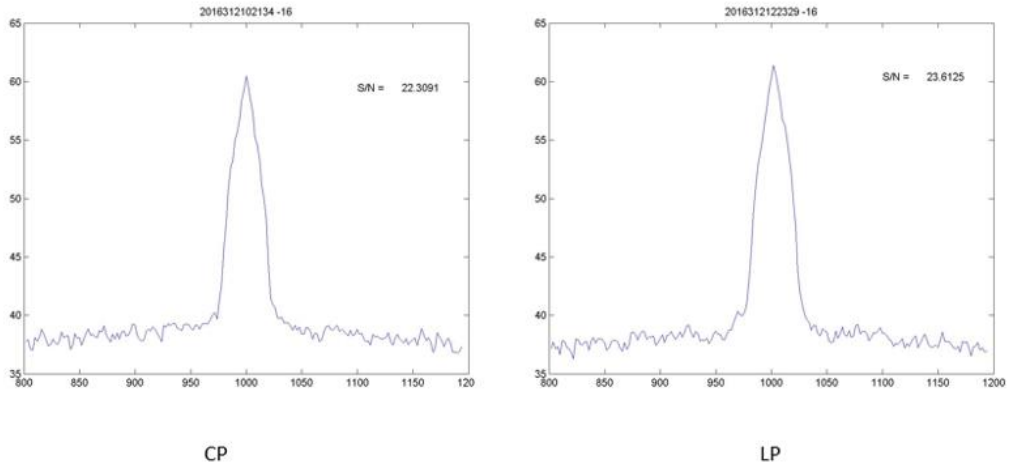

Fig 10 Log power plots of 16 accumulated echoes, with predicted signal width of 41Hz

Comparisons of LP to CP and CP to CP with LX1DB

After the tests with LX1DB reported above, where we both used CP, LX1DB changed to LP, using a feed with similar radiation characteristics to his CP one. His LP transmissions were received on both the TX and RX ports of my CP feed, and the results are shown in Fig 11.

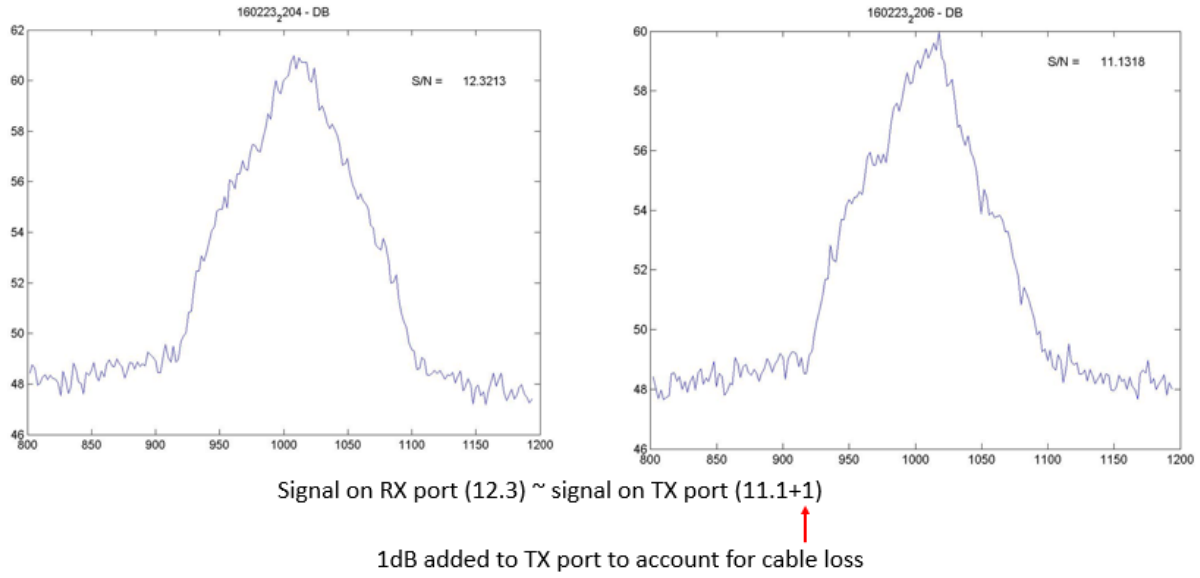

Fig 11 LP transmission from LX1DB received on TX and RX ports of G3WDG's CP feed

After accounting for the 1dB lower sensitivity of using the TX port on my feed, the levels of the signals are almost identical, as expected. What was not anticipated however, was that the S/N in the LP to CP test (12.2dB) was only 2dB down on the earlier CP to CP test (14.2dB), done only 30 minutes earlier with almost the same spreading. LX1DB noted in later discussions of these results that this lower than expected difference is something he has also noticed in the past.

Discussion

The lower S/N of CP-CP signals compared to LP-LP on the same system, together with only 2dB loss LP to CP and the observed 6.5-8dB XPD of CP to CP, seem to suggest that on 10GHz CP signals suffer more depolarization losses than LP, but the reason for this is not clear. This topic is discussed in Refs 6 and 7, where for the size of dishes used in all the tests in this paper a XPD figure of 6.5dB has been predicted theoretically. This alone would account for some of the observed apparent lower performance of CP, since nearly 25% of the returned power from the moon is "lost" into the opposite polarisation. The same reference suggests that little of this depolarization happens in the antennas, so must be largely down to the reflection at the moon.

Summary of findings

On 10GHz:

CP to CP performs somewhat worse than LP to LP

CP to LP only has 2dB loss

CP signal widths are the same as with LP

For tests under marginal conditions LP to LP with allowance for spatial offset is best.

Acknowledgements

I would like to thank OK1KIR, LX1DB and HB9Q for their contributions to this work and for many valuable discussions, and SM6FHZ for proof reading this paper and his useful suggestions.

References

1. http://lea.hamradio.si/~s57uuu/emeconf/ltsgocir.htm
2. http://www.2ingandlin.se/10GHz%20septum%20feeds%20for%20EME_A.pdf
3. http://www.illipe.se/EME_2013/Building_the_FHZ_Kumar_feed_by_SM6PGP.pdf
4. Experiences with building septum CP dish feeds without machine tools by Charlie Suckling, G3WDG DUBUS 4/2015 _http://tinyurl.com/zwbxrcv
5. A New Method for Microwave EME Doppler Shift Compensation by Mirek Kasal, OK2AQ and Charlie Suckling, G3WDG DUBUS 1/2016 http://www.urel.feec.vutbr.cz/esl/files/EME/Doc/Documents.html
6. http://www.attplus.cz/hamradio/projekty/article/cppl_b.pdf
7. http://www.om6aa.eu/Introduction_10_FV.pdf

K1JT - New Codes, Modes and Tools for Weak-Signal Communication

Joe Taylor (email: joe@princeton.edu)

WSJT-X: New Codes, Modes and Tools for Weak-Signal Communication

Joe Taylor
K1JT

EME Conference
Venice
Aug 21, 2016

"JT" Weak-Signal Software

- ***WSJT*** – VHF-and-up: meteor scatter, EME, ionoscatter, aircraft scatter, …
- ***MAP65*** – Wideband EME, adaptive polarization
- ***WSPR*** – Quasi-beacon mode, QRP propagation testing
- ***WSJT-X*** – All bands, many modes
  - ➔ Many VHF-related features
  - ➔ >4000 users, world-wide

WSJT-X

G3WDG received at OK1KIR

JT9E-H 10 GHz

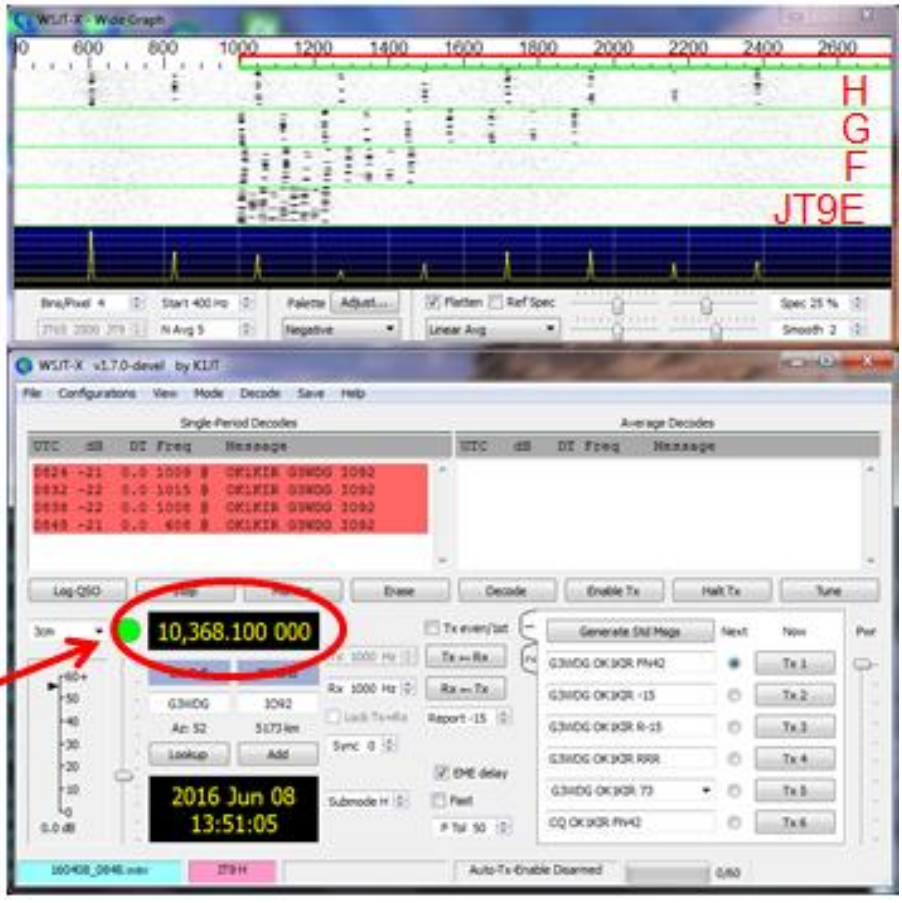

Codes ? Modes ??

- "Code" – symbols to represent information
  - Character-by-character: Morse (CW), baudot, ASCII, FSK441, JTMS, …
  - Block messages: Reed-Solomon, Convolutional, Turbo, LDPC, QRA …

- "Mode" – signaling method and protocol: coding, modulation, symbol rate, block size, …
  - SSB, CW, FSK441, JT65, JT4, JT9, JTMSK, …

JT4, JT9, JT65, JTMSK, …
Block-Structured Messages
Standard QSO

CQ K1ABC FN42

K1ABC W9XYZ EN37

W9XYZ K1ABC -22

K1ABC W9XYZ R-19

W9XYZ K1ABC RRR

K1ABC W9XYZ 73

Relevant VHF+ Propagation Types

Fading rates ↓

- Tropospheric scatter
- Multi-hop (weak) sporadic-E ?
- EME (VHF, UHF, microwave …)

} slow

- Ionospheric scatter
- Aircraft scatter
- Meteor scatter

} fast

Modes in *WSJT-X*

Scatter → "Fast"

- **ISCAT**
- **JT9 E-H**
- **JTMSK**
- **MSK144 ***

EME, QRP → "Slow"

- **JT65**
- **JT4**
- **JT9**
- **QRA64 ***
- **WSPR**

Echo

* Experimental

Why so many modes?

- Different propagation types
- Select code and optimize parameters for each purpose
  - Fading depth
  - Fading rate
  - Doppler spread
  - Stability and synchronizing requirements
- Also: learn as we go …

Mode design: Tunable parameters

- Block message structure
- Compression ➔ source encoding
- Error control coding
- Modulation type
- Bandwidth ➔ symbol rate
- Synchronization method
- Information throughput rate

Selected Mode Parameters

Mode	Block Code (k,n)	Q	Modulation	Symbol Rate (Hz)	Sync Fraction	Message Length (s)
JT4	206,72	2	4-FSK	4.375	0.50	47.1
JT9	206,72	8	9-FSK	1.736	0.19	49.0
JT65	63,12	64	65-FSK	2.692	0.50	46.8
QRA64 ?	63,12	64	65-FSK	2.692	0.50	46.8
JT9H fast	206,72	8	9-FSK	200	0.19	0.43
JTMSK	198,72	2	MSK	2000	0.15	0.117
JTMSK sh	24,12	2	MSK	2000	0.31	0.0175
MSK144 ?	128,72	2	MSK	2000	0.11	0.072

Recent Advances in *WSJT-X*

- Platform independence (Windows, Linux, OS X, …)
- Rig control for nearly all radios
- Accurate frequency calibration
- Added modes: WSPR, fast JT9, JTMSK, MSK144, QRA64
- Franke-Taylor decoder

Franke-Taylor Decoder for JT65

- Open source
- Soft decision
- Performs better than Kötter-Vardy
- *QEX* for May-June 2016 (link on WSJT web site)
- As implemented in *WSJT-X*, includes multi-pass decoding

Franke-Taylor Decoder

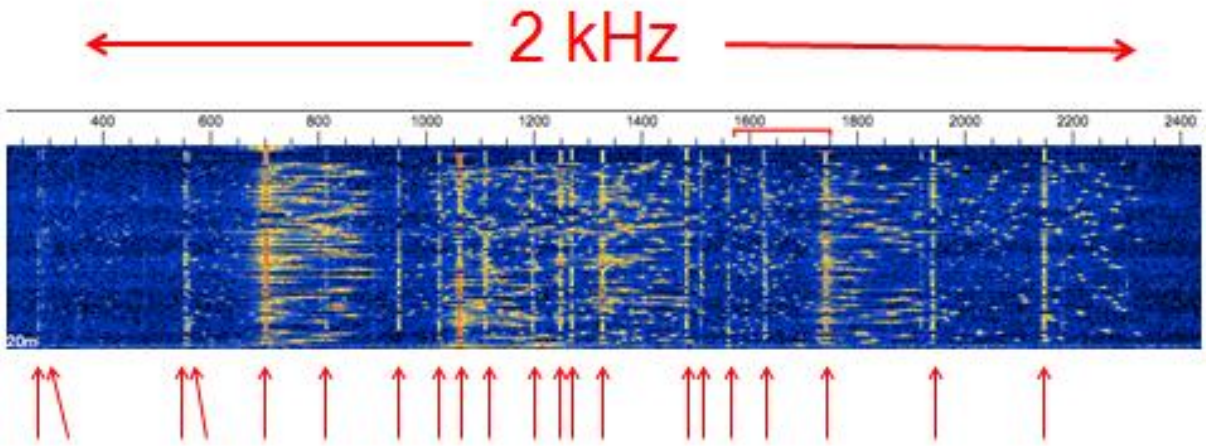

21 JT65A signals, all decoded !

New VHF+ Features in *WSJT-X*

- Transverter offsets
- JPL/NASA planetary ephemeris
  - ➔ Moon tracking, EME Doppler
- Automatic Doppler tracking
- Enhanced Echo mode
- Auto-sequencing for fast modes

… Brief guided tour …

WSJT-X Configuration

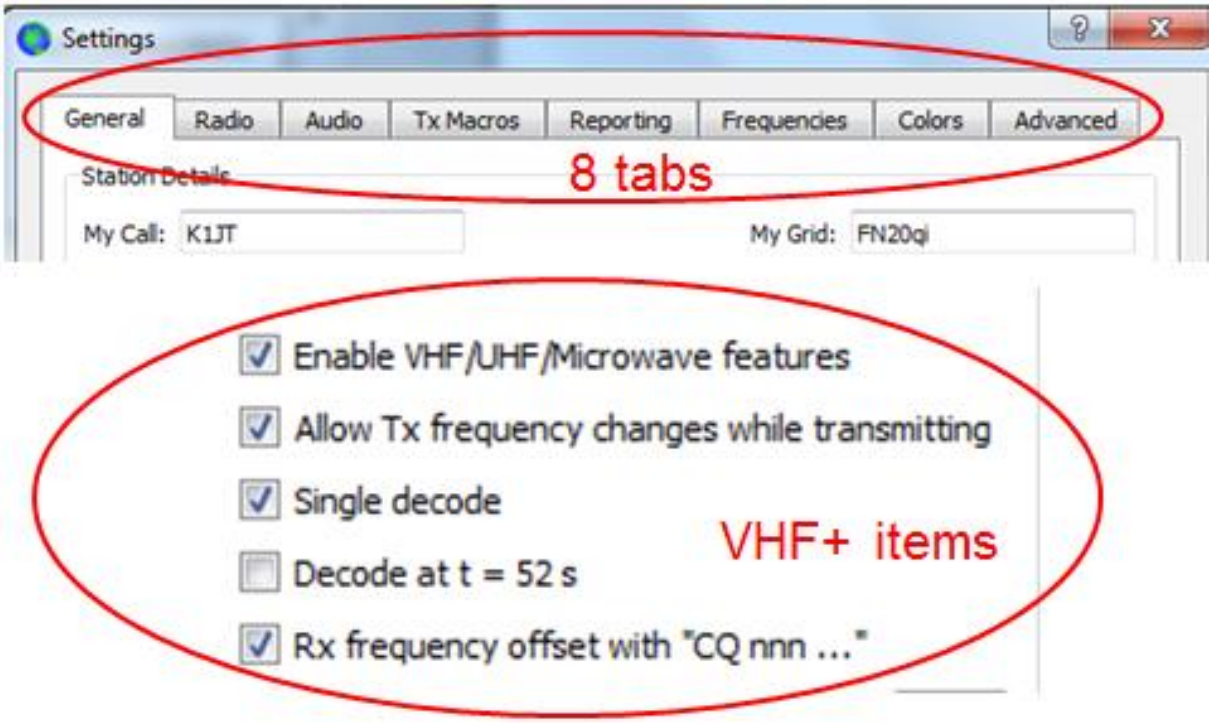

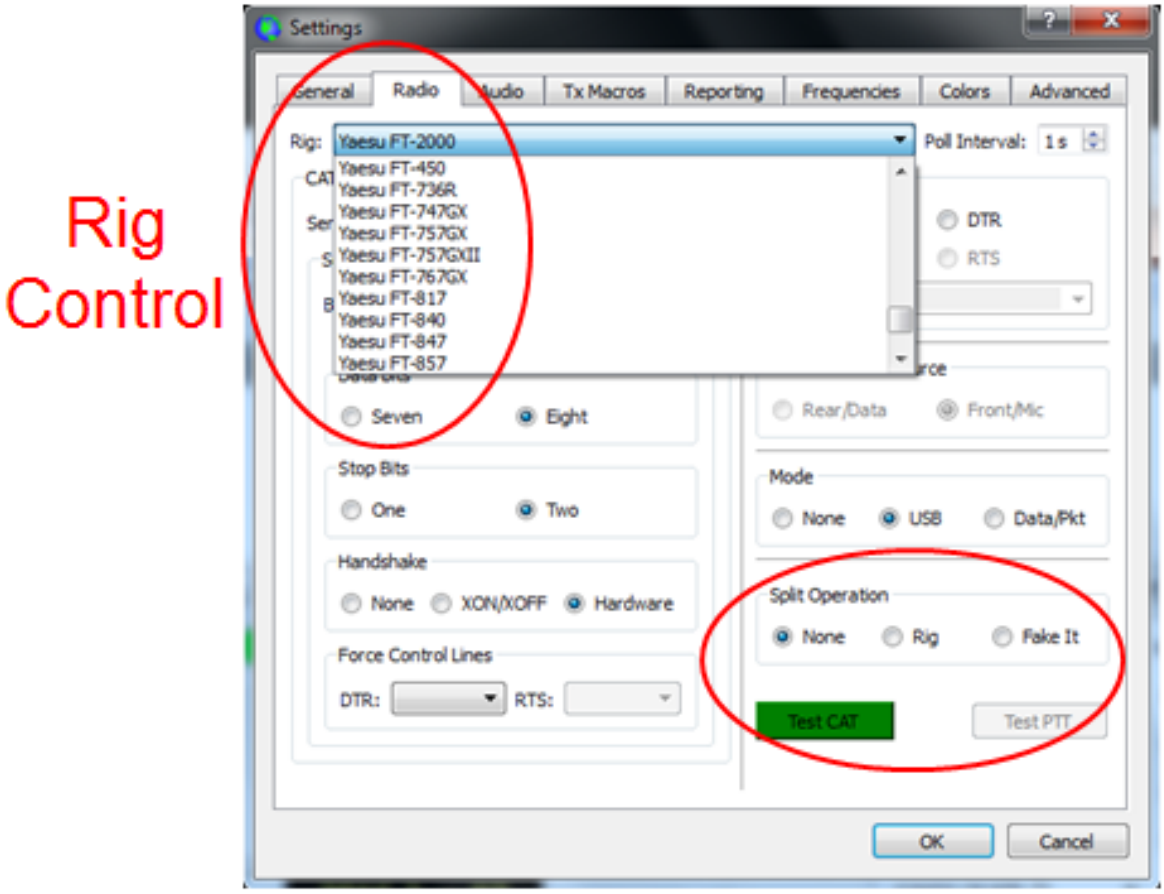

Frequency Settings

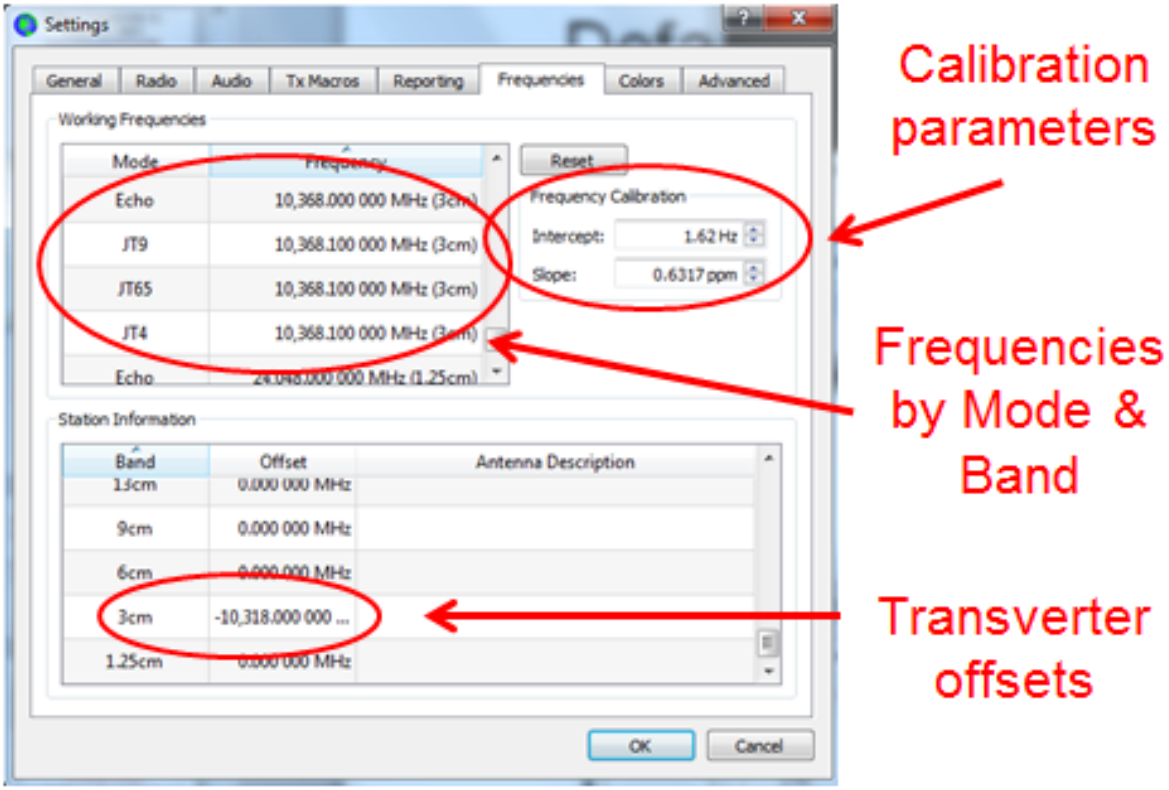

TS-2000X Frequency Calibration

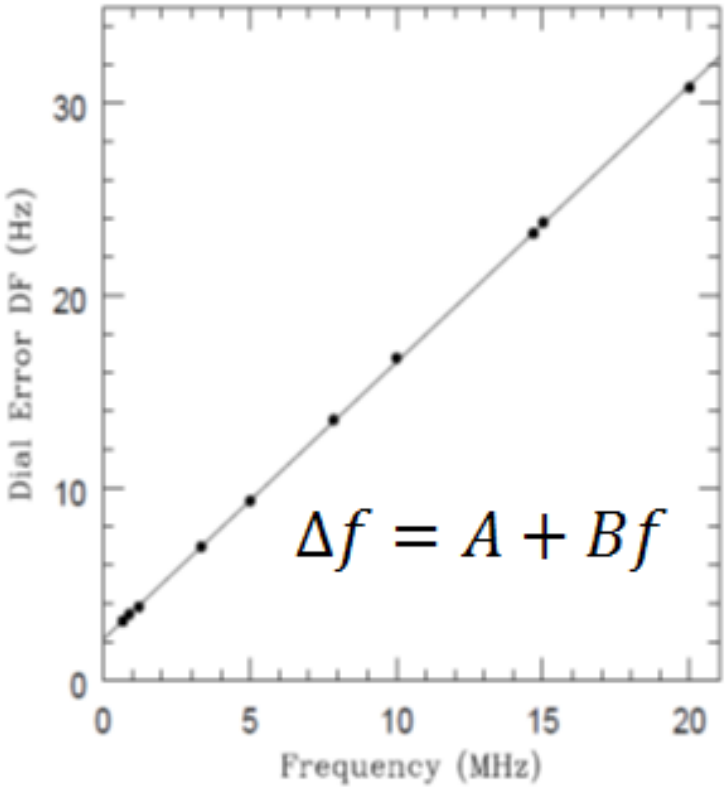

Automatic Doppler tracking

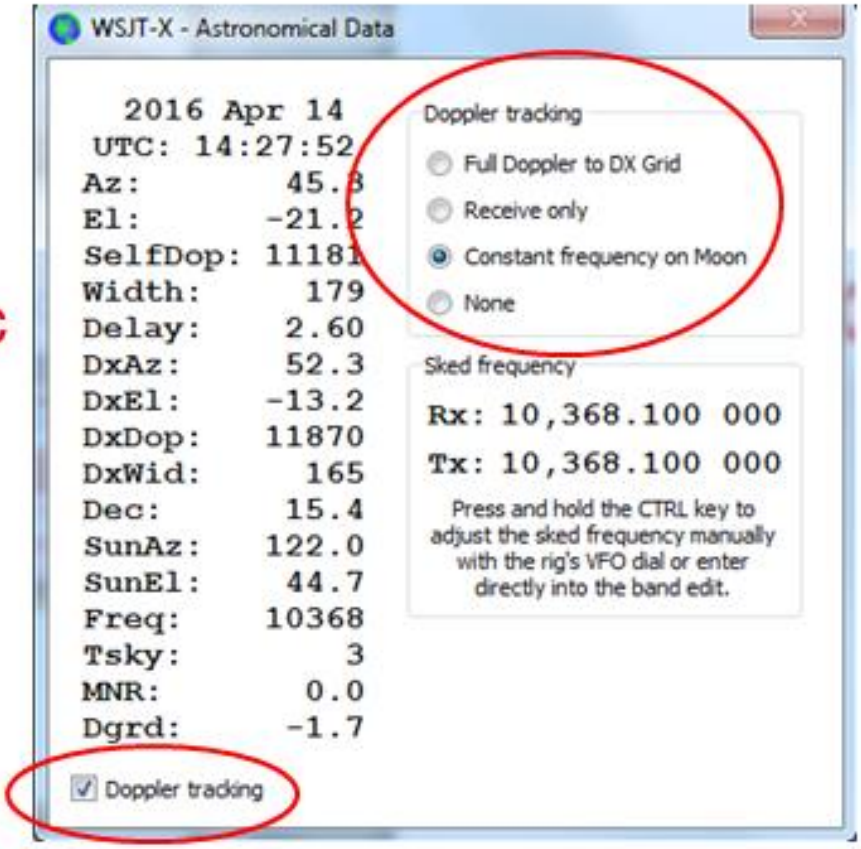

Echo Mode – G3WDG – 10 GHz

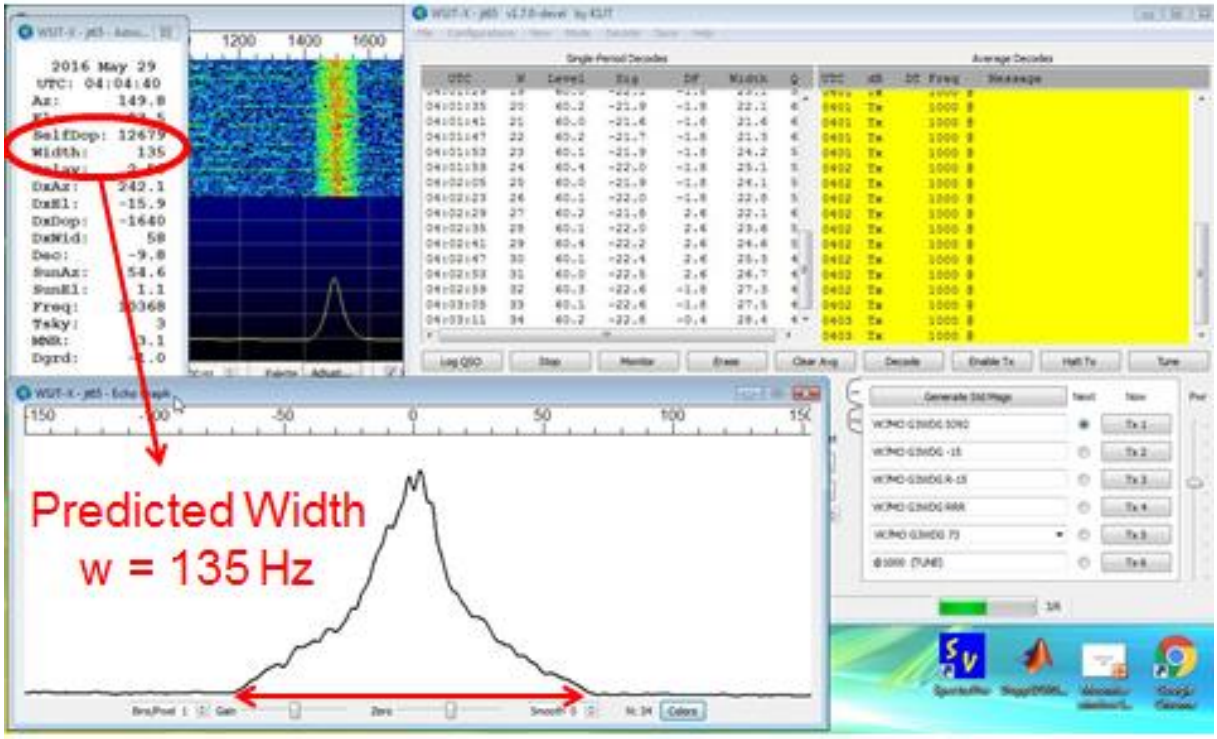

Single-pulse Echo

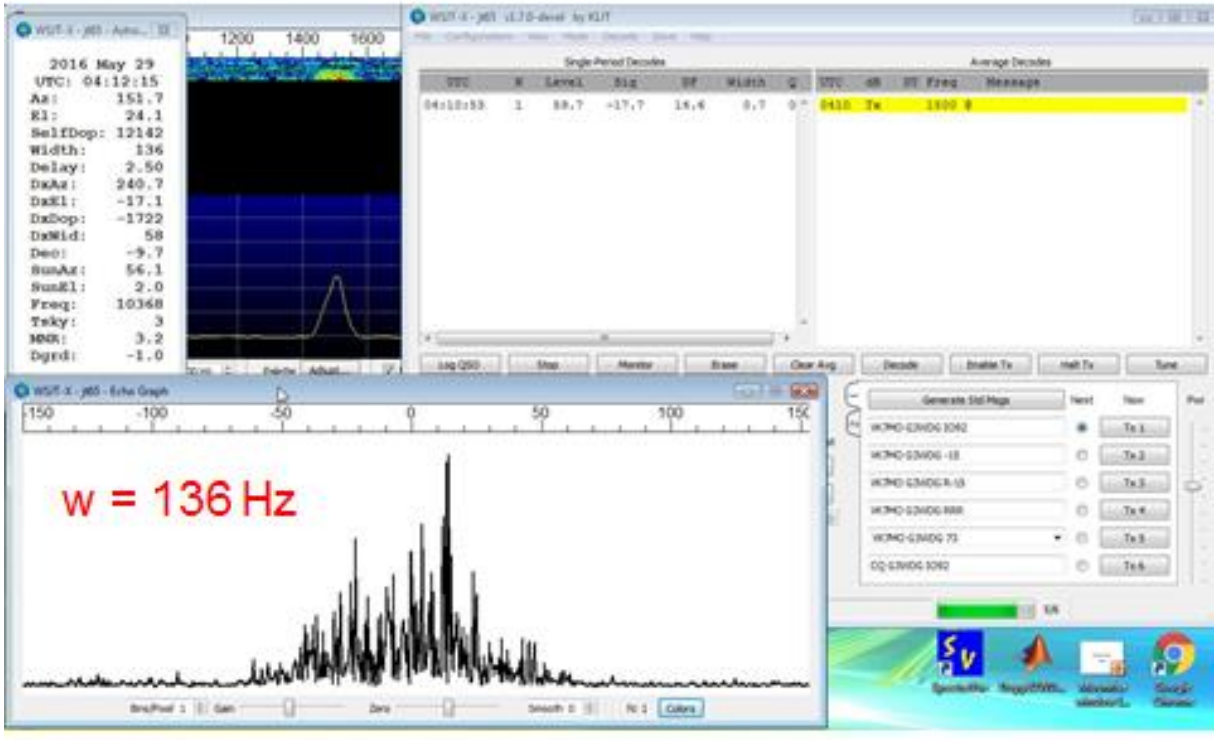

Doppler tracking by *WSJT-X*

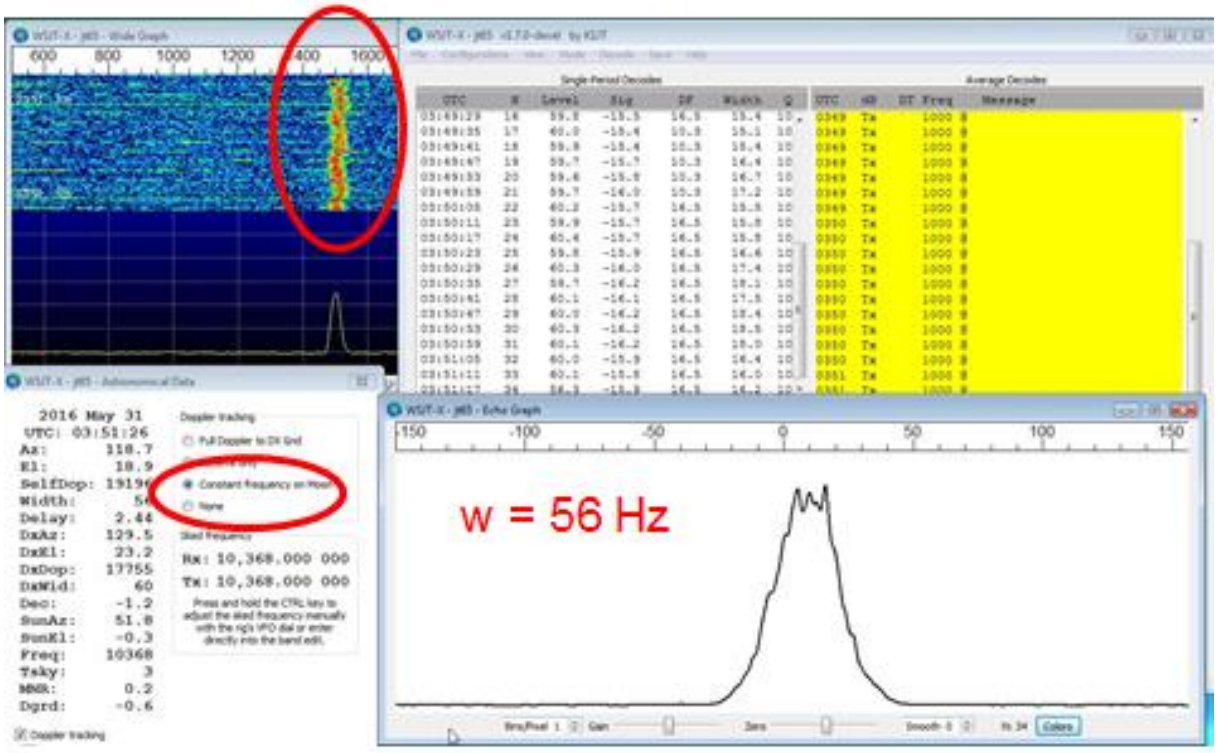

Doppler steering by transverter LO

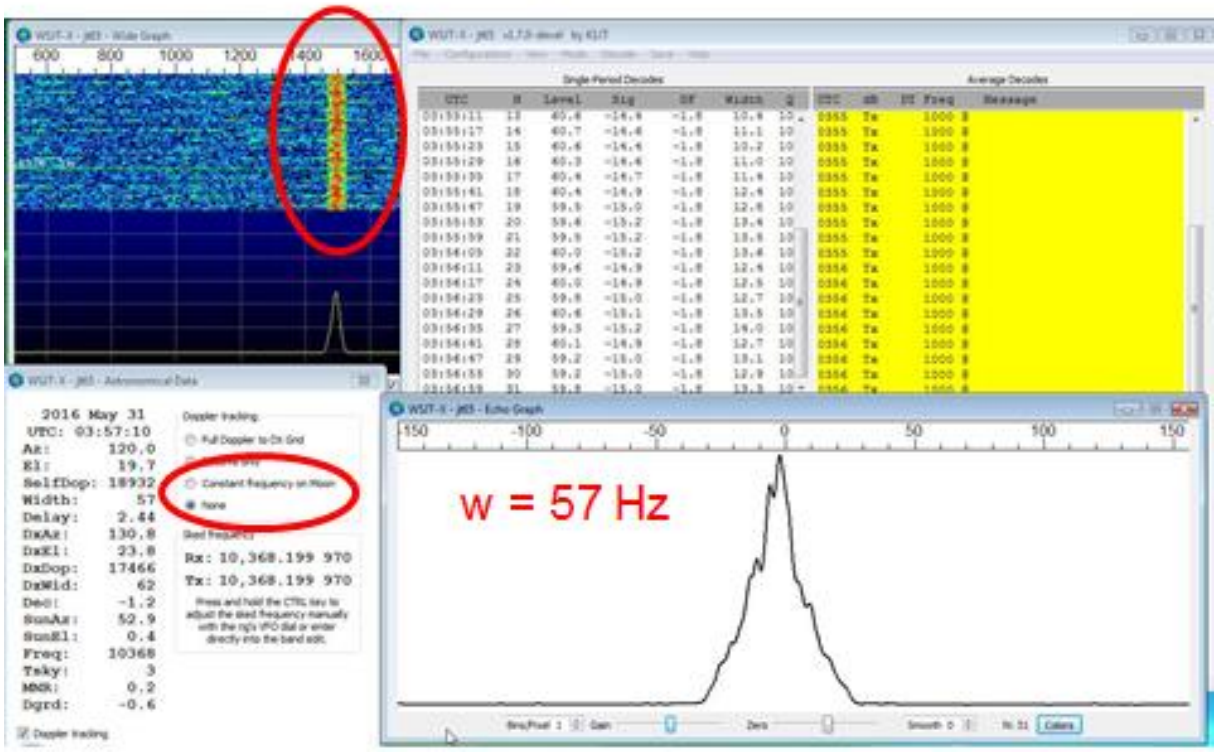

Close to libration minimum

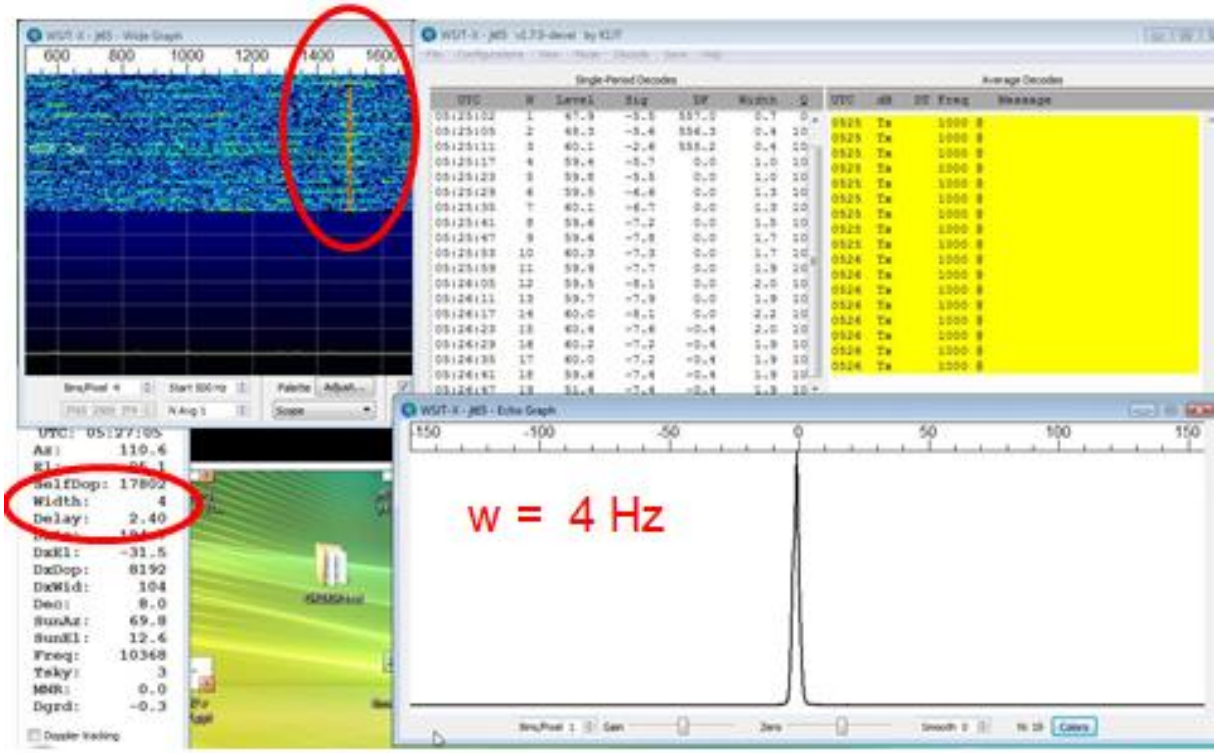

Just for fun: JTMSK echoes

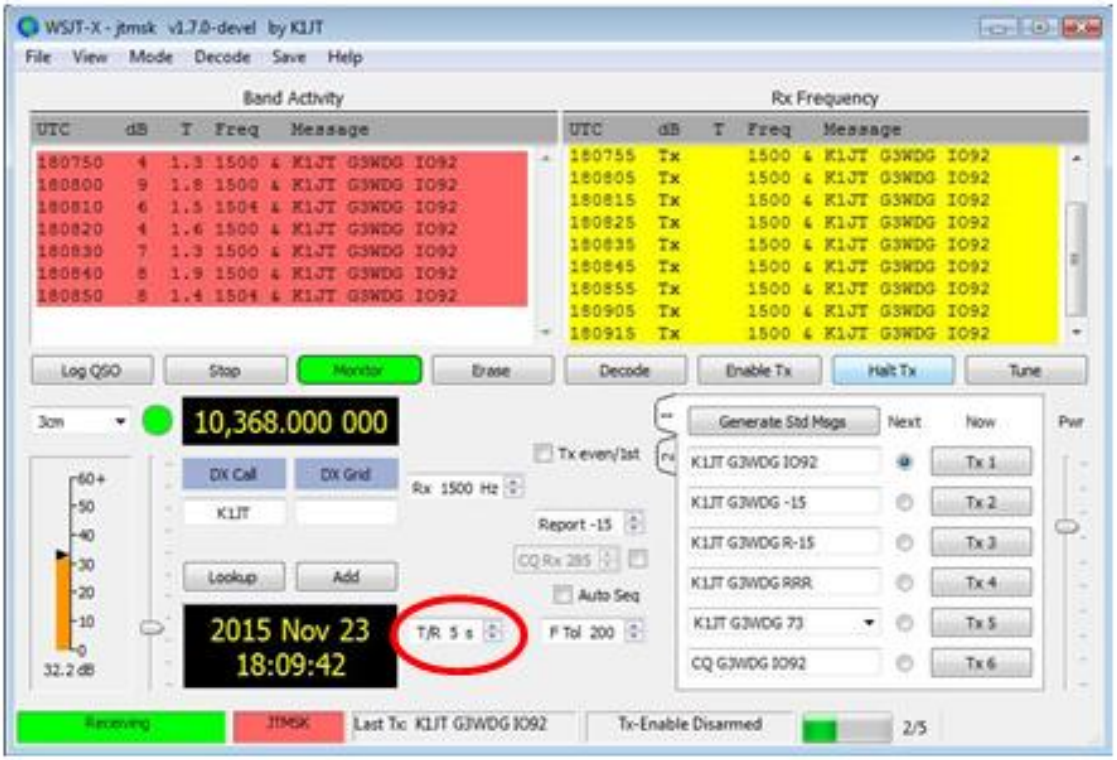

Echo Mode – K1JT – 144 MHz

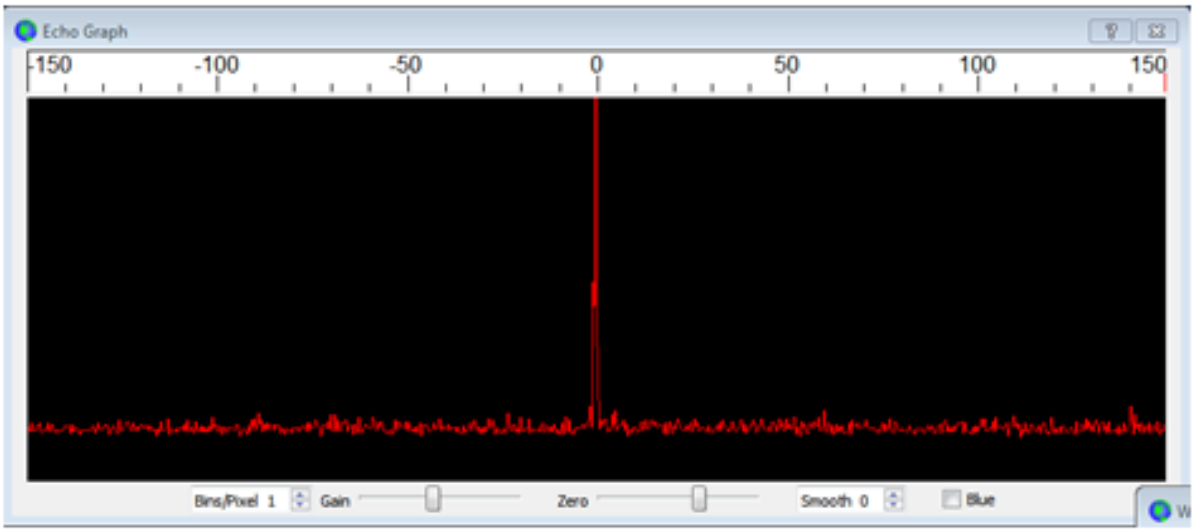

Logging, Reporting, UDP Server

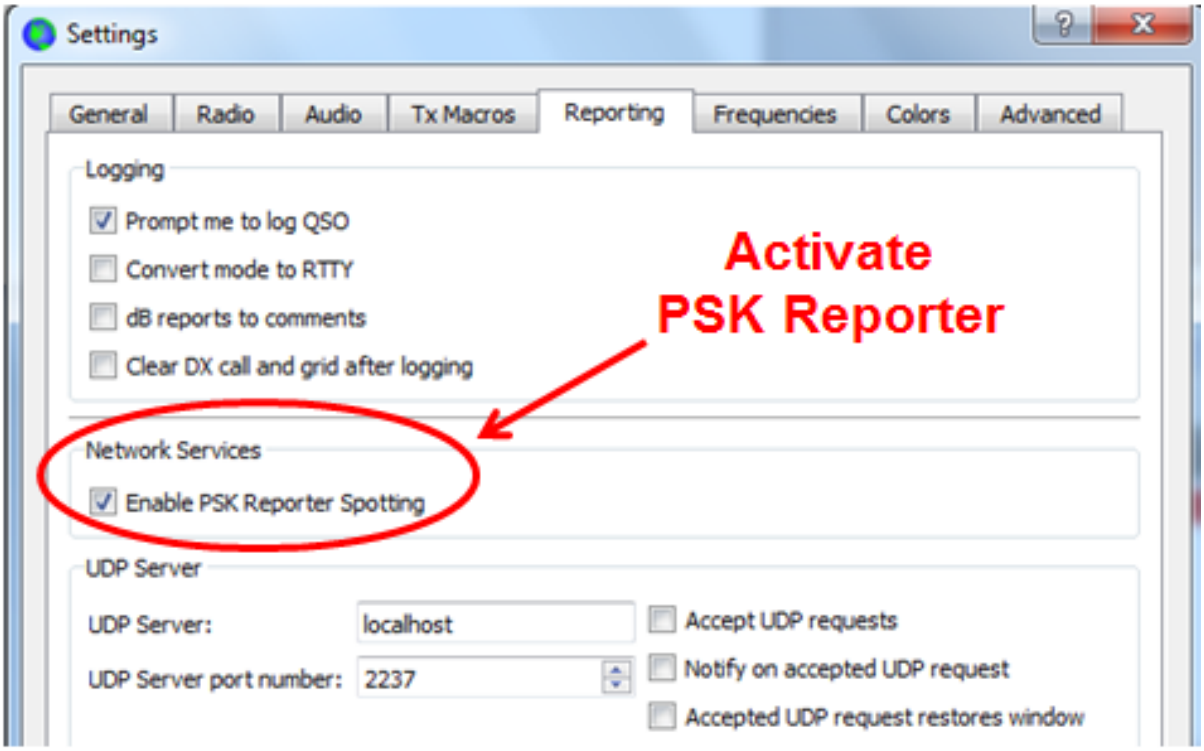

PSK Reporter - 6 m – JT modes

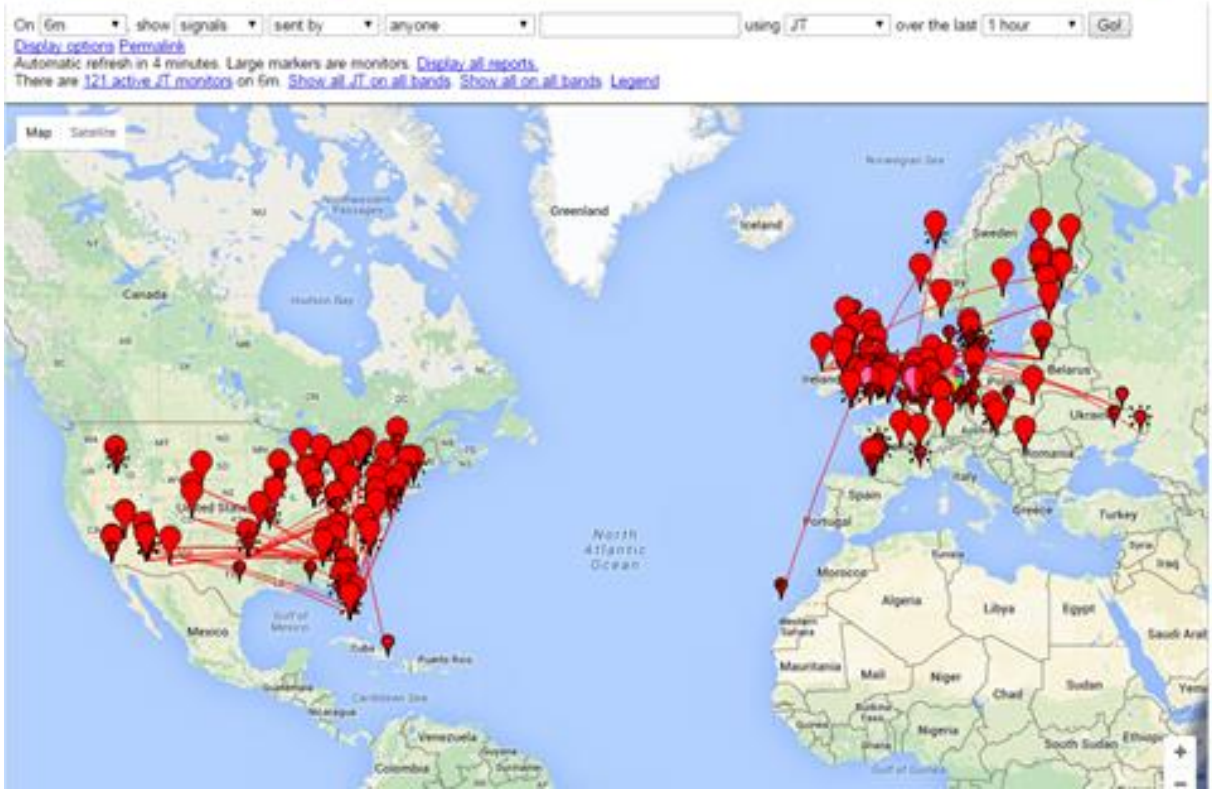

EME modes

- 50 MHz: **JT65A**
- 144, 222, 432 MHz: **JT65B**
- 1296 MHz: **JT65C**
- 2.3+ GHz depends on Doppler spread
  ➔ **JT65C, JT4F, JT9F, (QRA64 ?)**

Don't forget: In some ways,
➔ EME gets easier as frequency increases!

VK7MO – 10 GHz – 76 cm dish

G3WDG ➔ VK7MO
10 GHz – JT65C

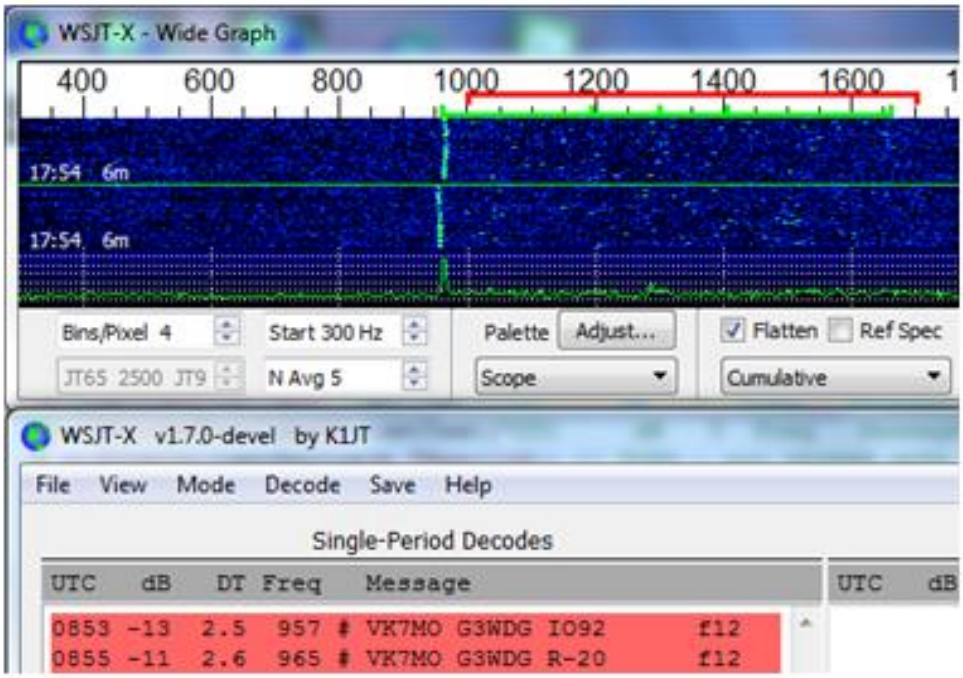

G3WDG ➔ VK7MO
10 GHz – JT9F

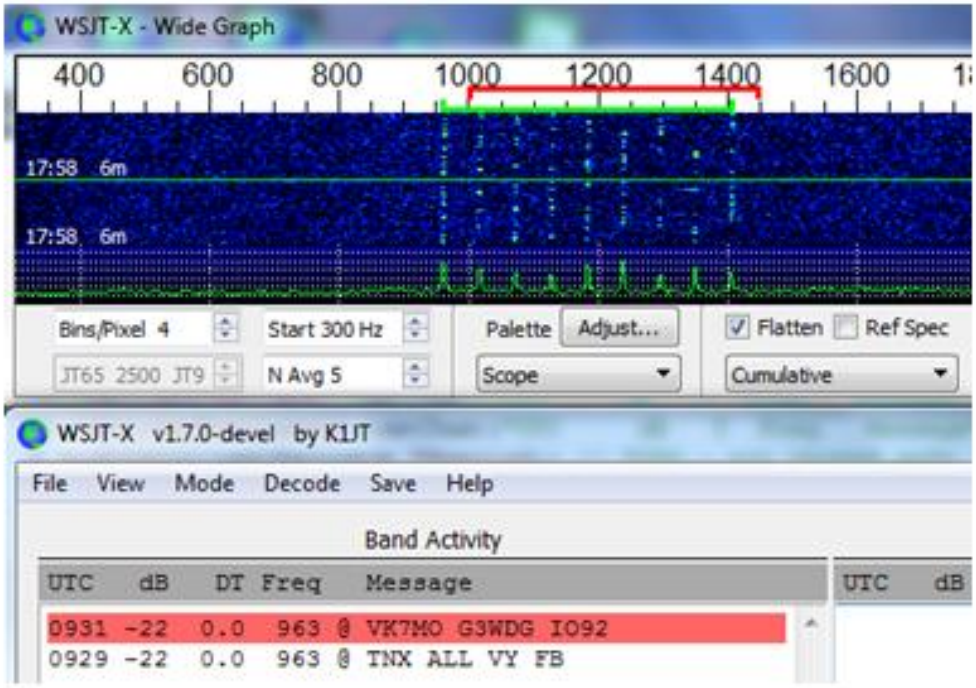

OK1KIR ➔ G3WDG

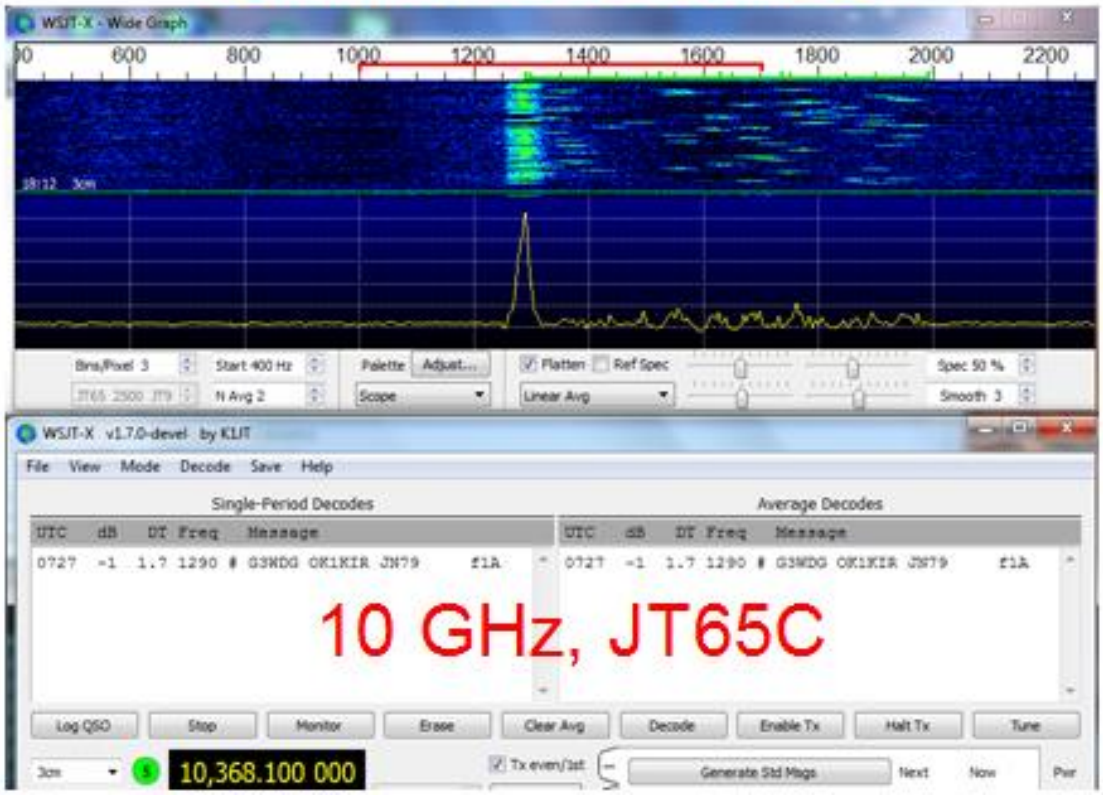

G3WDG ➔ OK1KIR, 10 GHz

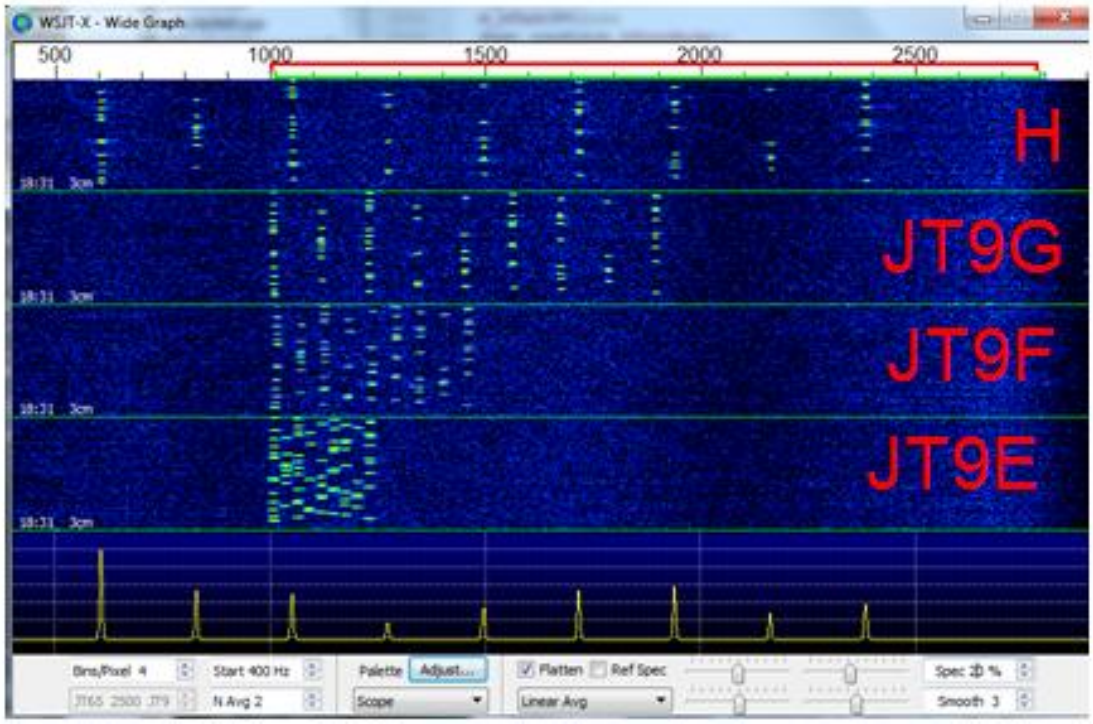

QRA64 mode

- Drop-in replacement for JT65
- Simulation tests
- On-the-air EME tests
- New sync scheme
- Further tests now being made …

Scatter Modes

- Ionospheric scatter (6m, 4m) **JT9G,H**
- Meteor scatter (6m, 4m, 2m, …) **JTMSK**
- → 800 – 2000 km, any time!

- Aircraft scatter (10 GHz) **ISCAT, JT9H**
  (up to ~800 km)

50.260 MHz Ionoscatter, JT9H

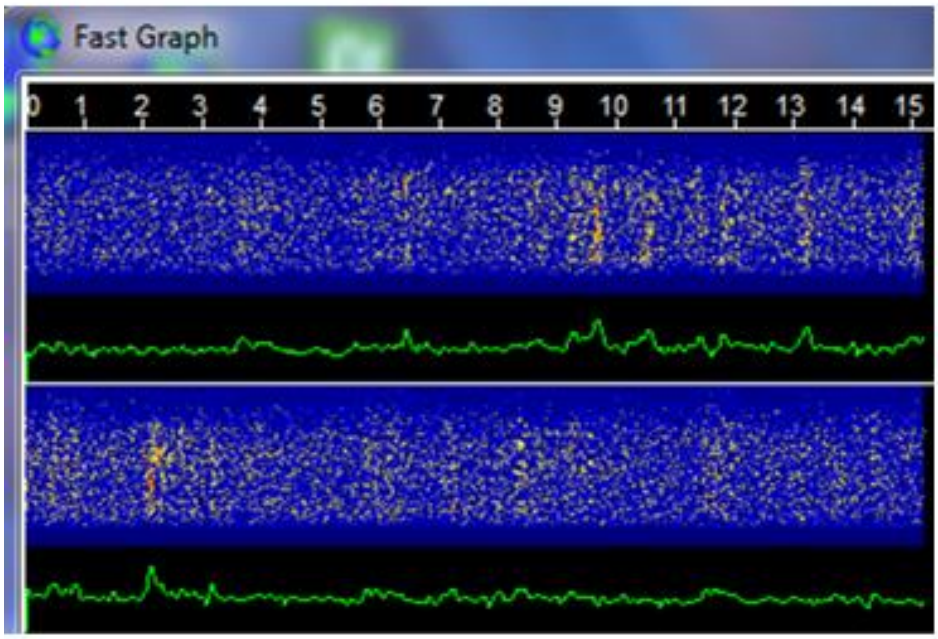

Up to 2000 km, any time!

Time (s) →

50.280 MHz – JT9G – 15 min

UTC	dB	T	Freq	Message
180730	-4	12.3	700	@ AB1NJ N0LWF -15
180815	-5	11.1	700	@ AB1NJ N0LWF RRR
180845	-5	12.8	700	@ AB1NJ N0LWF 73
180845	-7	3.8	700	@ AB1NJ N0LWF RRR
180915	-3	4.2	700	@ AB1NJ N0LWF 73
181115	-6	12.8	700	@ K1JT N0LWF R-09
181145	-4	13.2	700	@ K1JT N0LWF R-09
181215	-9	13.6	700	@ K1JT N0LWF -09
181245	-1	3.4	700	@ K1JT N0LWF RRR
181315	-2	3.4	700	@ K1JT N0LWF 73
182200	-6	7.7	700	@ K1JT ND0B -05
182230	3	11.5	700	@ K1JT ND0B -05
182300	2	11.1	700	@ K1JT ND0B RRR
182300	-2	3.0	700	@ K1JT ND0B R-05
182330	10	0.0	700	@ K1JT ND0B RRR
190430	-4	11.9	650	@ CQ N8CGY EN74
190730	3	8.5	650	@ CQ N8CGY EN74

N0LWF
EN10
1820 km

ND0B
EN07
2140 km

N8CGY
EN74
940 km

JTMSK, 50.280 MHz

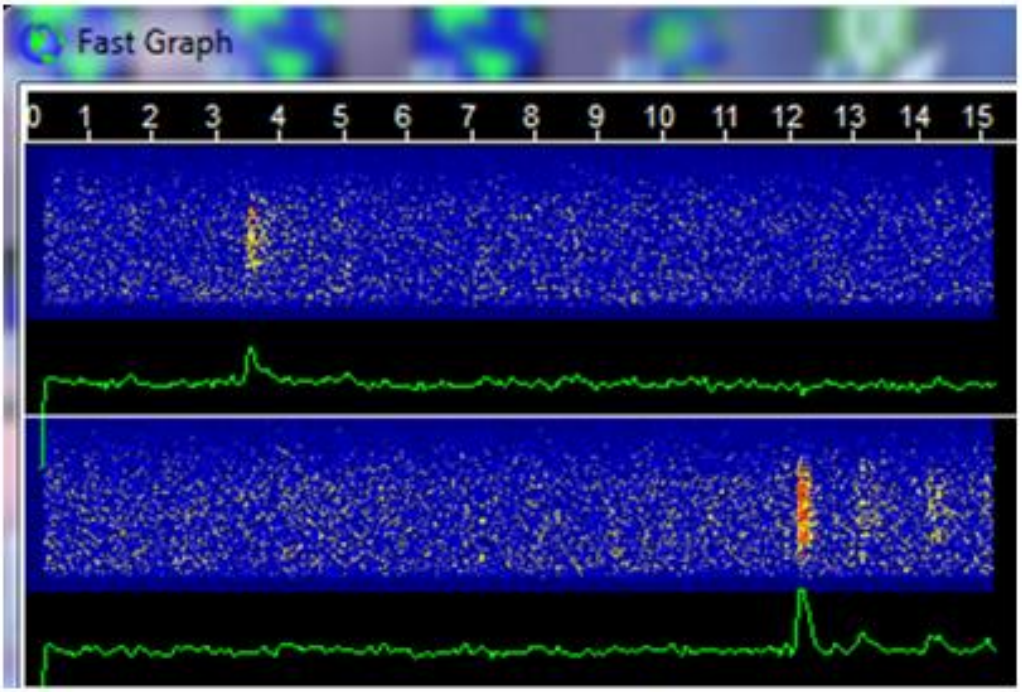

Time (s) →

VE1SKY (received at K1JT)

Testing
JTMSK
50 MHz
30 min

UTC	dB	T	Freq	Message
115515	3	1.7	1500	& K1JT VE1SKY +07
115615	1	3.1	1500	& K1JT VE1SKY +07
115745	7	7.7	1500	& K1JT VE1SKY R+03
120045	1	9.1	1500	& TNX 73 GL
120215	4	7.7	1500	& K1JT VE1SKY 73
121045	7	9.7	1500	& K1JT VE1SKY +10
121215	3	11.1	1504	& K1JT VE1SKY RRR
121245	4	2.8	1470	& K1JT VE1SKY RRR
121415	6	2.6	1500	& K1JT VE1SKY 73
121545	4	9.0	1504	& JTMSK IS FB
121615	6	12.0	1500	& K1JT VE1SKY FN74
122015	3	6.9	1500	& K1JT VE1SKY R+05
122045	2	9.7	1500	& FB JOE SKY
122245	3	9.6	1500	& TNX 73 GL
122445	2	7.2	1500	& ZIPSEND73
122815	4	9.1	1504	& RR RELEASE

K1JT (received at VE1SKY)

UTC	dB	T	Freq	Message
115400	1	8.4	1496	& VE1SKY K1JT FN20
115430	5	12.0	1504	& VE1SKY K1JT FN20
115500	3	3.2	1496	& VE1SKY K1JT FN20
115630	3	12.1	1500	& VE1SKY K1JT +07
115800	2	11.1	1500	& VE1SKY K1JT RRR
115830	4	4.0	1500	& VE1SKY K1JT RRR
115900	0	6.4	1500	& VE1SKY K1JT RRR
115930	3	12.3	1500	& VE1SKY K1JT RRR
120000	1	8.2	1530	& VE1SKY K1JT RRR
120100	2	7.9	1500	& VE1SKY K1JT RRR
120130	2	7.8	1500	& VE1SKY K1JT RRR
120200	2	9.8	1500	& VE1SKY K1JT RRR
120230	2	8.2	1500	& VE1SKY K1JT 73
120300	3	1.5	1500	& VE1SKY K1JT 73
120500	1	0.8	1500	& VE1SKY K1JT FN20
120600	3	0.8	1500	& VE1SKY K1JT 73
120630	1	4.4	1500	& VE1SKY K1JT FN20
120700	1	14.1	1500	& VE1SKY K1JT FN20
120730	1	1.3	1500	& VE1SKY K1JT FN20
120900	1	13.8	1500	& VE1SKY K1JT FN20
120930	0	11.0	1500	& VE1SKY K1JT FN20
121000	3	1.1	1500	& VE1SKY K1JT FN20
121030	5	6.6	1500	& VE1SKY K1JT FN20
121100	3	4.4	1534	& VE1SKY K1JT +08
121130	3	5.1	1491	& VE1SKY K1JT R+08
121200	4	5.4	1500	& VE1SKY K1JT R+08
121230	0	6.0	1491	& VE1SKY K1JT 73
121300	2	4.6	1500	& VE1SKY K1JT +04
121330	4	6.4	1500	& VE1SKY K1JT 73
121530	2	5.5	1500	& BACK TO TOP
121630	3	14.1	1500	& VE1SKY K1JT +04

UTC	dB	T	Freq	Message
121700	0	11.0	1500	& VE1SKY K1JT +04
121730	3	8.5	1500	& VE1SKY K1JT +04
121830	3	2.8	1500	& VE1SKY K1JT +04
122000	4	10.8	1496	& VE1SKY K1JT +04
122030	3	13.7	1500	& VE1SKY K1JT RRR
122100	4	14.4	1496	& VE1SKY K1JT 73
122130	1	13.2	1509	& TNX GOOD TEST
122200	2	1.0	1500	& TNX GOOD TEST
122230	2	12.7	1504	& TNX GOOD TEST
122330	3	9.9	1500	& OPEN RELEASE?
122430	2	3.4	1500	& OPEN RELEASE?
122500	1	0.5	1500	& DECODER OK
122530	3	13.9	1500	& DECODER OK
122600	2	6.4	1500	& DECODER OK
122730	2	3.3	1500	& FIX GUI NEXT
122830	4	8.1	1538	& QRT AT 1230

144.118 MHz: K1JT at VE1SKY
(barely audible…)

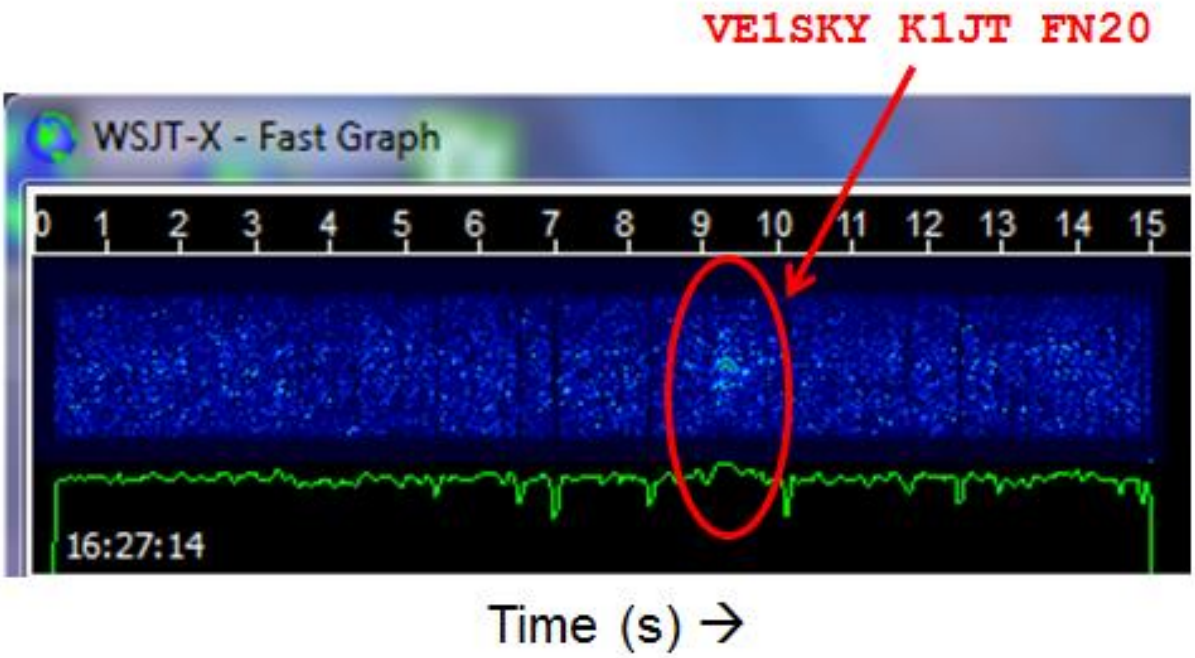

144 MHz
JTMSK

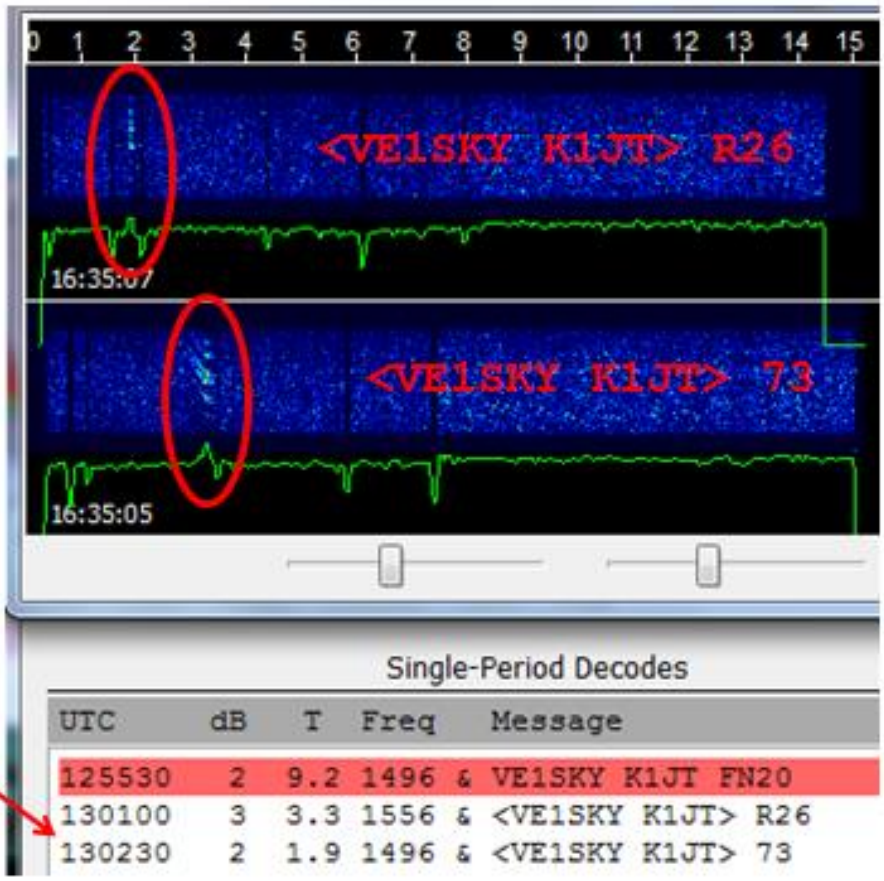

Short
Messages

Single-Period Decodes

UTC	dB	T	Freq	Message
125530	2	9.2	1496	& VE1SKY K1JT FN20
130100	3	3.3	1556	& <VE1SKY K1JT> R26
130230	2	1.9	1496	& <VE1SKY K1JT> 73

Message duration

JTMSK: long 117 ms, short 17.5 ms

MSK144: 72 ms, short 16 ms

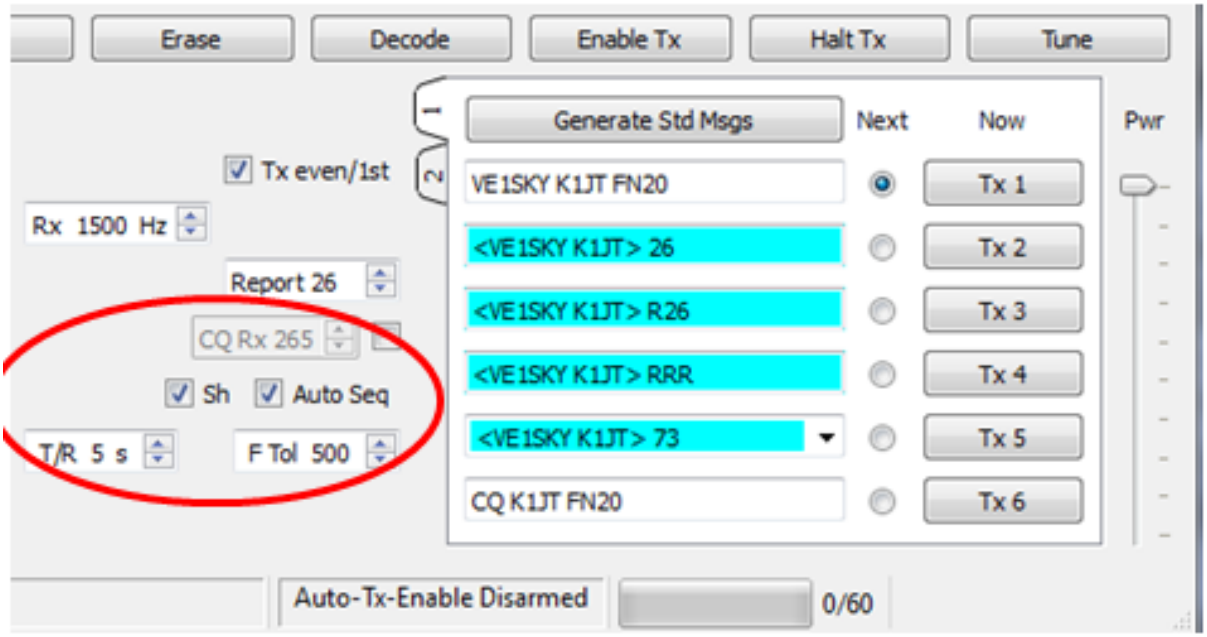

MSK144 First QSO

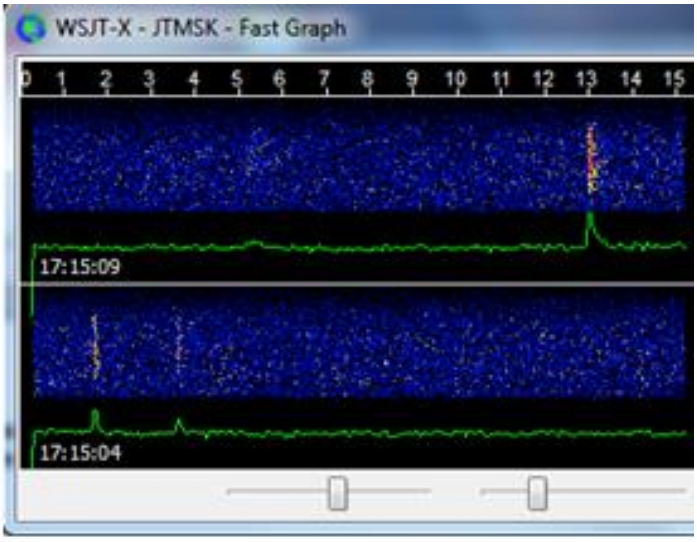

UTC	dB	T	Freq	Message
171015	Tx		1000	& CQ K1JT FN20
111630	0	5.6	1591	& K1JT AB1NJ FN34
171045	Tx		1000	& AB1NJ K1JT +00
111830	2	1.6	1590	& K1JT AB1NJ R+00
171115	Tx		1000	& AB1NJ K1JT RRR
112000	4	4.7	1560	& K1JT AB1NJ 73
112000	4	4.7	1560	& K1JT AB1NJ 73
171145	Tx		1000	& AB1NJ K1JT 73

Special Acknowledgments

WSJT-X now has **many** contributors!

Special thanks for recent enhancements to:

KI7MT: Software developers kit

G4WJS: Rig control, program structure

K9AN: FT decoder, MSK144

IV3NWV: QRA64

VE1SKY, G3WDG, VK7MO, OK1KIR: Tests

VK5MC - Techniques used in construction of a home brew 10 mt parabolic antenna

Chris Skeer (email: cjskeer@bigpond.com)

Introduction: Home brew parabolic dishes in Australia

Home brew dishes are not very common in VK. Pioneers in this field were the late Ray VK3ATN and the late Ron VK3AKC. Ray had an operational 16 foot dish, 27 foot dish and also had under construction a 50 foot dish, unfortunately the latter two were never erected.
Ron Wilkinson VK3AKC had an operational 20 foot dish in Geelong, this was used on tropo and EME for 1296 MHz and it was this dish which was given to me and which I rebuilt back in 1977. This experience gave me the opportunity to see any construction faults and design problems to be overcome with any construction of a larger dish.

20 foot dish rebuilt at VK5MC in 1977.

Design factors needed for the new larger dish

Strength of hub – to grab and hold shape

The hub is really the most important part of the dish, it the foundation of the reflecting surface and needs to be strong enough and structurally sound to hold its shape as the dish tips over. It is also the interface between the dish and the tower that it is mounted on so you need to have something solid to grab. In my case the complete dish weighs 600 kilo and 500 kilos of this is contributed by the hub. It is constructed using 25mm galvanised pipe, with a 300 mm diameter central stress tube of 8mm steel.

Hub in the workshop

No strain on surface shape by feed

As the dish ribs were of a light material, the feed structure was to be supported independently of the reflecting surface to prevent distortion. The feed support arm was made to fit behind the surface and was firmly attached to the centre of the hub.

The feed support arm made the access to the feed very simple as all it needed was a pivot point with a strong hinge and a winch to lower and raise the feeds. Without this arm, the feed would be at least 6 metres in the air making access difficult. This approach was also used by PA3CSG although I like to think my method is stronger.

Smaller F/D for better G/T

The earlier dish had an F/D of 0.6 which was the design figure of that period, it maximised the gain for the dual mode Turrin feed. In those days, with noise figures of 2 dB for the best preamplifiers, the noise temperature of the antenna was not of any consideration. These days 0.25 dB is achievable and a dish with less spill over is required to get a better receive performance. The F/D of 0.42 results in a better receiver performance and suits a large number of different feed designs. Giving the antenna a better gain/temperature performance on receive

Hub at the workshop with back feed arm being positioned behind a rib

Feed in lowered position showing easy access

Computer control with absolute encoders

My earlier dish used some Selsyn motors, which we geared in such a way to make a two dial indicator, one showing the complete 360 degrees with 10 degree marks, the other with parts of 10 degrees. This could not be computerised. Some pulse counters were employed in later times but were never really a success. The absolute encoders I have used with the VK5DJ tracking system make use of the AS5040 chips, which for my system on 1296 MHz with a 3dB beam width of 1.2 degrees, seems to perform faultlessly. The controller is very compatible with a wide range of indicator devices including a simple potentiometer.
Thanks to John VK5DJ who took up the challenge to use some new technology with the absolute encoder chips and created the tracking software for the PICs.
I was uncertain in the development of the system that it would be good enough for the large dish, the encoders looked too simple to give the high resolution required to work, but my worry was soon dismissed. Higher resolution encoders are now available.
All I have to do is listen and not worry about keeping up with the moon; it is all done for me.
See VK5DJ web site (vk5dj.com) for more information on this tracking system.

Construction problems

How strong does it need to be?

One of the design problems I faced was “How strong does it really have to be?” To a certain extent this was really “What do I have available to do the job, and will it stand up to the strain?” In practice it meant we solved strength problems as they revealed themselves.

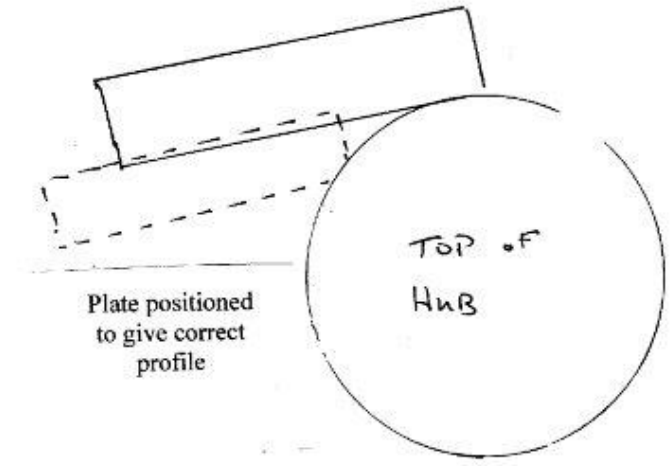

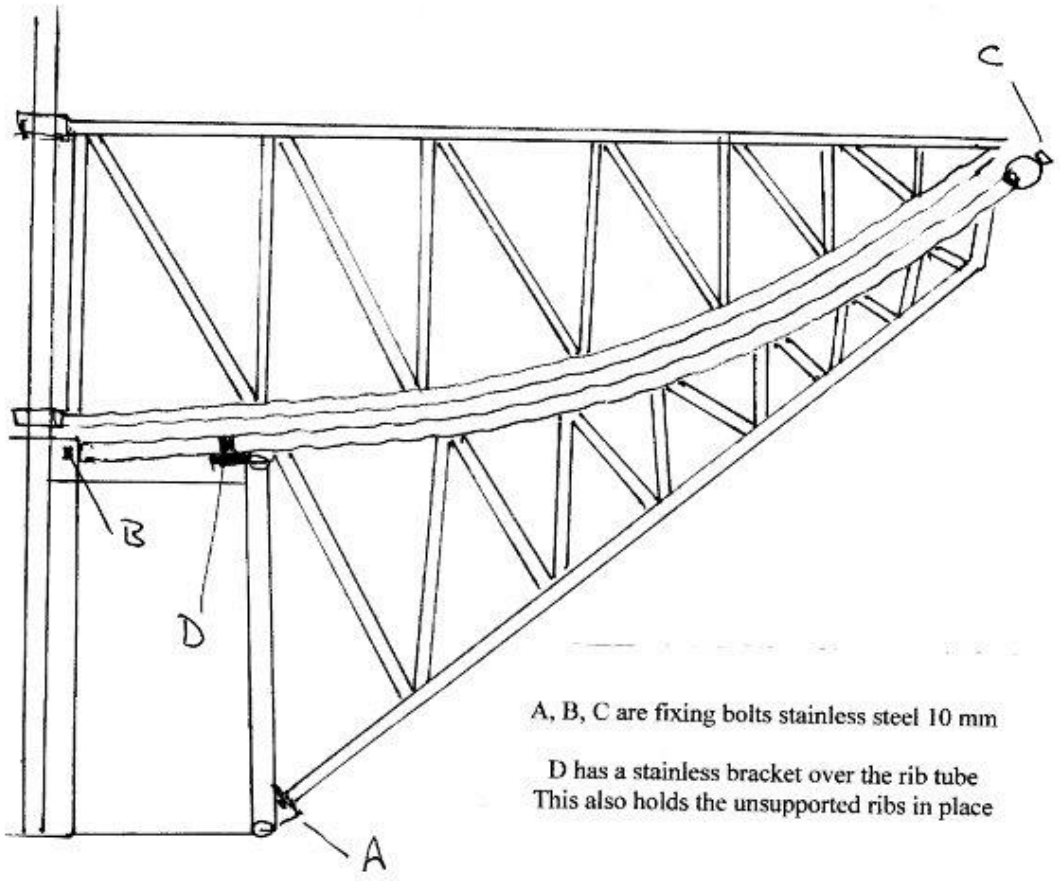

Fine adjustments of the ribs

While making the hub I found it difficult to bend the pipe and keep to a precise measurement, so it was made as well as I could. The precise position for the rib was fixed with a small support plate welded to the top and bottom fixing points of the outside of the hub. This gave me a rib accuracy of 5 mm or thereabouts.

Azimuth drive hydraulic motor and worm drive

Azimuth platform

The azimuth platform consists of 6 metre lengths of 300 mm RSJ steel with the 5 metre vertical supports of a similar material, ex ETSA power pole. This is supported on some steel wheels. The structure rotates on a circular concrete pad with a radius of 4 metres and some spokes to tie it into the central locating shaft. Even with this solid structure I did find that the vertical supports were twisting with the dish at low elevations, and a solid cross member was put at the top of the vertical supports.

Hydraulic system – pump size, lockout valves and restrictors.

I did not wish to use all of the available electricity supply (I have a SWER line) to drive a large 3 HP electric motor for the hydraulic pump. My flow requirement was small for elevation, but a little larger for azimuth so it is a compromise. Elevation positioning is made with two hydraulic rams and a lockout valve while azimuth control is made by driving one wheel using a 30/1 worm drive and a small hydraulic motor.

I started with a medium size pump which I had been given and soon realised after some research into the use and design rules of a hydraulic system that the pump I had was too large to drive with a 1 HP motor. A search was made of the entire farm for a pump that may suit my requirement; the smallest one was tested and found to be suitable for the task but unfortunately the windrower had priority. Luckily we were able to obtain one from a machinery grave yard at the right price. Perhaps a power steering pump from a vehicle would have been also suitable? To make sure that elevation control was slow; 0.8 mm restrictors were made and put on the hydraulic rams.

Winners

Scrap steel was used to make the supporting structure. This came from locally available scrapped steel/concrete power poles. The pipe used in the counter weight arms and the rear feed arm support were originally used in a "monkey bar" structure at the local football club playground and scrapped due to safety regulations. So costs were minimal.

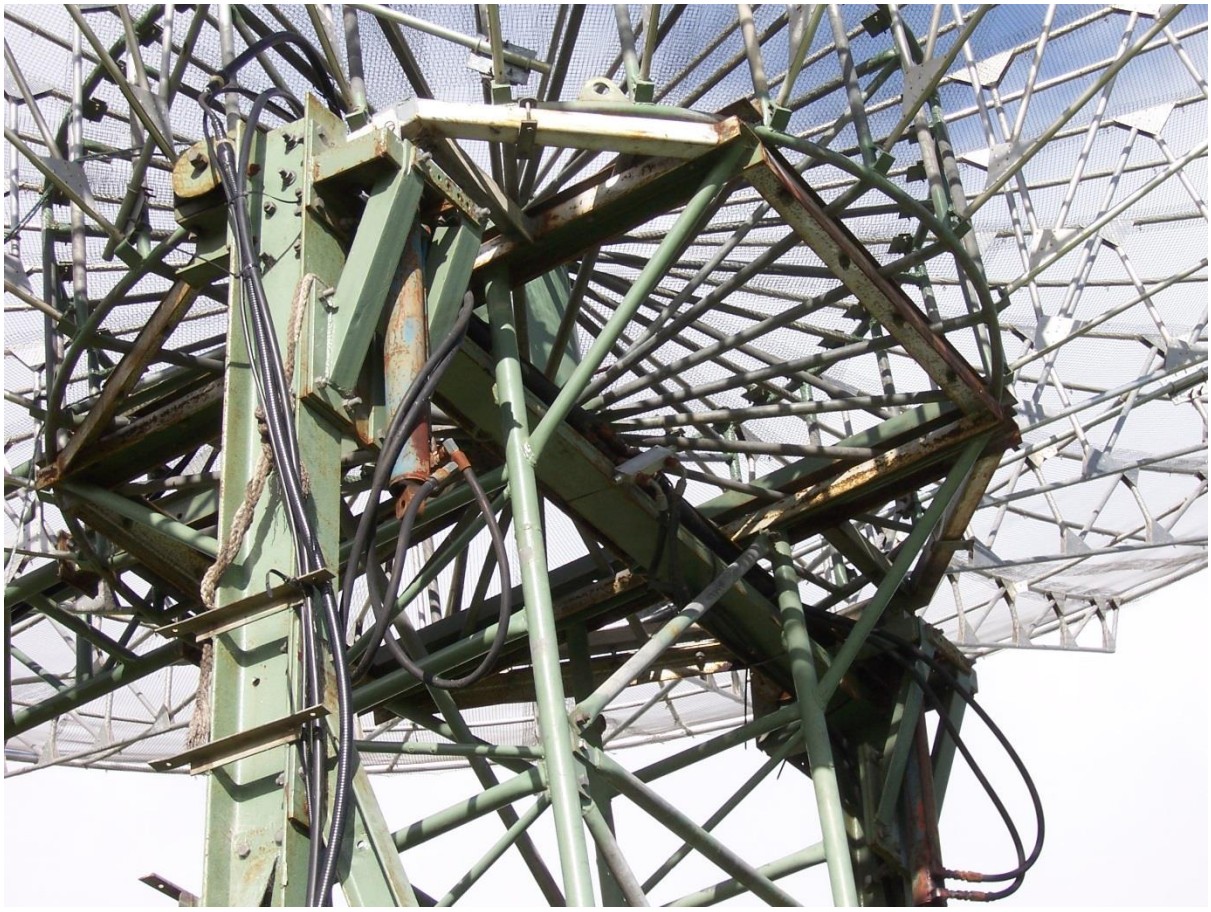

Back of the dish showing two hydraulic rams

Welding of plugs

The ribs were made of 22.2 mm x 1.5 mm round aluminium tube; it would have been much easier to attach these to the hub if they were square material.
Tapped aluminium plugs were made up and welded into the ribs where they attach to the hub and the outer ring. This resulted in a very strong structure. I used Eutectic welding rods and oxy/gas welding equipment for this task.
Stainless steel 10 mm bolts were used for the attachment points.

Stainless steel ties from craypots

Tying the mesh to the ribs needed to be quick and simple, with no corrosion worries. I came across some stainless steel ties used locally to make crayfish pots, these were ideal for the job as they could be purchased with the loops in the end, ready for the twister tool more commonly used when tying the reinforcing mesh together for concrete. 600 ties were used for the job.

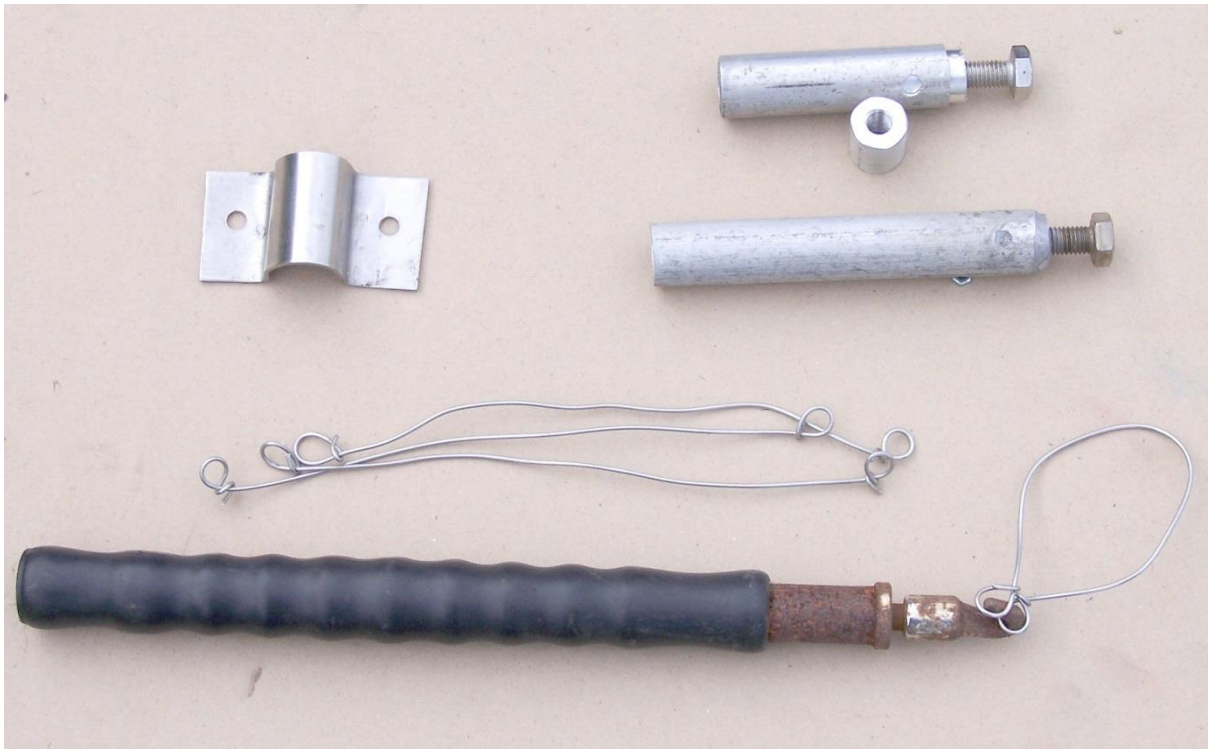

At the top are the attachment brackets and plugs while the bottom items are stainless steel ties and the twister tool mesh in pie sections.

The mesh

Laying a flat mesh on a curved surface can at times result in a lot of bubbles or kinks where the mesh is not tight, causing gain loss at the higher frequencies. I found using a pi section to cover the surface worked out extremely well, the small section cut off at the centre of the dish was put on the outside section resulted in very few bubbles in the surface with no waste of material. The mesh used was 900 mm wide, a 12mm hole and a wire diameter of 0.9 mm. During manufacture the mesh was hot dipped galvanised after welding.

Hardwood block bearings for AZ and EL

Red gum blocks were used for elevation and central azimuth location bearings. I have used this type of bearings on rollers around the farm and I am always surprised how long they last, they will not seize, with a little bit of grease pumped in occasionally, they will do the job for quite a while.

Feed arm focus

Final focus point turned out to be a lot simpler that I had expected, as the arm is adjusted by a winch. The process was: check the sun noise, wind the feed arm in/out for maximum noise, and make a small adjustment of the support arm to keep the feed still pointing at the centre of the dish. Once found a shim was made to fit the retaining clamp to the correct angle, so that it could be held at the correct position.
I did make the feed on a sliding structure but have not found this to be required owing to the ease of adjustment of the arm. But best of all the feeds can be wound down very simply to be worked on at ground level.

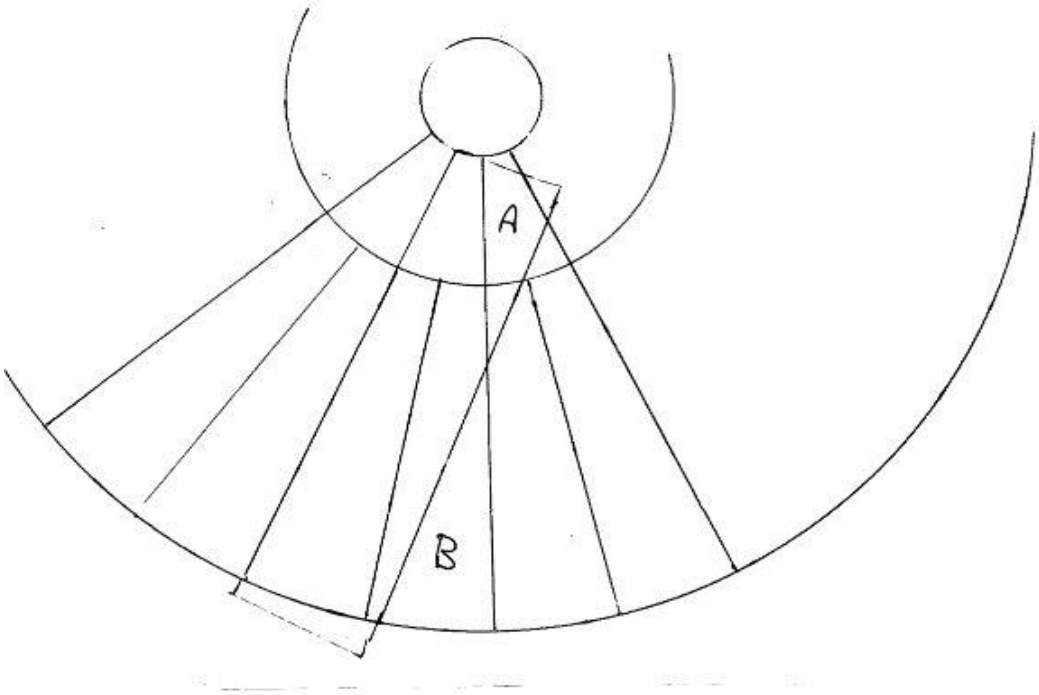

Part A was cut off and placed at B

Mesh at the edge of the dish , section of pi added to the outside

Feed arm and elbow in place

Location

I realise I am fortunate to be currently living on a farm with a bit of room, to be also on a small rise is a plus. I have used what was available; on the hill was once a windmill and tank stand. The stone tank stand now holds the control and transmitting equipment. The dish is positioned as close as possible to it and the operational room is some thirty metres away to the south of the dish.

Moon rise and moon set are virtually unrestricted.

Initial reactions and solution

To start with I was very disappointed with the performance bring obtained. Sun noise and sky termination figures were lower than expected and echoes were not there. Many checks of coaxial connectors and preamplifiers were made with no improvement. In desperation it had to be some common factor to both transmit and receive paths. While making another preamp change with the feed down on the morning of an activity weekend I looked into the feed to check if the probes had not fallen off, to my amazement I could not see the bottom of the feed for straw. I had a resident engineer, who had built his nest, giving enough attenuation to upset the performance. Once removed, echoes were immediately received, sun noise lifted to an expected level and many more stations were now audible

9.8 metre dish started by Eric VK5LP in 1985, completed 2008 by VK5MC

Noise measurements to date and echoes on 1296 MHz

I am currently seeing moon noise of 0.7 DB. Sun noise approximately 18db, perhaps I may be able to get a little more from this when time permits. Echoes have been detected down to 10 watts input to the coax cable at the transmitter.

I wish to acknowledge the help of my friends during the construction; it is not something to tackle without some help

VK5LP for his start with the project, he did the hard work of making the 24 ribs. He also purchased the rolls of mesh for the project.

VK5NC for the engineering help and design technical advice.

VK5DJ for the state of the art stand-alone tracking system. See VK5DJ beam controller web site.

Also a list of people who have contributed something VK5AVQ, VK5ZOO,VK5HDW,VK5DK, VK5JL, VK5MQ, VK5ZGY, VK5APN,VK5EE,VK5AV, VK5NY,VK3AFW, VK3ZQB, VK3XPD, VK3XD,OZ4MM, HB9BBD,VE7BBG, G4DDK.

G4HUP - Azimuth Drives for Small Dishes

Dave Powis (email: g4hup@outlook.com)

Abstract

The majority of the small dishes (<3m dia) available to amateurs for EME work are really intended for fixed pointing applications, such as CATV head-end sites or dedicated broadcast applications. Thus the dish mounts are of the 'point and forget' type. The amateur has two options in using such dishes - either a polar mount, or a full Azimuth/Elevation drive. Even dishes that are supplied with a polar mount require modification for EME use, but the subject of this paper is about providing full Azimuth and Elevation control of small dishes. The discussion is limited to small dishes, since the mechanical requirements for larger dishes are more stringent, due to wind loading effects.

Elevation drive of small dishes is relatively trivial, so the discussion will focus mainly on the azimuth requirements.

Introduction

Having been active at various time in the past on 144MHz and 23cm EME from home, I decided to get back on EME again, but this time on 3cm, using a relatively small dish -1.8m. The most significant mechanical obstacle was converting the dish from fixed heading usage to fully controllable, for moon tracking. This paper charts the development of the azimuth drive system.

Previous Experience

In 2006 I acquired a 2.4m prime focus dish, with a standard polar mount frame for head-end use. The dish was converted for use on 23cm with a full az/el drive system. An 18" satellite screw jack was used for the elevation drive, replacing the lead screw use in original service, and a pendulum and pot type elevation sensor was used.

To develop the azimuth drive required the provision of a thrust bearing to support the frame and dish, and a drive system capable of slow rotation. The dish frame was relatively easy to convert, by placing the thrust bearing inside the top of the support pole, and allowing the entire frame to rotate with the dish. The drive system was designed from a motorcycle drive chain, using the large and small sprockets. The large sprocket was modified to fit the outside of the dish support tube, and split into halves that could be clamped to the tube – see Fig 1. The small sprocket was on the drive shaft of the motor, which was attached to the dish frame, so that in operation the motor and the dish pulled themselves around the static large sprocket – the azimuth encoder was at the bottom of the drive shaft, and so was turning approx. 3 times faster than the dish rotation..

The system worked reasonably well - a number of successful contacts were made on 23cm using that dish, on the majority on CW and a few on JT. However, there were also some learning points from that exercise! Firstly, although the dish rotation at maximum speed seemed quite slow - it took approx. 70 seconds for a full 360°, experience proved that this was considerably too fast. When moon tracking, as the controller updated the dish position, it was moving too far at each step. The thrust bearing operation was not as smooth as I would have liked. The engineer who machined it for me did not follow my request, thinking that he had a better idea - I don't think he did!

Fig 1 - Detail of 2.4m prime focus dish azimuth drive

The frame tube rotating round the support tube was also not very smooth - it was quite difficult to get all the screws intended for fixed settings to just the right pressure to allow the dish to rotate freely - the outside of the support tube was not a smooth circle.

Finally, although this was not a factor in the operation of the drive, the W2DRZ control system I had elected to use was barely adequate for 23cm operation. It may have been better with a slower drive, but my main concern was that it did not have a capability to offset the dish from the calculated position. This was not a major issue at 23cm, where the beamwidth is about 5° for this size of dish, but since the profile of the Channelmaster dish was good to above 11GHz, it did rule out operation on the higher bands, where that capability is essential. It contributed to my decision to re-engineer the system.

In 2007/2008 I had the opportunity to work with the West Chester Radio Club, WC8VOA, in Cincinatti, where they had use of a 7.2m Vertex dish, and were trying to bring it into use on 3cm. Once we had acquired a suitable Rx system, I soon learned about dish offsetting!

Pictures of my 2.4 dish and the component parts can be found at [1] and the WC8VOA story is at [2] http://wc8voa.org/eme-station-information/

My current project

The drive to be described here is for a 1.8m Prodelin offset dish. I obtained a surplus dish in its manufacturers packaging several years ago, and have recently been working on a 3cm station using this dish. Again, the standard mount is designed for fixed service, but the type of modification I did on the 2.4m dish was not suitable for this mount. For the offset dish, the point at which the elevation pivots is in front of the centre of azimuth rotation, unlike the prime

focus dish where it is directly above the azimuth rotation. The dish azimuth arm, spine and feed mount are shown in DL4MEA's photograph at Fig 2.

Fig 2 - The basic Prodelin offset dish structure

This opened up another option - to insert a gearbox drive between the top of the head post and the azimuth arm of the dish. After considerable sketching and some measurements, it looked as though an extra height of about 150mm would result from introducing this gearbox, which I considered acceptable.

After researching available mechanical parts, I spent some time on my CAD program to get an idea of the dimensions. The initial plan view drawing is shown in Fig 3 below.

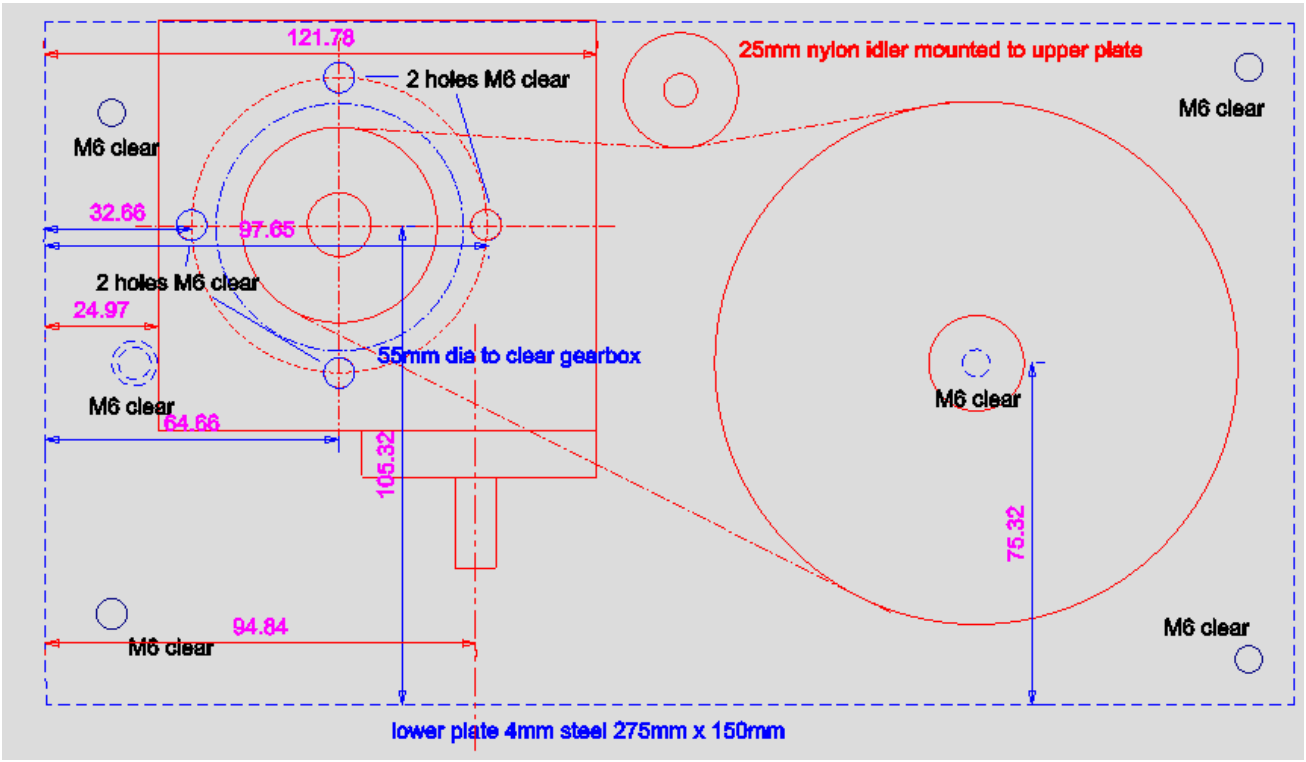

Fig 3 - Initial CAD drawing for dish drive - plan view

The objective was to achieve a drive 3 to 4 times slower than my original dish, so a worm drive motor was selected, and that was followed by an 80:1 second worm drive reduction gearbox. Final drive to the azimuth shaft was via a 2.5:1 reduction chain drive. I calculated that this should give around 4min for a complete revolution. A number of aspects of the initial design were modified after discussion with more experienced mechanical engineers, but the basic design concept has been carried through.

The first step was to build the drive system using MDF for the plates. This was easy and quick to do, and started to show up the minor changes that would be needed. A full working drive system was built this way, but without the chain tensioning and azimuth sensor system – Fig 4.

Fig 4 - MDF 'mock-up' of the drive system

On top of the upper plate is a thrust bearing to support the dish, and a large collar to secure the azimuth arm to. Initial tests showed that the drive system was rather slower than I had intended, so the final chain drive ratio was reduced a little. In other respects, the drive system did what was intended, and with the knowledge gained from the dummy build exercise, I had the confidence to cut some steel!

The top, bottom and motor plates are all 6mm mild steel. I had the outlines of these plates laser cut, since there is no distortion of the steel. The support pillars for the corners are 10mm threaded rod inside tube. A 20mm dia steel drive shaft is used for the output, with top and bottom bearings and a thrust bearing on the top plate. The upper support collar is machined to locate inside the thrust bearing, and on the top of the collar a plate is bolted to suppport the azimuth arm. See Figs 5 and 6

A considerable amount of lathe work went into creating the chain tensioning system and the azimuth sensor system - these were not off -the-shelf components. I had decided early on to use the OE5JFL EME controller system, so the MAB25 sensor is mounted on the bottom plate of the gearbox, and is driven by a 1:1 belt drive from the main shaft. I would have preferred to have it concentric on the shaft, but this was not possible without cutting holes in the support tube - which would have weakened it. The limit switches and the sensor terminations are on the top of the upper plate.

Fig 5 - Early stage build showing reduction gearbox and lower bearing in place

Fig 6 - Full gearbox with azimuth arm in place on thrust bearing

A small plastic enclosure is mounted on the top plate (Fig 7) so that all the sensor and control cables can be taken into one place. The sensor connections back to the JFL Controller are through an RJ45 connector at the back of the box, and the power connections for the motors are via separate cables.

Fig 7 – Detail of limit switches and terminal box on upper plate

Fig 8 – Dish spine in place on azimuth arm, with elevation jack

Elevation control is by a 24” heavy duty satellite screw jack, which sits in place of the original elevation bolt – Fig 8. Two lengths of 2” aluminium angle have been added to the back of the azimuth arm so that counter weights can be used to minimise the uneven load on the gearbox bearings.

For the elevation sensor, I decided to use an on-axis mounting for the sensor. I have previously used a pendulum type sensor, but without some damping of the pendulum arm, there is too much overshoot each time the drive is stopped. To ensure the axis of the sensor encoder is properly aligned with the axis of the elevation arm, the end of the elevation bolt was centre drilled in the lathe and tapped for an M6 bolt. An aluminium U bracket holds the sensor, as in Figs 9 and 10,

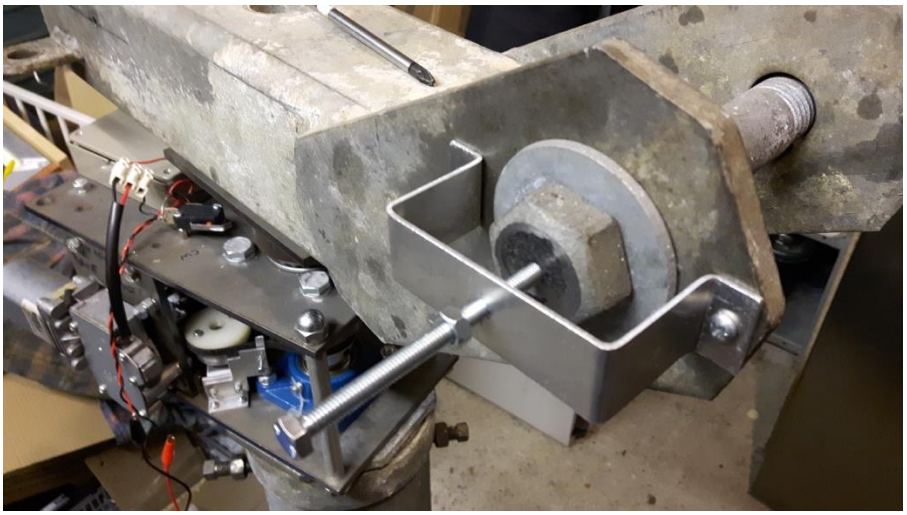

Fig 9 – Locating jig for the on-axis elevation sensor bracket.

and a piece of bar acts as the actuator, with a long M6 bolt threaded into the dish spine. A slot in the bar allows for any eccentricity in the mechanism.

Fig 10 – Completed elevation sensor assembly

Next Steps

Having reached the stage where the dish spine can be controlled in azimuth and elevation via the JFL controller, then whole assembly now needs stripping down and preparing for moving

onto the dish site – painting and weatherproofing of the mechanism of course, and the routing and securing of cables to provide a reliable connection whilst the assembly moves.

Final location

The dish is to be mounted on an ex-commercial pallet, which is already in place, with the cable duct back to the operating shack.

Fig 11 Pallet in place ready for dish drive and dish.

The pallet is mounted on 4 large concrete slabs with half-length wooden sleepers – this was done to avoid grass growing up around the base of the dish. In Fig 11 above, the white line that can be seen behind the pallet is on a true North-South axis, set up by both the pole-star and the midday sun shadow.

A 110mm dia flexible cable duct runs back to the shack, and equipment located at the dish is to be housed in a weatherproof ex-commercial housing, with plenty of heat sinking capability. This will be attached to the support pillar for the dish.

For another time?

Already, of course, there are things I can see that I would do differently if I repeated this project. Firstly, I would probably mount the drive motor at the end of the azimuth gearbox, rather than on the side. In its current location it may limit the rotation at the clockwise end of the travel, as compared to the anticlockwise end. This may not be an issue in practice, since at these heading the elevation of the moon will be very low, and it is likely that the back of the lower part of the dish spine will hit the support pole - 0° elevation will not be possible using the original dish parts. Until the full dish arm and feed support are assembled on the new mount, the actual minimum elevation achievable is not known.

To correct this, a complete new azimuth arm would need to be fabricated, moving the pivot point further forward. But this would completely change the balance of the dish and require much greater counterweighting at the rear. My feeling is that this is probably not justifiable, and would lead to a less stable final assembly.

I would also probably replace the chain drive in the gearbox with a toothed or ribbed belt drive, similar to those used for car cam-belts. Being more flexible than a chain, it should be easier

to tension up to eliminate backlash from the drive. This is a modification that could be applied to the existing system without significant re-engineering.

Fig 12 – Cable duct run to site

References

[1] Personal website G4HUP http://g4hup.com/

[2] West Chester ARA Ohio, USA 7.2m EME dish http://wc8voa.org/eme-station-information/

PA3FXB - Let's bounce (new frontiers at PI9CAM)

Jan van Muijlwijk (email: jvm@netvisit.nl)

Introduction

After the restoration in 2012/2013 and the great reopening of the dish by Joe K1JT in 2014, PI9CAM entered a new era. No more worrying about funds for the restoration. No more sleepless nights about what could possibly go wrong during the restoration process. The dish is as good as new now and we can start using it as much as possible!

We already did some very nice things with it right after the restoration like saving a satellite (TRITON-1) and the world's first moonbounce wedding, so where to go next…..

2014 – 2016

Of course we resumed our 'normal' operations like taking part in moonbounce activities and amateur radio astronomy observations.

Next to that we see a growing interest of the public to visit the dish. More and more groups of people contact us and ask for a guided tour at the dish. That's nice because that generates good exposure for our project. Within CAMRAS there is an ever growing group of volunteers that specialises in doing these guided tours!

Some highlights from the last two years are:

- Taking part in the JOTA using our WebSDR. Scouting groups built their own 70 cm antennas and saw their signals reflected off the moon via PI9CAM.
- An experiment with the professionals from LOFAR to generate 50 MHz moon echoes to make it possible to calibrate a LOFAR project. We had some results and the project is ongoing.
- Many art projects with our artist in residence Daniela de Paulis. Mainly about SSTV via the moon. Strong SSTV signals on 23 cm were sent by I1NDP, PY2BS, G4CCH and HB9Q. (thanks guys!) But we also streamed galactic noise via the internet to a museum where Daniela was doing a presentation. Some other artists joined us and worked with us on EME SSTV based art projects.
- Start of SETI@CAMRAS. A project to use the dish as an instrument to search for possible signals from extra-terrestrial intelligence. The objective is to observe and let the data crunching do via SETI@HOME, the very successful public domain SETI project of Berkeley University.
- The completion of the restoration DVD. A local volunteer film crew recorded many hours of great video during the restoration. CAMRAS hired a professional company to produce a high quality promotional DVD out of this material.
- A test on 6 cm. We entered the 6 cm activity weekend in June 2015. We used a very improvised setup mainly to test the performance of the dish at this high frequency. We once were on 6 cm before (ARRL contest 2009) but then the feed was mounted in an (much too) offset way and although we had some QSO's the results were not great. This time the feed was in focus and the dish performed as predicted!
- A test on 3 cm. Motivated by the success on 6 cm we wanted to try 3 cm. We know the mesh is too wide (approximately 7 x 7 mm) so the dish will be 'leaky' on 3 cm. And besides that it's way too big for 3 cm so our beam will be incredibly narrow. But just to know if and how good (or bad) it works it's a nice experiment. After some initial instability problems at the end of 2015 we had a nice result in May 2016. Results were as predicted!

We need to do some more testing but we might be able to use the dish for some 3 cm EME QSO's!

- Of course we were there on January 10 2016 when the 70th anniversary of moonbounce was celebrated by bringing the N2MO dish 'on the moon'. This dish is situated at the location where project Diana was done 70 years ago.
- In April 2016 we hosted the second EUCARA (European Conference on Amateur Radio Astronomy) which was a great success.
- In May 2016 we worked with ESA to solve the problems that occurred with the Italian CubeSat ES@T-II. We received strong signals of the sat but the sat did not react to our commands.

A new challenge

Andreas DJ5AR and I (PA3FXB) had several QSO's on 23 cm using the ISS as a passive reflector. After many tests and failures our first QSO succeeded in May 2013. We had our first QSO in CW, but we also managed an SSB QSO and we also used several digital modes. Andreas and I both use a 3 m dish and we were surprised by the strong signals we got from the ISS reflections. So we got the idea to take this satellite reflection thing one step further….

Trying to use the much smaller 'normal' satellites as a passive reflector!

That would not be possible with our small dishes. So to make up for the smaller satellite we used the 25 m Dwingeloo dish (PI9CAM).

What makes sat bounce so difficult?

First of all ISS is huge compared to other satellites!

The 'bigger' ones are about 20 times smaller than ISS….

They move very fast: 28.000 km/h. That makes tracking very difficult.

Our small 3 m dishes can move very fast. We both use SPID rotators. PI9CAM is a 120 ton construction. Nevertheless it can move surprisingly fast! We can track low and fast sats till about 45 degrees of elevation. Higher orbits are too fast for our monumental dish…

This fast movement of the sats causes a very big and fast changing Doppler shift. So big and fast that it's almost impossible to compensate it manually. Automatic and very accurate Doppler control is necessary to make this work.

First test

Our first test for this project was on February 2014.

We asked several big EME stations to look for satellite reflections.

The following stations tried to spot our tiny reflections: HB9Q, G4CCH, I1NDP, OE5JFL, PA3DZL and DJ5AR. All but one of those stations could not track the sats fast enough.

Moonbouncers are used to track the slow moving moon and not those speeding sats….

Only Hannes OE5JFL saw a short and weak reflection of our sat bounced signal!

So we knew it was possible!

The long road to a QSO…

There are many satellites orbiting the earth. How to select the best ones for a sat bounce QSO? Size matters! The bigger, the better… in general. There is a parameter that's very handy to select the best sats. Radar cross section (RCS)!

On the internet lists are available of the RCS of most sats.

There is one problem however… RCS is defined as the reflectivity on 10 GHz.

We do 1296 MHz. Quite a difference.

If a sat is a simple structure, like a cube or a ball the RCS on 10 GHz will be very comparable to the RCS on 1296 MHz, but if a sat is a fuzzy object with all kind of solar panels, antenna rods and other extensions it's much more difficult to compare RCS on those two frequencies.

Still it's the only figure we have so we use RCS to select the 'biggest' satellites.

Then there is distance. The lower the sat the closer it will get to our antennas, but the lowest sats are the fastest ones so they are more difficult to track and will go too fast for the PI9CAM dish sooner.

We still choose the lowest and most close sats because in the link budget calculation distance is in there to the forth power! So a small change of distance has a big effect on signal strength.

Doppler shift compensation is a very important issue as the Doppler shifts are huge and almost impossible to compensate manually. Andreas uses an SDR and he wrote software for it to compensate for Doppler. At PI9CAM we use a TS2000X and after a long search we found the software SatPC32 able to control the transceiver and to compensate Doppler.

Time is an important thing too as we need some common window to exchange the necessary information for a valid QSO. At PI9CAM we are only allowed to transmit above 10 degrees of elevation and we lose most sats around 45 degrees of elevation. This limits the QSO window very much, so we need to use fast ways to communicate.

What mode shall we use?

Because many sats are old and no longer controlled, they tumble more or less. This tumbling causes fading and very often we simply see/hear no reflections at all for a while. This behaviour forces us to use a timed way of TX/RX. Now to find the best amount of time for RX/TX periods. We tried CW 30 seconds but that appeared too long and often too weak. We went to the digital formats that are available in WSJT. We used FSK441, ISCAT and JTMS but the shortest times possible in those modes are 30 seconds. That appeared to be too long. We came close in completing a QSO a few times but just missed the final rogers every time…

A big step toward a QSO was WSJT-X. One of the new modes in this software is JT9.

JT9 comes in different 'flavours'. We chose the one with the biggest tone spreading (JT9H) because its robustness to drift (Doppler….) is probably the best. The great thing about JT9 is that one can choose 5, 10, 15 and 30 second TX/RX periods!

5 seconds is very short as we learned that often a small manual correction because of racing Doppler is needed, so we started to test with 10 second periods.

This paid off as we finally completed a sat bounce QSO on December 8 2015.

After many days of testing and after many tries via a multitude of satellites DJ5AR and PI9CAM finally had a QSO using OKEAN-O as a passive reflector.

This project took us almost two years but we loved every moment. We learned a lot about satellites, tracking, Doppler, software, etc. etc., but most of all it was BIG FUN!

During our presentation we will show you some pictures and we will play the sounds of the world's first small sat bounce QSO for you ☐

Andreas Imse DJ5AR

Jan van Muijlwijk PA3FXB (team PI9CAM)

VK5MC - Early EME operation using a Rhombic on 144 MHz

Chris Skeer (email: cjskeer@bigpond.com)

Introduction

Recently I had the task of removing a piece of history from my landscape in the form of a 144 MHz EME rhombic antenna. It had stood the test of time and over the years provided a lot of interest to others and good memories for me. Although its removal was a sad occasion I decided to record its history and share it with others.

It all began as a result of the 1971 SERG (South East Radio Group) VHF field day weekend at Jones' Ridge, south east of Mt Gambier and just over the border into Victoria. From there we heard Ray VK3ATN working an American station on 2 metres. The thought went into my mind that it would be nice to do something like that, but how?

During the next few months I made a study of the Moonrise and Moonset times as published in the South Australian Advertiser. However the information was not very helpful, if you have ever tried to see the moon rise during the day you will realize why.

Ray VK3ATN obviously had a system that was working so it was decided to pay a visit to Birchip during March. Trevor VK5NC (VK5ZTN at the time) came with me and has been involved with this project ever since.

Ray was very helpful and gave us details of his rhombic; he showed us what equipment he was using, and a list of Ray's windows were noted. No doubt he has had many visitors over the years interested in EME, as I have also had, but not many take up the challenge.

Ray VK3ATN was the first to develop and utilise the rhombic antenna for EME use on 144MHz in Australia. His first contact was with K2MWA in 1966 closely followed by K6MYC.

After the trip to Birchip it was decided that rhombics were the way to go as I had a suitable area to do it and yagis at that time were not quite as refined as they are today. As the local TV station had recently started up it was decided to put an advert in the local papers to see if I could get some of the towers that were now obsolete. The phones ran hot for a week, many pipe, tubular steel and winch up towers were obtained, and with most people pleased to see them removed from their back yards.

During July 1972, 122 pounds of hard drawn copper wire was purchased at a cost of $81-19 and some six-inch long strain insulators were obtained from America. From the information that Ray had given us I knew that his antenna was at 55 degrees from true north, but I was some two hundred kilometres to the West. As we only had a few degrees to play with how would we get our direction correct? On the sixth of July, Ray had a window so I got up at about 3 am at moon rise and put in two star droppers in line with the Moon. I now knew exactly were to point the rhombic.

Ray VK3ATN had carefully selected his antenna position to catch the moon on its northerly peak in declination, to allow for a couple of days of operation together each month. Figure 1 gives a plot of the azimuth moon rise over a month.

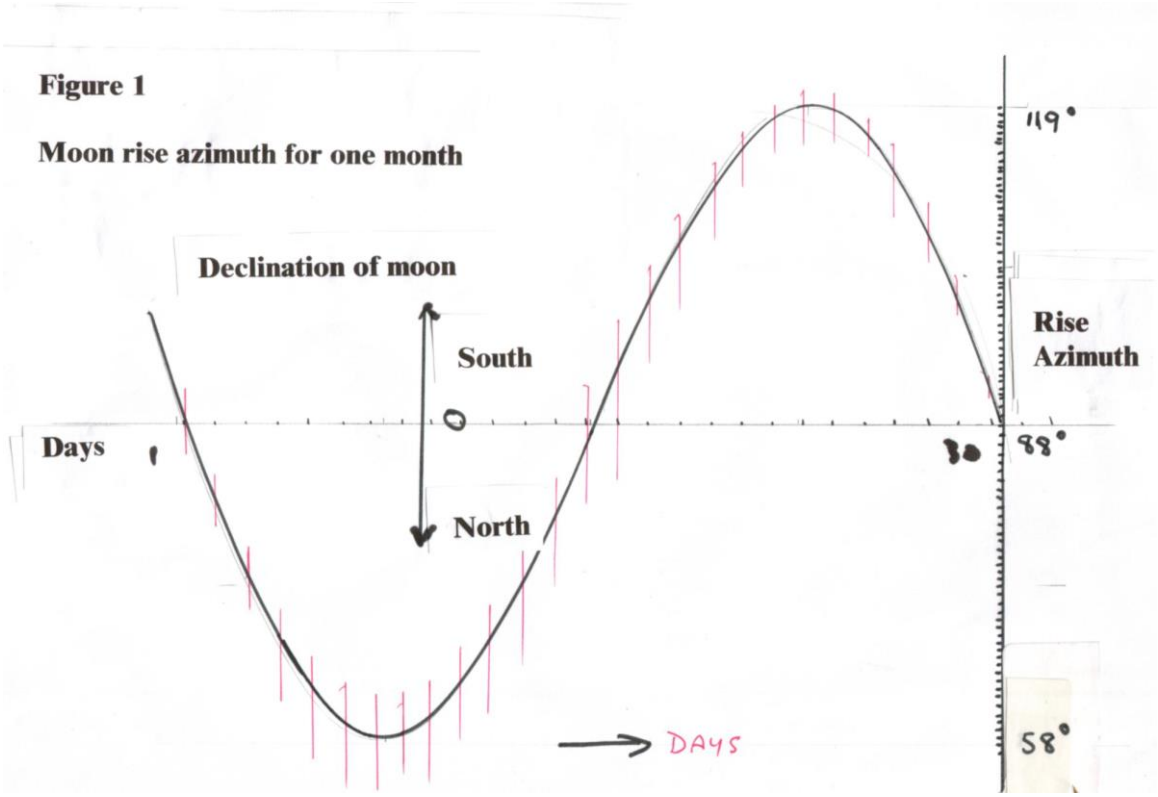

The first rhombic to be put up for moon rise was 342 feet per leg, making it 680 feet long with a feed angle of ten degrees. It was a four-layer antenna, each layer stacked six feet apart and used about a mile of copper wire. The rhombic crossed a country road with three of the towers in an adjoining paddock, the main feed tower was as close to the house as I could fit, but still had 150 feet of home made open wire feed back to the shack near the house. The mind boggles at trying to get permission from the local council to put up such a structure these days. Figure 2 gives the dimensions of the antenna using feet as the measurement, as it was in those days. Figure 2 gives the dimensions of the antenna using feet as the measurement, as it was in those days.

Figure 2

Antenna Dimensions

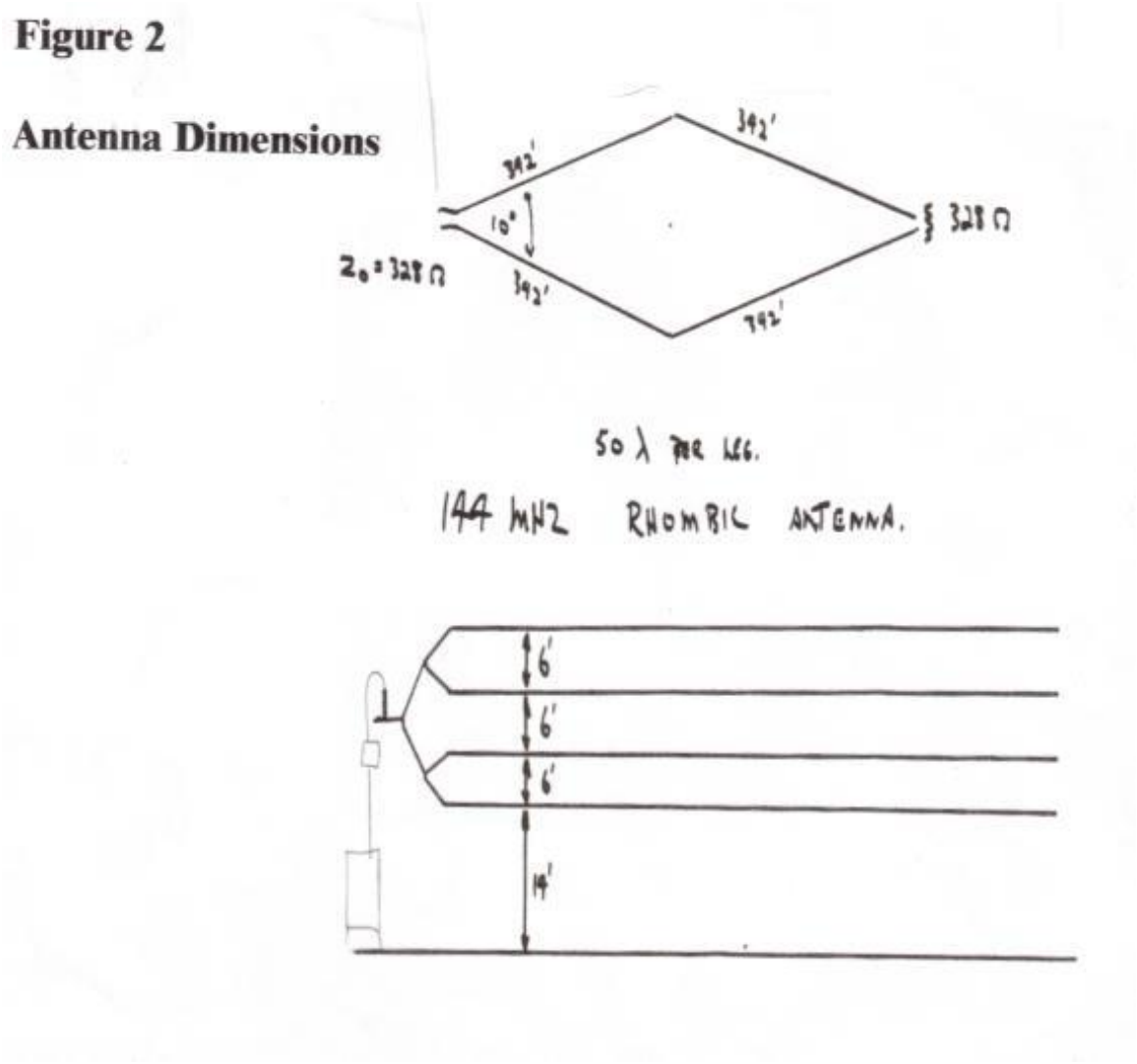

I can always vividly remember the first time I tried for an echo off the moon. When I lifted the Morse key after zero beating the receiver, "Bingo !!!" it was there. I heard echoes for seven and half minutes before they disappeared as I had actually started in the middle of the window of usable time. Over the next few months a plot of the antenna was made to see were I could actually hear echoes, and to determine where it was pointing in the sky. A rhombic such as this has a maximum gain not on the horizon but at a point where the sky wave and ground wave combine, in this case about three and a half degrees above. Figure 3 gives an indication of the antenna pattern and was built up using the times that echo's were heard.

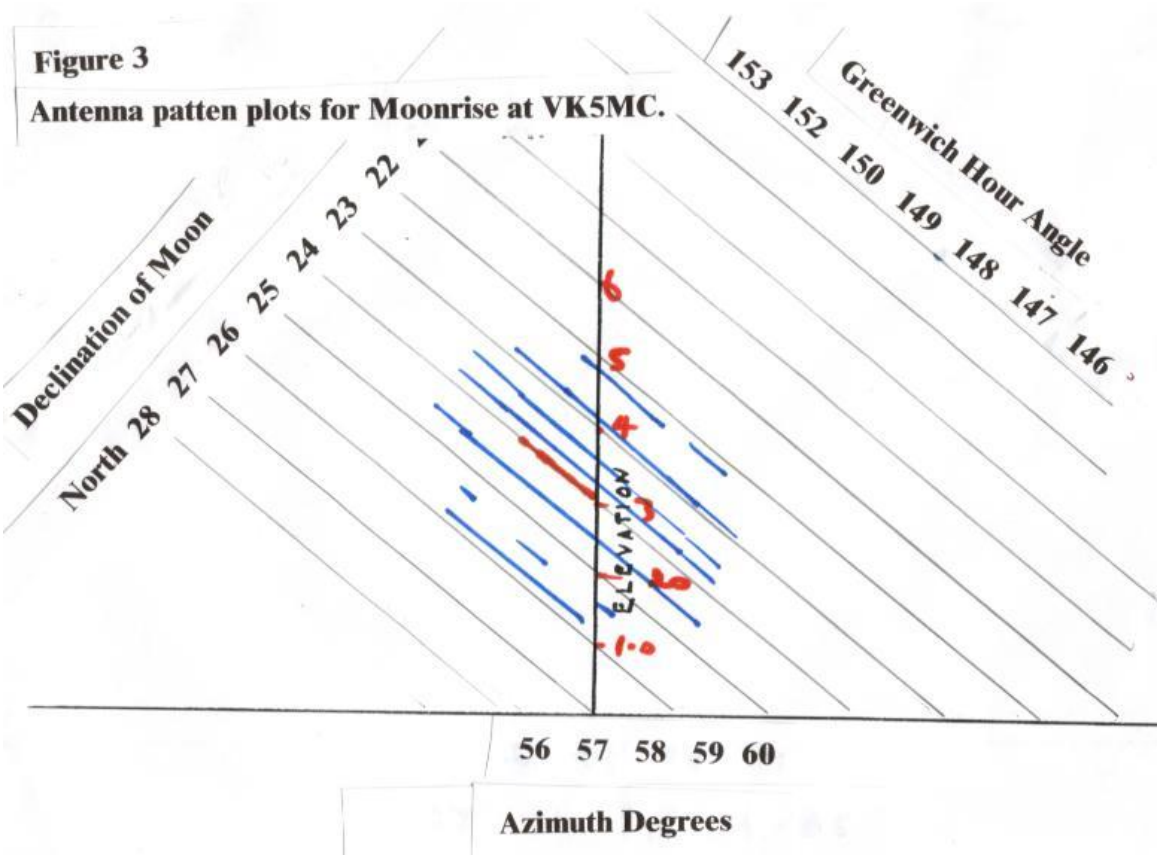

Once it was established where it was pointing in Greenwich Hour Angle and Declination, the only way of predicting when the moon was to be in the correct place was to purchase a Nautical almanac. This contained daily charts of the moon, sun and stars giving their Declination and Greenwich Hour Angle for each and every hour of the year. I would go through the days looking at the declination when this was acceptable, look at the GHA and calculate the centre time of the window. These normally occurred close together on a couple of days per month as Ray had carefully positioned his antenna at a position where the declination reaches a peak. If you plot the declination of the moon over a period of a month it will look like a sine wave, the antenna is positioned to be near the peak of the wave pattern, giving two or sometimes four consecutive days of useable window. When calculating the windows one has to be aware of the position of the sun, if it is too close nobody will be heard. On one occasion, when the sun was rising through the antenna, sun noise was measured at 18 dB over residual noise.

Later it was found that the calculated antenna gain for a four layer rhombic over good ground was 32.5 dbi according to an article, "The design of an optimum rhombic Antenna", by R.P.Decker. From the Collins radio Company. Information supplied to me recently by VK3AUU gives a computer plot of a single 50 wavelength rhombic.

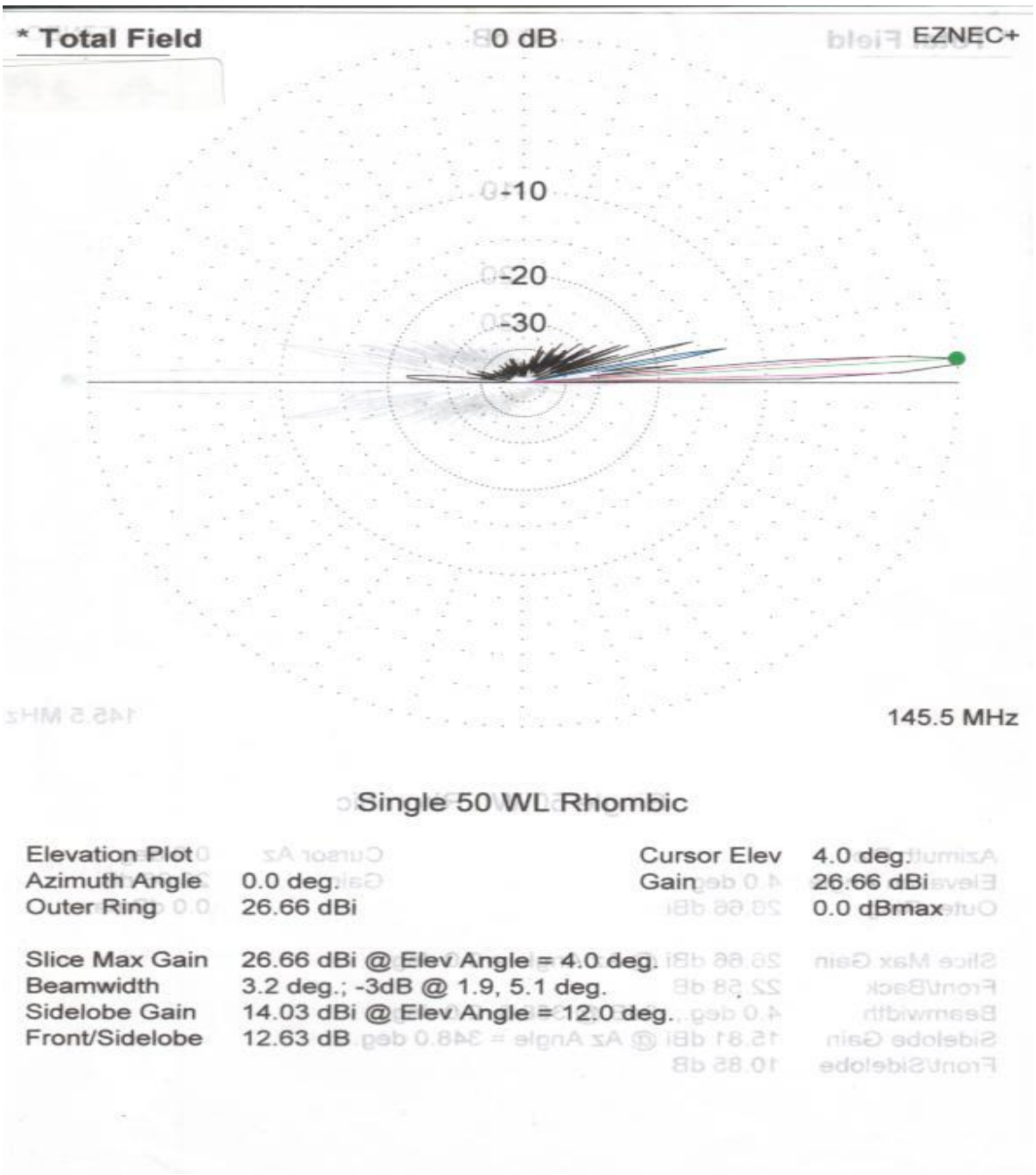

The first attempt at a CW contact was with Bob Sutherland W6PO; it must have been a Sunday afternoon as quite a gathering of SERG members was present. We could hear Bob quite well; he had a 1000 watt 8877 transmitter compared to our 4CX150A which gave around 100 watts out less the losses of 150 feet of open wire feed. Using the T M O reports used on EME (T= odd letters, M= most letters, O= all letters). His report received was "M" and no "Rogers", so it was not an official contact although we had heard him and he had heard us.

After several attempts I did have an "O" report contact with W6PO, on March 13 1973. Bob at that time was using a 160 element collinear antenna, a U-310 preamp and 8877 triode final amplifier.

A few months later, Lionel VE7BQH was heard with very good signals, "O" was sent to him but no report was received from him at all, very frustrated I took the tape recording to Trevor VK5NC. After listening to the tape he said "A good signal from him, but you were calling VE7BYH not VE7BQH that's why he did not give you a report". For those not familiar with Morse code a Q and a Y are a mirror image of each other and for an inexperienced operator as I was at that time it is easy under the pressure of the moment to get them wrong. Needless to say a month or so later I did correct my morse sending and had a contact with VE7BQH.

Almost all of the contacts that were made on 144 MHz EME were made on a random basis, all I did was publish a list of window times for the next six months, when the moon was in the correct place for me to use the moon. Whoever wished to make a contact with me could come up and call me. I would transmit on 144.012 and listen 144.000 to 144.010 for any calls. This would enable me to break way from the normal 2 minute transmit /receive periods if I thought signals were strong enough.

Early in the experimentation it became quite obvious that the only way to get a better signal up to the moon was to cut down the feed line loss. So a small shack was built at the feed end of the rhombic so that the transmitter could be as close to the antenna as possible, a preamplifier was also put at the antenna and the system was starting to work quite well.

Making skeds for a window six months in advance had its problems although I was working for myself and could take an hour off whenever I wished to although sometimes things clashed. One Saturday in March I was involved in a cricket final and could not be there for the window. After some instructions on how to turn on the tape recorder and tune the receiver, the XYL recorded the window for me and heard K8III, K2RTH and VE2DFO all calling me, to no reply as I was busy playing a cricket final.

On 12 December 1984 on a window when no other signals were being heard I was receiving some fairly strong echoes. It was decided to see how low a power could be detected. On that occasion a 10-watt button was put in the "Bird 43" wattmeter and echoes were detected 2db over the noise with 4 watts of power. Obviously on that occasion everything was working in favor and not against as they normally are when looking for echoes.

Over the years one could get a feel for the antenna. As it relied on ground reflection to help it perform, at the end of summer when the ground under neath the antenna was very dry the performance would not be as good as it was in the winter or spring. Faraday and libration fading were also noticeable, some times signals from other stations could be heard quite well but no echoes could be heard at all.

One very memorable contact on Dec 30th 1974, which is recorded on tape, occurred when the late Ron Wilkinson VK3AKC, a 1296 EME operator at that time and VK5NC were present in the shack. It was an evening moonrise and Kelly W8KPY was contacted on CW with 549 reports both ways, no O reports, as signals were fairly good. On his final 73s he requested that I go to SSB for a try, which we did. We heard him quite well and gave him "strength 5 readability 5" report. His report to us was 4x4 ; we received Rogers from him wishing us a good morning. Looking at the back of his QSL card Kelly noted that according to him it was the first ever SSB contact on 144 MHz from the United States to Australia.

It became fairly obvious during operation that I was hearing stations much better than they were hearing me. During 1975 a high power permit was applied for and obtained and the transmitter now was improved to a pair of 4CX250B with 600 watts output on 144 MHz.

IV3NWV - Q-ary Repeat-Accumulate Codes for Weak Signals Communications

Nico Palermo – IV3NWV (e-mail: nicopal@microtelecom.it)

Introduction

Whether coherent or incoherent signal detection is used, channel coding systems designed for amateur radio weak signal communications are currently based on strong, large constraint length convolutional codes or on Reed-Solomon codes.

The WSJT-X program [1], in example, offers four basic modes, namely JT4, JT9, JT65 and WSPR which use incoherent demodulation over an orthogonal MFSK signal set and a binary, k=32 constraint length, R=1/2 rate convolutional coding (JT4, JT9 and WSPR) with a moderate size signal constellation (4-FSK or 8-FSK), or a Reed-Solomon code and a larger 64-FSK signal constellation (JT65).

EMEpsk [2] instead attempts to estimate the channel state and coherently demodulate a BPSK signal using a large constraint length binary convolutional code.

While they are someway remarkably good, both convolutional codes and Reed-Solomon codes do not provide a performance which is very close to the limits predicted by information theory. This fact motivated a continuous research which in the '90s lead to the discovery of turbo codes by Berrou [3] , the rediscovery of the Gallager's LDPC (Low Density Parity Check) codes and the message passing decoding algorithm devised by David MacKay [4].

Here we present a particular class of LDPC codes named QRA, shortly for Q-ary irregular Repeat-Accumulate codes, which exhibit a performance which is closer to the limits predicted by theory. Despite their simplicity, QRA codes appear to be as good as the best known LDPC codes and, unlike them, can be encoded in a linear time [5]. Being non-binary, QRA codes are perfectly suited for a direct implementation on MFSK communication systems and offer a significant coding gain over conventional coded modulation systems based on convolutional or Reed-Solomon codes.

In Section I of this paper, 'QRA Code Basics', we will introduce QRA codes, how they can be concisely described by a graph and some heuristic rules which should help to design or at least to avoid selecting the worst of them.

Section II will present the results of the simulations and compare the coding system used by JT65 (RS(12,63) code over GF(64) + Koetter-Vardy RS soft-decoder) vs. a QRA(12,63) code over the same alphabet and a Q-ary MAPP (Maximum A Posteriori Probability) message passing decoder.

In Section III, 'Message Sequences Aided Decoding', we will explore in more detail the semantic and the redundancy of messages exchanged by two communication nodes (stations) in order to validate with sufficiently low uncertainty the information they have to exchange, as it normally happens when a 2-way connection (QSO) needs to be established and confirmed. We will show that in such a 2-way connection the correctly decoded messages received up to a particular connection phase can be used by a MAPP soft-decoder as a priori knowledge information and improve the receiver detection threshold as much as shorthands and low informative messages do, yet carrying full information, unlike the JT65 protocol shorthand messages, about the sender and recipient addresses.

Unlike the deep search algorithm used in JT65 which relies on a database of communication nodes or other information considered to be plausible, a MAPP decoder can improve its message detection sensitivity much just by exploiting the few messages it is receiving during a specific QSO. This decoding method is indeed inferior to a deep-search based message decoding, nonetheless 1) it provides a significant advantage over a system in which the semantic of the QSO is ignored and 2) it relies only on information received from the communication channel.

I - QRA Codes Basics

QRA codes are very simple codes.

In the most simple form of the encoding process, the K information symbols x_1, x_2,... x_K, each of them belonging to a finite field of size Q (the Galois field GF(Q)), are repeated accordingly to a repetition factor denoted with r_k, and produce the sequence of symbols:

$x_1\ x_1 \dots x_1$	$x_2\ x_2 \dots x_2$	$x_3\ x_3 \dots x_3$	...	$x_K\ x_K\ x_K \dots x_K$
repeat r_1 times	repeat r_2 times	repeat r_3 times		repeat r_K times

The repetition factors r_k don't need to be equal. In the case they are the code is called a regular code (all the information symbols are repeated by the same factor); if they don't, the code is called an irregular code (being the irregularity in the differences of the repeat factors used for each information symbol).

Example: consider a sequence of K=4 symbols {A, b, f, J} which is the information we want to send. We decide to repeat the first symbol 'A' three times (r_1=3), the second and the third symbols 'b' and 'f' five times (r_2=r_3=5) and the last symbol 'J' six times (r_4=6).

The repeated sequence of symbols will be therefore: AAAbbbbbfffffJJJJJJ, and the sequence r_1=3, r_2=5, r_3=5, r_4=6 is the sequence of the repeat factors.

The sequence of repeated information symbols is then reordered accordingly to a given permutation sequence Π and produce as output the sequence of symbols:

$x_{\pi 1}\ x_{\pi 2}\ x_{\pi 3}\ x_{\pi 4}\ x_{\pi 5}\ x_{\pi 6}$ .... $x_{\pi M}$

where $M = \sum_{n=1}^{K} r_n$ is the length of the sequence of the repeated information symbols.

The M parity checks of the code are generated from the above sequence using a recursive formula which generates a sequence of check symbols y_m as a 'weighted' accumulation of the input sequence $x_{\pi 1}$:..$x_{\pi M}$:

$y_0 = 0;$

$y_m = y_{m-1} + w_m \cdot x_{\pi m}$

$m = 1,2,3,...,M$

where w_m are non-null multiplicative factors, called weights, taken from the GF(Q) field. The '+' and the ' · ' operators are not the normal algebraic operators but the additive and the multiplicative operators on the GF(Q) field (see Appendix A).

The encoder output codeword $\underline{x}$ is formed concatenating the sequence of the original K information symbols $x_1...x_K$ with the sequence of the M parity check symbols $y_1...y_M$ computed by the accumulator obtaining a K+M = N symbols sequence:

$\underline{x} = (x_1, x_2, \dots x_N) = (x_1, x_2, \dots x_K, y_1, y_2, \dots y_M)$

The rate of RA codes constructed in this way is R = K/(K+M) and since $M = \sum_{k=1}^{K} r_k$ is always larger than than K when $r_k>1$, the code rate can't be larger than 1/2 and, for practical reasons, it's usually much smaller (R<1/4).

To construct RA codes with a larger rate the sequence of symbols $x_{\pi 1}:..x_{\pi M}$ is grouped in groups of *a>1* symbols per group (*a* is named the grouping factor of the code), all the symbols in a group are xor-ed together and only a parity check per group is generated. In this case the code rate is R = K/(K+M/a) and thus can be higher than the rate of a code in which no symbol grouping is used.

All the QRA codes constructed in this way are called systematic codes (their codewords contain an explicit copy of the source information symbols) and, as we will see later, they are particularly useful in the case that some information symbols are known in advance by the decoder.

As any other linear code, QRA codes may be described by a graph which, besides being extremely important for decoding purposes, provides an immediate sight of the underlying code structure.

For this purpose we denote each of the N symbols x_n of a codeword with a circle (named a variable node) and each of the M check equations $y_m = y_{m-1} + w_m \cdot x_{\pi m}$ with a box (named a check node). Then we connect circles to boxes with edges to indicate which code variables are involved in which code checks. The resulting graph is named a Tanner graph [6] and for an irregular QRA code it looks like in Fig. 1.

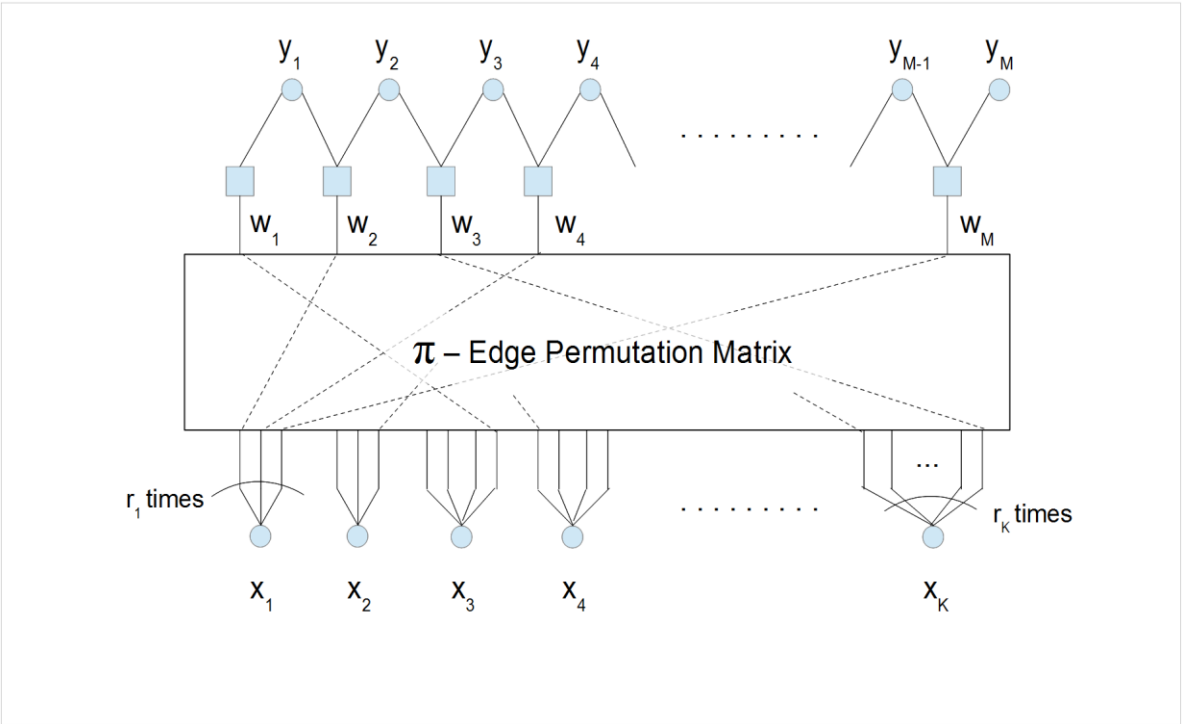

Fig. 1 – The Tanner graph of an irregular QRA Code with grouping factor a=1.

The circles $x_1..x_K$ are the variable nodes associated with the (systematic) information symbols, the circles $y_1..y_M$ are the variable nodes associated with the parity check symbols and the boxes are the check nodes which represent the code parity equations.

From Fig.1 we can see that the variable degrees, that's to say the number of check nodes a variable node is connected to is no more than max (r_k) and that the check nodes degree, that's to say the number of variables connected to a check node, is not larger than three. So far, if we described this code with a MxN parity check matrix H, the matrix for which each codeword of the code satisfies the set of M equations $H\underline{x} = 0$) each of its row would have no more than three non-null entries (the maximum check degree) and each of its columns would have no more than max (r_k) non-null entries (the maximum variable degree), being the average value lower than this maximum.

The parity check matrix of a QRA code is therefore very sparse (few non-null entries per row and few non-null entries per column) and suggests that both regular and irregular QRA codes are, by definition, Low Density Parity Check codes indeed!

From Fig. 1 we see also that an irregular QRA code can be designed with some freedom degrees and that it is completely described by three sets of variables:

- the set of the repetition factors $r_1...r_K$ and the grouping factor *a*,
- the edge permutation matrix π which permutes the repetitions of the information symbols,
- the parity nodes weights $w_1...w_M$

Therefore, which choice of the sequence of repetition factors, grouping factor, edge permutation matrix and code weights leads to the code which, once decoded, offers the lowest word error rate at a given Eb/No ratio? Unlike convolutional and RS codes, QRA codes and LDPC codes lack a true algebraic framework and their construction is often based on a random Montecarlo approach in which a candidate code with some desired properties is simulated, its word error rate curve computed and eventually selected if its performance is better than the average.

The Tanner graph of the code, along with what we know about the message passing decoding, gives some hints on the codes we should avoid. Such hints help to select a 'better than the average' code in a class but the problem is still open, at least for short codes.

So far, how to design and select the proper repetition factors, the edge permutation matrix and the code check weights (a further freedom degree that binary RA codes have not to deal with) when the code is made by very few information symbols?

I (partially) solved this problem with few selection guidelines which helped me finding codes which looks not very bad and at least outperform the Reed-Solomon code used in JT65 quite abundantly.

These rules are rather intuitive and they are listed here below:

a. Systematic symbols repetition factors:

  - irregular codes are always better than regular codes, repetition factors should be properly selected from the set of the integer numbers {3..10},
  - repetition factors lower than three lead to codes with low codeword weights which can be likely confused in a short code decoder and should be avoided,

b. Edge permutation matrix:

  - cycles in the resulting code Tanner graph should be as large as possible. Fig 1, in example, shows that there's a cycle of six edges, which touches the variables x_1, y_2 and y_3. Short cycles limit the ability of a message passing decoder to compute exact probabilities and should be avoided.

- the edge permutation matrix must be designed so that short length cycles are avoided. The minimum cycle length in a code is called 'girth'. Low code girths lead to undesirable information correlation when the code is decoded iteratively by the message-passing algorithm. Design the edge permutation matrix so that the code girth is at least 6.

c. Check node weights:

- weights should be selected in order to maximize codewords distance. In binary codes weights can't be different from 1 (the only non null element of GF (2)), but with Q-ary codes we have a further freedom degree which helps to keep such a distance larger than that of any binary code.

- the weights which refer to the same information symbol (as i.e. w_1, w_4 and w_M which weight the information symbol x_1 as shown in Fig. 1) must be properly selected. In the QRA codes presented in this paper we choose these weights so that for any information symbol x_j the associated weights $w_k(j)$, with $k=1..r_j$ obey the rules:

  1) $\sum_{k=1}^{z} w_k(j) \neq 0$ for any $z<r_j$, and

  2) $\sum_{k=1}^{r_j} w_k(j) = 0$

While someway arbitrary, the weighting rules grant that the accumulator of the code is terminated to zero for any codeword in the code. The consequence of this choice is not trivial. It can be demonstrated that under the framework of iterative, turbo-like decoding and as shown in [7], the EXIT chart [8] of the constituent accumulator sub-code have the property that the extrinsic information $I_{ex}(I_a)$ provided by the accumulator decoder when it is fed by perfect a priori knowledge ($I_a=1$) is $I_{ex}(1)=1$ for any input SNR. This property boosts the ability to successfully decode the received signal whenever a sufficient amount of a priori knowledge about the transmitted codeword is available to the decoder.

II - Simulations Results.

To compare the performance of a QRA code and decoder with the performance of some already well known coding scheme, I searched for some irregular QRA codes with the same parameters of the Reed-Solomon code used in Joe Taylor's JT65 mode, that's to say a code with K=12 information symbols and a codeword length of N=63 symbols taken from an alphabet of Q=64 symbols. To accomplish this task I wrote an algorithm which implements the code design guidelines mentioned in section I and obtained some few codes whose performance I then evaluated with a MAPP soft-decoder for Q-ary LDPC codes based on the message passing algorithm. A description of this decoder is available in Appendix B.

Performance simulations have been made for two type of channel models, the classical AWGN (Additive White Gaussian Noise) model, and the flat block-fading Rayleigh model. For this last model we assume that the channel is affected by a frequency flat fading and that the N multiplicative channel gains a_n which affect the received symbol amplitude are normally distributed complex variables, uncorrelated from symbol to symbol, with average squared amplitude $\bar{a}_n^2 = 1$ for each of the n=1..N codeword symbols.

Fig. 2 shows the Word Error Rate of the 64-ary QRA(12,63) code/decoder in a AWGN channel and compares it with the code/decoders performance used in JT65. The curve of the QRA code is labeled 'QRA' and was obtained allowing the decoder to iterate for a maximum of 100

iterations. The curves labeled FT, KV and BM refers respectively to the Franke-Taylor soft-decoder, to the patented Koetter-Vardy decoder used in earlier implementations of JT65 and to the Berlekamp-Massey hard-decision decoder as published in [10].

The QRA code performance shown in Fig. 2 is referred to the code QRA(12,63) for the 64-FSK modulation whose parameters are listed in Appendix A. On the AWGN channel this code offers a gain of about 1.3 dB over a RS(12,63) Reed-Solomon decoded by the FT decoder and about 1.6 dB over the KV decoder.

The code performance is remarkable, especially in consideration that the theoretical minimum Eb/No ratio at which a 64-FSK system with incoherent demodulation using a code rate R=12/63 (and infinitely long codewords) can communicate with an arbitrary small error rate in a AWGN channel is about 2.1 dB [11]. This is known as the Shannon Limit or the channel capacity. The QRA(12,63) coding system Eb/No threshold, arbitrarily taken at a 50% word error rate, is about 2.7 dB and only 0.6 dB far away the channel capacity. Note also that, at practical word error rates of few percents, the distance of the QRA decoder from the Shannon limit is half the KV decoder distance.

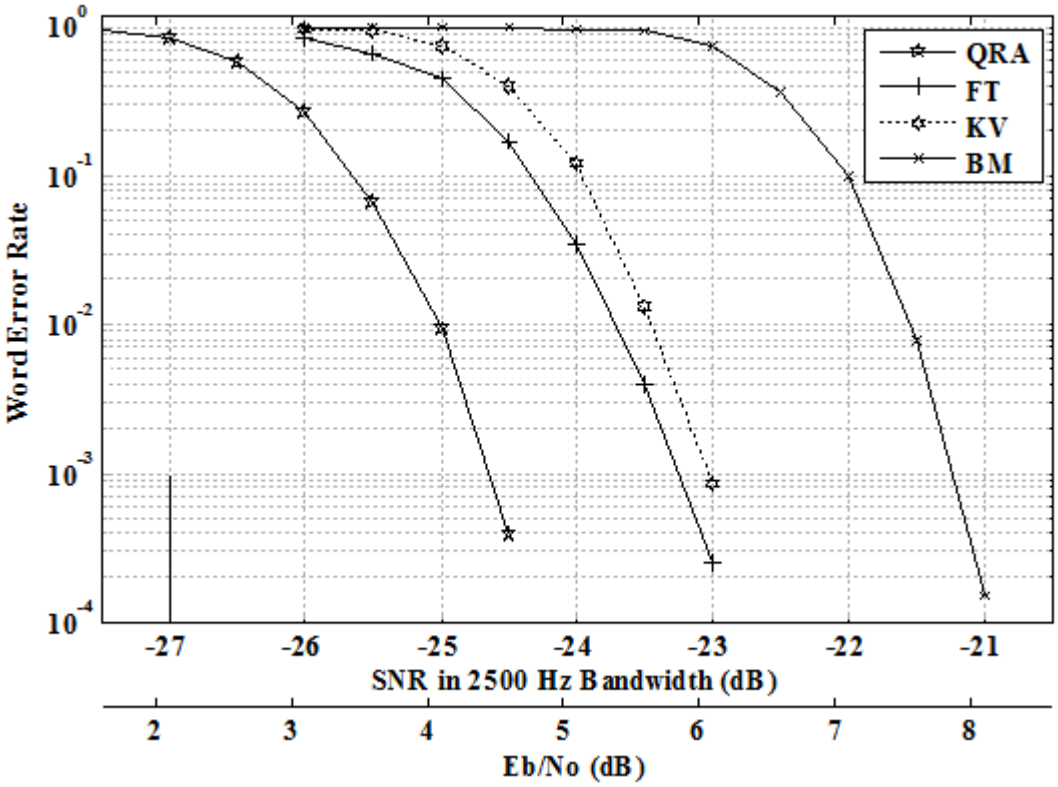

Fig. 2 – Word Error Rate of the QRA(12,63) code with the message passing decoder on the AWGN channel compared with the RS(12,63) Reed-Solomon code decoded by the Franke-Taylor (FT), the Koetter-Vardy (KV) and the hard-decision Berlekamp-Massey (BM) decoders used in JT65. The vertical bar at Eb/No = 2.1 dB is the Shannon capacity limit of a 64-FSK channel with incoherent demodulation and code rate R=12/63.

The horizontal axis scales used in Fig. 2 are the Signal to Noise Ratio in a 2500 Hz reference bandwidth and the Eb/No ratio. The relationship between the SNR in a given bandwidth and the Eb/No ratio depends on the Eb/No ratio through the system effective communication bit rate Rb, the reference bandwidth B and the ratio between the symbols used for synchronization purposes (Nsync) and the information-carrying data symbols (N) accordingly to the formula:

$$SNR = \frac{Rb}{B}\left(1 + \frac{Nsync}{N}\right)\frac{Eb}{No}$$

In JT65, for instance, we have Rb = 72 bit/46.81 s = 1.538 bit/s, Nsync=63 and N=63. Therefore, once expressed in dB, the SNR scale is offset by -29.1 dB respect to the Eb/No scale.

Note that, as the performance of a coding system in terms of the Signal to Noise Ratio in an arbitrary noise bandwidth depends on the effective communication rate Rb and the Nsync/N ratio, the SNR scale is useful to compare different coding systems only when they operate at exactly the same rate and with the same pilot/data symbols ratio. Nonetheless, as long as a coding system performance is evaluated in an AWGN channel, the communication rate is totally irrelevant. When expressed as a function of the Eb/No ratio the word error rate of a coding system is exactly the same whether the communication rate is 1 Bit/s or 1 GBit/s. Of course, since the energy spent per transmitted bit is a product between power and time, the faster the communication rate is, the shorter the bit time interval and the higher the power required to achieve the same error rate of a slower system.

Fig. 3 shows the QRA(12,63) message passing decoder performance as a function of the maximum number of iterations it is allowed to run. Ten decoder iterations are not sufficient to propagate all the available information to the code graph nodes and the decoder performance, while still better than the KV decoder, is less than optimal. This happens because with the message passing algorithm it takes k iterations for any information message to propagate and reach a destination node which is 2*k edges far away from the information source node. The QRA(12,63) code accumulator chain is ~100 edges long and it takes fifty iterations for a message originated by the first accumulator symbol to reach the last one. Nonetheless, twenty decoder iterations are sufficient to get out of the code almost all of its coding power and the full coding gain is achieved with 100 iterations. The effective decoding time has a small, less than linear dependence on the maximum number of the iterations as most of the successful decodes occur within a number of iteration which is usually less than the allowed maximum.

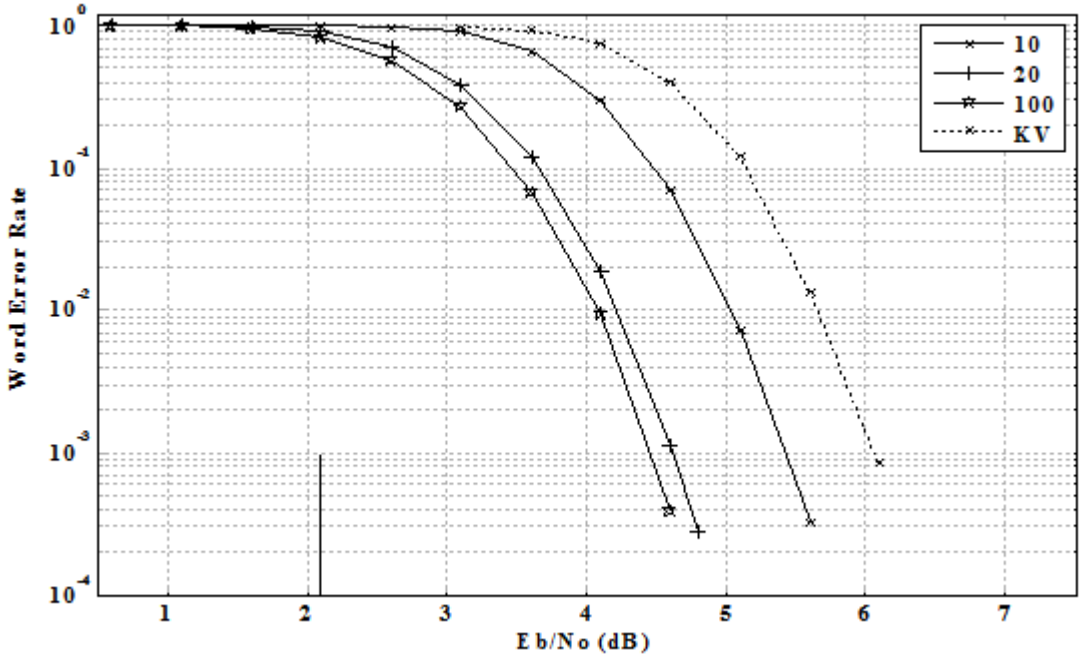

Fig. 3 – QRA(12,63) code performance as a function of the maximum number of iterations the message passing decoder is allowed to run. The KV RS(12,63) Reed-Solomon soft-decoder performance curve is plotted for reference. The vertical bar at Eb/No = 2.1 dB is the Shannon capacity limit of a 64-FSK channel with incoherent demodulation and code rate R=12/63.

Simulations results for the Rayleigh block-fading channel are shown in Fig. 4. The percentage copy curve of the QRA(12,63) code with the message passing decoder is labeled with QRA. The performance of the RS(12,63) code used by JT65 and decoded with the Franke-Taylor decoder is labeled with FT. The simulation of the QRA code assumes that no word is lost in the synchronization process and that the energy losses due to impairments in the synchronization process are negligible. A maximum of 100 iterations are used in the message passing decoder. The curves labeled DS, FT and BM are those published in [10].

We see that for the Rayleigh channel the coding-gain of the message passing decoder versus the FT decoder is 1.5 dB, thus even higher than that achieved in the AWGN channel, and almost independent on the percent copy.

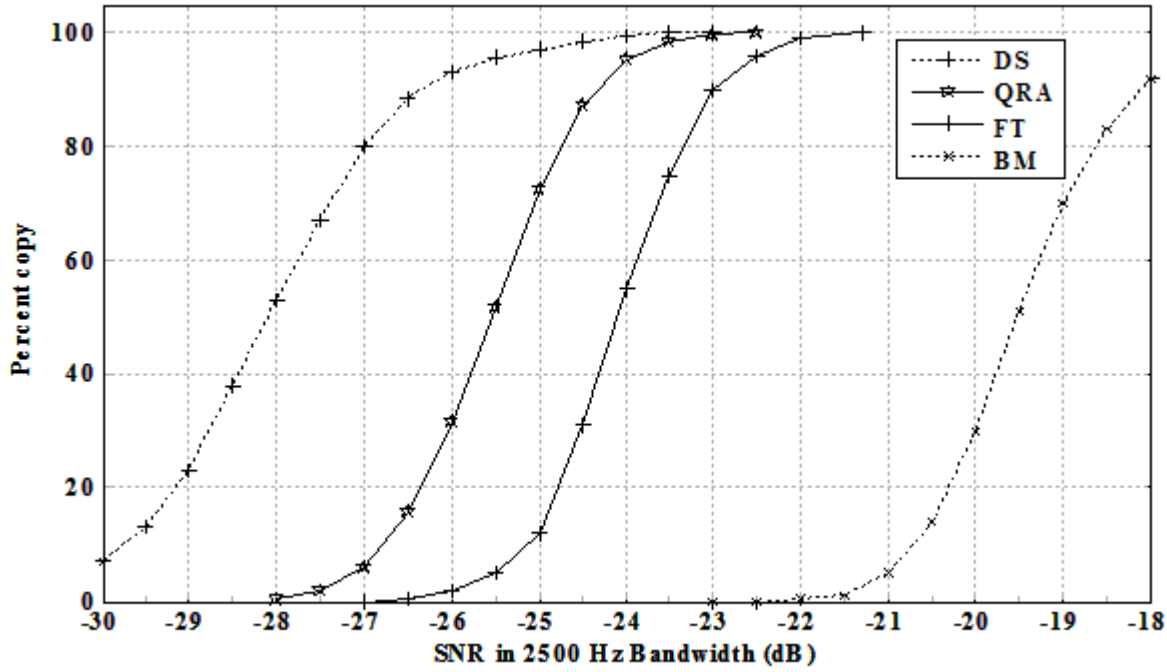

Fig. 4 – Percent copy for the QRA(12,63) code and message passing decoding versus the RS(12,63) code and FT decoding for the Rayleigh channel. The JT65 Deep-Search (DS) and BM decoders curves added for reference.

It should be observed, anyway, that while the QRA curve refers to a "block-fading" channel model, the FT curve refers to a different "1 Hz Doppler-spread" fading channel model and that a direct and more accurate comparison should take into account the differences between them.

It is also important to note that any soft-decoder aimed to achieve the channel capacity needs very accurate channel observations and symbol reliabilities. The message passing decoder makes no exceptions to this rule and in all the simulations it is fed by a symbol reliability metric which models accurately what the theory asks for. As we know from the statistics of a MFSK signal with incoherent demodulation, symbols likelihoods are proportional to a non-linear function of the amplitudes of the received symbol. The exact relationship between the likelihoods of the received amplitudes vector $\underline{r}$ given that the transmitted symbol x was X_j is:

$$\text{Prob}\,(\underline{r} \mid x=X_j) = \Lambda j(\underline{r}) \propto I_0\left(r_j \sqrt{Es}/\sigma^2\right) \quad ,$$

where r_j is the j-th component of the received amplitudes vector, Es is the symbol energy, σ^2 is the noise variance per signal dimension ($\sigma^2 = No/2$) and $I_0(.)$ is the modified Bessel function of the first kind of order zero.

Therefore, to exactly evaluate the likelihoods from the received amplitudes we need to know both the noise variance and the symbol energy Es. In a 64-FSK system with a codeword length of some tens of symbols the noise variance can be evaluated with a good approximation but, since the codeword is not sufficiently long, the estimation of the symbols energy can be affected by large errors that do not allow to compute the required likelihoods with sufficient precision. To overcome this problem the decoder is fed with likelihoods assuming that the symbols energies are those which we would receive at the decoding threshold of the code. This choice is of course optimal only when the received signal is right at the decoding threshold and for the AWGN channel only.

III – Message Sequences Aided Decoding.

Consider a minimal QSO between the two EME stations IV3NWV and SM5BSZ.

The sequence of messages exchanged by them may look as the following:

1 - CQ IV3NWV JN66 …

2 - IV3NWV SM5BSZ JO89 …

3 - SM5BSZ IV3NWV -599 …

4 - IV3NWV SM5BSZ -599 …

5 - SM5BSZ IV3NWV 73 …

6 - IV3NWV SM5BSZ 73 …

where the ellipsis symbol … indicates that, in the attempt to complete the QSO, when a reply from the destination station has not been copied a message can be eventually repeated by the sender.

As done in JT65 and in order to reduce to the essential the amount of the information which each message carries, we can encode any of these messages dedicating 28 bits to encode the call sign of the message source, 28 bits to the call sign of the message destination and 16 bits to encode Maidenhead locators, particular call sign prefixes or suffixes, signal reports or shorthand messages.

Despite this 'source coding' operation, we note that the sequence of messages exchanged in a QSO contain still a large amount of redundancy. The sender and destination call signs, for instance, are repeated over all the QSO.

In the example above, if SM5BSZ wishes to reply a call, he needs at least to wait for a call. In this case he does not need to listen to every possible message but just to those that begin with a CQ. Once he has received a CQ call, and after he replied to the IV3NWV call with message #2, he can found himself in two situations: 1) IV3NWV hasn't copied message #2 and continue to send a CQ with message #1 or, 2) IV3NWV has copied SM5BSZ's reply and is going to answer him with a report sent with message #3 in which both the addresses of the message are already known by the recipient.

This example shows that as long as the QSO proceeds to its conclusion, the stations which are participating to it need to receive less and less information from the other party. JT65 already exploits this opportunity in a simple way and, to improve the decoding ability of recipients, it

sends the last messages of a QSO as handshakes, especially encoded messages which do not convey any address information.

A different decoding approach is to explicitly exploit the information received up to some phase of a QSO and use it as an 'a priori' knowledge which can be passed to the decoder in order to improve its sensitivity. Such a knowledge is passed to the QRA soft-decoder as a probability distribution. In example, if we assume that a symbol in a message is already known, we first pass to the decoder a probability distribution in which we set to zero all the distribution entries that we exclude as possible outcomes; then we let the decoder run and find the best estimation of the message symbols we still know nothing about. What we desire to be excluded from the decoding process is simply assigned a null probability. Following this approach I've simulated the performance of the decoder accordingly to the message fields that are already known by the receiver during the QSO accordingly to the phase the QSO has reached.

In the first phase of the QSO (messages #1 and #2 of the example above) each of the two stations decoders are waiting for a message which is either a CQ call or a reply in which the destination address of a message is his own call-sign. SM5BSZ is waiting for a CQ, IV3NWV is waiting for a reply directed to himself. In both of these cases we can drive the decoder with an a priori knowledge of 28 bits, which is the size of the destination address field, and look for the decoding performance we obtain when such an amount of information is provided to the decoder.

In the second phase of the QSO (messages #3 and #4) both the stations already know that any further message in the QSO have both a specific destination and a source address. In this phase of the QSO, the two stations are actually exchanging their signal reports, and they can drive the decoder with an a priori knowledge of 56 bits, the amount of information contained in the first two fields of a JT65 message. Finally, in the last phase of the QSO, the two stations need only to send an acknowledgment message to confirm what received up to the second phase. We can continue to consider this acknowledgment as a message in which the third field of the JT65 protocol has the intended meaning. In this phase the decoder can be fed with an a priori knowledge of all of the constituent 72 bits of the message (both addresses are known, third field known). This is equivalent to decode real shorthand messages and we might expect to get out from the decoder the same performance obtained when they are used.

Note that, since in each phase of the QSO a station could receive the repetition of a message sent in a previous phase (this happens whenever the other party has not decoded our last reply and retries a transmission), the decoder must be occasionally run twice, once for any of the two messages that the receiver expects in a particular QSO phase. From a practical point of view, the decoder needs the intrinsic symbols information, that's to say the likelihoods computed from the channel observations; thus we can simply mask to zero all the likelihoods which we do not consider plausible.

In Fig. 5 we show the performance of a decoding system based on this approach when the QRA(12,63) code is decoded with some amount of known information and a block-fading Rayleigh channel model is assumed.

The curve labeled AP28 refers to the decoding of messages in which the first 28 bit field of the message is known to the receiver. This situation happens whenever we are waiting for a CQ call or for a a reply to our own call-sign (in this case the destination address of the reply message is our call sign, therefore we already know it in advance).

The curve labeled AP56 refers to the decoder performance when both the sender address and the destination address of the incoming message are known by the receiver, as it happens when the receiver is waiting for a signal report, an acknowledgment or some other shorthand information.

The sensitivity to CQ calls and replies directed to the caller (curve AP28) is 2.5 dB better than the sensitivity obtained with the RS code and the FT decoder currently used in JT65.

The sensitivity to signal reports and shorthand messages (curve AP56), which still carry 16 bits of unknown information, is remarkably superior to that of the deep-search algorithm. This is not really surprising, anyway. The deep-search is a maximum likelihood algorithm which looks for the most probable codeword among a restricted set of candidates; the QRA decoder computes symbol-wise probabilities which, being marginal distributions (or weighted averages) of all the possible cases, produce a better estimate of the transmitted symbol messages. Such a better sensitivity suggests that a more uniform content among messages could help lowering the decoding threshold even more. The Maidenhead locator, in example, could be transmitted before the end of a QSO and prior to the final acknowledgments. In this case the CQ/reply messages in the initial phase of the QSO would contain only 28 bit of information, being the other 44 bits (the 28 bits destination field and the 16 bits field used by the third field of a JT65 message) already known by the receiver.

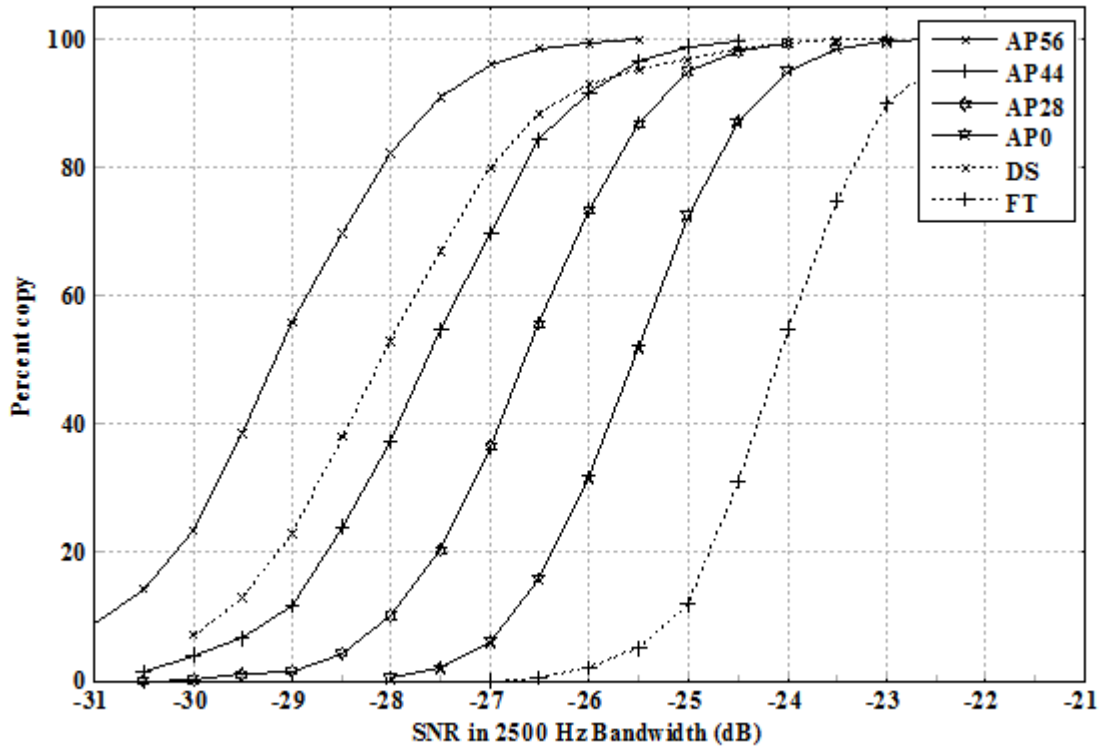

Fig. 5 – Word Error rate of the QRA(12,63) decoder in the Rayleigh channel as a function of the of the a priori (AP) knowledge available to the receiver. The curves AP'nn' indicates the decoder performance when 'nn' bits in a message are known in advance by the receiver. The curve labeled AP0 is the decoder performance when we have no knowledge of the incoming message, as it happens for instance when the message is a plain JT65 text message. This is the same curve that we named QRA in Fig. 4.

The performance of this messaging scheme is shown by the curve labeled AP44 and is just 0.5 dB away from the deep-search algorithm despite we are not using any knowledge other than that we are expecting to receive a call or an answer directed to ourselves. The decoding threshold of a QSO initiated in this way is 3.5 dB better than that of the FT decoder although, to achieve this remarkably good performance, the QRA decoder still uses information received from the communication channel only.

IV – Conclusions

A software package for encoding and decoding the QRA codes I've presented in this paper is going to be published as open source under a GNU GPL license in the hope that it will be useful to the EME digital modes community.

I would like to thank Leif Åsbrink, SM5BSZ for his fruitful suggestions and the encouraging attention he deserved to me during this development. I'd like to thank Joe Taylor, K1JT which along these years always provided me the information and the tools I needed to start this development from.

Finally, a special thank to Andrea Montefusco, IW0HDV which helps me whenever there's some source code to port in OSs other than the one I'm used to work with.

APPENDIX A.

64-ary QRA(12,63) Code Parameters

The irregular QRA(12,63) code on GF(64) whose performance has been shown in Section II and compared with the RS(12,63) code used in JT65, has been designed following the guidelines indicated in Section I and its parameters are listed here below.

Information symbols repetition factors r_k:

3, 3, 3, 3, 4, 4, 4, 5, 5, 5, 6, 7

Note 1: the first information symbol is repeated three times, the last one 7 times.

Edge permutation matrix:

3, 11, 0, 1, 7, 8, 6, 5, 10, 4, 11, 9, 0, 2, 6, 7, 8, 4, 11, 5,

10, 2, 1, 9, 3, 8, 4, 11, 5, 7, 10, 9, 6, 3, 11, 5, 8, 10, 0, 7,

9, 11, 4, 2, 10, 6, 8, 1, 9, 7, 11, 10

The grouping factor is a=1.

Note 2: the twelve systematic symbols of the code are numbered from 0 to 11. Accordingly to Fig. 1 the first accumulator check input is connected to information symbol #3, the second input to information symbol #11 and so on. The shortest cycle in this code has length 8.

Weights w_k:

39, 0, 34, 16, 25, 0, 34, 48, 19, 13, 29, 56, 0, 5, 39, 42, 31, 0, 10, 0,

57, 62, 33, 43, 0, 14, 22, 48, 28, 20, 5, 45, 16, 43, 17, 4, 32, 0, 31, 0,

0, 28, 57, 0, 18, 0, 60, 0, 10, 31, 57, 27

Note 3: weights are given as discrete logarithms in base α, where α is a primitive element of the GF(64) field (see note 5 below for more).

Note 4: both the edge permutation matrix and the weights are sequences of 52 entries while the code has only 51 check variables. The last entry in the tables is not used by the encoder (but it is used by the decoder) and ensures that the implicit 52nd code accumulator check symbol is always 0 whatever the information symbols are.

Note 5: (A very short tutorial on finite fields).

A finite field is a set of elements in which additions and multiplications are defined much as the ordinary operations on an infinite field like that of the integer numbers:

- The addition has a neutral element called 0 such that for any element α in the field $\alpha+0=\alpha$.

- The multiplication has a neutral element called 1 such that for any element α in the field $\alpha\cdot 1=\alpha$.

- Both the addition and the multiplication are symmetric in their operands.

$\alpha+\beta=\beta+\alpha$ and $\alpha\cdot\beta=\beta\cdot\alpha$.

- Every element α has an additive inverse which, for finite fields of size $Q=2^q$, is α itself ($\alpha=-\alpha$)

- Every element $\alpha \neq 0$ has a multiplicative inverse α^{-1} such that $\alpha\cdot\alpha^{-1}=1$.

- Taken a field element α, with $\alpha \neq 0$ and $\alpha \neq 1$, we can form the sequence of elements α, $\alpha\cdot\alpha=\alpha^2$, $\alpha\cdot\alpha\cdot\alpha=\alpha^3$, etc.... Each of the elements of this sequence must belong to the field but, since the number of the elements if finite, not all the powers of α are distinct.

We call α a primitive element of a field the element for which all the powers α^0, α^1, α^2, α^3, ..., α^{Q-2} are distinct elements of the field. Every element but the 0 can be expressed as a power of the primitive element. We define the discrete logarithm in base α of an element β, $\log_\alpha(\beta)$, as the integer number j such $\beta=\alpha^j$. The first entry in the code weights table above (39) means that the weight associated with the first accumulator input is α^{39}.

- Any primitive element α of a finite field is a root of an irreducible polynomial G(x) of degree $q=\log_2(Q)$ with binary coefficients a_q, so that $G(x) = x^q + a_{q-1}\,x^{q-1} + a_{q-2}\,x^{q-2} + \cdot\ldots + a_1\,x + a_0 = 0$. This generator polynomial allows to express any element of the field as a linear combination of the first q-1 powers of a primitive element α of the field:

$0 = 0\cdot\alpha^{q-1} + 0\cdot\alpha^{q-2} + \ldots + 0\cdot\alpha^1 + 0\cdot\alpha^0$

$1 = 1\cdot\alpha^0$

$\alpha = 1\cdot\alpha^1$

$\alpha^2 = 1\cdot\alpha^2$

…

$\alpha^q = a_{q-1}\cdot\alpha^{q-1} + a_{q-2}\cdot\alpha^{q-2} + \ldots + a_1\cdot\alpha^1 + a_0\cdot\alpha^0$ (as dictated by the generator polynomial)

$\alpha^{q+1} = \alpha\cdot\alpha^q = a_{q-1}\cdot\alpha^q + a_{q-2}\cdot\alpha^{q-1} + \ldots + a_1\cdot\alpha^2 + a_0\cdot\alpha^1 =$

$a_{q-1}(\,a_{q-1}\alpha^{q-1} + a_{q-2}\alpha^{q-2} + \cdot\ldots + a_1\alpha^1 + a_0\alpha^0) + a_{q-2}\alpha^{q-1} + \ldots + a_1\alpha^1 + a_0\alpha^1 =$

$(a_{q-1}+a_{q-2})\alpha^{q-1} + (a_{q-1}a_{q-2}+a_{q-3})\alpha^{q-2} + \ldots + (a_{q-1}a_1+a_0)\alpha^1 + (a_{q-1}a_0)\alpha^0$

…

Thus any element of the field can be expressed by a unique q-uple of binary digits.

For the QRA(12,63) code presented here the primitive element α of the field is a root of the polynomial is $P(x)=x^6 + x + 1$, so that $\alpha^6 + \alpha + 1 = 0$ or $\alpha^6 = \alpha + 1$ and the relationship between the element fields, their discrete logarithm and their binary representation is shown in the following table:

El	Log	Binary	El	Log	Binary	El	Log	Binary	El	Log	Binary
0	-	000000	α^{15}	15	101000	α^{31}	31	100101	α^{47}	47	100111
1	0	000001	α^{16}	16	010011	α^{32}	32	001001	α^{48}	48	001101
α^{1}	1	000010	α^{17}	17	100110	α^{33}	33	010010	α^{49}	49	011010
α^{2}	2	000100	α^{18}	18	001111	α^{34}	34	100100	α^{50}	50	110100
α^{3}	3	001000	α^{19}	19	011110	α^{35}	35	001011	α^{51}	51	101011
α^{4}	4	010000	α^{20}	20	111100	α^{36}	36	010110	α^{52}	52	010101
α^{5}	5	100000	α^{21}	21	111011	α^{37}	37	101100	α^{53}	53	101010
α^{6}	6	000011	α^{22}	22	110101	α^{38}	38	011011	α^{54}	54	010111
α^{7}	7	000110	α^{23}	23	101001	α^{39}	39	110110	α^{55}	55	101110
α^{8}	8	001100	α^{24}	24	010001	α^{40}	40	101111	α^{56}	56	011111
α^{9}	9	011000	α^{25}	25	100010	α^{41}	41	011101	α^{57}	57	111110
α^{10}	10	110000	α^{26}	26	000111	α^{42}	42	111010	α^{58}	58	111111
α^{11}	11	100011	α^{27}	27	001110	α^{43}	43	110111	α^{59}	59	111101
α^{12}	12	000101	α^{28}	28	011100	α^{44}	44	101101	α^{60}	60	111001
α^{13}	13	001010	α^{29}	29	111000	α^{45}	45	011001	α^{61}	61	110001
α^{14}	14	010100	α^{30}	30	110011	α^{46}	46	110010	α^{62}	62	100001

Additions between elements are simply the xor of the binary representations of the arguments. Multiplications can be carrier out noting that each element of the field (but the 0) can be seen as the power of a primitive element and that, when two elements are multiplied, their exponents must be summed (modulo 63) and then the primitive element exponentiated to this sum to get the final result.

For what concerns the code properties, the choice of the generator polynomial is irrelevant, being any particular choice just a different map of the binary q-uples which represent the field elements.

APPENDIX B.

MAPP Decoding of Q-ary LDPC codes. The Message Passing Algorithm.

LDPC codes can be efficiently decoded by the message passing algorithm, a method strictly connected with what in the '90s were already known by the artificial intelligence community under the name of Pearl's "Belief Propagation" algorithm [9].

The MAPP (Maximum A Posteriori Probability) decoding problem we are concerned with is rather simple to state:

- Given the observations on the received signal, any eventual a priori knowledge we have on the transmitted symbols of a codeword and for each information symbol in a codeword:

A. Compute the a posteriori, symbol-wise probability that a symbol was sent,

B. Select as the best estimate of the transmitted symbol the symbol value which looks

more likely and maximizes the statistical probability computed at point A.

Although simply to state, when the underlying math of the problem is explored in detail, the task looks extremely complex and, before the message passing algorithm became known, it was indeed something really formidable to solve.

Consider a transmission system that encodes messages in N symbols codewords, that each of the codeword symbols x_n , (n=1..N), is encoded mapping each symbol to a signal waveform and then sent over a memoryless communication channel which add some noise to these waveforms.

At the receiving site, the receiver correlates the received signal with the (known) waveforms used by the transmitter and, for each symbol of the codeword, produces a set of observations s_n (n=1..N) which gives some information on the transmitted symbols.

If we are using a Q-ary code, a MFSK modulation which maps each symbol value to one of the available modulation tones and an incoherent demodulator, each of the s_n observations is in fact a vector of size Q of real numbers and we usually denote it with the underlined symbol $\underline{s}_n$ to indicate that it is a vector.

Under these assumptions and accordingly to the formulation of the MAPP decoding problem we would like to:

A. For every value X_1, X_2, …, X_N the transmitted symbols x_1,x_2,...x_N could assume, compute the a posteriori codeword probability:

Prob {$x_1=X_1$, $x_2=X_2$, $x_3=X_3$, … $x_N=X_N$ given the observations $\underline{s}_1$, $\underline{s}_2$, $\underline{s}_3$, …, $\underline{s}_N$)

B. For every value X_n that the symbol x_n can assume compute the symbol-wise probability:

Prob {$x_n=X_n$ given the observations $\underline{s}_1$, $\underline{s}_2$, $\underline{s}_3$, …, $\underline{s}_N$)

C. For each symbol x_n , choose $\hat{X}_n$ as the the best estimate of the transmitted symbol x_n so that:

$\hat{X}_n$ = value which maximizes Prob {x_n=X_n given the observations $\underline{s}_1$, $\underline{s}_2$, $\underline{s}_3$, …, $\underline{s}_N$)

It is known that, in general, the exact solution of this problems is of exponential complexity.

In step A, in example, we have to compute a function for every possible combination of the transmitted information symbols, a task which is prohibitive when a codeword has more than very few (>3) tens of information bits. Furthermore, if this step looks not sufficiently complex, we then have to compute the probability at step B which can be computed summing the probability at step A over all the combination of symbols but the one we are interested in (this operation is called probability marginalization) and to do this summation for each of the codeword information symbols.

The message passing algorithm [4] [12] is a powerful tool which exploits the fact that the a posteriori probability Prob {x_1=X_1, x_2=X_2, x_3=X_3, … x_N=X_N given the observations $\underline{s}_1$, $\underline{s}_2$, $\underline{s}_3$, …, $\underline{s}_N$), and any of its marginal distribution, can be computed quickly and exactly when the Tanner graph of the code is a tree and it can be factorized into products which can be orderly evaluated.

Accordingly to Bayes' rule about conditional probabilities we know that Prob {x given y} (we will indicate this probability with the symbol p(x|y)) is:

$$p(x|y) = p(y|x)\, p(x) / p(y)$$

We note that if we want to look for the x that maximize p(x|y), the factor p(y) appears in the equation as a multiplicative constant and we can ignore it simply writing:

$$p(x|y) \propto p(y|x)\, p(x)$$

with the meaning that the a posteriori probability p(x|y) of x given the observation y is proportional to the probability p(y|x) of the observation y given x, which is called the likelihood of y given x, multiplied by the a priori probability p(x) of the variable x.

Thus we can rewrite the a posteriori symbols probability of a codeword as:

$$p(x_1, \dots x_N \mid \underline{s}_1, \dots, \underline{s}_N) \qquad p(\underline{s}_1, \underline{s}_2, \underline{s}_3, \dots, \underline{s}_N \mid x_1, x_2, \dots x_N)\, p(x_1, x_2, \dots x_N)$$

For a memoryless channel each observation $\underline{s}_j$ depends only on the transmitted symbol x_j and the likelihood $p(\underline{s}_1, \underline{s}_2, \underline{s}_3, \dots, \underline{s}_N \mid x_1, x_2, \dots x_N)$ can be factorized as a product of terms $p(\underline{s}_j \mid x_j)$, j=1..N.

We also note that the a priori probability $p(x_1, x_2, \dots x_N)$ depends both on the code we are using and on the knowledge we may have on any of the transmitted information symbols.

In example if the code we are using imposes the parity check equation $x_1+x_{10}+x_{54} = 0$ we know that this probability $p(x_1, x_2, \dots x_N)$ must be null for any codeword in which the equation $x_1+x_{10}+x_{54} = 0$ is not satisfied. This indicates that also $p(x_1, x_2, \dots x_N)$ can be factorized in a product of terms and we can write:

$$p(x_1, x_2, \dots x_N) = f_1(\underline{X}_1)\, f_2(\underline{X}_2) \dots f_M(\underline{X}_M)\, p_1(x_1) p_2(x_2) \dots p_K(x_K)$$

where: 1) each of the terms $f_m(\underline{X}_m)$ represents a code constraint (a parity check equation) which depends on a subset $\underline{X}_m = \{ x_{m1}, x_{m2} .. x_{mM} \}$, m=1..M, of codeword symbols and evaluate to 1 or 0 if the symbols involved in the set $\underline{X}_m$ satisfy the m-th parity check equation of the code or not, and 2) $p_1(x_1)p_2(x_2)...p_K(x_K)$ represent the a priori probability we have of the information symbols contained in a codeword.

Under the above hypothesis we can rewrite the a posteriori probability of a codeword given the channel observations, the code constraints and the a priori probabilities of the codeword symbols as a product of terms:

$$p(x_1, x_2, \ldots, x_N \mid \underline{s_1}, \underline{s_2}, \ldots, \underline{s_N}) = \prod_{n=1..\mathrm{N}} p(\underline{s_n} \mid x_n) \cdot \prod_{m=1..\mathrm{M}} f_m(\underline{X_m}) \cdot \prod_{k=1..\mathrm{K}} p_k(x_k) \quad (1)$$

The marginal, symbol-wise a posteriori probability of the symbol x_k , for any k=1..K, can be then computed summing the codeword probabilities over all the codeword symbols except the symbol x_k:

$$p(x_k \mid \underline{s_1}, \underline{s_2}, \ldots, \underline{s_N}) = \sum_{x_1} \sum_{x_2} \ldots \sum_{x_{k-1}} \sum_{x_{k+1}} \ldots \sum_{x_N} \prod_{n=1..\mathrm{N}} p(\underline{s_n} \mid x_n) \cdot \prod_{m=1..\mathrm{M}} f_m(\underline{X_m}) \cdot \prod_{k=1..\mathrm{K}} p_k(x_k)$$

or more shortly as:

$$p(x_k \mid \underline{s_1}, \underline{s_2}, \ldots, \underline{s_N}) = \sum_{\neg x_k} \prod_{n=1..\mathrm{N}} p(\underline{s_n} \mid x_n) \cdot \prod_{m=1..\mathrm{M}} f_m(\underline{X_m}) \cdot \prod_{k=1..\mathrm{K}} p_k(x_k) \quad (2)$$

where with $\sum_{\neg x_k} \ldots$ we indicate that the summation is done over all the variables except x_k.

Eq. (1) shows that the APP (A Posteriori Probability) of a codeword is simply a product of factors which involves a set of variables and we can represent it in a graphical way using a Tanner graph as we do with codes: we indicate each variable $x_1,\ldots,x_N$ with a circle, each factor of the equation with a box and then we connect the circles (the equation variables) to the boxes (the equation factors) they are referred by with edges. The factors graph we obtain in this way is identical to the Tanner graph of the code with just a small difference: the code variables are now connected to the additional factors $p(\underline{s}_j|x_j)$ which represent the channel observations and the factors $p_k(x_k)$ which represent the a priori information we have on code the information symbols.

The factors graph for the RA code presented in Section I is shown in Fig. 6.

The message passing algorithm exploits the factorization shown in the factors graph to compute iteratively the a posteriori probabilities we are interested into in an very efficient way.

To carry out this task it simply considers variables and check equations as sources and receivers of messages. Such messages are probability distributions. They are computed accordingly to the type of the graph nodes they are involved into and iteratively sent along the graph edges.

Each iteration of the message passing algorithm consists of two steps:

a. compute messages directed from boxes to circles given the messages received by circles,

b. compute messages directed from circles to boxes given the messages received by boxes

The message passing algorithm is started at step a) initializing the messages directed towards each graph circle to the probability distributions coming from the channel observations and any a priori information (the boxes labeled $p_n(x_n)$ and $p(\underline{s}_n|x_n)$). As in this initialization phase no information is still available from the code checks $f_1,\ldots,f_M$, all the boxes $f_1,\ldots,f_M$ are initialized to send to the circles they are connected to a message which corresponds to a uniform probability distribution.

At step b), once every circle in the graph has been provided by messages on any of the edges it is connected to, for any of the edges that connects it to a box, it computes a message directed to that box as the product of all the incoming messages but the message coming from that box.

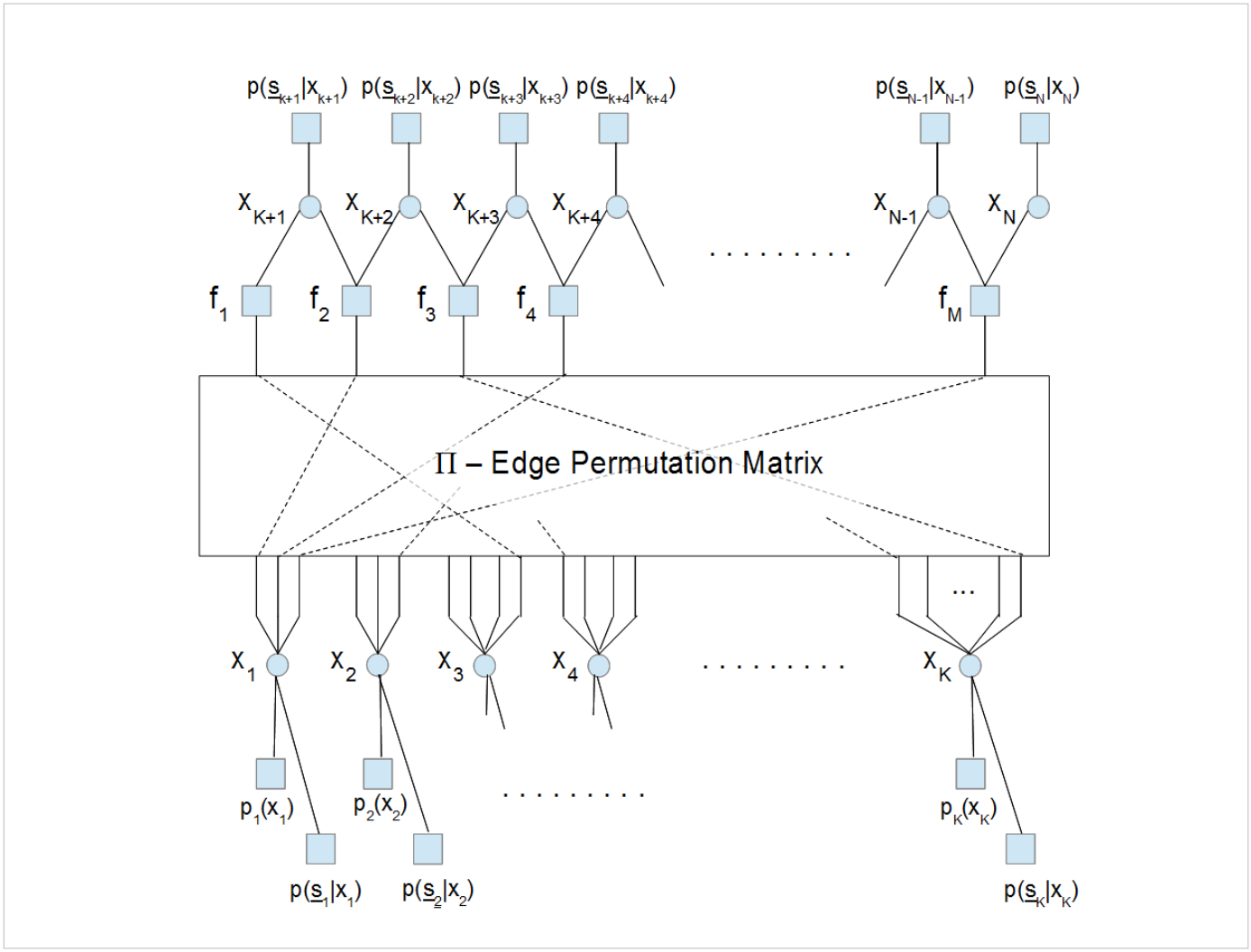

Fig. 6 – The factors graph for the computation of a posteriori probabilities in a RA code. The circles x_n represent the code symbols. The boxes f_m represent the factors associated with the code parity check constraints. The boxes labeled $p_k(x_k)$ indicate the factors associated with the codeword symbols a priori information and the boxes labeled $p(\underline{s}_n|x_n)$ represent the symbols likelihoods (the channel observations).

If we indicate with v_n the generic variable (circle) of the graph, with C(n) the set of the checks it is connected to in the factor graph, with $msg(c_m \rightarrow v_n)$ the message received by the variable v_n by the code check c_m and with $msg(v_n \rightarrow c_m)$ the message sent by v_n to c_m, the variable to check message update rule of step b. can be concisely expressed as:

$$msg(v_n \rightarrow c_m) \propto \prod_{j \in C(n),\, j \neq m} msg(c_j \rightarrow v_n), \quad n = 1..N, \forall m \in C(n) \qquad \text{v} \rightarrow \text{c step}$$

This update rule simply states that the probability of a product of (statistically independent) terms is proportional to the product of their probabilities, i.e. that $p(x)=p_1(x)p_2(x)...p_{...}(x)$, therefore, whenever we have some statistically independent evaluations of the variable v_j we can output their product as result. The proportionality constant is determined noting that the output $msg(v_n \rightarrow c_m)$ must be a probability distribution and its elements must sum to unity. Therefore the actual messages output by the v→c step are normalized accordingly to:

$$msg'(v_n = V_k \rightarrow c_m) = \frac{msg(v_n = V_k \rightarrow c_m)}{\sum_{j=1..Q} msg(v_n = V_j \rightarrow c_m)}, \; k=1..Q$$

where $V_1,V_2,..V_Q$ are the values a variable can assume and Q is the cardinality of the code alphabet.

After the first iteration the checks to variables messages msg($c_m \rightarrow v_n$) of step a. are updated noting that if we need to compute the probability of a variable involved in a parity equation, instead of making a product of probability functions, we have to make convolutions.

Suppose, in example, that we want to compute the probability of the variable x_1 given the constraint $x_1+x_2+x_3=0$ (mod2) and the probabilities $p(x_2)$ and $p(x_3)$. To compute the probability that x_1 assumes a particular value X_1 we have to consider all the cases for which $X_1 + x_2+x_3=0$, that's to say sum the product of the probabilities that $x_2=0$ and $x_3=X_1$, $x_2=1$ and $x3=X_1+1$ (note that we are working with sums mod2) and so on.

If we indicate with V(m) the set of variables connected to the check c_m , the msg($c_m \rightarrow v_n$) update rule of step a. is therefore:

$$msg(c_m \rightarrow v_n) = \sum \prod_{j \in V(m),\ j \neq n} msg(v_j \rightarrow c_m) \qquad m = 1..M, \forall n \in V(m) \qquad c \rightarrow v \text{ step}$$

where we have indicated with the symbol $\sum \prod \cdots$ the convolution of its arguments.

After a given number of iterations are made the a posteriori probability of each variable is computed as the product of all the messages coming from the factors it is involved with:

$$app(v_n) \propto \prod_{j \in C(n)} msg(c_j \rightarrow v_n)$$

Note that this computation is identical to the $v \rightarrow c$ step with the only difference that now the product is made on all the inbound edges connected to a variable.

Finally, the last step of the decoding process consist in selecting as the best estimate of the transmitted symbols, the variable value which maximizes the a posteriori probability computed in this way. Once this symbols selection is done we check if all the parity equations of the code are satisfied and declare a successful decode whenever this happens. If at least one parity equation is not satisfied we have two choices: 1) continue with the $v \rightarrow c$ and $c \rightarrow v$ steps iteration to produce new (and possibly more accurate) values for the symbols a posteriori probabilities or, 2) stop the algorithm after a maximum number of iteration is reached and declare a decoding failure.

It should be noted that the message passing algorithm computes the exact marginal a posteriori symbol probabilities only in the case that the factors graph is a tree, that's to say in the case it has no cycles. When the code graph has cycles, as it happens for any practical code, the algorithm do not produce the results an exhaustive computation of all the $2^{K \cdot \log_2(Q)}$possible cases would deliver. Yet it has a complexity which, unlike exhaustive evaluations, goes linearly with the codeword length and it is still asymptotically optimal.

Despite this linear dependence on the codeword length, the message passing algorithm is quite computational intensive, especially for Q-ary codes in which Q is large.

In the $v \rightarrow c$ step we have to compute M products between probabilities distributions of size Q, for a total of about $M\,Q\,C$ real numbers multiplications per iteration, where C denotes the average number of factors a variable is connected to.

The $c \rightarrow v$ step is even more complex as, for any code factor and for any code variable we have to compute a convolution between $\bar{V}$ probability distributions of size Q, where $\bar{V}$ indicates the average number of variables per code factor,

for a total of $M \; Q^2 \; \bar{V}$ real numbers multiplications per iteration and therefore with a quadratic complexity over the code alphabet size Q. Luckily, these convolutions can be computed in a faster way using an algorithm that is similar to the FFT (Fast Fourier Transform) based convolution where time sequences are transformed in the frequency domain, the frequency domain spectral components are multiplied together and then transformed back in the time domain. The only difference with FFT-based convolutions is that, in the case we need to convolve sequences indexed over symbols belonging to a finite field GF(Q), we use the FWHT (Fast Walsh-Hadamard Transform) in place of the FFT. When computed in this way each convolution requires $3Q \log_2(Q)$ operations and a significant computational saving is available when Q>16.

Bibliographic References

[1] http://physics.princeton.edu/pulsar/K1JT/ - Joe Taylor - K1JT

[2] http://www.dj5hg.de/digitalmodes/emepsk_userguide.pdf - Klaus von der Heide – DJ5HG

[3] "Near Shannon limit error-correcting coding and decoding: Turbo-codes. 1" – C. Berrou, A. Glavieux, P. Thihimajshima – ICC '93 IEEE Conference on Communications, May 1993.

[4] "Information Theory, Inference and Learning Algorithms" - David J.C. MacKay – Cambridge University Press, 2003

[5] "Irregular Repeat-Accumulate Codes" - H. Jin, A. Khandekar, R. McEliece - 2nd Conference on Turbo Codes – Brest, France, September 2000

[6] "A recursive approach to low complexity codes" - R.Tanner, IEEE Transactions on Information Theory, September 1981

[7] "Design of serially concatenated systems depending on the block length" - M. Tuechler, IEEE Transaction on Communications, Feb. 2004

[8] "Convergence Behavior of Iteratively Decoded Parallel Concatenated Codes" - Stephan ten Brink, IEEE Transaction on Communications, October 2001

[9] "Turbo Decoding as an Instance of Pearl's Belief Propagation Algorithm" - R. McEliece, D. MacKay, J.F. Cheng, IEEE Journal on Selected Areas in Communications, February 1998.

[10] "Open Source Soft-Decision Decoder for the JT65 (63,12) Reed-Solomon Code" – Steven Franke, Joe Taylor – QEX May/June 2016 issue, also available here: http://physics.princeton.edu/pulsar/K1JT/FrankeTaylor_QEX_2016.pdf

[11] "Capacity Approaching Codes for Non-Coherent Orthogonal Modulation" – A. Fabregas, A. Grant - IEEE Transactions on Wireless Communications, November 2007

[12] "Factor Graphs and the Sum-Product Algorithm" - F.R. Kschischang, B.J. Frey, H.A. Loeliger, IEEE Transactions on Information Theory, February 2001

I0NAA - The stealth dish

Mario Natali (email: mario.natali@gmail.com)

The stealth dish

AGENDA

- Why a stealth dish.
- Mechanical design.
- Technical characteristics.
- Results obtained.
- Future plans.

The stealth dish

Why a stealth dish...

✓ **Visibility** → ***Low***

➢ *Limits as much as possible visibility when not in use*

✓ **Safety** → **High**

➢ *Makes access to the feeder easy and safe*

✓ **Maintainability** → **High**

➢ *Makes the set-up time short and repeatable*

The stealth dish

Why a stealth dish... : Challenges and advantages

CHALLANGES

- ✓ Accuracy and repeatibility of positioning.
- ✓ Complex mechanism.
- ✓ Much higher overall weight.
- ✓ Stability.

ADVANTAGES

- ✓ Very easy access to the feeder.
- ✓ «curiosity» minimization...
- ✓ No need to use stairs.
- ✓ Lower overall profile when in «resting» position that minimize lightening risk.
- ✓ .... Good sleep during thunderstorms .....

EME Conference 2016, Venice — Impedimentum pro occasione capere — Mario Armando Natali, I0NAA

The stealth dish

Why a stealth dish .... : a bit of history

..... From Braunau am Inn to Assisi

EME Conference 2016, Venice — Impedimentum pro occasione capere — Mario Armando Natali, I0NAA

The stealth dish

Mechanical design : tower design

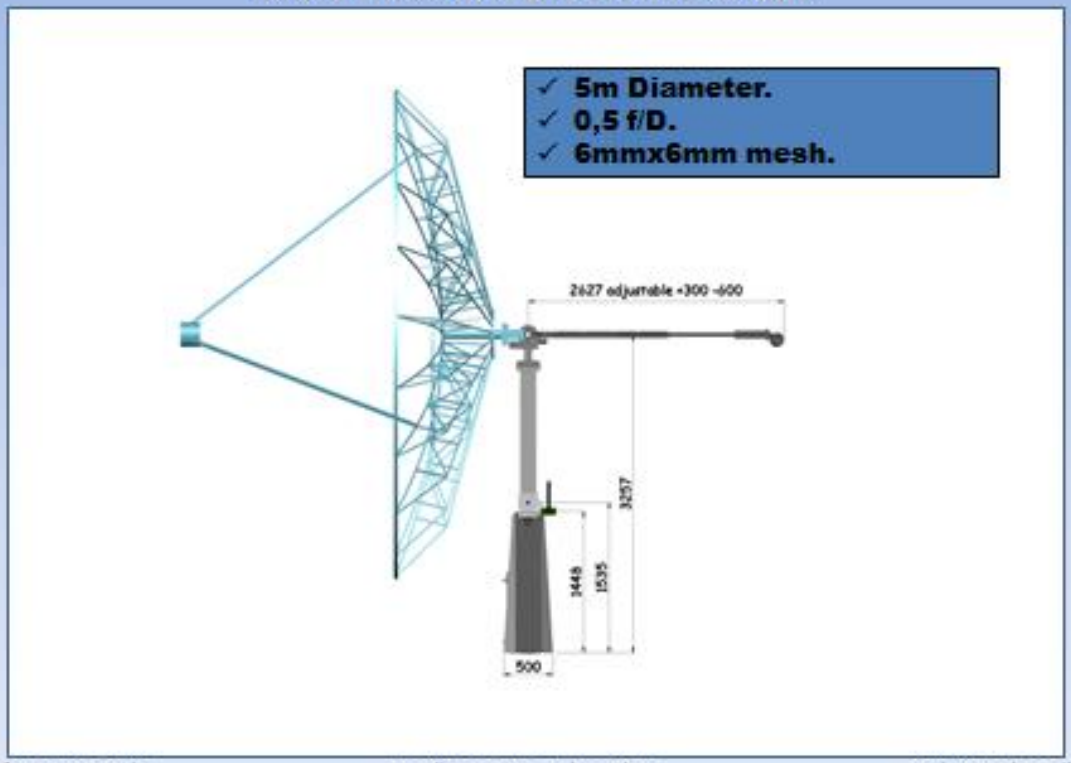

The stealth dish

Mechanical design : tower design

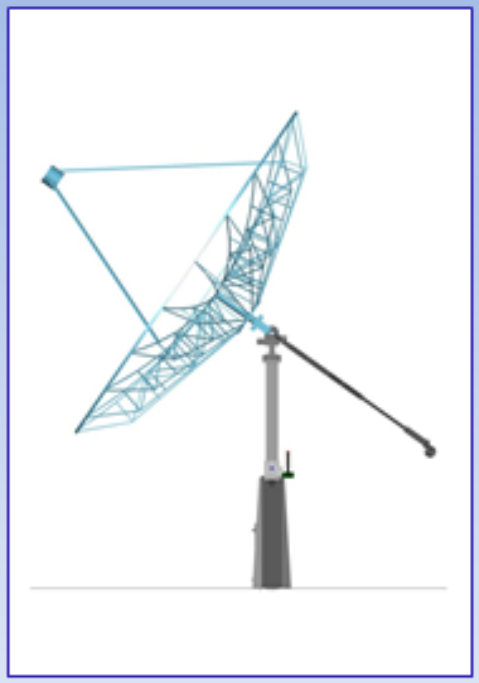

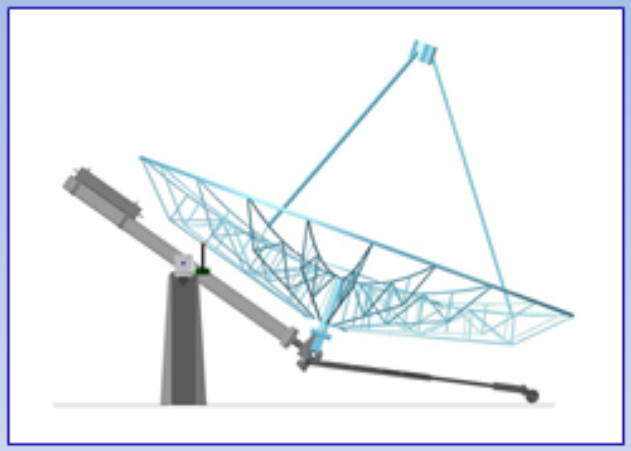

- ✓ Total weight about 1,000Kg.
- ✓ Counterweights ..... with wheels.
- ✓ Tilting system built with standard gearbox.
- ✓ 15 minutes from operations start to first echo.

The stealth dish

Mechanical design : the plinth

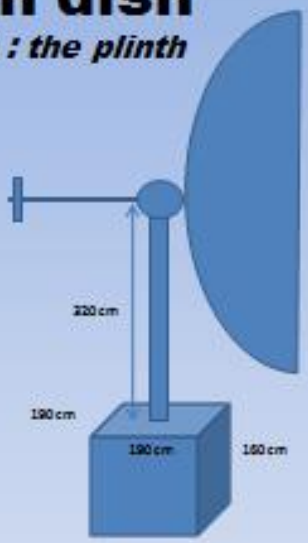

- ✓ **Stabilizing moment = 14,650 Kg.**
- ✓ **Tilting moment =6,900 Kg. (wind @ 100Km/h)**
- ✓ **η (stabilization moment) = 2.11.**

EME Conference 2016, Venice *Impedimentum pro occasione compare* *Mario Armando Natali, I0NAA*

The stealth dish

Technical characteristics : the station

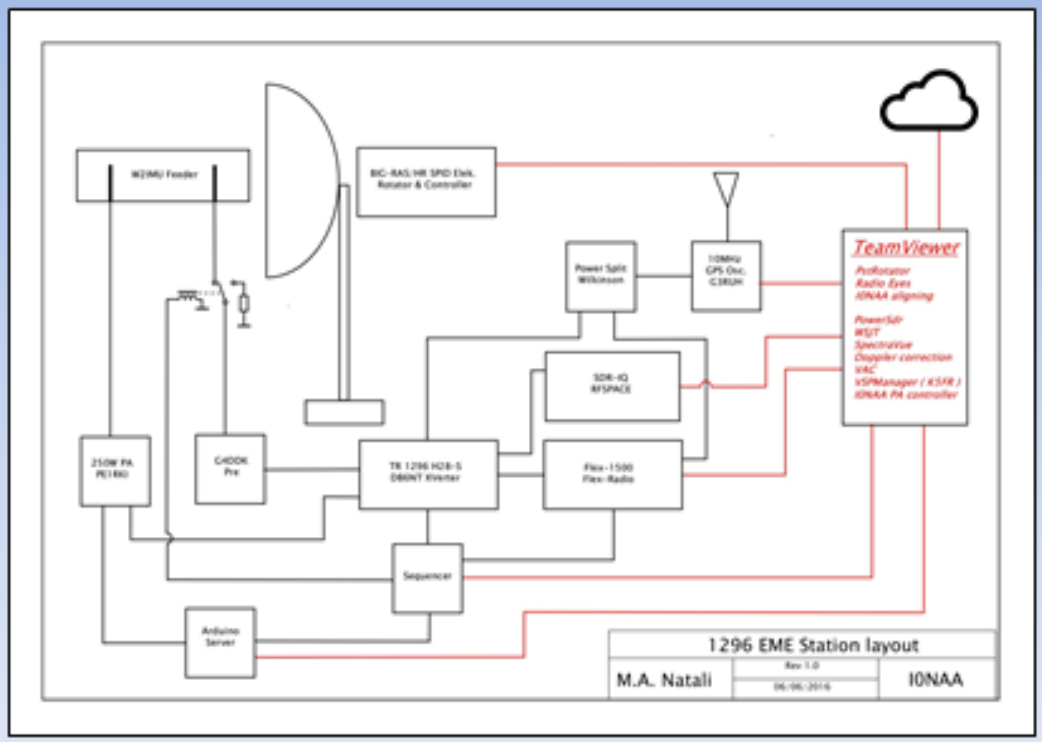

EME Conference 2016, Venice *Impedimentum pro occasione compare* *Mario Armando Natali, I0NAA*

The stealth dish

Technical characteristics : the feeder

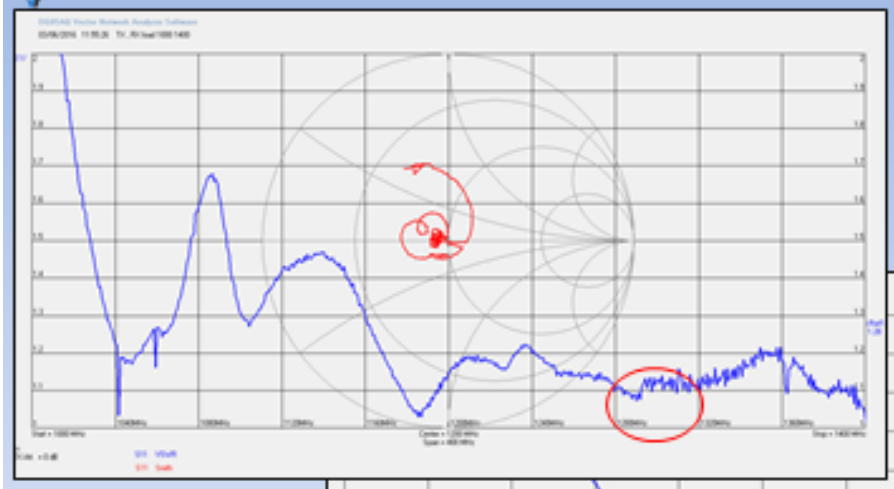

Very good S11 response over large bandwidth.

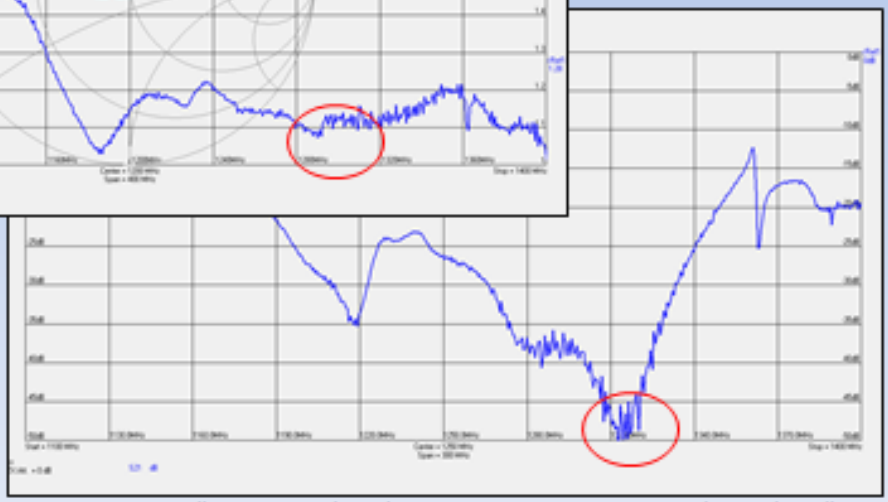

Pretty good crosstalk response at the target frequency.

EME Conference 2016, Venice *Impedimentum pro occasione compare* *Mario Armando Natali, IONAA*

The stealth dish

Technical characteristics : the results

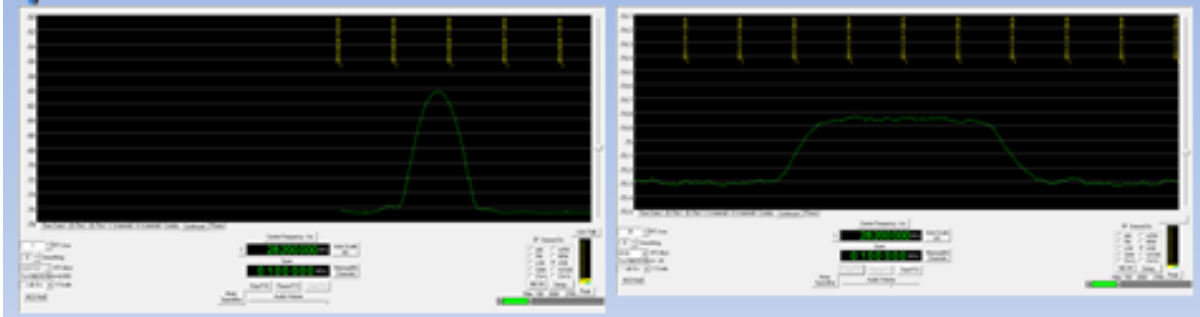

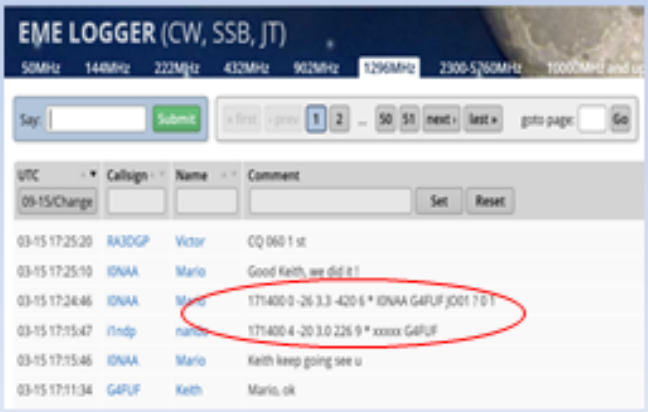

- Very consistent measurements of Cygnus-A @ 0,58dB Vs. 0,63dB Reference (92,1%).
- Very good measurement of sun noise @ around 96% Vs. Reference.
- Some problemon sidelobes to be fixed.
- «Theoretical» result achieved comparing reception of the same signal with Nando I1NDP !!!

EME Conference 2016, Venice *Impedimentum pro occasione compare* *Mario Armando Natali, IONAA*


The stealth dish
Software tools : EZmoon
INPUT PARAMETERS
OUTPUT PARAMETERS
FORMULA
Very basic worksheet to evaluate the EME path with formulas in evidence to allow good understanding and easy customization.
Go to download section of ARI PG http://www.aripg.it/
EME Conference 2016, Venice
Impedimentum pro occasione cumpare
Mario Armando Natali, IONAA


The stealth dish
Technical characteristics : the results
Echo with 220W.
JT65C QSO with SP5GDM.
EME Conference 2016, Venice
Impedimentum pro occasione cumpare
Mario Armando Natali, IONAA

The stealth dish

Future plans : automatic alignment

- ✓ **The main problem with the stealth dish is the repeatability of the alignment.**

The very narrow HPBW (about 3 Deg.) requires strict control of orientation and the incremental encoders (Hall sensors) of SPID BIG-RAS/HR , together with the tower tilting mechanism, impose a re-alignment at the beginning of each session.

- ✓ **The re-alignment is done manually calculating an offset and it is quite easy to perform during the day with the sun ... but becomes much more difficult without the sun !**
- ✓ **Absolute encoders are the obvious answer .... But this is too easy ..... ☺**

The stealth dish

Future plans : automatic alignment

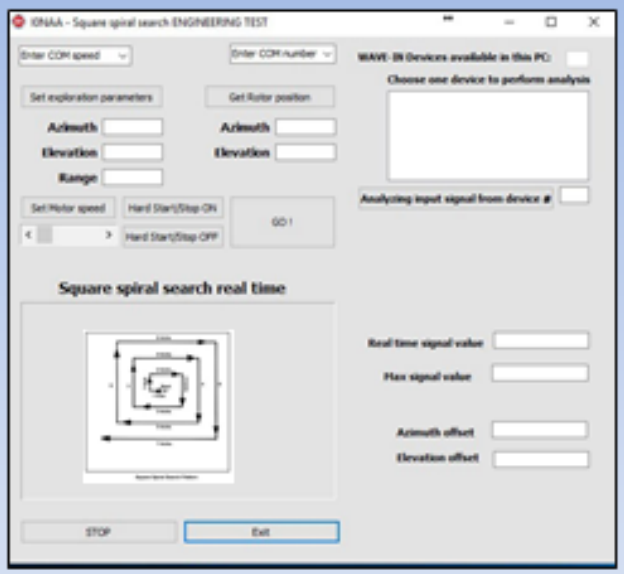

Rotator controller

RX Audio

Square Spiral Search Pattern program is in development and I plan to release it for SPID BIG-RAS/HR rotator in October. This program will use the latest firmware release from SPID that will allow better motor control to minimize start-stop oscillations.

The stealth dish

Future plans : the sky ...

- ✓ **The next challenge is the reception of pulsars ....**
- ✓ **Pulsars reception is an outstandig «methodology» to fine tune an EME station and to understand digital signal processing.**
- ✓ **The start to this long journey was the development of a program that can predict the «detactability» of a pulsars comparing the MDS (Minimum Detectable Signal) of a station with pulsar flow data derived from ATNF pulsar catalogue.**
- ✓ **The MDS is calculated entering standard station parameters and integration bandwidth / time.**
- ✓ **The program is also able to track / predict the position of the most important radio sources.**

EME Conference 2016, Venice *Impedimentum pro occasione capere* *Mario Armando Natali, IQ9AA*

The stealth dish

Future plans : Murmur

Go to download section of ARI PG http://www.aripg.it/

EME Conference 2016, Venice *Impedimentum pro occasione capere* *Mario Armando Natali, IQ9AA*

The stealth dish

Conclusions : the beauty of the antennas

oe5jfl

i0naa

.... who said that hamradio is not romantic .....

EME Conference 2016, Venice — Impedimentum pro adsalam compare — Mario Armando Natali, I0NAA

The stealth dish

EZMoon

INPUT PARAMETERS									
Frequency	MHz	1.296	Line loss before LNA	dB	0,10	Mean distance	Km	380.000
TX antenna gain	dBi	33,00	LNA noise figure	dB	0,33	Mean diameter	Km	3.470
RX antenna gain	dBi	33,00	LNA gain	dB	33,00	Mean reflectivity	%	7
TX Power	Watt	350,00	Line loss after LNA	dB	0,30	Sky temperature (TSky)	K	100
TX line loss	dB	0,10	RX noise figure	dB	0,00			
			Bandwidth	Hz	3.000			
OUTPUT PARAMETERS									
ERP	Watt	687.601	Line loss before LNA	dB	0,90	Receiving system noise factor	F	1,23
ERP	dBw	30,33	Line noise factor before LNA	F	1,03	Receiving system noise figure	dB	0,83
RADAR Equation	dB	67,01	LNA gain	dB	0810	Noise temperature of receiving system	K	53,93
Path loss	dB	271,18	LNA noise factor	F	1,00	Overall noise temperature (including TSky)	K	153,93
			Line loss after LNA	dB	0,29	Overall noise power (including TSky)	dBw	-172,93
			Line noise factor after LNA	F	1,13			
			RX noise factor	F	3,31			
EXPECTED SNR (Sout)	dB	-9,83						

FORMULA

ERP	=TX Power*(POWER(10;((TX antenna gain+TX line loss)/10)))
ERP	=10*LOG10(ERP)
RADAR Equation	=10*LOG10(4*Mean distance*2)/Mean diameter*2)
Path loss	=(33.03+20*LOG10(Frequency)+20*LOG10(Mean distance*2)+RADAR Equation-10*LOG10(Mean reflectivity/100))
Line loss before LNA	=POWER(10;(-Line loss before LNA/10))
Line noise factor before LNA	=POWER(10;(Line loss before LNA/10))
LNA gain	=POWER(10;(LNA gain))
LNA noise factor	=POWER(10;(LNA noise figure/10))
Line loss after LNA	=POWER(10;(-Line loss after LNA/10))
Line noise factor after LNA	=POWER(10;(Line loss after LNA/10))
RX noise factor	=POWER(10;(RX noise figure/10))
Receiving system noise factor	=B13+((B10-1)/B11)+((B10-1)/(B18*B11))+((B17-1)/(B13*B18*B11))
Receiving system noise figure	=Line noise factor before LNA*((LNA noise factor-1)/(Line loss before LNA)+(Line noise factor after LNA-1)/(LNA gain*Line loss before LNA))+ ((RX noise factor-1)/(Line loss after LNA*LNA gain*Line loss before LNA))
Noise temperature of receiving system	=(10^(Receiving system noise figure/10)-1)*290
Overall noise temperature (including TSky)	=Noise temperature of receiving system+Sky temperature (TSky)
Overall noise power (including TSky)	=10*LOG10(Bandwidth *1.38E-23*Overall noise temperature (including TSky))
EXPECTED SNR	=ERP-Path loss-Overall noise power (including TSky)+RX antenna gain

Mario Natali, I0NAA

K1DS - Please Don't Throw Tomatoes—The ARRL EME Contest

Rick Rosen (email: rick1ds@hotmail.com)

For the past 4 years, I have been the author of the ARRL EME Contest Results, published in capsule form in QST and with more complete commentary and results on-line. In this role, I have been able to review the log summaries and scores of the moon-bouncers, and solicit their comments and feedback on the contest. As the use of the WSJT suite of digital communications programs has continued to grow, with the establishment of beacons on 1296MHz and 10GHz, and with changes in the rules allowing for self-spotting, there has been both growth in participation and controversy over how these changes are affecting the ARRL EME Contest.

Since first being licensed in 1959 as a Novice level amateur radio operator, I have operated VHF. When I first started we were permitted CW, MCW and voice privileges on 2 meters, and aside from my military surplus HF equipment, I had a homebrew acorn tube transceiver for 2m and then a Heathkit "Twoer." Although I was fascinated by various reports of EME communications over the years, it wasn't until the 1990's when NC1I came to RI with his 432MHz gear that I saw and heard an EME station and QSO. When I moved to PA in 1997, I was closer to Al K2UYH, Marc N2UO, Russ K2TXB, Roger W3SZ, and Joe K1JT. I became a member of the Mt. Airy VHF RC, known as the Packrats, edited their monthly newsletter, eventually served as president of the club for 5 years, and as a result had closer relationships with these hams who were members. I got to experience EME operations at both Al and Joe's stations, and with a lot of their encouragement, I started to make some of my own EME QSO's, 2m CW with a single Yagi, 70cm CW with a pair of Yagis, 23cm CW with a 3m dish, and this past year, a few CW QSOs on 13cm. This year I also made my second JT65 EME QSO, finally getting the computer and radio to play together. Because I live in a community that does not allow outdoor antennas, I have a radio van and trailer mounted antennas that I assemble to operate on a limited portable basis, and then have to disassemble all the gear and antennas to storage after the activity. It has been a challenge and struggle, but very rewarding.

I attended my first International EME meeting with my XYL Jani in Prague 14 years ago, and we have been at every one since. I have met so many of the active EME group, and Jani has been welcomed by the spouses. This has been a great learning experience, and quite rewarding to get EME QSL cards from around the world. What also has struck me is the great diversity that we have. We hail from all around the globe. We have licensing authorities and various radio privileges that are varied. We have those involved for EME for half a century or more, and those who are just thinking about how they can make their first EME contact. There are stations operating from decommissioned commercial and research dishes, and those with a single yagi, with everything in-between. With improvements in technology, we have EME beacons, a host of digital communication options, chat rooms and reflectors, greater transmit power generation and more sensitive receive capability. The highly prized Worked All Continents, Worked All States and DXCC awards have been achieved on several bands. With all of these changes, there has been both increased excitement and consternation.

I was hesitant to volunteer to talk about any potential changes in the ARRL EME Contest rules. In this forum, it can be quite controversial, hence my presentation title. I am a member of the ARRL, but I am a volunteer author and have never been a member of any of the committees. I do not know if this exercise and forum will have any impact on the ARRL EME Contest. As an author and EME op, I have been able to see and hear much feedback about the contests and their rules. I am also aware of the changes at ARRL over the years. There was a time when

every entrant in every activity had their call listed in QST. Over time, as publishing costs continued to rise and the availability of internet web space was inexpensive, there was a shift in contest reporting, with the highlights and limited commentary and top winners cited in QST, and a more generous document and full results published online. There have also been changes in the amount of space dedicated to activities that are more and less popular among the ham community. The VHF/UHF/microwave Spring and Fall Sprints (4 hour single band or microwave activity nights) have been removed from ARRL sponsorship and are supported by the volunteer efforts of some radio clubs. The results of the ARRL EME Contest and the ARRL 10GHz and Up Contest have had their appearance in QST dramatically shortened due to the limited number of logs received. This year, the longstanding ARRL UHF Contest is not being sponsored by the ARRL because of declining log submissions, but has been picked up by a group of active VHF/UHF/microwave hams. The hope is that with greater participation, and rule changes, it may become an ARRL event again in the future. There is also the opportunity for other independent groups or individuals to sponsor EME activity and the ARRL can give these activities publicity. We have to remember that there are limits to the resources that can be devoted to a small segment of the ham population. With just a few more than 100 log entries, and perhaps a world-wide participation of 500 hams in a contest, it is difficult to draw an organization's attention.

With all of the foregoing explained, let's take a brief look at what has happened in EME contesting and activity over the past few years. DUBUS sponsors EME activities for 12 moon passes per year. ARI sponsors activities for 4 moon orbits per year; two of them overlapping with the 6 moon pass activities of ARRL. The 2m ATP CW events occur over 8 moon orbits, with 3 of them overlapping DUBUS events. Lastly, there are 14 weekend days that there are terrestrial VHF and up events in the US and EU. The number of logs received by DUBUS over the past 10 years for their single band events has declined dramatically for 2m, dropped modestly for 70cm, and has shown growth on all other higher bands. There are still only between 20 and 40 logs submitted for the higher microwave events. The ARRL rules take a different approach, having multiple microwave bands used for the first weekend and then multiple bands through 23cm for the second two weekends. The difference here has been that the number of logs that show 2m activity has been steady and rising, while the number of submitted logs with microwave activity on 13cm and above has declined. Could this be just chance variation, or is it indicative of a trend? DUBUS is dropping both the 2m and 70cm Digital EME Championships due to the lack of log entries. The ARRL EME Contest has shown growth of digital activity and the number of log entries.

The feedback and thoughts from the brief on-line survey will also be reviewed here. At the time of writing, there were just over 100 survey responses to the link posted on the various internet moon reflectors. As more come in they will be added to the analysis. There are no surprises in the results. Respondents showed capabilities greatest on 2m and slightly decreasing with each higher band, with the exception of 10GHz, which seems to be growing. Bands for 6m, 1.25m (222MHz) and 33cm (902MHz) were not included in the survey, as these are neither popular EME contest bands and some are also not available in all countries. Activity in events was greater than 50% by respondents, with the ARRL contest having the biggest draw of 82% of those surveyed. Use of SSB was noted for 43%, while both CW and digital operation were done by over 70%. Of those who do not or no longer enter the ARRL contest, about 25% indicated they were concerned about digital and self-spotting issues. Ten percent cited concern over dates and paper log entries. Many emphasized these reasons in their comments. Almost 50% of respondents asked for single band weekend events and also separate digital and CW activity. I am sure that all of the EME community understands the hazards and risks of band feed changes in the dark and the terrible accident in 2012 that befell Philippe F2TU. There was modest support for increasing the point value for QSOs on higher bands and also for being able to add points for both CW and digital contacts with the same station. There were mixed

comments about self-spotting. Some feel it is inappropriate for a contest, while others are very pleased to use it for the more difficult microwave and cross-band contacts and for communication with small stations. Some felt that there should be regional awards. I thought that having all three weekends be all-band could have helped the issue of single band issues, having 6 separate passes for those with all of the microwave capabilities, while others could concentrate on the lower bands with their stations, and/or changing some of the award categories.

When all is said and done, there may be opportunity for some independent sponsorship of single band weekends, modest incremental change to the ARRL contest and award categories, or things just might remain the same. We know that change is a constant. It brings opportunity and challenge. I remember the book, "Who Moved My Cheese? An Amazing Way to Deal with Change in Your Work and in Your Life," published in 1998, a motivational tale by Spencer Johnson written in the style of a parable or business fable. Check it out on Wikipedia. As trends and changes develop, they will induce further contest modification as has already happened for both ARRL and DUBUS.

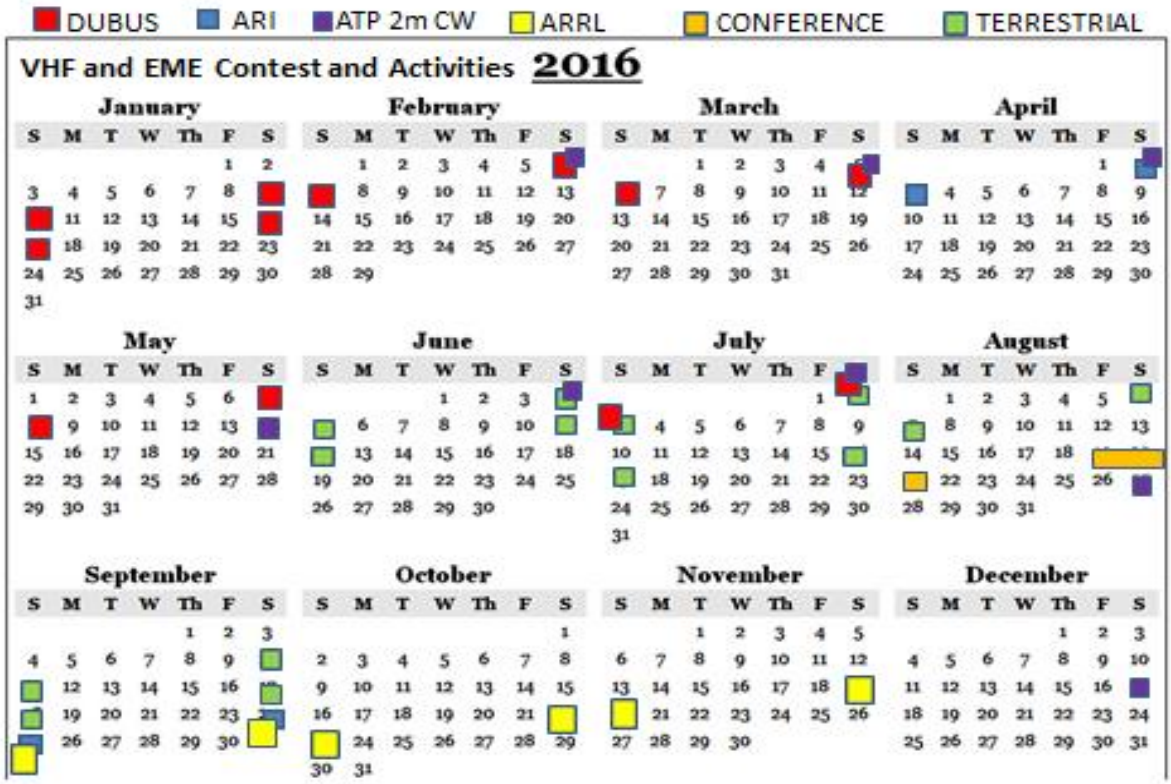
DUBUS
ARI
ATP 2m CW
ARRL
CONFERENCE
TERRESTRIAL
VHF and EME Contest and Activities 2016
January
February
March
April
May
June
July
August
September
October
November
December

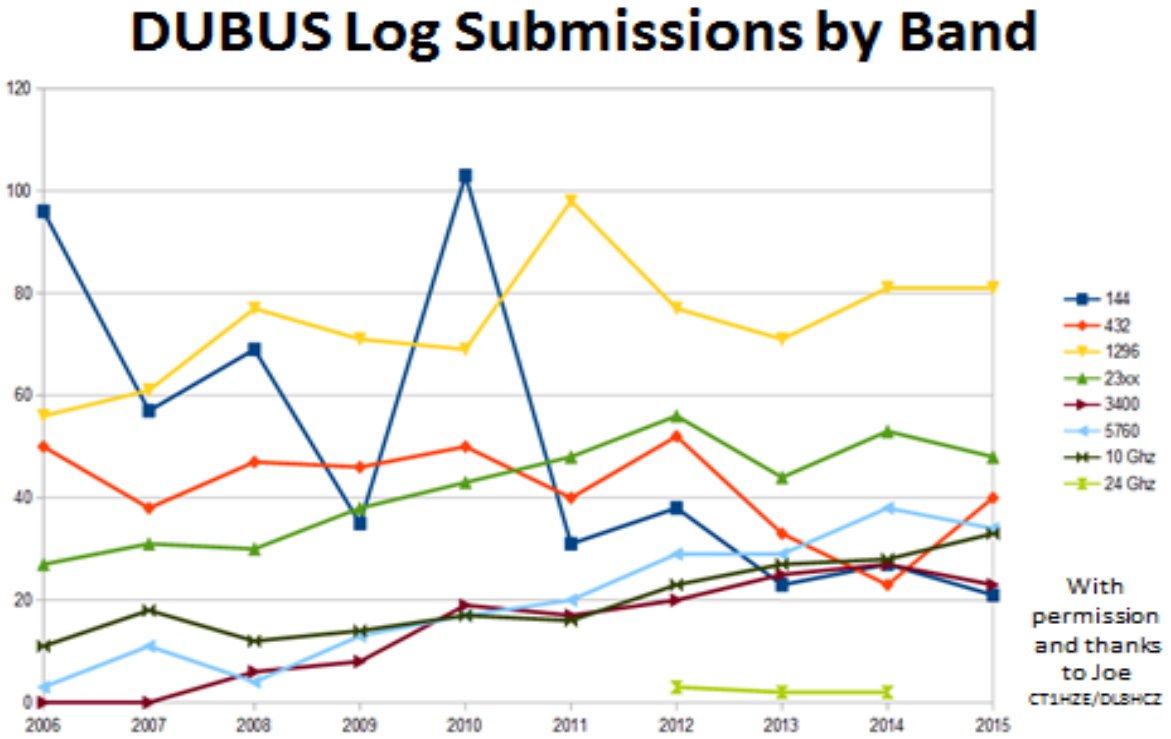
DUBUS Log Submissions by Band
120
100
80
60
40
20
0
2006
2007
2008
2009
2010
2011
2012
2013
2014
2015
144
432
1296
23xx
3400
5760
10 Ghz
24 Ghz
With permission and thanks to Joe
CT1HZE/DL8HCZ

DUBUS 2015 CW EME Contest

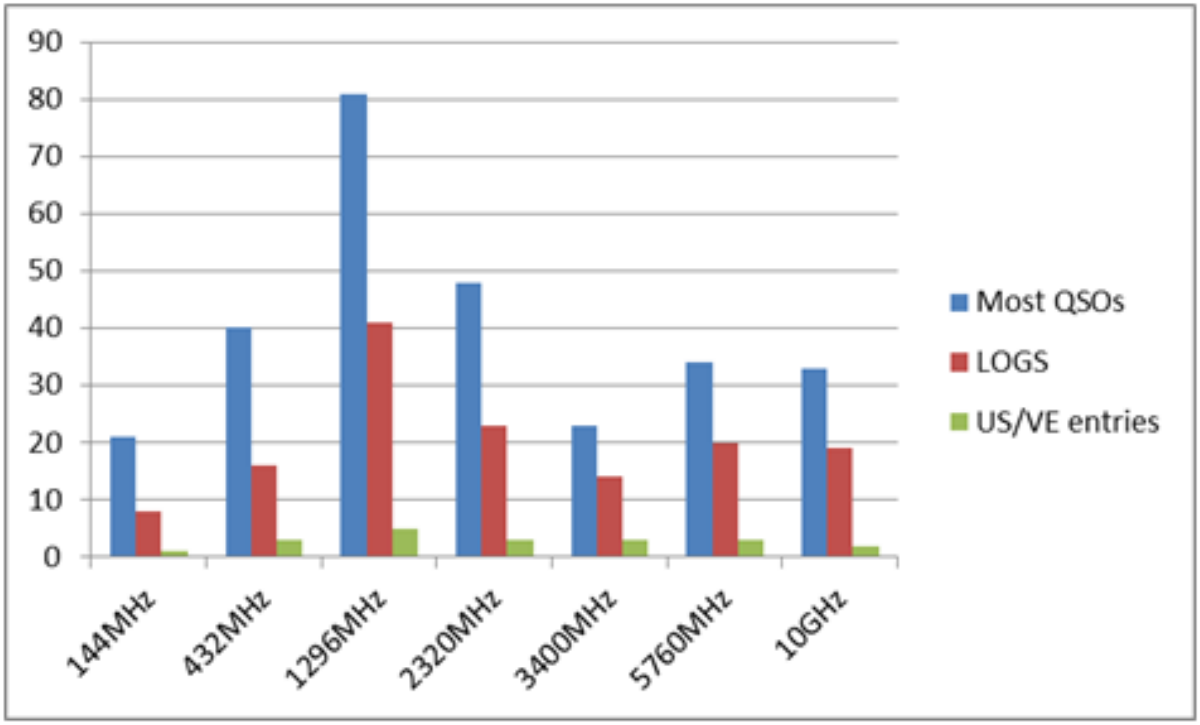

Comments on the DUBUS 2015 European CW Contest

"Activity was poor on 2m but better on 70cm compared to 2014. 23cm is still **THE** band, but 10GHz becomes very popular now too. At least 34 stations were active in the contest, that seems to be an all time high. Activity and entries on 13, 9 and 6cm were about the same as last year, maybe slightly less. "

73 Joe, DL8HCZ/CT1HZE

DUBUS 2015 Digital EME Championship

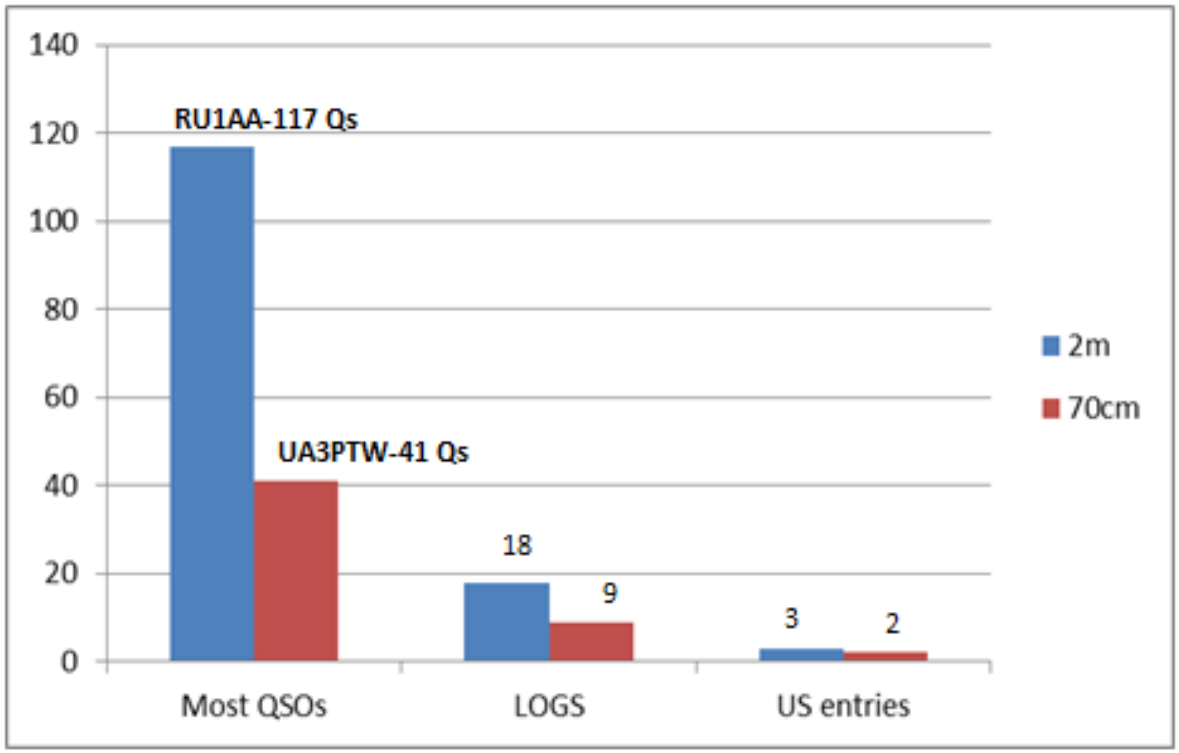

DUBUS 2m Digital EME 2015

"Thanks to all who sent an entry. Entries are down 50% vs 2015. This is a clear vote. There are just a few EME Ops left who like to invest some time into a contest, most operators nowadays just hunt for new DXCCs and initials which is totally ok. The effort to promote and evaluate such a contest and send out awards is simply too big for this low level of participation. So, this was the last 2m Digital EME Championship. Maybe we will be back with another contest concept in the future."
73 de Joe CT1HZE/DL8HCZ (18 logs)

DUBUS 70cm Digital EME 2015

"Thanks to all who sent an entry. Over 40 stations were active on the band, but just 9 sending an entry. This is the reason why this is the last 70cm Digital EME Championship. We think there are enough other EME contests (ARRL, ARI) which cover 70cm digital."

73 de Joe, CT1HZE

ARRL EME Log Submissions by Band

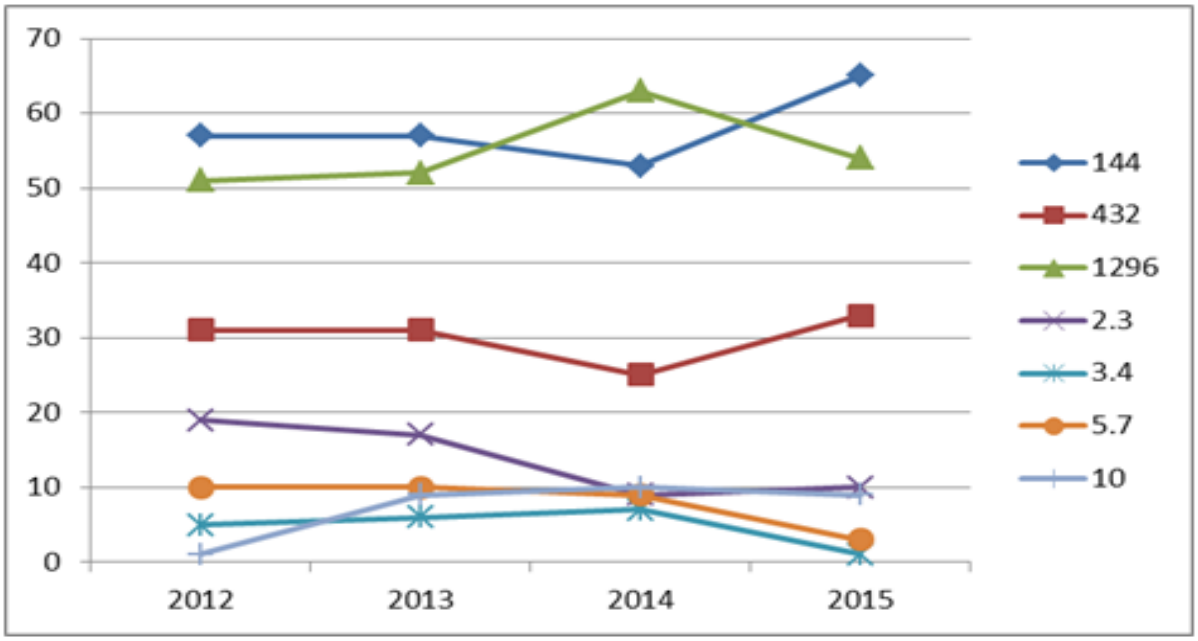

ARRL EME Contest Logs

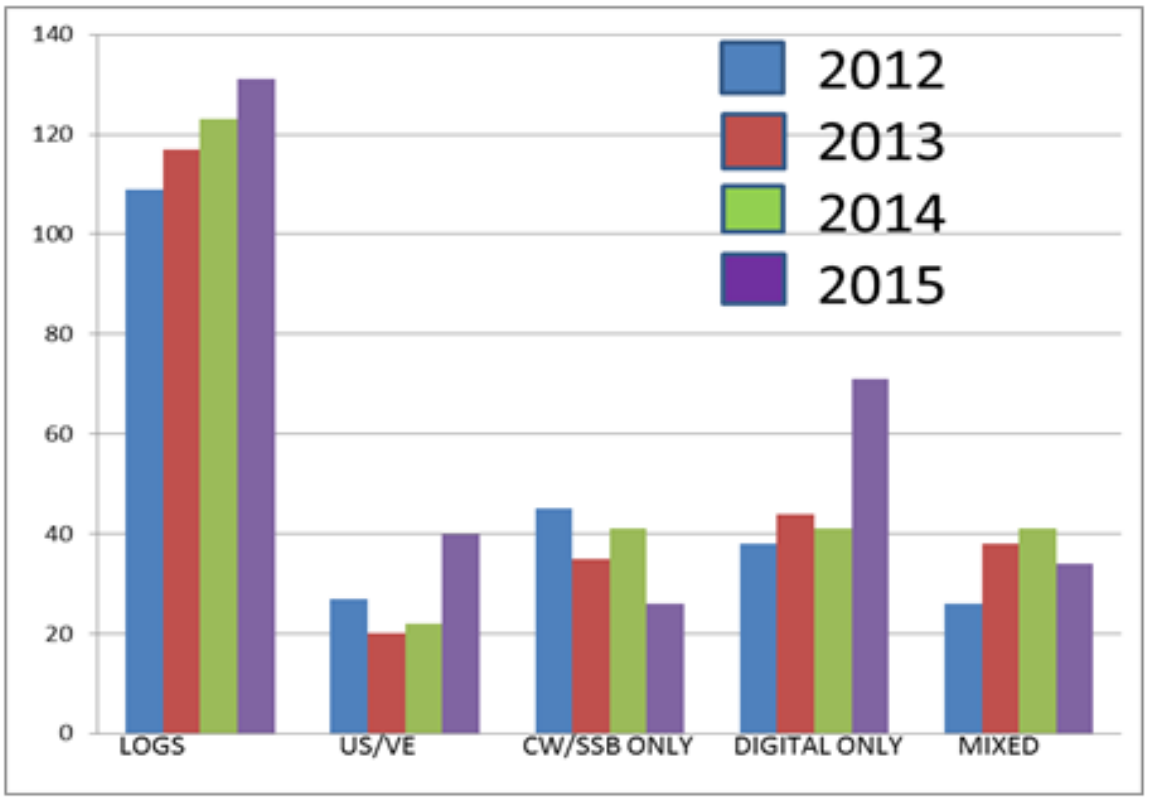

ARRL EME QSOs by Band

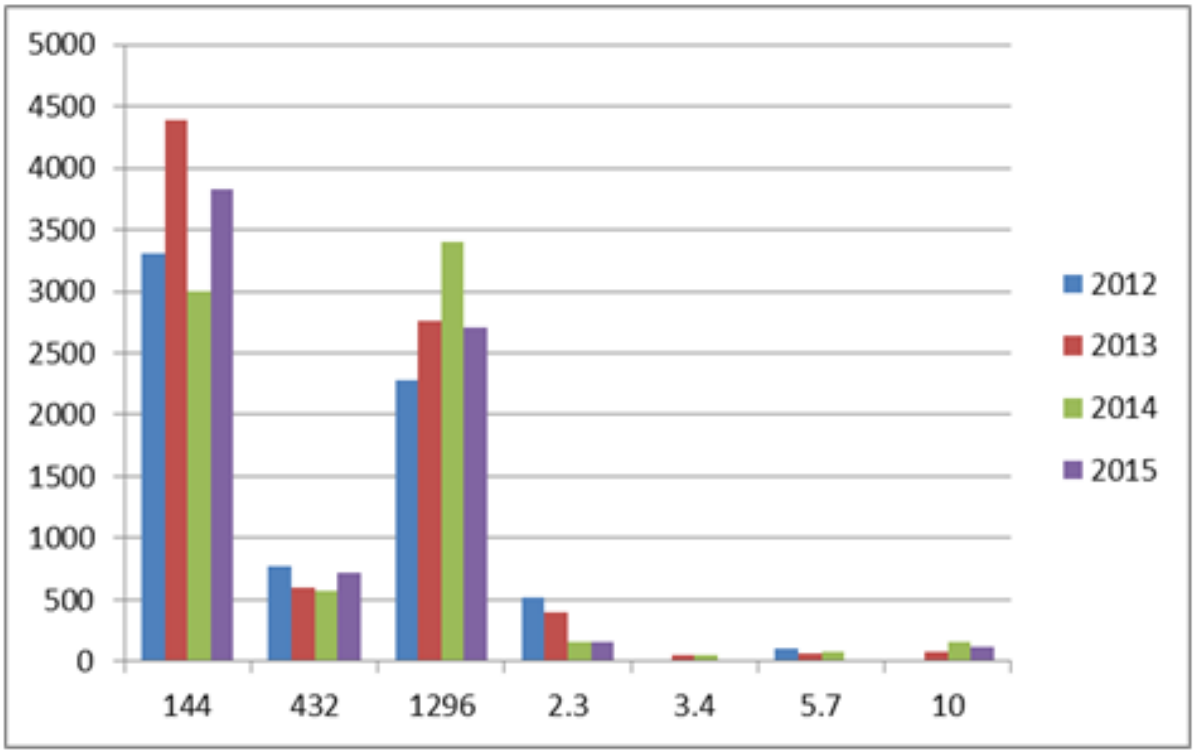

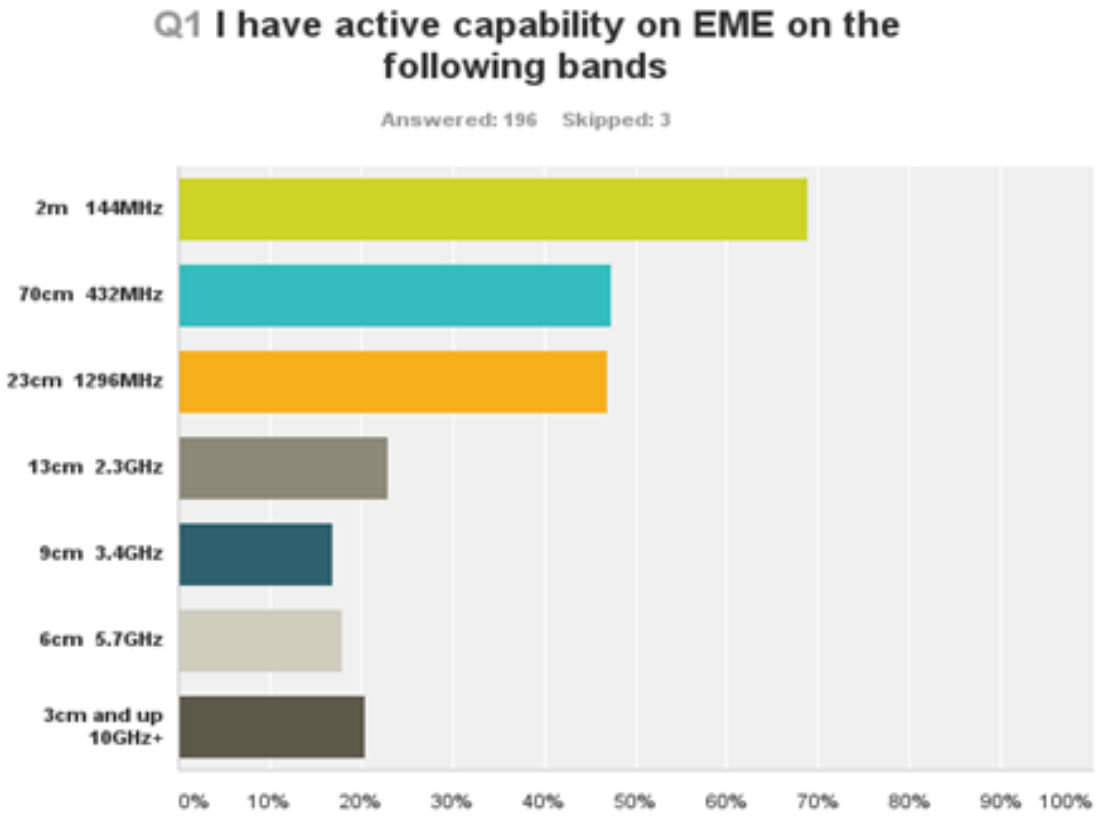
Q1 I have active capability on EME on the following bands
Answered: 196 Skipped: 3
2m 144MHz
70cm 432MHz
23cm 1296MHz
13cm 2.3GHz
9cm 3.4GHz
6cm 5.7GHz
3cm and up 10GHz+
0% 10% 20% 30% 40% 50% 60% 70% 80% 90% 100%

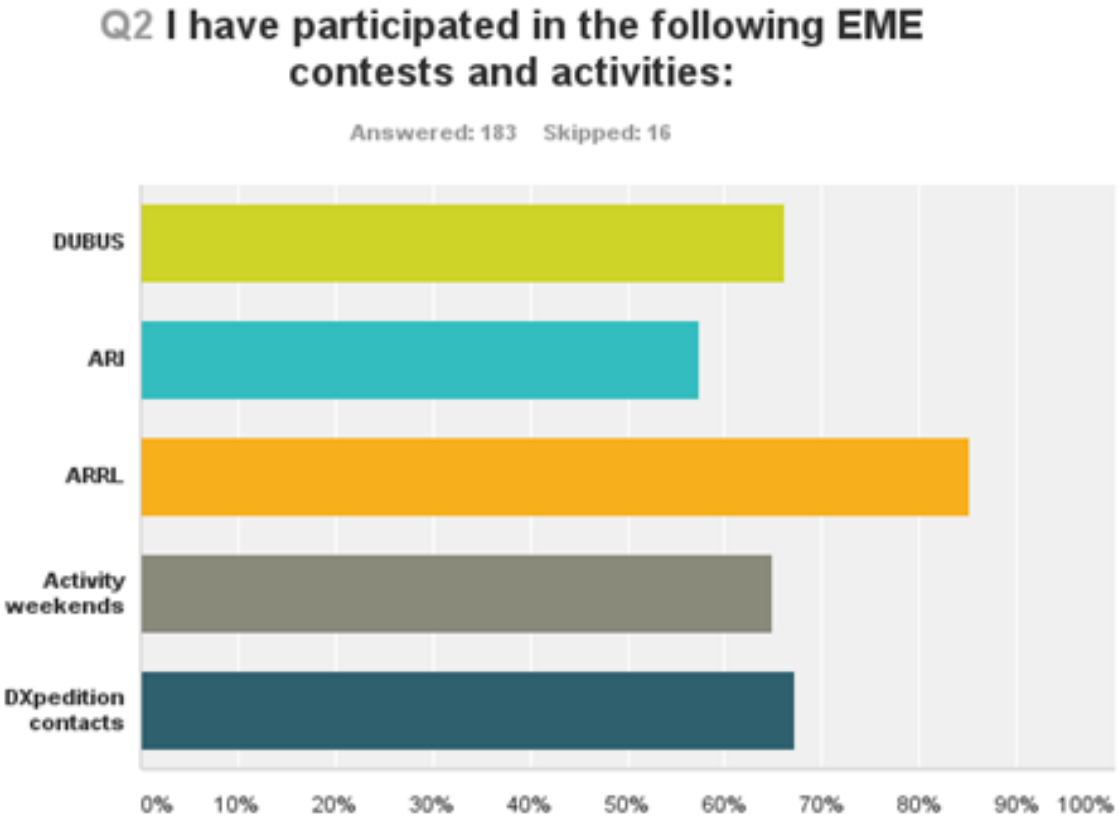
Q2 I have participated in the following EME contests and activities:
Answered: 183 Skipped: 16
DUBUS
ARI
ARRL
Activity weekends
DXpedition contacts
0% 10% 20% 30% 40% 50% 60% 70% 80% 90% 100%

Q3 I have operated the following modes:

Answered: 197 Skipped: 2

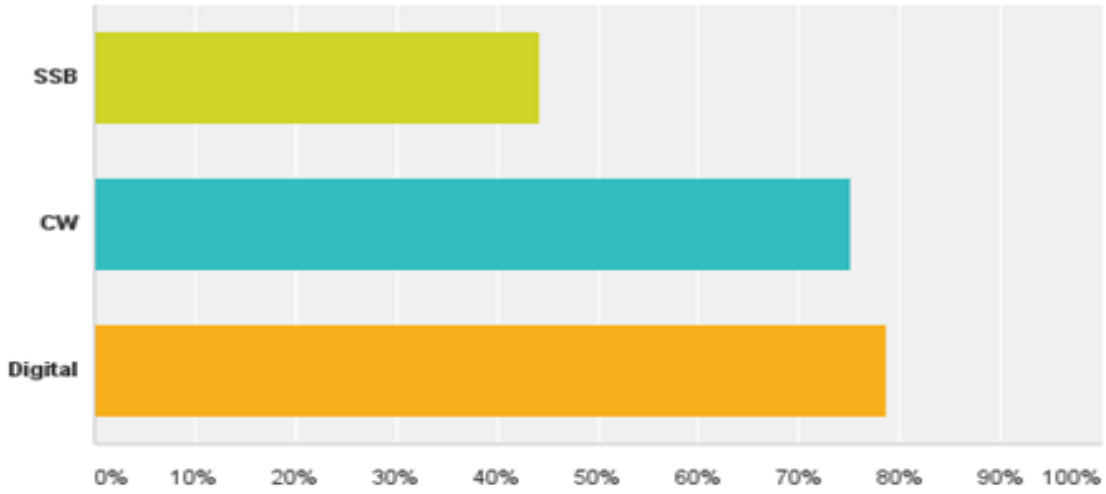

Q4 Have you participated in the ARRL EME Contest?

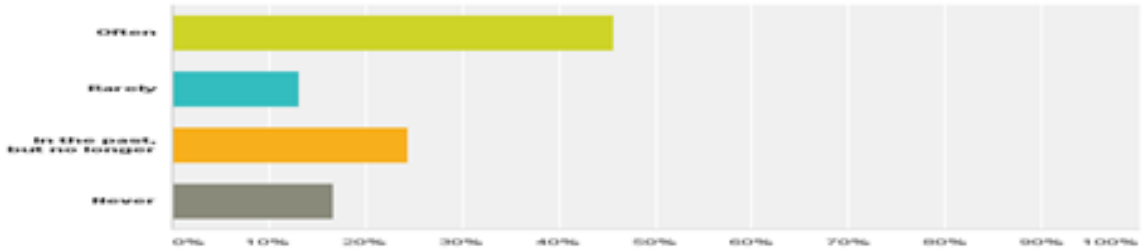

Q5: If you have never or are no longer participating in the ARRL EME contest, please indicate the reason(s):

Answer Choices	Responses	
No current active EME capabilities	4.8%	5
I do not want to send in a paper log, only prefer electronic submission	13.5	14
I am not interested in EME contests	12.5	13
I am concerned about the rules changes allowing digital QSOs	23	24
I am concerned about the rules change allowing self-spotting	23	24
The dates are problematic	9.6	10
Other (please specify)	55	57
Total Respondents: 104		

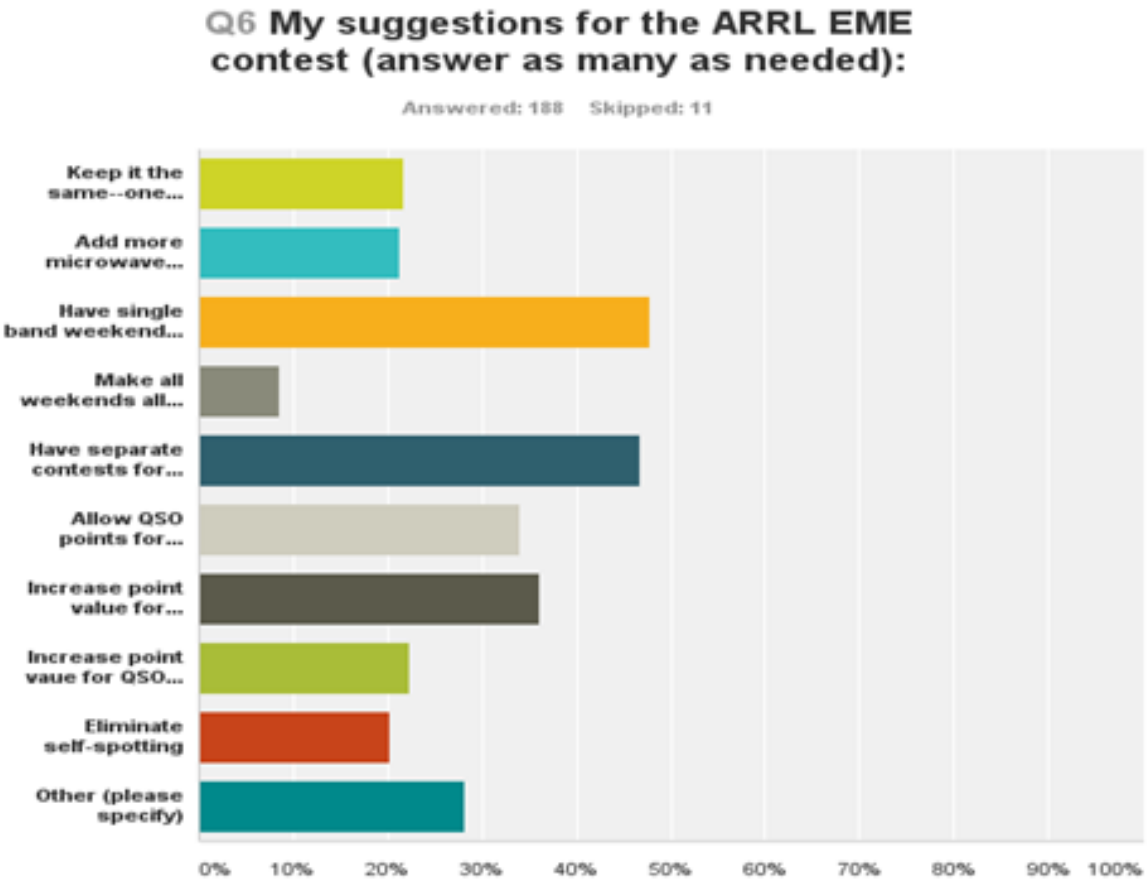

Is Change Needed?

- DUBUS and ARRL EME contest participation is strong and growing.
- Other ARRL VHF contests award higher band QSO points
- QSO information exchange and scoring is problematic
- Mode use has shifted
- More new participants with very modest stations
- Number of logs submitted validates contest support
- Technology has advanced capabilities
- A minority of >=2GHz capable stations participate

2015 ARRL Contest Logs Received

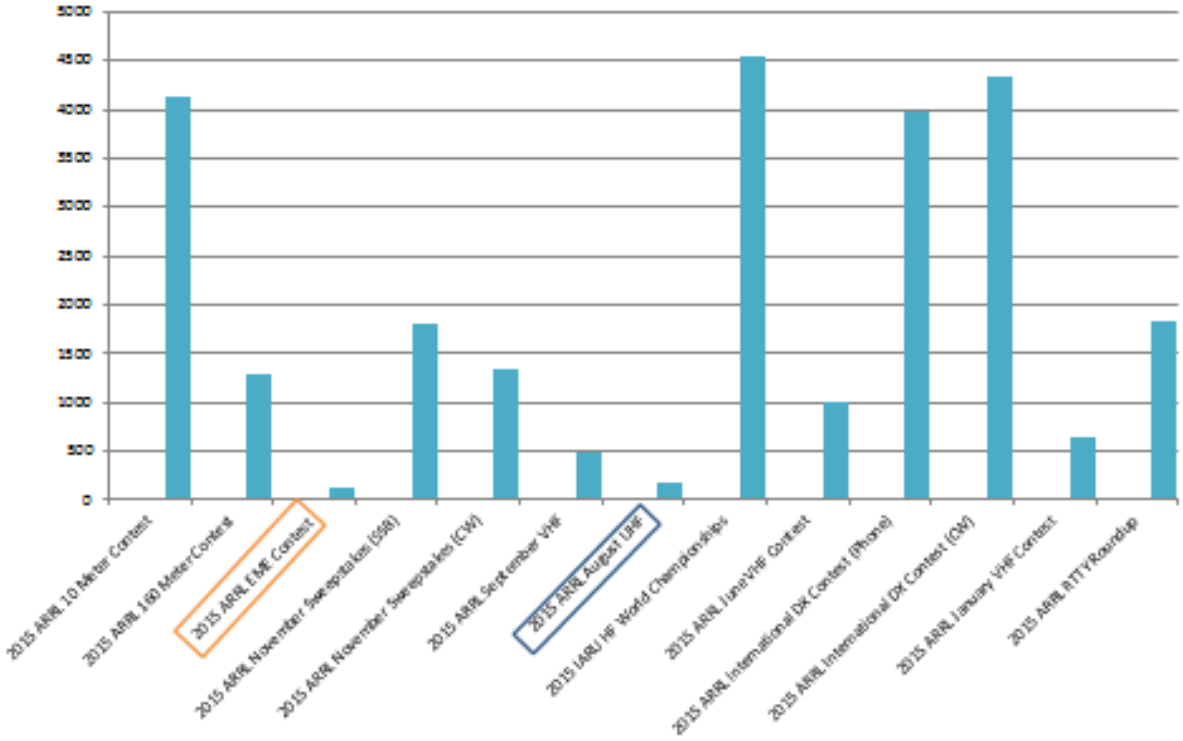

Is Change Possible?

- Participation is measured by log submission
- Contest changes have been responsive to activity trends and technology developments
- Some contests have been eliminated from ARRL sponsorship due to low participation
- ARRL has Ad-Hoc VHF contest committees, Radiosport Manager, Board of Directors
- Independent EME activity sponsors possible

Can We Adapt?

- We are ambassadors for a unique form of radio communication
- We are highly technical and capable
- We are energetic and constantly push the envelope
- We are a diverse group of EME ops representing many diverse interests
- We need to be inclusive
- All voices need to be heard and considered
- EME contesting and activity brings us together